JYU DISSERTATIONS 503

Juulia Lautaoja

Muscle metabolism and intercellular crosstalk

Effects of *in vitro* exercise and changes in muscle size

UNIVERSITY OF JYVÄSKYLÄ
FACULTY OF SPORT AND HEALTH SCIENCES

JYU DISSERTATIONS 503

Juulia Lautaoja

Muscle Metabolism and Intercellular Crosstalk

Effects of *in Vitro* Exercise and Changes in Muscle Size

Esitetään Jyväskylän yliopiston liikuntatieteellisen tiedekunnan suostumuksella
julkisesti tarkastettavaksi yliopiston Liikunta-rakennuksen salissa L 304
toukokuun 6. päivänä 2022 kello 12.

Academic dissertation to be publicly discussed, by permission of
the Faculty of Sport and Health Sciences of the University of Jyväskylä, in building
Liikunta, auditorium L 304 on May 6, 2022 at 12 o'clock noon.

JYVÄSKYLÄN YLIOPISTO
UNIVERSITY OF JYVÄSKYLÄ

JYVÄSKYLÄ 2022

Editors
Simon Walker
Faculty of Sport and Health Sciences, University of Jyväskylä
Timo Hautala
Open Science Centre, University of Jyväskylä

ISBN 978-951-39-9084-8 (PDF)
URN:ISBN:978-951-39-9084-8
ISSN 2489-9003

Permanent link to this publication: http://urn.fi/URN:ISBN:978-951-39-9084-8

ABSTRACT

Lautaoja, Juulia
Muscle metabolism and intercellular crosstalk - effects of *in vitro* exercise and changes in muscle size
Jyväskylä: University of Jyväskylä, 2022, 116 p.
(JYU Dissertations
ISSN 2489-9003; 503)
ISBN 978-951-39-9084-8

Skeletal muscles have an active role in the regulation of the whole-body metabolism in health and disease. Maintenance of skeletal muscle mass is important for everyday life as well as for better prognosis against muscle wasting diseases, such as cancer cachexia. Along with its role in the wasting conditions, skeletal muscle is also a key tissue in exercise. In addition to traditional endocrine organs, such as pancreas, skeletal muscles can also produce and release signaling molecules, collectively known as exerkines, that finetune metabolism in the recipient cells and tissues. The purpose of this dissertation was to examine skeletal muscle physiology, metabolism, and secretome in response to changes in muscle size and to muscle cell contractions. To address these interactions, both animal and cell models were used. More specifically, muscle wasting induced by the C26 colon carcinoma cells *in vivo* and myostatin *in vitro* were used to model muscle atrophy. The blockade of myostatin and activins, negative regulators of muscle size, was used to reverse muscle wasting *in vivo*. The direct skeletal muscle-specific effects of myostatin were studied using muscle cells. Muscle cell contractions induced by exercise-like electrical pulse stimulation *in vitro* were used to mimic *in vivo* exercise. The main findings of this dissertation were that cancer greatly disturbed skeletal muscle and serum metabolomes. These disturbances could not be rescued by the reversal of muscle wasting using myostatin and activin blocker. Myostatin had expected effects on signaling in the myoblasts, but the differentiation of the murine C2C12 cells into myotubes decreased this response. Human muscle cells appeared to maintain their responsiveness to myostatin better, also after differentiation. Myotube contractions induced many expected, but also newly detected intra- and extracellular changes at the metabolome and transcriptome levels. Based on these omics-analyses, the observed changes were mainly related to energy metabolism, contractility, and inflammatory response. This dissertation provides novel insights into skeletal muscle and exercise research that may improve development of better *in vivo* and especially *in vitro* models to study not only skeletal muscle physiology per se, but also the mediators and the mechanisms of intercellular crosstalk in different conditions.

Keywords: physical activity, physical inactivity, skeletal muscle, myotube, intercellular crosstalk, electrical pulse stimulation, exercise

TIIVISTELMÄ (ABSTRACT IN FINNISH)

Lautaoja, Juulia
Lihasten aineenvaihdunta ja solujen välinen vuorovaikutus – lihassolujen liikunnan ja lihaskoon muutosten vaikutukset
Jyväskylä: University of Jyväskylä, 2022, 116 s.
(JYU Dissertations
ISSN 2489-9003; 503)
ISBN 978-951-39-9084-8

Luurankolihaksilla on tärkeä rooli toimintakykyisen arjen ylläpitämisessä niin terveillä ihmisillä kuin lihaskatoa edistävää tautia, kuten syöpää sairastavilla potilailla. Suurempi luurankolihasmassa on yhdistetty parempaan selviämiseen syövästä, joten on tärkeää ymmärtää paremmin, miten lihaskadon ehkäisy vaikuttaa luurankolihasten aineenvaihduntaan. Lihaskadon lisäksi luurankolihaskudos on tärkeä liikunnassa. Perinteisten umpirauhasten lisäksi myös lihakset tuottavat ja vapauttavat verenkiertoon säätelytekijöitä, jotka muokkaavat kohdekudosten aineenvaihduntaa. Nämä tekijät kuitenkin tunnetaan vielä varsin huonosti, joten niiden tutkiminen on tärkeää. Tämän väitöskirjan tarkoitus oli tutkia, miten luurankolihaksen koko ja supistukset vaikuttavat lihaksen fysiologiaan ja erityisesti aineenvaihduntaan. Hiirten kokeellinen syöpä mallinsi luurankolihasten katoa, joka kumottiin estämällä lihaskasvun negatiivisten säätelijöiden, myostatiinin ja aktiviinien vaikutukset liukoisella kasvutekijäreseptorilla. Solumallilla tutkittiin muun muassa myostatiinin suoria vaikutuksia luurankolihaksen aineenvaihduntaan. Liikunnankaltaista lihassolujen sähköstimulaatiota käytettiin mallina lihassupistuksista. Tämän väitöskirjan päätulokset olivat, että kokeellisen syövän aiheuttama lihaskato häiritsi suuresti luurankolihaksen aineenvaihduntaa ja monien molekyylien pitoisuuksia niin lihaksessa kuin veressä. Lihaskadon estämisen vaikutukset luurankolihaksen aineenvaihduntatuotteisiin jäivät syövän vaikutusta pienemmiksi. Näin ollen lihaskadon ja syövän aiheuttamat vaikutukset luurankolihaksessa ja veressä eivät todennäköisesti johtuneet muutoksista luurankolihaksen koossa. Hiiren, mutta ei ihmisen lihassolulinjan erilaistuminen lihassäikeiksi muutti niiden vasteita myostatiinille. Lihassolujen supistukset saivat aikaan sekä odotettuja että odottamattomia fysiologisia muutoksia niin lihassolujen sisällä kuin niiden ulkopuolella. Havaitut muutokset liittyivät muun muassa energia-aineenvaihduntaan, supistuskykyyn ja tulehdusvasteisiin. Tämän väitöskirjan tulokset lisäävät ymmärrystä lihas- ja liikuntatutkimuksesta eläin- ja solumalleilla sekä mahdollistavat parempien tutkimusmallien kehittämisen, erityisesti solutasolla.

Avainsanat: fyysinen aktiivisuus, fyysinen inaktiivisuus, luurankolihas, lihassolu, solujen välinen vuorovaikutus, sähköstimulaatio, liikunta

Author

Juulia Lautaoja, MSc
NeuroMuscular Research Center
Faculty of Sport and Health Sciences
University of Jyväskylä
P.O. Box 35
FI-40014 University of Jyväskylä, Finland
juulia.h.lautaoja@jyu.fi
ORCID: 0000-0003-2037-829X

Supervisors

Associate Professor Juha Hulmi, PhD
NeuroMuscular Research Center
Faculty of Sport and Health Sciences
University of Jyväskylä
Jyväskylä, Finland

Satu Pekkala, PhD, Academy Research Fellow
Docent at the University of Turku
Faculty of Sport and Health Sciences
University of Jyväskylä
Jyväskylä, Finland

Reviewers

Professor Cora Weigert, PhD
Institute for Clinical Chemistry and Pathobiochemistry
University of Tübingen
Tübingen, Germany

Associate Professor Severine Lamon, PhD
Centre for Physical Activity and Nutrition Research
School of Exercise and Nutrition Sciences
Deakin University, Melbourne
Victoria, Australia

Opponent

Professor Ketan Patel, PhD
School of Biological Sciences
University of Reading
Reading, Great Britain

ACKNOWLEDGEMENTS

The main work presented in this dissertation was carried out at the Faculty of Sport and Health Sciences at the University of Jyväskylä. I wish to thank the Faculty for providing me high-quality facilities and experienced staff to work with. The mass spectrometry analyses were conducted at the Shanghai Jiao Tong University, while nuclear magnetic resonance spectrometry (Department of Chemistry) and messenger RNA sequencing (Department of Biological and Environmental Sciences) were conducted at the University of Jyväskylä. Financial support for the study was received from the Academy of Finland, the Cancer Society of Finland, the Finnish Cultural Foundation, Emil Aaltonen Foundation and the Faculty of Sport and Health Sciences.

I wish to express my deepest gratitude to my supervisor Associate Professor Juha Hulmi for all the help, guidance and support during this journey. Six years ago, Professor Heikki Kyröläinen sent me to knock on your door when I needed a master's thesis topic. I was glad to be accepted to your group despite of my, so to say, limited music taste. However, other strengths, presumably related to other types of heavy metal, may have compensated this musical drawback. Juha, you are very good at knowing when to provide extra backup and when to give space for us students to make our own decisions. As I have enjoyed being part of your research group, I really hope that someday we could work together again.

Secondly, I would like to sincerely thank my second supervisor Dr. Satu Pekkala. You have always been there for me, both professionally and personally. You have always cleared time from your busy schedule to help me if I have had any questions or problems. I really appreciate that as well as our informal discussions, for example, about (rescue) dogs and mushroom hunting. Both you and Juha have told me to slow down when I have stubbornly tried to keep up with my sometimes tight and overoptimistic schedule. Other times you have pushed me to keep the very core of my work clear in mind. "So what?" is a question that I will carry with me as one of the key lessons learned.

I wish to thank the pre-examiners of my dissertation, Professor Cora Weigert and Associate Professor Severine Lamon, for their constructive, justified and valuable comments. Your feedback really improved my thesis. I also want to thank Professor Ketal Patel for accepting the invitation to come to Jyväskylä and to be my opponent.

I would like to acknowledge all the collaborators and co-authors with whom I have had a privilege to work with over the years. Of these, I wish to mention Dr. Olli Ritvos and Dr. Arja Pasternack for providing us the soluble activin receptor and the recombinant myostatin protein as well as guidance for the biology of these fascinating proteins. I wish to thank Professor Sulin Cheng, Professor Perttu Permi and Professor Marja Tiirola as well as their research groups for conducting the omics analyses. These methods and results form the core of my thesis and the observed results provide novel insights to the studied research topics. The help I have received from Dr. Maciej Lalowski, Dr. Thomas O´Connell and Dr. Tia-Marje Korhonen for the bioinformatics has been indispensable and I

wish to thank you all for you time and effort. It has been a pleasure to work with you all. I would sincerely like to express my gratitude to Dr. Anita Kopperi who taught me all the basics about cell culturing. Without you everything would have been a lot harder! You were a patient teacher who pushed me to try, and fail, and then try again. This might not be the easiest or the fastest way to do a PhD, but I certainly got the most out of it! I wish to thank Dr. Sira Karvinen for your incredibly positive attitude and teaching methods, without you I might have hit rock bottom with you-know-what! You have taught me many high-end and already forgotten lab methods and given me great advice regarding the future in academia. I really look up to you as a scientist, which is why I am very grateful for your guidance. Regarding the early set-up of the electrical pulse stimulation project, I would like to thank Dr. Hannah Crossland for the help and ideas. Your guidance was extremely important.

I have had an opportunity to work with three bright and hardworking bachelor's and/or master's students, Mr. Sakari Mäntyselkä, Mr. Miika Moilanen and Ms. Juuli Peräkylä. I am sure that we all learned a lot during these processes, and I am very grateful for your valuable help. It is nice to see that most of your work was or will be published at some point in scientific journals. I am very glad that you Sakari continued as a PhD student in Juha's group, I am eager to follow your path towards a scientific career. Without your assistance and countless hours of literature digging, especially with the metabolomics, my thesis might look a lot different.

There are not enough words to express my gratitude to Dr. Tuuli Nissinen, you have been like a big sister to me during my MSc and PhD. Thank you for your encouraging guidance and trust, they have helped me to become the scientist I am today. I really appreciate the time and effort you have put into helping me with various issues, big and small. I have really enjoyed working with you, and hopefully we could do that again at some point, but I value our free time activities even more. The lunch breaks and get-togethers with the smaller or extended Maca group have been very important to me. Our dog walks have been a welcomed break to busy everyday life and our discussions about the latest plot twists in the life of Manu, Äijä and others has made my day! Overall, I am glad to call you not only a colleague, but also a dear friend.

Next, I would like to sincerely thank Dr. Jaakko Hentilä, if Tuuli is my lab-sister, you are my lab-brother. You have always helped me if I have had any (IT) issues, and as an easy-going and practical person you have balanced me and Tuuli. Of course, this works vice versa! There are quite a few things (reagents, equipment and your jacket…) that we have helped you to find from the lab, Lozzi, Ilokivi or somewhere else. We have had some crazy WB days, but we have always managed with those! One great memory was our conference trip to London, it was so nice to spend time together, again, not only as colleagues but also as friends!

I also wish to thank Dr. Enni Hietavala, you have given me perspective to academia and life in general. Tuuli and you have developed an eye for "abstract art" and you willingly share the best bits with the Maca group, which is also a

platform for alternative thoughts and discussion about them. A warm, collective thank you for your friendship all Maca members, Tuuli, Enni, Jaakko and Anita! A multidisciplinary aspect to my PhD journey was provided by the Afterit group, consisting Dr. Donna Niemistö, Dr. Kirsi Keskinen, Ms. Mari Kääpä and Mrs. Heidi Leppä. Thank you all for the peer support!

I have received a bucketful of help from our skilled laboratory staff. I wish to thank Mervi Matero, Hanne Tähti, Bettina Hutz, Leena Tulla, Aila Ollikainen, Risto Puurtinen, Susanna Luoma, Tanja Toivanen, Jukka Hintikka, Ulla-Maria Sahinaho, Jouni Tukiainen and our laboratory manager Dr. Maarit Lehti. It has been a pleasure to work with you all, there has never been a problem so big or question so small that some of you could not be able solve it! Especially you Mervi have always cheered my days with good (bad) humor and variably deep conversations, I appreciate that. And remember, no matter where we are, our hearts will always beat for a very special city! Thank you Dr. Laura-Ylä-Outinen for sharing your knowledge about cell culturing, I am sure that many of us will learn a lot from you! I also wish to thank Katja Pylkkänen and Minna Herpola for your help with various practical issues from which I could not have coped without you. Finally, thanks to all the fellow PhD students and staff working in the Biology of Physical Activity, the community and the atmosphere have been very supportive and encouraging.

Viimeisimpänä haluan kiittää perhettäni, kiitos kaikesta siitä tuesta ja kannustuksesta, jota olen teiltä saanut. Se on ollut todella tärkeää, sillä aina välillä omat valinnat ja päätökset epäilyttävät ja näinä aikoina tuki on ollut arvokasta. Kiitän Janne sinua siitä, että olemme antaneet toisillemme mahdollisuuden tehdä sitä, mitkä kumpikin oikeasti haluaa ilman, että se olisi toiselta pois. Keskustelut ja ratkaisut eivät ole aina olleet lähimainkaan helppoja, mutta ilman niitä me emme olisi tässä.

Jyväskylä 1.3.2022
Juulia Lautaoja

LIST OF ORIGINAL PUBLICATIONS

This dissertation is based on the following original research articles that are referred by their Roman numerals in the text:

I **Lautaoja, J.H.**, Lalowski, M., Nissinen, T.A., Hentilä, J., Shi, Y., Ritvos, O., Cheng, S. & Hulmi, J.J. (2019). Muscle and serum metabolomes are dysregulated in colon-26 tumor-bearing mice despite amelioration of cachexia with activin receptor type 2B ligand blockade. American Journal of Physiology - Endocrinology and Metabolism, 316(5), E852-E865.

II **Lautaoja, J.H.**, Pekkala, S., Pasternack, A., Laitinen, M., Ritvos, O. & Hulmi, J.J. (2020). Differentiation of the murine C2C12 myoblasts strongly reduces the effects of myostatin on intracellular signaling. Biomolecules, 10(5), 695.

III **Lautaoja, J.H.**, O´Connell, T.M., Mäntyselkä, S., Peräkylä, J., Kainulainen, H., Pekkala, S., Permi, P. & Hulmi, J.J. (2021). Higher glucose availability augments the metabolic responses of the C2C12 myotubes to exercise-like electrical pulse stimulation. American Journal of Physiology - Endocrinology and Metabolism, 321(2), E229-E245.

IV **Lautaoja, J.H.**, Karvinen, S., Korhonen, T-M., O´Connell T.M., Tiirola, M., Hulmi, J.J. & Pekkala, S. Contraction-induced changes in the C2C12 myotube transcriptome, but not myomiRNA release, are augmented by higher glucose availability. Manuscript in preparation.

The first publication was designed by Juha Hulmi, Tuuli Nissinen and Jaakko Hentilä, while I participated in designing the experimental approaches for publications II–IV together with Juha Hulmi and Satu Pekkala. The sample collection for study I was conducted by Tuuli Nissinen and Jaakko Hentilä. For studies II to IV, I performed the experiments and sample collection together with Sakari Mäntyselkä (III), Juuli Peräkylä (III), Sira Karvinen (IV) and Satu Pekkala (IV). The ^{1}H-NMR spectroscopy (III) was conducted at the University of Jyväskylä by Perttu Permi and Sakari Mäntyselkä with the bioinformatics analysis conducted by Thomas O´Connell, Sakari Mäntyselkä and I. For study IV, I conducted the RNA-sequencing libraries that were sequenced in collaboration with Marja Tiirola's group (University of Jyväskylä). Throughout experiments I to IV, I have conducted most of the biochemical analyses (Western blots, qPCRs, ELISAs and lipid extractions) as well as most (I, III–IV) or all (II) the data handling and statistical analyses (I–IV) for the publications as well as prepared most of the figures (I–IV). I had the main responsibility of the writing process in all the manuscripts.

ABBREVIATIONS

ALK	Activin-like receptor
AMPK	AMP-activated protein kinase
ATP/AMP	Adenosine triphosphate/monophosphate
BCAA	Branched chain amino acid
BCFA	Branched chain fatty acid
BMP	Bone morphogenetic protein
C26	Colon-26 carcinoma
DEG	Differentially expressed gene
DM	Differentiation medium
DMEM	Dulbecco's modified eagle's medium
DNA	Deoxyribonucleic acid
EL-EPS	Exercise-like electric pulse stimulation
ERK1/2	Extracellular signal-regulated kinase 1/2
EV	Extracellular vesicle
FBS	Fetal bovine serum
GDF	Growth differentiation factor
GM	Growth medium
IL	Interleukin
MAPK	Mitogen-activated protein kinase
miRNA, miR	Micro-RNA
mRNA	Messenger RNA
MS	Mass spectrometry
mTOR(C1)	Mechanistic target of rapamycin (complex 1)
NF-κB	Nuclear factor κB
^{1}H-NMR	Proton nuclear magnetic resonance
PBS	Phosphate buffered saline
P/S	Penicillin-streptomycin
RNA	Ribonucleic acid
(s)ACVR(2B-Fc)	(Soluble) Activin receptor (type 2B with Fc domain)
SAPK/JNK1/2	Stress-activated protein kinase/c-Jun N-terminal kinase 1/2
Smad	Mothers against decapentaplegic homolog
TCA cycle	Tricarboxylic acid cycle
TGF-β	Transforming growth factor-β
VO_2 max	Maximal oxygen uptake

CONTENTS

1 INTRODUCTION

Metabolism, derived from the Greek word *metabole*, meaning "change", is a broad concept that includes all the chemical reactions in an organism that sustain life. Metabolism can be divided into catabolic and anabolic processes that either breakdown or synthesize compounds, respectively. The field that studies individual small molecules and metabolites is termed metabolomics and the term metabolome was first introduced more than two decades ago (Oliver et al. 1998). Among other factors, changes in the gene expression regulates skeletal muscle metabolism and the method to examine the sum of the RNA transcripts is named transcriptomics, a method developed in the early 1990s (Lowe et al. 2017).

Many distinct conditions are known to disturb the metabolism of the skeletal muscle, which is an essential tissue from many perspectives. Skeletal muscles comprise almost 40% of the body mass and besides locomotion they participate in glucose disposal, act as amino acid reservoirs, maintain energy homeostasis and metabolic capacity as well as prevent many pathological and chronic conditions through exercise and exercise-induced signaling (Ato et al. 2017; Lee & Jun 2019; Pedersen & Saltin 2015; Schnyder & Handschin 2015; Wolfe 2006). Skeletal muscle plasticity enables the tissue to rapidly modify its metabolism in response to changes in the environmental conditions and energy demand. This is critical because up to 75% of the whole-body metabolism in the human body occurs in the skeletal muscle (Trovato et al. 2019). Adaptations of the skeletal muscle to new conditions induced, for example, by dietary modifications, exercise or diseases can promote changes in the energy metabolism and in the regulation of muscle mass by altering the levels of transcription, translation and metabolites (Egan & Zierath 2013; Hoffman 2017).

Numerous factors regulate skeletal muscle size, that is the balance between protein synthesis and breakdown. These factors include mechanical stimuli, nutrition, hormones, age, the level of physical activity and various diseases (Evans et al. 2008; Wackerhage et al. 2019). In general, inadequate macromolecule and/or energy intake, lack of exercise and multiple pathological conditions can enhance protein breakdown, leading to extensive muscle loss (atrophy) and thereby reduced quality of life and life expectancy (Evans et al. 2008).

Controversially, the combination of adequate nutrition, (resistance) exercise, and recovery are the preconditions for positive protein balance resulting in enhanced protein synthesis and muscle growth (hypertrophy) (Atherton & Smith 2012). Resistance training is an effective and healthy countermeasure of muscle wasting (Argilés et al. 2019), but in many situations it is not feasible, at least not alone. Therefore, other means to reduce muscle wasting in diseases such as cancer cachexia have been investigated, of which blocking myostatin and activins has been one potential candidate (Hulmi et al. 2021). The effects of myostatin and activins, two well-known regulators of muscle growth and size, on whole-body metabolism have been investigated with basic physiological methods, but before conducting the present dissertation, there were no comprehensive studies on the effects of these future candidate drugs on skeletal muscle and serum metabolomes. Moreover, the underlying molecular mechanisms of the cancer-induced effects on skeletal muscle metabolism are not fully understood and development of a simple *in vitro* skeletal muscle atrophy model would enable researchers to address these questions.

It is well known that exercise is an effective and inexpensive way to maintain and increase skeletal muscle mass as well as to prevent and reduce obesity and many other diseases (Pedersen & Saltin 2015). A growing body of literature demonstrates that during exercise skeletal muscles can express, produce, and secrete/release signaling factors, exerkines, to the circulation (Safdar et al. 2016). These exerkines are able to modify the metabolism of the nearby and/or distant recipient cells and tissues (Pedersen et al. 2007; Safdar et al. 2016). Importantly, recent recognition of skeletal muscle as a secretory organ has opened a new, unexplored research area in exercise physiology. Although the knowledge of new exerkines is rapidly expanding, small metabolites, for example, have remained understudied, especially in *in vitro* models. More research is therefore needed to better elucidate the mechanisms and mediators that promote exercise-induced health benefits.

This dissertation aimed to study the effects of (1) cancer cachexia–induced skeletal muscle wasting and (2) maintenance of skeletal muscle mass by blocking myostatin and activins on skeletal muscle and serum metabolomes. A further aim was to (3) develop an *in vitro* skeletal muscle atrophy model to study the molecular mechanisms of muscle wasting. Beyond wasting models, this dissertation aimed to study the effects of (4) exercise-mimicking myotube contractions on intra- and extracellular adaptations using different omics-approaches.

2 LITERATURE REVIEW

2.1 Principles of skeletal muscle mass regulation

Skeletal muscle mass is a result of the changes occurring in protein balance, which is regulated by the rate of muscle protein synthesis and breakdown (Figure 1). When the protein balance is positive, meaning when protein synthesis exceeds protein breakdown, skeletal muscle mass increases in a process called hypertrophy. There are certain requirements for the enhanced protein synthesis and thus for hypertrophy, including appropriate diet (i.e., adequate energy and macronutrient intake) and physical activity level (exercise) (Atherton & Smith 2012). If these requirements are not met and the protein balance is below the level needed for the maintenance of the muscle mass, protein breakdown is enhanced resulting in decreased skeletal muscle mass (muscle atrophy). Various diseases, such as cancer, can promote muscle atrophy, which has been related to poor prognosis and quality of life (Hulmi et al. 2021). Muscle atrophy can result from reduced protein synthesis and/or increased protein degradation (Fearon et al. 2012). Both hypertrophy and physical activity as well as atrophy and inactivity have been extensively studied over the years by various omics-methods (Gallagher et al. 2016; Hoffman 2017). However, more studies are needed to better understand the mechanisms behind these opposing conditions.

2.1.1 Muscle protein synthesis

The mechanistic target of rapamycin (mTOR) complex 1 (mTORC1) is a master regulator of multiple important processes, including muscle protein synthesis (Laplante & Sabatini 2009). Various factors, such as energy availability, amino acids, growth factors and stress finetune cell growth by regulating mTORC1 signaling (Figure 1). Although mTORC1 is one of the major regulators of muscle size, mTORC1-independent hypertrophy mechanisms may also exist

(Ogasawara et al. 2019). Additionally, even though hypertrophy is commonly observed as increased myofibril cross-sectional area, myofibril number may also in some cases contribute to muscle hypertrophy (Jorgenson et al. 2020).

In response to growth factors, inactivation of the inhibitory upstream regulators promotes mTORC1 signaling and anabolic processes in the skeletal muscle (Laplante & Sabatini 2012). Besides inhibitory molecules, mTORC1 activity is regulated by amino acids and cellular localization. The mTOR–associated protein known as Raptor facilitates amino acids to the proximity of mTORC1 (Laplante & Sabatini 2012). When amino acids are present, mTORC1 translocates to the lysosomal surface to be fully activated via Rag GTPases and Ragulator-Rag complex (Laplante & Sabatini 2012). Indeed, the translocation has been thought to be needed for the amino acid–dependent mTORC1 activation and thus protein synthesis promotion is reliant on the availability of the suitable building blocks, that is, amino acids (Sancak et al. 2010).

Downstream mediators of mTORC1, such as p70S6 kinase, eukaryotic initiation factor 4E-binding protein 1 and ribosomal protein S6 (Figure 1) (Browne & Proud 2002; Gingras et al. 1999; Ma & Blenis 2009; Wullschleger et al. 2006) promote protein synthesis. Activation of these mediators is required for initiation of cap-dependent translation, enhanced messenger RNA (mRNA) biogenesis and translation elongation (Laplante & Sabatini 2012). The growth– promoting effects of mTORC1 can be regulated by inhibiting autophagy, a process in which proteins are catabolized (Laplante & Sabatini 2009). However, chronically enhanced mTORC1 signaling leads to impaired autophagy, which may lead to atrophy (Castets et al. 2013). Indeed, the balance between anabolic and catabolic processes is finely tuned in the skeletal muscle for optimal adaptation.

2.1.2 Muscle protein degradation

During atrophy and protein breakdown, the number of intracellular organelles and proteins decreases, thus causing a decrease in the skeletal muscle mass (Figure 1). Protein degradation can occur in different cellular compartments, such as in the lysosomes or in the proteasomes (Nandi et al. 2006). The two main catabolic machineries, ubiquitin-proteasome and autophagy-lysosome systems, are responsible for the disposal of misfolded and non-functional proteins and peptides (Nandi et al. 2006; Rabinowitz & White 2010). Ubiquitination is used to specifically label those proteins that are directed for degradation in proteasomes and this requires activation of atrophy-related genes, such as muscle-specific ubiquitin E3 ligases (Nandi et al. 2006; Rabinowitz & White 2010).

Restricted availability of energy and amino acids enhances protein breakdown. Indeed, decreased appetite during many diseases or starvation results in a lack of suitable substrates required for mTORC1 activation and translation initiation (Kim et al. 2013). Furthermore, energy deficiency promotes AMP-activated protein kinase (AMPK)-mediated signaling to conserve ATP by inhibiting anabolic processes and by favoring catabolic reactions leading to, if prolonged, muscle atrophy (Kahn et al. 2005). Besides nutritional contribution, other factors induce atrophy. It has been shown that one pathway that promotes skeletal

muscle atrophy includes mothers against decapentaplegic homolog (Smad)2 and Smad3 that act via activin receptor type 2A and type 2B (ACVR2A/B) (Lee et al. 2005). The ACVR2A/B is activated by the members of the transforming growth factor-β (TGF-β) family, such as myostatin, activins, and growth differentiation factors (GDF) (Lee et al. 2005). The TGF-β members are vital for the normal cellular metabolism but under pathological conditions, for example during cancer cachexia, they can induce muscle atrophy (Rodriguez et al. 2014; Zhou et al. 2010). Once activated by the ligand binding, ACVR2A/B promotes processes that lead to the phosphorylation of the transcription factors Smad2 and Smad3 (Bloise et al. 2018; Burks & Cohn 2011; Derynck & Zhang 2003) and finally to upregulated expression of target genes, including ubiquitin E3 ligases (Bodine & Baehr 2014). The detailed mechanisms of the ACVR2A/B activation and signaling are described in the sections 2.2.3 and 2.2.4. Next, features of cancer cachexia, a common atrophy-causing disease, are discussed.

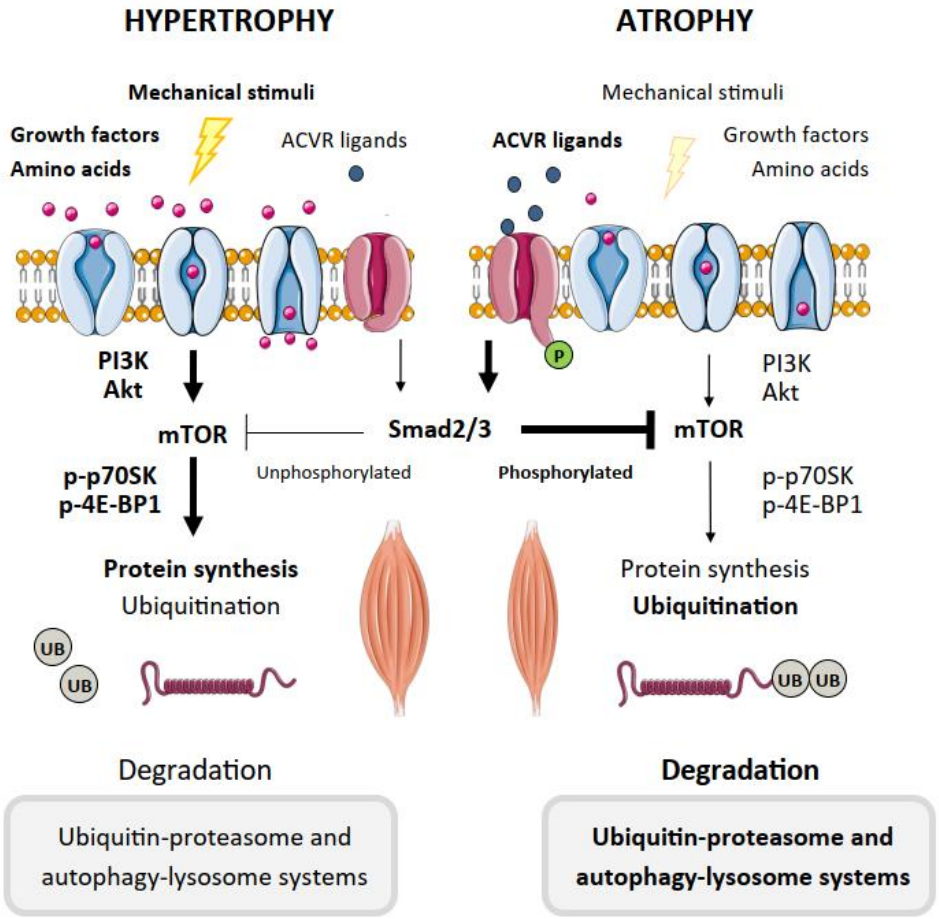

FIGURE 1 Simplified presentation of the major pathways and processes regulating skeletal muscle mass. ACVR, activin receptor type 2A/B; PI3K, phosphoinositide 3-kinase; Akt, protein kinase B; mTOR, mechanistic target of rapamycin; p70SK, p70S6 kinase; 4E-BP1, eukaryotic translation initiation factor 4E-binding protein 1; Smad, small mothers against decapentaplegic; p, phosphorylated; UB, ubiquitin. Images were obtained from https://smart.servier.com.

2.2 Skeletal muscle metabolism in catabolic conditions

2.2.1 Cancer cachexia

Cancer cachexia is a life-threatening disease that negatively affects the metabolism of multiple organs, such as skeletal muscle, heart, liver, and adipose tissue (Argilés et al. 2014). Cachexia is characterized with ≥ 5% weight loss within the last six months thus causing skeletal muscle atrophy that can be accompanied with or without reduced adipose tissue mass (Fearon et al. 2011). Although cachexia has been related to poor prognosis of cancer and to cancer-related deaths already since the 1930s (Warren 1932), it can also occur during other diseases, such as chronic heart failure and chronic kidney disease (Evans et al. 2008). In addition to body weight changes, other symptoms including systemic inflammation, reduced food intake, and anorexia are common during cachexia (Evans et al. 2008) and these symptoms may contribute to the reduced tolerance to anticancer treatments (Penna et al. 2019). Importantly, although medication can improve appetite and some individuals, especially those in the early stage of cachexia, can benefit from dietary counseling, cachexia cannot be reversed by nutritional strategies alone (Argilés et al. 2019).

It has been shown that maintenance of both skeletal muscle mass and function are important during cancer cachexia (Hardee et al. 2019; Nissinen et al. 2018; Zhou et al. 2010). This is important because it is reported that protein synthesis decreases and/or protein breakdown increases during the development of cachexia partly via tumor-derived pro-inflammatory cytokines (i.e., tumorkines) (Argilés et al. 2014; Tsoli & Robertson 2013). Myostatin and activins are common tumorkines that act via canonical (Smad-dependent) and non-canonical (Smad-independent) pathways (Derynck & Zhang 2003) to regulate the balance between catabolic and anabolic processes. Besides affecting protein homeostasis, cancer cachexia has other prominent effects on the molecular mechanisms. Based on the preclinical cancer models, cachexia disrupts mitochondrial biogenesis and function, thus leading to reduced oxidative metabolism together with muscle atrophy (Hardee et al. 2019). The causal role of adequate skeletal muscle mass and mitochondrial adaptations on improved cancer survival remains to be established, especially in humans (Hulmi et al. 2021). In the following section, cancer-induced changes on the skeletal muscle and serum metabolomes are reviewed.

2.2.2 Cancer-induced changes in skeletal muscle and serum metabolites

Skeletal muscle. By releasing energy and other required resources, skeletal muscle and adipose tissue wasting promote tumor growth. Omics studies have shown that cancer cachexia impairs skeletal muscle metabolism by targeting, for example, proteins, lipids, and carbohydrates (Der-Torossian et al. 2012; Gallagher et al. 2016). Skeletal muscle atrophy releases amino acids that can be used by the tumor during cachexia (Vettore et al. 2019). Alternatively, amino acids can be used by the liver for the synthesis of acute phase response proteins (Reeds et al.

1993), which aim to minimize the trauma-induced damage in the body (Stephens et al. 2008). Unlike contractile proteins, acute phase response proteins are rich in aromatic amino acids and their synthesis may accelerate skeletal muscle atrophy (Reeds et al. 1993). Besides protein breakdown, processes related to energy metabolism including glycolysis, tricarboxylic acid (TCA) cycle (Der-Torossian et al. 2013b), glycogenesis, and glycogenolysis (Tseng et al. 2015) have been shown to be affected in colon 26 carcinoma (C26) tumor-bearing mice. Simultaneously, oxidative stress, redox homeostasis, and the pentose phosphate pathway were also affected by the C26 cancer (Der-Torossian et al. 2013b; Tseng et al. 2015). Similarly, in other experimental cancer models glucose and amino acid metabolism were impaired in the BGC823 tumor-bearing mice (Cui et al. 2019a), while in glioma-bearing mice processes related to glucose, lipid, protein, and TCA cycle metabolism were affected, which was inferred from the decreased content of skeletal muscle glucose, glycerol and 3-hydroxybutyrate as well as increased amino acid content (Cui et al. 2019b). Overall, these results demonstrate that cancer cachexia significantly impairs skeletal muscle metabolism. However, although the severity of cachexia regulates the magnitude of the metabolic responses (Cui et al. 2019a), little is known about the metabolite level responses to the pharmacological maintenance of the skeletal muscle during cachexia.

Serum. A less invasive method to study cancer-induced changes on the whole-body metabolomics is to use serum or plasma samples, an approach which has identified biomarkers related to cancer and cancer progression (Giskeødegård et al. 2019). Cachectic and non-cachectic patients have large inter-individual variation in serum metabolites measured within a single day (Fujiwara et al. 2014), which may be related to progression stage of the disease or the duration of the experiment (Ballarò et al. 2016). Because serum metabolites have been used as markers of cachexia and/or muscle loss (Miller et al. 2019), the intra-day and/or inter-individual variation in the serum metabolome can make interpretation and comparison of the results between studies complicating.

Based on the serum metabolomics from the experimental cancer models, the C26 tumor-bearing have been reported to suffer from hyperlipidemia, hyperglycemia, and lower level of circulating branched chain amino acids (BCAAs) (Der-Torossian et al. 2013a). Similar to this murine model of cachexia, Yang and colleagues reported that the levels of triglycerides, free fatty acids and glucose were higher in the serum of cachectic in comparison to pre-cachectic cancer patients (Yang et al. 2018). In contrast, other studies have observed decreased circulating glucose level in cachectic mice (O'Connell et al. 2008; Pin et al. 2019).

The rate of weight loss has been shown to be a distinctive factor affecting serum metabolome in cachexia, and 40 metabolites, including fatty acids, lipids and L-phenylalanine, have been associated with the loss of ≥ 5% of body weight (Miller et al. 2019). In addition, altered serum amino acid profile (increased phenylalanine and glycine; decreased glutamine, alanine, and histidine) has been associated with systemic inflammation and progression of cachexia (Sirniö et al. 2019). However, some of the results have been inconsistent among studies, although glutathione, isoleucine and leucine were elevated in all disease stages

(Yusof et al. 2018). More studies are needed to determine reliable serum markers of skeletal muscle atrophy and cachexia.

2.2.3 Activin receptor ligands in cancer cachexia

Thus far, over 30 genes encoding the TGF-β family members have been identified. They are divided into two branches: (1) the TGF-β/activin branch and (2) the bone morphogenetic protein/GDF branch (Derynck & Budi 2019). Under normal conditions, these factors are important regulators of cell growth, differentiation, migration, and apoptosis, while during many diseases dysregulated signaling of a few TGF-β family members, such as myostatin and activins, can lead to muscle atrophy and increased risk of mortality (Schmierer & Hill 2007). Indeed, tumor-derived TGF-β family members promote mobilization of suitable substrates for tumor growth, thus enhancing, for example, skeletal muscle and adipose tissue wasting (Dschietzig 2014).

ACVR2A/B is a cell-surface serine/threonine kinase that binds, for instance, myostatin, activins and GDF11 (Sartori et al. 2021b) and thus these TGF-β family members are referred to as activin receptor (ACVR) ligands. Myostatin, which is also known as GDF8, was first identified from mice over two decades ago by Alexandra McPherron, Ann Lawler and Se-Jin Lee when they reported that myostatin acts as a negative regulator of muscle size (McPherron et al. 1997). The authors demonstrated that myostatin null mice exhibited increased musculature and lower fat mass in comparison to wild-type mice (McPherron et al. 1997). Muscular phenotype has been observed in both the young and the older myostatin null mice, although the body mass of the older mice was more similar with the wild-type mice due to the deficiency in the development of normal fat stores (Peake et al. 2015). Interestingly, despite increased musculature, myostatin null mice exhibit impaired muscle function and decreased exercise capacity (Amthor et al. 2007; Mouisel et al. 2014). Endurance exercise has been shown to improve muscle function and oxidative properties of the myostatin null mice as well as to drive wild-type like phenotype by reducing muscle fiber size and muscle mass (Matsakas et al. 2010, 2012).

In contrast to the myostatin null genotype, overexpression of myostatin has been shown to promote cachexia-like symptoms including muscle wasting and decrease in body mass (Dschietzig 2014; Peake et al. 2015). Because, for instance, some tumors express myostatin (Han et al. 2018) that acts via Smad signaling (Han et al. 2013), myostatin has become an attractive target for the development of anti-atrophy therapies. However, although different approaches have been developed to block myostatin (Dschietzig 2014; Lee & Glass 2011) and some anti-myostatin therapies are under clinical trials (Argilés et al. 2019), the relevance of myostatin on muscle wasting in cancer is still not completely understood (Penna et al. 2019).

Besides myostatin, another widely studied group of the TGF-β members are activins. Activins exist in five dimeric forms with different combinations of the β subunits, of which the most studied one is activin A (βAβA) (Bloise et al. 2018). Activin A was first identified by Vale and colleagues (Vale et al. 1986) and then

named by Ling and colleagues (Ling et al. 1986) at the end of the 1980s. Activins act as antagonists of inhibins, of which the latter prevents the secretion of follicle stimulating hormone from the pituitary (Bloise et al. 2018). Besides inhibition of myogenesis and negative regulation of muscle growth, muscular properties, such as force production and mitochondrial capacity, are also modified by activin A (Bloise et al. 2018). Furthermore, activin A reduces protein synthesis and promotes protein breakdown in the skeletal muscle (Bloise et al. 2018) and the circulating activin A levels have been shown to predict survival in cancer patients (Loumaye et al. 2017).

Another TGF-β family member, GDF11, was characterized by Nakashima and colleagues in 1999 (Nakashima et al. 1999), while other groups studied it at the same time (Gamer et al. 1999; McPherron et al. 1999). To date, GDF11 has been reported to regulate, for example, muscle, bone, and nervous system development (Zhang et al. 2017). GDF11 has almost identical actions in striated muscle as myostatin (Rodgers & Ward 2021).

Because myostatin, activin A and GDF11 all belong to the same TGF-β family, they share many similar signaling properties accompanied also with unique features. Normally, bioavailability of myostatin and activins is strictly regulated at the level of translation, secretion, and receptor binding both intra- and extracellularly (Weiss & Attisano 2013). Some of the ACVR ligands, such as myostatin, are produced as a large pre-propeptide complex containing a signal peptide, a long N-terminal pro-peptide and a C-terminal mature peptide (Derynck & Budi 2019) (Figure 2). To obtain a functional protein, two cleavages are required after translation (Otto & Patel 2010). Firstly, signal peptide, which was important for the processing and secretion of the protein, is removed (Peake et al. 2015). Secondly, the pro-peptide, which was vital for the proper protein folding, is proteolytically cleaved (Cotton et al. 2018; Gray & Mason 1990; Harrison et al. 2011; Walker et al. 2018). After these cleavages, two mature peptides form a dimer and the latent, inactive protein is ready to be secreted. In the circulation, the bioavailability of the mature protein can be regulated by the non-covalent binding of the protein to the extracellular matrix components (Peake et al. 2015) or the circulating protein is in a latent, inactive form (Wolfman et al. 2003). Bone morphogenetic protein-1/Tolloid metalloproteinases cleave myostatin from the latent complex and release active myostatin to the circulation to enable receptor binding (Wolfman et al. 2003).

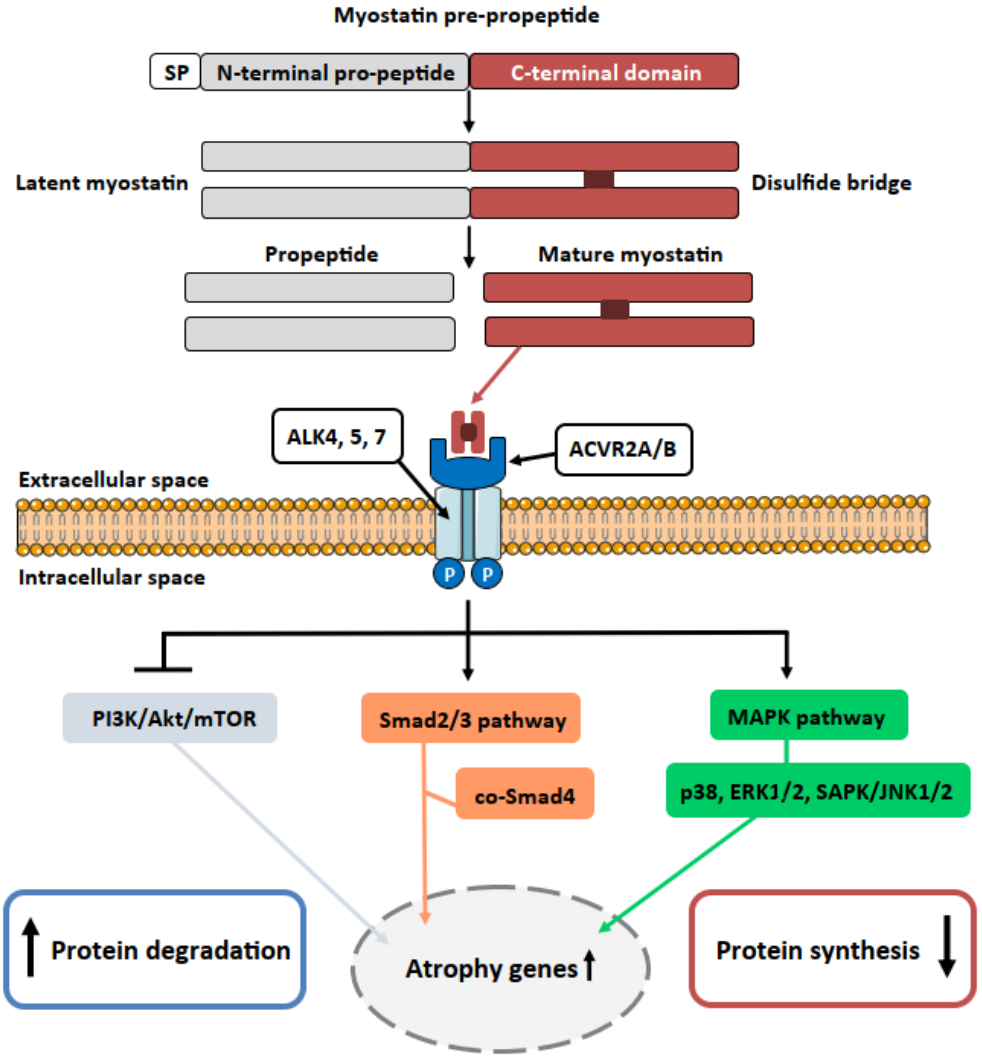

FIGURE 2 Processing of the latent myostatin pre-propeptide to mature bioactive myostatin and straightforward presentation of the myostatin-induced signaling in the cells. ACVR2B/A, activin receptor type 2A/B; Akt, Akt kinase/protein kinase B; ALK, activin-like receptor; ERK1/2, extracellular signal-regulated protein kinases 1/2; MAPK; mitogen-activated protein kinase; mTOR, mammalian target of rapamycin; PI3K, phosphoinositide 3-kinase; SAPK/JNK1/2, stress-activated protein kinase/c-Jun N-terminal kinase 1/2; Smad, mothers against decapentaplegic homolog; SP, signal peptide. Modified from (Huang et al. 2011; Verzola et al. 2019). Images were obtained from https://smart.servier.com.

2.2.4 Activin receptor ligand-mediated signaling in cancer cachexia

Canonical Smad-dependent signaling. Among other receptors, the TGF-β family members mediate their effects through activin type 2 and type 1 receptors (Derynck & Budi 2019). Overall, there are five type 2 and seven type 1 receptors that reside as monomers, heterodimers, or homodimers on the recipient cell membranes (Derynck & Budi 2019). Myostatin, activins and GDF11 mediate their effects by binding to the ACVR2A/B coupled with type 1 receptors activin-like

receptor (ALK)-4, ALK-5 or ALK-7 to form a hetero-tetrameric complex (Derynck & Budi 2019). Once the ligand is bound, conformational changes promote the type 2 receptors to phosphorylate serine and threonine resides at the regulatory domain of the type 1 receptors (Derynck & Budi 2019; Massagué et al. 2005). This initiates the canonical Smad-dependent signaling pathway mediated via Smad2 and Smad3 (Derynck & Budi 2019) (Figure 2).

Once the phosphorylated Smad2 and Smad3 are released into the cytoplasm, they translocate together with the co-Smad4 into the nucleus to modulate expression of several hundred different genes (Zi et al. 2012). Among these genes are myogenic differentiation 1, myogenic factor 5 and myogenin, which are all important mediators of skeletal muscle development and myogenesis (Elkina et al. 2011). The expression of these genes is downregulated by the ACVR ligands, thus resulting in impaired muscle function (Ge et al. 2011; Langley et al. 2002). Other negative effects on skeletal muscle mass mediated via Smads include enhanced expression of the muscle ubiquitin E3 ligases (Bodine & Baehr 2014), which promote protein ubiquitination and degradation (Bodine & Baehr 2014; Rabinowitz & White 2010). That being said, not all E3 ligases, such as atrogin-1 are ideal markers of protein breakdown because in some cases they can mainly target regulators of protein synthesis (Attaix & Baracos 2010). The Smad2 and Smad3 can also decrease mTOR activity, but the underlying mechanisms are unclear (Sartori et al. 2021b).

Interestingly, another level of complexity to the described Smad signaling was recently added when findings showed that many bone morphogenic proteins can interact with Smad1/5/7, which may interfere myostatin and activin signaling pathways (Sartori et al. 2021b). Thus, unlike myostatin, activins, and GDF11, these TGF-β member proteins induce, not inhibit skeletal muscle hypertrophy (Sartori et al. 2013, 2021a; Winbanks et al. 2013). However, these are not discussed further since they are not in the scope of this dissertation. Furthermore, other TGF-β family members, such as some of the bone morphogenic proteins in addition to myostatin and GDF11 mentioned above, can also bind at least weakly to ACVR2A/B (Townson et al. 2012) thus showing relatively high unspecificity of this signaling pathway.

Non-canonical Smad-independent signaling. Some of the TGF-β family members including myostatin and activins can also mediate their actions via non-canonical Smad-independent pathways (Rodgers & Ward 2021). Examples of these pathways are mitogen-activated protein kinase (MAPK) and phosphatidylinositol-3-kinase/Akt/mTOR pathways (Derynck & Budi 2019) (Figure 2). Among other effects (Rodgers & Ward 2021), myostatin has been shown to target Akt/mTOR signaling (Trendelenburg et al. 2009), while activin A acted via the MAPK pathway (Ding et al. 2017). The MAPKs (p38 MAPK (p38), stress-activated protein kinase/c-Jun N-terminal kinase 1/2 (SAPK/JNK1/2), and extracellular signal-regulated kinase 1/2 (ERK1/2)) are commonly increased during inflammation or diseases and their chronic activation has been related to dysregulation of muscle growth and differentiation *in vitro* and *in vivo* (Huang et al. 2007; Penna et al. 2010; Philip et al. 2005; Yang et al. 2006; Zhang et al. 2011).

However, MAPK signaling does not exclusively induce negative effects as they also respond to different physiological signals, such as exercise (Hulmi et al. 2012; Lessard et al. 2018) and acute increases in these markers have been related to improved health (Kramer & Goodyear 2007). Indeed, MAPKs are important not only because they regulate muscle functions but also due to their effects on energy metabolism (e.g., fatty acid and carbohydrate uptake and oxidation) as well as mitogenic functions and oxidative capacity (Kramer & Goodyear 2007).

Overall, myostatin and activins as well as other members of the TGF-β family have multiple distinct signaling pathways that, for example, during cancer cachexia have detrimental effects on skeletal muscle metabolism. However, it remains poorly understood how ACVR ligand blocking during cancer cachexia affects skeletal muscle metabolism. More research is needed on this topic.

2.3 Skeletal muscle metabolism in exercise

2.3.1 Energy sources and ATP production mechanisms

Energy Sources. Most of the metabolic processes in the skeletal muscle are fueled by ATP derived mainly from carbohydrates and fats (Hargreaves & Spriet 2020). Transition from rest to exercise rapidly multiplies energetic needs because the metabolic rate can increase even by 100-fold (Hargreaves & Spriet 2020). To support the desired exercise intensity, the readily available energy sources (i.e., skeletal muscle ATP and phosphocreatine stores) are utilized. Additionally, intramuscular triglycerides and glycogen as well as plasma glucose and free fatty acids refuel the ATP stores in the skeletal muscle (Hargreaves & Spriet 2020). In 1993, Romijn and colleagues introduced the classical model in which the relationship between energy substrate preference, exercise intensity and duration were presented (Romijn et al. 1993). This model illustrates that during low and moderate intensity exercise (< 65% of maximal oxygen uptake, VO_2 max), plasma free fatty acids and intramuscular triglycerides are mainly oxidized, while during high intensity exercise (in humans about 80% of VO_2 max), carbohydrates (intramuscular glycogen and in less extent plasma glucose) are the main energy source over fats (Romijn et al. 1993; Spriet 2014; Watt & Cheng 2017). It is hypothesized that the greater ATP/O_2 ratio of the carbohydrates could explain the decreased fat usage during intensive exercise (Spriet 2014), which is reasonable because ATP yield from fats is almost 10% less efficient than from aerobic carbohydrate oxidation (Hargreaves & Spriet 2020). However, when the exercise duration increases (and intensity decreases), the usage of fats is enhanced partly due to promoted catecholamine signaling and depleted carbohydrate stores (if not fulfilled by carbohydrate ingestion during exercise) (Melzer 2011).

ATP production mechanisms. Exercise-induced increase in the energy demand can be fulfilled by anaerobic (O_2-independent) or aerobic (O_2-dependent) pathways and the selection is mainly based on the intensity and duration of the exercise. More specifically, short- and long-duration low-intensity exercise

utilizes aerobic, while short-duration (< a few minutes) high-intensity exercise favors anaerobic energy production pathways (Melzer 2011). ATP derived anaerobically from phosphocreatine breakdown and the conversion of glycogen to lactate fuels short exercise bouts, such as sprints and jumps (Hargreaves & Spriet 2020). Although anaerobic glycolysis is a rather inefficient ATP production pathway by providing only two ATPs per one glucose molecule or three ATPs per one glycogen molecule (i.e., below 10% of the 36 ATPs released by aerobic glucose oxidation) (Melzer 2011), it is almost 100 times faster than oxidative phosphorylation (Stojan & Christopher-Stine 2015). Although anaerobic pathways provide ATP rapidly for explosive exercise bouts, their reservoirs are short-lived. Indeed, aerobic ATP production from muscle glycogen stores through oxidative phosphorylation becomes dominant already after 1 minute of exercise (Hargreaves & Spriet 2020).

The whole-body energy metabolism and substrate (e.g., glucose, free fatty acids) availability are strictly regulated during exercise and previous studies have suggested that also skeletal muscle takes part in these events. Indeed, skeletal muscles secrete factors that communicate together with other tissues and in response, for example, adipose tissue can release free fatty acids to the circulation to maintain muscle contractions (Fiuza-Luces et al. 2013). The following section will review the role of skeletal muscle as a secretory organ that is able to promote tissue crosstalk. In addition, different types of exercise-responsive signaling mediators are reviewed.

2.3.2 Skeletal muscle as a secretory organ during exercise

Already 60 years ago, Goldstein suggested that skeletal muscle might release humoral factors to the circulation because muscle contractions were detected to affect other organs (Goldstein 1961). This was a hallmark statement, because traditionally it has been thought that only the conventional endocrine organs (e.g., pancreas, pituitary gland, and thyroid gland) are able to release hormones and signaling molecules that modify the metabolism of the recipient tissue or organ. To date, it is widely accepted that part of the health-beneficial effects of exercise are mediated via exercise and/or muscle contraction-induced secretory molecules (Fiuza-Luces et al. 2013; Whitham & Febbraio 2016). These signaling mediators regulate several processes, such as skeletal muscle growth and lipid metabolism in an auto-, para- and/or endocrine manner, which enables the body to adapt to exercise-induced requirements (Huh 2018). However, there are challenges to study the exercise-induced changes of the skeletal muscle *in vivo* both within the tissue and in the secreted fraction (secretome). For instance, other organs and tissues also secrete identical signaling molecules, such as interleukin (IL)-6, into the circulation during exercise and thus it is impossible to distinguish from where the molecules originate (Lombardi et al. 2016). Indeed, this limits the ability to specify the muscle-specific contribution to the circulating signaling mediator pool. For this reason, research on *in vitro* muscle contraction/exercise is also needed to enable exclusive examination of the skeletal muscle secretome.

After the recognition of skeletal muscle as a secretory organ capable of releasing signaling factors into the circulation at rest and during exercise, the muscle-derived mediators had to be identified and categorized. Pedersen and colleagues classified myokines as "*cytokines or other peptides produced, expressed and released by muscle fibers*" (Pedersen et al. 2007), while Weigert and colleagues termed muscle-derived exercise-responsive metabolites with signaling properties as myometabokines (Weigert et al. 2014). Finally, Safdar colleagues expanded these definitions by classifying myokines and other molecules (e.g., metabolites, nucleic acids and extracellular vesicles) released from any tissue in response to exercise as "*exerkines*" (Safdar et al. 2016) (Figure 3). However, it should be emphasized that currently none of the identified muscle-derived factors are solely expressed and secreted by the skeletal muscle (Catoire & Kersten 2015). Instead, many of them are produced by multiple other cell types, such as immune cells, adipocytes, and hepatocytes (Hoffmann & Weigert 2017). In other contexts, these factors could be called adipokines, adipomyokines (Raschke & Eckel 2013) or hepatokines (Weigert et al. 2019). Nomenclature can be confusing, and it is usually dependent on the context of the study. This dissertation focuses on a variety of skeletal muscle-derived factors secreted or released in an exercise-induced manner, so the term *exerkine* will be used in the following sections.

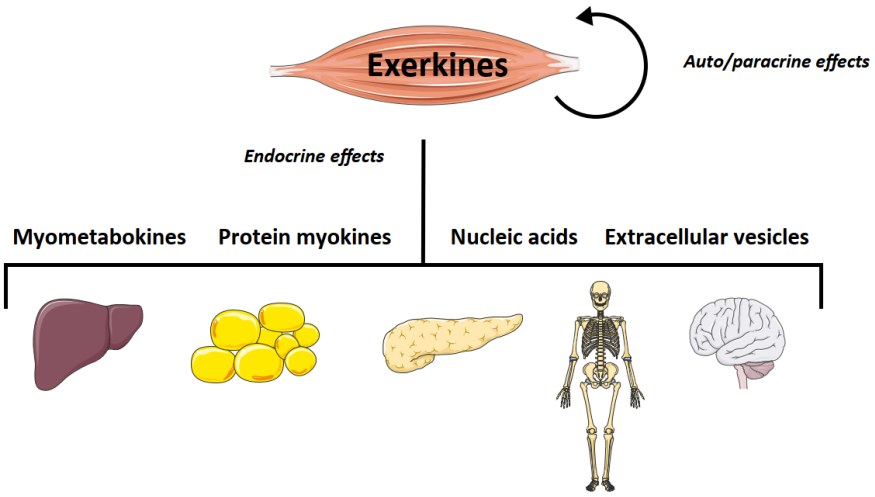

FIGURE 3 Skeletal muscle as a secretory organ. A variety of muscle-derived exerkines regulate metabolism of skeletal muscle in auto- and/or paracrine manner or other tissues such as liver, adipose tissue, pancreas, bone, and brain in an endocrine manner. Images were obtained from https://smart.servier.com.

The number of the detected and identified exerkines increases constantly (Murphy et al. 2020; Severinsen & Pedersen 2020). Due to this expansion, the function and biological activity of all currently known exerkines are not thoroughly understood and more research is needed. Additionally, because several signaling factors can be secreted from tissues other than skeletal muscle, it remains to be determined whether the origin of the mediator differently affects its target or function. However, due to the large proportion of the whole-body mass

(30–40%) and great vascularization, most likely the main contribution to the circulating exerkine pool during exercise is obtained from the skeletal muscle (Piccirillo 2019). Furthermore, exercise type (acute bout or training) and intensity, skeletal muscle fiber type as well as other factors can affect the release of exerkines (Catoire & Kersten 2015; Piccirillo 2019) and this area of research is currently underappreciated. The next three chapters aim to introduce and review different types of exerkines and elucidate the effects of a few of the best-known molecules of each group.

2.3.2.1 Myometabokines

Although omics, such as proteomics and transcriptomics, have recently become widely popular in the study of skeletal muscle metabolism (Hoffman 2017), metabolites are a less studied population of molecules despite their important role in metabolism. However, some individual muscle-produced metabolites and their functions in intercellular signaling have been determined.

One of the best-described exercise-induced changes in the energy-related metabolites during and after moderate- to high-intensity exercise is enhanced glycolysis, which is usually inferred from increased lactate content in the circulation. Previously, lactate has been considered to cause fatigue and hinder muscle contraction (Brooks 2020; Melzer 2011), but recent studies have shown that lactate is an important energy substrate, gluconeogenic precursor, and signaling molecule that has been overlooked in the past (Brooks 2020). Furthermore, lactate is produced also under fully aerobic conditions, although to a lesser extent, and thus it has been considered to be a link between aerobic and anaerobic pathways (Brooks 2020). Lactate is favored over glucose and free fatty acids in the working skeletal muscle and heart due to the cell–cell lactate shuttling and it has been reported to inhibit mitochondrial fatty acid uptake and β-oxidation in the skeletal muscle (Brooks 2020).

Of the individual lipid-derived metabolites regulating energy metabolism, glycerol, which is an end-product of lipolysis, is related to enhanced fatty acid utilization (Lewis et al. 2010). Additionally, 3-hydroxybutyrate, a common ketone body serves as an energy substrate and intermediate for the formation of acetyl-coenzyme A and succinyl-coenzyme A (Newman & Verdin 2014). Additionally, other fatty acid-derived metabolites, such as acetate and acetoacetate that serve as energy sources especially during fasting or prolonged exercise are shown to be increased after exercise in various biofluids (Schranner et al. 2020).

Increased catabolism of the branched chain amino acids (BCAA) during exercise has been hypothesized to enhance fatty acid oxidation via glyceroneogenesis and thus suggested to improve metabolic health (Kainulainen et al. 2013). The breakdown products of the BCAA catabolism can be directed into the TCA cycle or lipid metabolism (Kainulainen et al. 2013). A few examples of these products are ketogenic metabolites 2-oxoisovalerate and 3-methyl-2-oxovalerate (Schranner et al. 2020). Besides BCAA, glucogenic and ketogenic amino acids are important in the maintenance of energy homeostasis. They can, however, have systemic effects as well. For example, glutamine is a versatile molecule because

it can be converted to other amino acids, fatty acids or nucleotides and it can be used for ATP production via TCA cycle (Pedersen et al. 2020). The systemic role of alanine is related to the energy metabolism through glucose-alanine cycle (Schnyder & Handschin 2015). Related to energy metabolism, many of the TCA cycle intermediates, such as citrate, succinate, fumarate and malate have been reported to be altered in the blood after exercise (Lewis et al. 2010; Maurer et al. 2021; Sakaguchi et al. 2019). A recent study even suggests that almost all TCA cycle intermediates may increase in the cells and in the circulation after exercise (Maurer et al. 2021).

Most of the above mentioned metabolites have been determined by analyzing *in vivo* biofluids (e.g., blood, sweat, saliva or urine) that contain mainly unphosphorylated metabolites because the phosphorylated molecules, such as ATP or glucose-6-phosphate, cannot diffuse through the membrane due to their negative charge (Schranner et al. 2020; Westheimer 1987). As stated above, the problem with biofluid metabolomics in myometabokine research is the contribution of all other non-muscular organs to the metabolite pool studied. Additionally, biofluid analyses do not reflect intracellular changes. Indeed, Zhang and colleagues reported that comparison of the metabolite profiles of the skeletal muscle interstitial fluid and blood after *in vivo* exercise demonstrated that these two are not directly comparable (Zhang et al. 2018). More specifically, the authors demonstrated that the most altered biologically functional groups after exercise were metabolites related to amino acids, fats and carbohydrates but the individual metabolites within the aforementioned groups differed among interstitial fluid and blood (Zhang et al. 2018). This highlights the importance of the exclusive examination of skeletal muscle cell-derived factors using a suitable study approach, such as interstitial fluid or arteriovenous difference *in vivo* (Murphy et al. 2020; Zhang et al. 2018) or myotube contractions, passive stretching and/or pharmacological exercise mimetics, such as an AMPK activator 5-aminoimidazole-4-carboxamide-1-β-d-ribofuranoside or Ca^{2+} ionophore caffeine (Carter & Solomon 2019; Nikolić et al. 2017; Ren et al. 2021) *in vitro*.

2.3.2.2 Protein myokines

The local regulators of skeletal muscle size, such as myostatin and many interleukins, promote processes related to muscle regeneration, satellite cell activation, myogenesis, and growth (Fiuza-Luces et al. 2013; Severinsen & Pedersen 2020). The mediators regulating local energy metabolism indirectly, such as fatty acid uptake into the skeletal muscle, include angiopoietin-like 4 and myonectin (Catoire & Kersten 2015; Fiuza-Luces et al. 2013). Myokines having a dual effect on muscle size and metabolism regulation include apelin, brain-derived neurotropic factor, IL-6, musclin and secreted protein acidic and rich in cysteine (Catoire & Kersten 2015; Fiuza-Luces et al. 2013; Laurens et al. 2020a; Lee & Jun 2019; Severinsen & Pedersen 2020). High vascularization is critically important for efficient muscle metabolism, and exercise is known to improve aerobic capacity by enhancing angiogenesis and mitochondrial biogenesis. Protein myokines regulating these processes, such as fibroblast growth factor-21, follistatin-like 1,

IL-6, myonectin and vascular endothelial growth factor, have been identified to be secreted during and/or after exercise (Fiuza-Luces et al. 2013; Lee & Jun 2019).

Exercise-induced infiltration of immune cells, such as macrophages, to the skeletal muscle due to tissue damage has been associated with enhanced recovery (Catoire & Kersten 2015). The CC-chemokine ligand 2 (CCL2, also known as monocyte chemoattractant protein 1) and chemokine C-X3-C motif ligand 1 have been shown to promote muscle repair and macrophage infiltration into the skeletal muscle (Catoire & Kersten 2015), thus contributing to skeletal muscle-specific adaptations to exercise.

Systemic protein myokines affecting adipose tissue, such as myostatin, fibroblast growth factor-21, GDF15, IL-6, irisin, and myonectin, regulate fuel availability by affecting glucose and fatty acid uptake into the adipocytes, lipolysis, white adipose tissue browning, and brown adipose tissue thermogenesis (Catoire & Kersten 2015; Fiuza-Luces et al. 2013; Hoffmann & Weigert 2017; Laurens et al. 2020a, 2020b). Similarly, fibroblast growth factor-21, IL-6, and myonectin also affect liver metabolism by promoting fatty acid uptake and oxidation, ketogenesis, glucogenesis and glucose release (Catoire & Kersten 2015; Fiuza-Luces et al. 2013; Laurens et al. 2020a). Exercise-induced pancreatic β-cell regulation through IL-6 and irisin may increase insulin secretion, and some exerkines (e.g., brain-derived neurotropic factor, fibroblast growth factor-21 and irisin) have been suggested to also modulate cognition and neuroplasticity (Laurens et al. 2020a). Finally, bones are also targeted by protein myokines, including interleukins (Lombardi et al. 2016). More research is needed to better understand the contraction-induced changes in the regulation of protein myokine metabolism at transcriptional and translational levels.

2.3.2.3 Extracellular vesicles and microRNAs

Extracellular vesicles (EV), including exosomes, microvesicles, and apoptotic bodies, are a heterogeneous group of spherical lipid structures differing in size, composition and morphology (Yáñez-Mó et al. 2015). Exosomes are released into the extracellular space after exocytosis of multivesicular bodies (O´Brien et al. 2020; Rome et al. 2019), while microvesicles bud from the plasma membrane (Rome et al. 2019). Apoptotic cells release apoptotic bodies as blebs (Yáñez-Mó et al. 2015). EVs are found practically from all biofluids *in vivo* and in cell culture media *in vitro* (Safdar & Tarnopolsky 2018).

Sample extraction and purification protocols determine the examined EV pool (Simonsen 2017). The size ranges of each EV population have recently been debated without achieving a consensus. Some research groups, therefore, do not specify the vesicle population studied. Instead, a broader definition, such as exosome-like vesicles (ELV) or EVs are used. In this dissertation, the term *EV* will be used. Related to the overlapping in vesicle size, the tracing of EVs can be complicated. This is why surface proteins or microRNA (miRNA) content have been used to identify especially skeletal muscle-derived EVs (Vechetti et al. 2021).

Exercise has been reported to be a strong stimulus to enhance EV release from the skeletal muscle to promote intercellular communication (Rome et al.

2019; Trovato et al. 2019). For example, Whitham and colleagues demonstrated that EVs released during endurance exercise accumulate into the liver and they were rich in glycolytic enzymes and exerkines (Whitham et al. 2018). Indeed, a growing body of evidence suggests that EVs can mediate multisystemic adaptations induced by exercise via transportation of exerkines (Safdar & Tarnopolsky 2018). The EVs are able to transport different types of selectively packaged functional cargo including proteins, lipids, metabolites, nucleic acids and sugars to nearby and/or distant destinations (De Gasperi et al. 2017; Lovett et al. 2018; Rome et al. 2019; Safdar & Tarnopolsky 2018). This dissertation will focus on EV microRNAs (miRNA).

miRNAs are small, 19-22 nucleotides long signaling molecules that regulate gene expression mainly at the post-transcriptional level (Forterre et al. 2014). Exercise-induced effects of miRNAs include regulation of aerobic capacity by modifying mitochondrial biogenesis, myocardial remodeling, skeletal muscle angiogenesis, and substrate metabolism (Safdar & Tarnopolsky 2018). Due to feasible availability and rapid responses, miRNAs are attractive biomarkers of various conditions, including exercise (Hiam & Lamon 2020).

EVs containing skeletal muscle-enriched miRNAs (myomiRNAs), which are ≥ 20-fold more abundant in the skeletal muscle than in other tissues, are thought to mediate some of the systemic effects of exercise (Lovett et al. 2018). Indeed, many myomiRNAs, including miR-1, miR-133a, miR-133b and miR-206 as well as other miRNAs are responsive to exercise (Vechetti et al. 2021; Wang & Wang 2016). Despite increasing attention to miRNAs in recent years, it is not clear whether *in vitro* myotube contractions promote miRNA packing to the EVs. The next chapter introduces the reader to an exercise-mimicking *in vitro* model.

2.4 Electric pulse stimulation as an *in vitro* exercise mimetic

2.4.1 History

Because certain aspects of exercise research are challenging, time-consuming and expensive to conduct using *in vivo* subjects or animal models, alternative approaches were needed. *In vitro* models provide a flexible platform for rather inexpensive studies and they are also an ethically reasonable alternative for *in vivo* experiments. To be accepted as an *in vitro* exercise-mimicking model, myotubes need to produce the same key physiological responses as observed during and after *in vivo* exercise. First, the innervation of the muscle cells was replaced by electrical stimulation. Already in the 1970´s chicken muscle cells were electrically stimulated to study the regulation of acetyl choline receptors and innervation (Shainberg & Burstein 1976). The following studies focused on stimulation-induced changes in the myosin heavy chain isoforms (Düsterhöft & Pette 1990; Naumann & Pette 1994; Wehrle et al. 1994) and Ca^{2+} signaling (Brown et al. 1995; Thelen et al. 1997). Two decades ago, electrical stimulation was reported to increase myotube glucose uptake and improve insulin responses (Aas et al. 2002)

as well as to enhance lactate secretion and glycogen mobilization (Elsner et al. 2003; Marotta et al. 2004). Although these studies were able to mimic many of the physiological changes induced by exercise, the Kanzaki lab has been considered a pioneer in the development of the *in vitro* exercise mimicking model. The research team published many seminal reports demonstrating that electrical pulse stimulation (EPS) induced *de novo* sarcomere assembly (Fujita et al. 2007), increased ATP hydrolysis, glucose transporter 4 recycling, phosphorylation of common exercise responsive proteins – including AMPK and MAPKs (Nedachi et al. 2008) – and exerkine secretion (Farmawati et al. 2013; Nedachi et al. 2009). In Figure 4, the history of the *in vitro* exercise-mimicking model development is briefly summarized.

During the last decade, the number of studies utilizing skeletal muscle-specific exercise-like EPS (hereafter referred to as EL-EPS as recommended by Carter & Solomon (2019)) as an *in vitro* exercise mimetic has skyrocketed (Nikolić et al. 2017). The studies have focused on, but not been limited to, examining EL-EPS-induced metabolic effects in myotubes (Abdelmoez et al. 2020; Hong et al. 2017; Lambernd et al. 2012; Li et al. 2019; Nikolić et al. 2012) as well as identification and validation of novel contraction-responsive exerkines (Pourteymour et al. 2017; Raschke et al. 2013; Scheler et al. 2013). A few studies have also aimed to develop a resistance exercise protocol resulting in myotube hypertrophy and/or increased mTORC1 signaling (Scheler et al. 2013; Tarum et al. 2017; Valero-Breton et al. 2020). Different omics-methods have become increasingly popular, such as proteomics (Laurens et al. 2020b; Reimann et al. 2017), transcriptomics (Pillon et al. 2020; Scheler et al. 2013; Sidorenko et al. 2018; Y. Tamura et al. 2020) and even trans-omics (combination of omics) (Hoshino et al. 2020). The intercellular cross-talk has been studied by applying EL-EPS conditioned medium to other cell lines, such as hepatocytes (Evers-van Gogh et al. 2015), adipocytes (K. Tamura et al. 2020), monocytes (Miyatake et al. 2016), endothelial cells (Chaweewannakorn et al. 2020; Ishiuchi et al. 2018; Zhao et al. 2018) and β-cells (Barlow et al. 2018; Barlow & Solomon 2019; Christensen et al. 2015). Furthermore, as an additional validation of the suitability of EL-EPS for exercise research, comparison of the voluntary wheel running in mice and *in vitro* EL-EPS resulted in similar molecular responses (Son et al. 2019). The majority of studies using EL-EPS have utilized short- or long-term low-frequency protocols that mainly induce similar responses as acute exercise bouts do (Nikolić et al. 2017). The EL-EPS studies have resulted in an enormous list of protocols with variable settings (Nikolić et al. 2017).

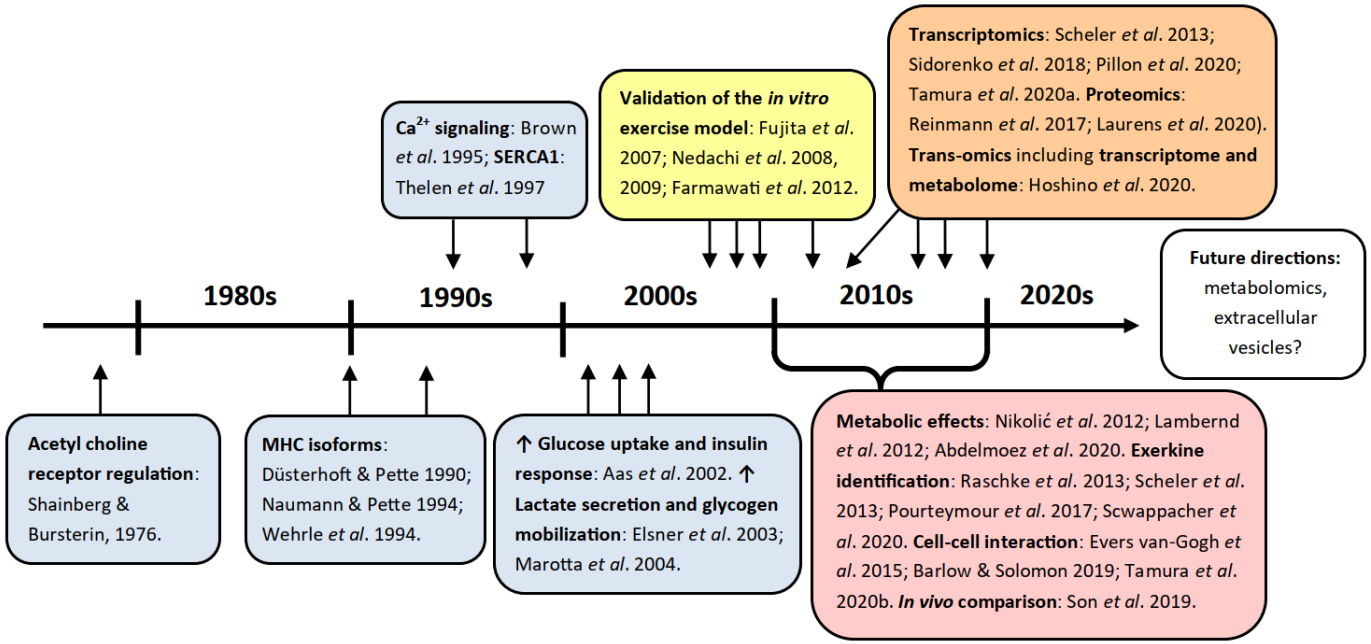

FIGURE 4 Development of the *in vitro* exercise-like electrical pulse stimulation model from the 1970s to 2020s. A few of the most relevant studies are presented to demonstrate the process of the model development and the study interests in different times. The Kanzaki lab (yellow background) published hallmark studies validating the model for *in vitro* exercise research. MHC, myosin heavy chain; SERCA1, sarco/endoplasmic reticulum Ca^{2+}-ATPase 1.

The EL-EPS approaches have been divided to low (≤ 5 Hz) and high (≥ 30 Hz) frequency protocols lasting less than eight hours, while long-term (≥ 24 h) protocols utilize only low-frequency stimulation (Nikolić et al. 2017). Most of the studies reviewed by Nikolić and colleagues applied short-term low-frequency EL-EPS on myotubes originated from rodents or human (Nikolić et al. 2017), while long-term studies were a minority. The murine C2C12, rat L6 and various primary or commercial human skeletal muscle cell lines are the most commonly used in EL-EPS studies (Nikolić et al. 2017), but their species-specific properties may induce distinct responses to EL-EPS (Abdelmoez et al. 2020).

The major benefit of the EL-EPS approach is that it enables exclusive examination of intra- and extracellular changes. Despite the heterogeneity of the EL-EPS protocols published, myotube contractions induce many of the key physiological changes observed during *in vivo* exercise (Carter & Solomon 2019; Nikolić et al. 2017), thus making it a suitable model for studying skeletal muscle and exercise *in vitro*. Lastly, it is worth noting that EL-EPS-related research is not limited to 2D models. Instead, 3D EL-EPS models have been developed (Hernández-Albors et al. 2019; Mestre et al. 2018; Nakamura et al. 2021), but this dissertation will focus only on the 2D studies. In the next two sections, EL-EPS-mediated intra- and extracellular changes are reviewed.

2.4.2 Intracellular responses to EL-EPS

Since the initial validation of the EL-EPS model by the Kanzaki lab, metabolic changes have been studied extensively. The EL-EPS has been reported to increase mitochondrial content (Nikolić et al. 2012) as well as to enhance glucose uptake and oxidation (Lambernd et al. 2012; Nikolić et al. 2012) partly via upregulated glucose transporter 4 translocation (Hu et al. 2018; Li et al. 2018). Simultaneously, myotube contractions have promoted anaerobic glycolysis (i.e., lactate production and secretion), as well as utilization of phosphocreatine and ATP (Lambernd et al. 2012; Nikolić et al. 2012). The glycogen content has been reported to decrease in EL-EPS medium similar to serum *in vivo* (Son et al. 2019), while in cell lysates the glycogen has been shown to decrease (Li et al. 2018; Park et al. 2019) and to increase (Farmawati et al. 2013) after EL-EPS. Further, long-term EL-EPS was reported to induce glycogen synthesis with simultaneous increase in glycerol release and palmitate oxidation (Laurens et al. 2020b). In contrast to glucose metabolism, the EL-EPS protocols have been shown to have controversial effects on fatty acid uptake and oxidation (Lambernd et al. 2012; Li et al. 2019; Nikolić et al. 2012), which may be partly due to measurement protocol, the fatty acid analyzed (e.g., palmitate or oleate) or donor-specific characteristics (Feng et al. 2015; Lambernd et al. 2012; Nikolić et al. 2012). More specifically, fatty acid oxidation has mainly increased or remained unaltered after EL-EPS (Feng et al. 2015; Lambernd et al. 2012; Li et al. 2019; Løvsletten et al. 2020; Marš et al. 2020; Nikolić et al. 2012). Similar to *in vivo* exercise, contraction-induced generation of reactive oxygen species (Hoshino et al. 2020; Liu et al. 2021) has also been reported after EL-EPS.

At the level of translation, multiple exercise-related signaling cascades including phosphorylation of AMPK, MAPKs, and acetyl-CoA carboxylase have been shown to increase after both *in vivo* exercise and *in vitro* EL-EPS (Nikolić et al. 2017). Additionally, inhibitory-κB kinase β/nuclear factor (NF)-κB as well as phosphoinositide 3-kinase/Akt/mTOR pathways have also been analyzed after the EL-EPS (Hoshino et al. 2020; Nikolić et al. 2017; Scheler et al. 2013; Tarum et al. 2017; Valero-Breton et al. 2020), and the responses are highly dependent on the EL-EPS protocol used. The protein contents of myosin heavy chain isoforms have been examined in addition to the gene transcripts (Fukushima et al. 2021; Marš et al. 2020; Nedachi et al. 2008; Nikolić et al. 2012) similar to oxidative phosphorylation (Nikolić et al. 2017). Fewer studies have examined signaling pathways related to resistance exercise (Scheler et al. 2013; Tarum et al. 2017; Valero-Breton et al. 2020).

At the level of transcription, EL-EPS has been reported to upregulate, for example, exerkine expression (Chen et al. 2019; Fukushima et al. 2021; Nedachi et al. 2008, 2009; Scheler et al. 2013). Related to myotube differentiation and ability to contract, myosin heavy chain isoforms are also affected by EL-EPS (Fukushima et al. 2021; Lambernd et al. 2012; Marš et al. 2020). The EL-EPS-induced Ca^{2+} signaling has been reported to regulate 30% of the differentially expressed genes (DEGs) (Sidorenko et al. 2018), while in another study 800 DEGs were reported after the EL-EPS with time-dependent changes partly regulated by reactive oxygen species (Hoshino et al. 2020). The comparison of the low- (twitch) and high-frequency (tetanus) protocols resulted in similar metabolic adaptations and partly the same genes were affected after EL-EPS (Tamura et al. 2020). Son and colleagues reported that voluntary wheel running and short-term high-frequency EL-EPS enhanced gene expression of the myogenic markers and antioxidant enzymes (Son et al. 2019). Furthermore, glucose availability of the resting C2C12 myotubes has been reported to modify gene expression (MacDonald et al. 2020), thus highlighting that nutrient availability should be better taken into account in future EL-EPS studies.

Lastly, regardless of the cell line used, the myotube contractions are not visible immediately after the electrical current is applied to the media. The reason for the delayed response is the assembly of the contractile units within the cells, for example reorganization of the cytoskeleton and *de novo* formation of sarcomere structures (Fujita et al. 2007; Lambernd et al. 2012). Thus, if the stimulation time is shorter than the time to detect visible contractions, changes in the studied parameters can possibly be caused by Ca^{2+} flux rather than contractions *per se*.

2.4.3 Extracellular responses to EL-EPS

Exercise-induced changes do not occur only in the skeletal muscle because skeletal muscle cells secrete exerkines as described in section 2.3.2. However, most of the EL-EPS studies to date have mainly analyzed cytokines, proteins, and peptides from the cell culture media, while metabolites and extracellular vesicles have received less interest. That being said, many studies have measured media glucose and lactate contents as markers of increased uptake and anaerobic

glycolysis, respectively (Carter & Solomon 2019; Nikolić et al. 2017). Cell viability has been assessed from the media because if EL-EPS induces cell death or disrupts cell membrane integrity, intracellular enzymes, such as lactate dehydrogenase, leak into the media (Nikolić et al. 2017).

Many of the exerkines have been identified from blood samples after *in vivo* exercise (see the section 2.3.2.) and although *in vitro* approaches are becoming increasingly popular, they have almost exclusively focused on protein myokine identification. Nikolić and colleagues listed many exerkines that have been identified after EL-EPS, including C-C motif chemokines (e.g., CCL2 and CCL21), fibroblast growth factors, different interleukins, angiopoietin-like 4 (Nikolić et al. 2017), while others have reported dozens more (Raschke et al. 2013; Scheler et al. 2013). However, the molecular mechanisms and target tissues of the identified exerkines remain mainly unknown. Further studies are therefore warranted.

Myotube cultures always contain myoblasts that also express cytokines, such as IL-1ra, IL-6 and CCL2, but the constitutive exerkine expression is greater in the myotubes (Peake et al. 2015). Moreover, EL-EPS does not promote IL-6 secretion from the myoblast, thus highlighting the major role of the myotubes as the primary origin of exerkines (Farmawati et al. 2013; Peake et al. 2015). It is also critical to note that the type, duration, and intensity of the EL-EPS can have a great impact on the expression and secretion of exerkines, suggesting that their metabolism is strictly regulated (Peake et al. 2015). As a conclusion, although EL-EPS as an *in vitro* exercise-mimicking model is suitable to study intra- and extracellular responses to myotube contractions, more studies are needed to better understand how these identified mediators affect intra- and intercell metabolism and communication. Another aspect neglected in previous EL-EPS studies is the lack of examination of the effects of nutrition contraction-induced responses within the myotubes.

3 PURPOSE OF THE STUDY

The aims of this dissertation were to study the effects of (1) muscle size regulation by cancer cachexia and activin receptor ligands and (2) muscle contractions using exercise-mimicking stimulation of myotubes. The main focus was on intra- and extracellular responses (i.e., muscle metabolism and secretome, respecively).

The specific aims were to study:

1. The effects of blocking myostatin and activins on skeletal muscle and serum metabolome during experimental cancer. (I)

   Hypothesis: Muscle wasting is accompanied by changes in skeletal muscle and serum metabolome and those are in part rescued by blocking myostatin and activins.

2. The effects of myostatin and other tumorkines on myogenic C2C12 and CHQ cell lines. (II)

   Hypothesis: Myostatin and tumorkines dysregulate myoblast differentiation into myotubes, induce signaling via catabolic pathways, and downregulate anabolic pathways in myoblasts and myotubes.

3. The effects of chronic low-frequency exercise-like electric pulse stimulation on the myotube and media metabolites, intracellular signaling, and substrate utilization in the C2C12 myotubes under variable nutrient avaliability. (III)

   Hypothesis: Exercise-like electrical pulse stimulation activates similar pathways as shown after *in vivo* exercise, promotes the release/secretion of exercise-induced metabolites, and enhances both glucose and lipid metabolism. Nutrient availability regulates intra- and extracellular responses to myotube contractions. (IV)

4. The effects of chronic low-frequency exercise-like electric pulse stimulation on the C2C12 myotube transcriptome and extracellular vesicle miRNA content under variable nutrient availability.

Hypothesis: Exercise-like electrical pulse stimulation promotes the expresson of contractily proteins and various exerkines in myoubes. To promote intercellular communication, the same miRNAs are packed into extracellular vesicles and released to the cell culture media as have been reported to occur during *in vivo* exercise. Nutrient availability affects gene expression and the pathways, which are up- and downregulated.

4 MATERIAL AND METHODS

4.1 Animals

BALB/c male mice (BALB/cAnCrl, Charles River Laboratories, Germany), aged 5–6 weeks, were housed under standard conditions (temperature 22 °C, 12:12 h light/dark cycle). Water and food pellets were provided *ab libitum* (R36; 4% fat, 55.7% carbohydrate, 18.5% protein, 3 kcal/g, Labfor, Stockholm, Sweden).

4.1.1 Ethics statement

The animals were treated in accordance with the European Legislation for the protection of vertebrate animals used for experimental and other scientific purposes. The National Animal Experiment Board approved the protocols used and the guidelines of the committee were followed when experiments were conducted (permit number: ESAVI/10137/04.10.07/2014). Additionally, ethical standards of the 1964 Declaration of Helsinki and its later amendments were followed.

4.2 Cell lines

The murine C2C12 myoblasts were purchased from American Type Culture Collection (ATCC, Manassas, VA, USA). Murine colon-26 carcinoma (C26) cells were a kind gift from Dr. Fabio Penna (obtained from Prof. Mario P. Colombo). The primary human CHQ myoblasts, derived from quadriceps muscle biopsy of a 5-day-old infant (Edom et al. 1994), were a kind gift from Dr. Vincent Mouly and Dr. Eija Laakkonen. The satellite cell proliferation potential reduces with age (Schultz & Lipton 1982), which is why infant cell line was selected. Because

immortalization only restrains senescence (Zhu et al. 2007; Thorley et al. 2016), examination of the immortalized C2C12 and non-immortalized CHQ cells in the same study (II) is justified. All the described cell experiments were performed in a humidified environment at 37 °C and 5% CO_2.

4.2.1 C2C12 myoblasts (II-IV)

The murine C2C12 myoblasts were cultured in a growth medium (GM) containing high glucose (4.5 g/l) Dulbecco's Modified Eagle Medium (DMEM, #BE12-614, Lonza, Basel, Switzerland) supplemented with 10% (v/v) fetal bovine serum (FBS, #10270-106, Gibco, Rockville, MD, USA), 100 U/ml and 100 µg/ml penicillin-streptomycin (P/S, #15140, Gibco) and 2 mM L-glutamine (#17-605E, Lonza, or #25030, Gibco). For the experiments, myoblasts were seeded on 12- or 6-well plates (NunclonTM Delta; Thermo Scientific, Waltham, MA, USA). When the myoblasts reached over 90% confluence, the cells were rinsed with phosphate buffered saline (PBS, #10010, Gibco) and GM was replaced by differentiation medium (DM) containing high glucose DMEM, 5% (v/v) FBS, 100 U/ml and 100 µg/ml P/S and 2 mM L-glutamine to promote fusion into myotubes. Fresh DM was changed every second day. When a low glucose DMEM medium (1 g/l, #BE12-707, Lonza) was used in the experiments, the C2C12 cells were acclimatized to these conditions overnight.

4.2.2 CHQ myoblasts (II)

The primary human CHQ cells were cultured in a growth medium with a 4:1 ratio of GlutaMAX (#61965, Gibco) and Medium 199 (#41150, Gibco) supplemented with 20% (v/v) FBS and 50 µg/ml gentamicin (#15750, Gibco). For the experiments, myoblasts were seeded on 6-well plates (NunclonTM Delta). After reaching over 90% confluence, differentiation was promoted by replacing GM with DM, which contained 4:1 GlutaMAX and Medium 199, 50 µg/ml gentamicin and 10 µg/ml bovine insulin (#15500, Sigma-Aldrich, St. Luis, MO, USA) as previously described (Pekkala et al. 2015). The DM was not replaced during the differentiation.

4.2.3 C26 colon carcinoma cells (I-II)

For Study I, the C26 cells were grown in a high glucose medium (GlutaMAX, #10569, Gibco) supplemented with 10% (v/v) FBS and 100 U/ml and 100 µg/ml P/S. The C26 cells were harvested for injections by trypsinization with 0.25% Trypsin-EDTA (#15400, Gibco) and centrifugation at 390 g for 5 minutes. The cell pellet was suspended in sterile PBS and kept on ice until injections for the mice. For Study II, the C26 cells were grown in the same high glucose GM as described in the C2C12 myoblasts in the section 4.2.1. For the experiments, the C26 cells were maintained in GM or medium was switched to C2C12 DM described (section 4.2.1). The C26 cells were acclimatized to DM for 48 h prior to the experiment.

4.3 Experimental designs

4.3.1 *In vivo* C26 cancer experiments (I)

The mice were randomized into four groups containing healthy controls (CTRL, N = 9) administered with a vehicle (PBS) and the C26 tumor-bearing mice with a vehicle (C26+PBS) or soluble activin receptor type 2B (sACVR), either only before (C26+sACVR/b) or both before and after tumor formation (C26+sACVR/c). The mice were injected intraperitoneally (i.p.) with sACVR (5 mg/kg) or PBS (100 µl) every fourth day, in total three times before and after the C26 cell inoculation (days -11, -7, -3, 1, 5, and 9). On day 0, the C26 cancer cells (5 x 10^5 cells within 100 µl of PBS) or equal volume of PBS (control group) were inoculated to the interscapular region while mice were under anesthesia (60–70 mg/kg ketamine, and 9 mg/kg xylazine, i.p., Ketaminol® and Rompun®, respectively). Samples were collected on day 11. Experiment 1 was repeated to collect more samples for metabolomics analyses with all groups above except C26+sACVR/b. The final N sizes were N = 15 in CTRL, N = 13 in C26+PBS and N = 13 in C26+sACVR/c groups, respectively. Samples of the second experiment were collected when tumor growth and loss of body mass reached the levels of the first experiment (on day 13) (Figure 5).

4.3.1 *In vitro* myostatin and co-culture experiments (II)

All the myostatin and co-culture experiments independent of the cell line used (C2C12 or CHQ) were conducted on day 0-1 (myoblasts in GM) or on day 5-6 (myotubes in DM) post differentiation. Before the experiments, the wells were rinsed twice with PBS and fresh medium, depending on the differentiation state GM or DM with all the supplements, was added (Figure 5).

Protocol 1: Myostatin experiments. Prior to use, the inactive myostatin propeptide was activated by heating (5 min at 95 °C) to release the mature protein (Wolfman et al. 2003). The final myostatin concentration (100 ng/ml) was selected based on our dose-dependent bioassay (data not shown) and previous reports (Graham et al. 2017; Zhang et al. 2011). Due to the high conservation rate of the myostatin protein among human and mouse (99% identical), administration of activated mature myostatin on C2C12 and CHQ cell lines is justified (McPherron et al. 1997; Peake et al. 2015). The selection of the two time-points used (2 h and 24 h) were chosen to examine both acute and delayed or persistent changes (Ding et al. 2017; Graham et al. 2017; Rodgers et al. 2014). Myostatin experiments were replicated once, total N = 6 per group.

Protocol 2: Co-culture experiments. The C2C12 cells were grown as described above in section 4.2.1 and the C26 cells were grown in C2C12 GM or acclimatized for 48 h to C2C12 DM prior to the combination of the cell lines as demonstrated previously (Jackman et al. 2017). The C2C12 and C26 cells were seeded to Transwell® wells or 0.4 µm porous membrane inserts (Costar, Corning Incorporated, Corning, NY, USA), respectively and the C26 cells were grown on

a separate plate for 24 h allowing the cells to attach to the membrane. The two cell lines were combined on day 0 or day 5 post C2C12 differentiation and the C26 cells were approximately 80% to 90% confluent at this point. First, media were removed, wells and inserts were rinsed with PBS and fresh GM or DM depending on the differentiation stage of the C2C12 cells was added to both cell lines. Next, the C26 inserts were placed on top of the C2C12 wells for the 24-hour co-culture. The experiments were replicated once, total N = 6–8 per group.

4.3.2 *In vitro* exercise-like electrical pulse stimulation experiments (III–IV)

Protocol 1: EL-EPS for omics-analyses (III–IV). The C2C12 cell experiments were conducted on days 4–6 post myotube differentiation by using either high (HG) or low (LG) glucose medium. When a LG medium was used, the cells were acclimatized to lower glucose content overnight on day 4 post-differentiation. At this point, LG DM contained all the supplements. The next day (day 5), the wells were rinsed with PBS and serum-free HG or LG DMEM supplemented with 2 mM L-glutamine was added for 1 h (Furuichi et al. 2018). Next, the medium was removed, the wells were rinsed with PBS and fresh serum-free HG or LG DMEM supplemented with 2 mM L-glutamine was added. The low-frequency EL-EPS was applied for 24 h (1 Hz, 12 V, 2 ms) by placing the C-Dish carbon electrodes attached to C-Pace 100 machine (Ionoptix Corporation, Milton, MA, USA) to the wells. The samples were collected immediately after cessation of the EL-EPS (Figure 5). The experiments were replicated three times, total N = 6–8 per group (III) or N = 5 per group (IV). Additionally, stimulated and unstimulated fresh media controls (i.e., no cells/no power and no cells/power) were included to the metabolomics study (III) to exclude the stimulation effect alone, total N = 3 per group.

Protocol 2: EL-EPS for fat oxidation (III). The C2C12 cells were grown as in protocol 1. On day 4 post differentiation, the cells were acclimatized to 100 µM oleic acid – albumin from bovine serum (#03008, Sigma-Aldrich) and 1 mM L-carnitine (C0158, Sigma-Aldrich) in either serum-free LG or HG DMEM supplemented with 2 mM L-glutamine. The next day, the electrodes were placed directly to the wells and EL-EPS was applied overall for 24 h (1 Hz, 12 V, 2 ms). On day 6, after 22 h of stimulation, the EL-EPS was paused, medium was removed, and wells were rinsed with PBS. Next, fresh serum-free HG or LG DMEM supplemented with 2 mM L-glutamine, 100 µM oleic acid, 1mM L-carnitine and 1 µCi/ml radiolabelled [9,10-^{3}H(N)] oleic acid (24 Ci/mmol, NET289005MC, PerkinElmer, Boston, MA, USA) was added. Radiolabelled oleic acid was omitted from the negative controls. The remaining 2-hour EL-EPS was applied. The samples were collected immediately after cessation of the EL-EPS (Figure 5). The experiments were replicated independently three times, total N = 8–10 per group.

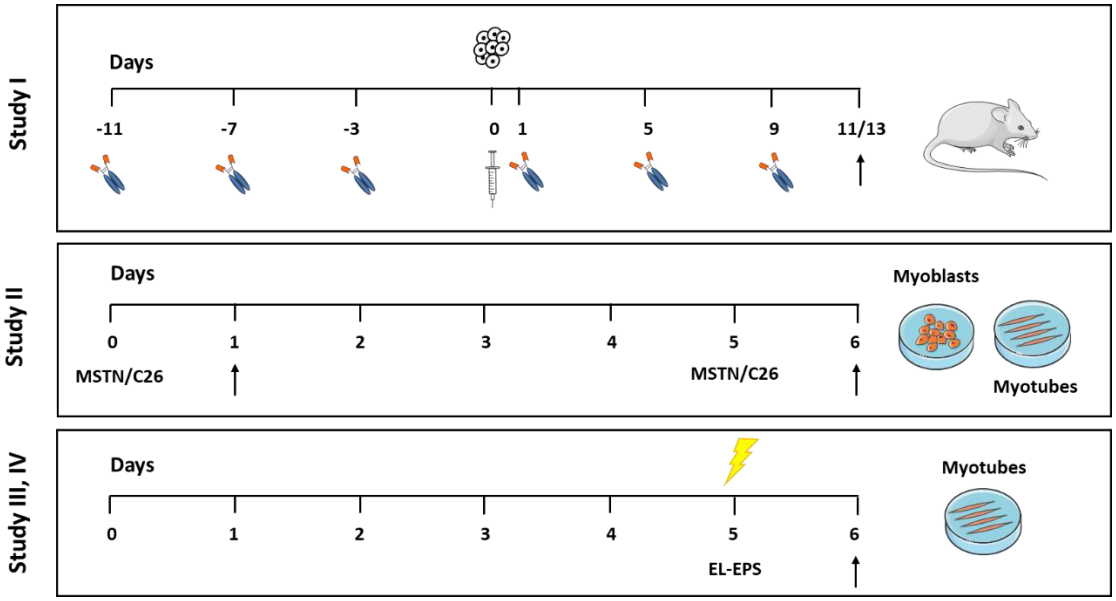

FIGURE 5 Simplified presentation of the experimental designs in *in vivo* (I) and *in vitro* (II-IV) studies. The syringe and cell cluster depicts C26 cancer cell inoculation, while receptors depict administration of soluble activin receptor type 2B or vehicle control. MSTN/C26 depicts administration of myostatin on the C2C12 or CHQ myoblasts (day 0) and myotubes (day 5) or beginning of the C2C12 and C26 Transwell® co-culture, respectively. Lightning demonstrates the administration of exercise-like electrical pulse stimulation (EL-EPS). Black arrows depict the time-points of sample collections. Images were obtained from https://smart.server.com.

4.4 Production of the recombinant proteins

The recombinant soluble ACVR2B-Fc (I) (Hulmi et al. 2013) and myostatin (II) proteins were produced in-house by Dr. Arja Pasterncak and Dr. Olli Ritvos at the University of Helsinki, Finland. The protocols were similar for both proteins and explained briefly below. First, PCR was used to amplify the ectodomain of human ACVR2B. The same was repeated for the C-terminally hexa histidine (His6)–tagged human IgG1 Fc domain. In the case of myostatin, latent precursor protein (Cotton et al. 2018; Gray & Mason 1990; Walker et al. 2018) was also amplified via PCR (both pro-domain and mature domain). The amplified PCR products were subcloned into pGEM-T easy (Promega, Madison, WI, USA) vector, sequenced, fused and finally cloned into the pEFIRES-p expression vector. Then the vectors were transfected into Chinese hamster ovary cells (CHO). For the protein production, CHO cell suspension was grown in CD OptiCHO medium (Gibco) supplemented with 2 mM L-glutamine in an orbital shaker. Next, the cell culture media were harvested by centrifugation and filtrated to collect the recombinant proteins. The silver-stained SDS-PAGE and Western blot analyses verified

high purity of the produced proteins and confirmed that most of the purified myostatin was in the mature form.

The produced sACVR2B-Fc is similar but not identical to the previously reported protein (Lee et al. 2005). The biological activity of the heat activated (5 min at 95 °C) myostatin was tested in human hepatocytes transfected with CAGA luciferase reporter construct as earlier with modifications (Kaivo-Oja et al. 2005). The dose dependent myostatin activity measured by luciferase assay reagent (Promega) was detected after 18-hour incubation at a concentration of 10–100 ng/ml. Two blockers of myostatin, sACVR2B-Fc and follistatin-288 (6-600 ng/ml), were able to abolish the activity of 10 ng myostatin dose-dependently.

4.5 *In vivo* and *in vitro* sample collections

In Study I, the mice were anaesthetized by intraperitoneal injection of ketamine (110–120 mg/kg, Ketaminol®) and xylazine (15–16 mg/kg, Rompun®) on day 11 or day 13 after C26 cell injection. Next, the mice were euthanized by cardiac puncture followed by cervical dislocation. The blood was collected into serum collection tubes (Biofuge 12, Heraeus, Hanau, Germany) followed by 10 minutes centrifugation at 2000 *g*, at room temperature (RT). The resulting sera were stored at -80 °C. The skeletal muscle (gastrocnemius and tibialis anterior) samples were weighted and snap-frozen in liquid nitrogen before storage at -80 °C.

In studies II to IV, the samples were collected immediately after the indicated incubation times. The cells and the media were collected for distinct analyses described in detail in the following sections. Table 1 describes the collected samples and conducted analyses in studies I to IV.

TABLE 1 The samples collected, and analyses conducted in studies I-IV.

Sample	Analysis	Study
M. Gastrocnemius	GC/TOF-MS, TG extraction	I
M. Tibialis anterior	WB	I
Serum	GC/TOF-MS	I
CHQ cells	WB, qPCR	II
C2C12 cells	^{1}H-NMR, RNA-seq, WB, qPCR	II-IV
C2C12 media	^{1}H-NMR, ELISA	III
C2C12 media EVs	NTA, EM, qPCR	IV

GC/TOF-MS, gas-chromatography/time-of-flight mass spectrometry; TG, triacylglycerol; WB, Western blot; qPCR, quantitative real-time polymerase chain reaction; ^{1}H-NMR, proton nuclear magnetic resonance spectroscopy; RNA-seq, messenger RNA sequencing; ELISA, enzyme-linked immunosorbent assay; EVs, extracellular vesicles, NTA, nanoparticle tracking analysis; EM, electron microscopy.

4.6 MS- and ^{1}H-NMR-based metabolomics

4.6.1 Tissue and serum preparation for CG/TOF-MS (I)

Skeletal muscle samples were homogenized for gas chromatography/time-of-flight mass spectrometry (CG/TOF-MS) analysis by 2 minutes of grinding (Jingxin science, China) followed by metabolite extraction using methanol-chloroform-water (1:2.5:1, v/v/v) solvent. Serum metabolites were extracted with methanol-chloroform (3:1, v/v). From this step forward, the preparation protocol was identical for both samples. After short mixing and 20-minute incubation at -20 °C, the samples were centrifuged at 15 000 *g* for 10 minutes at 4 °C. Next, the resulting supernatants were vacuum dried (Huamei, China), suspended to methoxyamine, mixed shortly, and shaken before adding N,O-bis(trimethylsilyl)trifluoroacetamide (BSTFA) and trimethylchlorosilane (Supelco, Bellefonte, PA, USA).

4.6.2 Cell lysates and media preparation for ^{1}H-NMR (III)

After the 24-hour EL-EPS, stimulated and non-stimulated C2C12 cell lysates and cell culture media with and without cells were collected for ^{1}H nuclear magnetic resonance spectroscopy (^{1}H-NMR) as described previously by Kostidis and colleagues (Kostidis et al. 2017) with slight modifications. Briefly, the media were shortly centrifuged and a pool of 200 µl aliquot per three wells was collected. Next, cold methanol was added to the pool and the mixtures were incubated for 30 minutes at -20 °C followed by centrifugation for 20 minutes at 16 000 *g* at 4 °C. The wells were washed with cold PBS and metabolic quenching was conducted by adding liquid nitrogen. The cells were scraped into 200 µl of lysis solution (90% 9:1 (v/v) aqueous methanol-chloroform), homogenates from three wells were pooled and centrifuged for 10 minutes at 16 000 *g* at 4 °C. All the supernatants were stored at -80 °C until use.

Prior to the ^{1}H-NMR analysis, the samples were lyophilized. The samples were reconstituted in 200 µl of sodium phosphate buffer in 99.8% D_2O (Acros Organics™, Thermo Scientific). The internal standard used in the study was 0.5 mM 3-(trimethylsilyl) propanesulfonic-d6 acid sodium salt (DSS-d6, IS-2 Internal Standard, Chenomx, Edmonton, Canada). Lastly, the samples were transferred to 3 mm ^{1}H-NMR-sample tubes (Norell Inc., Morganton, NC, USA) after mixing.

4.6.3 CG/TOF-MS and ^{1}H-NMR measurements (I, III)

The metabolite analyses of the *in vivo* samples were conducted using an Agilent 6890 gas chromatography (GC) system coupled with a Pegasus III Time-of-Flight mass spectrometer (TOF-MS). Trimethylsilytated (TMS) samples were separated by a DB-5ms capillary column (30 m x 0.25 mm, 0.25 µm, Agilent J&W Scientific, Folsom, CA, USA). A constant flow rate of helium was applied during measurements. The transfer line temperature was set at 270 °C and ion source at 220 °C.

The settings for electron impact ionization were set at 70 eV at full scan mode (*m/z* 30–600) to acquire the mass spectrometry data. The dwell time for each scan was 10 spectra per second, while the solvent delay was 7 minutes.

The ^{1}H-NMR spectra were collected using a Bruker AVANCE III HD NMR spectrometer, operating at 800 MHz ^{1}H frequency (Bruker Corporation, MA, USA) and equipped with a cryogenically cooled ^{1}H, ^{13}C, ^{15}N triple-resonance probehead. During the measurements, the sample temperature was set at 25 °C. In addition to ^{1}H one-dimensional NOESY experiments, heteronuclear ^{1}H-^{13}C heteronuclear single quantum coherence spectroscopy (HSQC) and ^{1}H-^{13}C HSQC-total correlation spectroscopy (HSQC-TOCSY), as well as homonuclear ^{1}H-^{1}H TOCSY and ^{1}H-^{1}H double quantum filtered correlation spectroscopy (DQF-COSY) two-dimensional spectra were used to confirm the identification of the profiled metabolites. The TopSpin 4.0.9 software (Bruker Corporation) was used for processing and analysis of the two-dimensional spectra.

4.6.4 Data analyses and metabolite identification (I, III)

Study (I). The GC/TOF-MS data were analyzed using ChromaTOF software (v 4.34, LECO, St Joseph, MI). Briefly, the .csv files were aligned with the Statistic Compare component followed by generation of three-dimension data sets. The peaks of one metabolite were combined after the removal of internal standards and known false positives. In each sample, the sum intensities of peaks were used for data set normalization. Metabolite identification was conducted as follows. The available reference standards, NIST 11 standard mass spectral databases and the Fiehn databases linked to ChromaTOF software, were used for annotation of the detected metabolites with both multivariate and univariate statistical significance (VIP > 1.0 and P < 0.05). Positive identification was accepted if the identified metabolite reached > 70% similarity with the reference standard. The GC/TOF-MS analyses enabled identification of 219 metabolites from skeletal muscle and serum. Based on the reporting threshold (i.e., metabolite was detected in over 30% of the animals), 156 metabolites were included in further analyses. To be eligible for further bioinformatic searches, metabolites must fulfill the inclusion criteria: after false discovery rate correction (FDR) < 0.05 and fold change (FC) > |1.2|.

Study (III). The obtained data were analyzed using Chenomx 8.5 or 8.6 software (Chenomx, Edmonton, Canada). The spectra were automatically zero-filled to the nearest power of two, which was at least twice as large as the number of points acquired. Automatic phase correction and baseline correction were used, and manual adjustments were conducted if necessary. Additionally, Chenomx software's reference peak–based shim correction tool was used to enhance the line shape of the spectra. Overall, ^{1}H-NMR analysis enabled identification of 39 and 37 metabolites from the cells and media, respectively, of which 37 and 34 were detected in 50% of the samples, thus meeting the reporting threshold for further analyses.

4.7 Nucleic acid analyses

4.7.1 RNA extraction (II, IV)

4.7.1.1 Myotube lysates (II, IV)

In Study II, TRI reagent solution (AM9738, Thermo Scientific) was used to extract total RNA from the myotube lysates according to the manufacturer's protocol. In Study IV, DNA/RNA Shield solution (#R1100, Zymo Research, Irvine, CA, USA) was used to extract nucleic acids from the cell lysates using Chemagic 360 automated nucleic acid extraction instrument (PerkinElmer).

4.7.1.2 Extracellular vesicles (IV)

First, the validation of the extracellular vesicle (EV) extraction from the C2C12 myotube culture media was conducted as previously described (Karvinen et al. 2020) using exoRNeasy serum/plasma midi kit (#77044, Qiagen, Hilden Germany). The representative EV extraction samples were analyzed at the EV Core (University of Helsinki, Finland) by visualization using electron microscopy (EM) imaging, while the size and number of the particles were quantified using nanoparticle tracking analysis (NTA) as previously described (Puhka et al. 2017). The results showed that the protocol was suitable for extraction of the EVs from the cell culture media.

After the protocol validation, the EV RNA extraction was conducted using exoRNeasy serum/plasma midi kit (#77144, Qiagen, Hilden Germany) according to the manufacturer's protocol. For the EV RNA extraction, media from two wells of a 6-well plate were pooled. During the EV RNA extraction, miRNeasy Serum/Plasma Spike-In Control Syn-cel-miR-39 (#219610, Qiagen) was added to be an internal control for RT-qPCR.

4.7.2 Reverse transcription and RT-qPCR (II, IV)

4.7.2.1 Cell lysates (II, IV)

For the cDNA synthesis, iScript™ Advanced cDNA kit for RT-qPCR (#172-5038, BioRad Laboratories, Hercules, CA, USA) was used according to the manufacturer's protocol in Study II. In Study IV, genomic DNA was first eliminated according to the manufacturer's protocol, followed by the cDNA synthesis using Maxima H first strand cDNA synthesis kit with dsDNase treatment (#K1682, Thermo Scientific). The RT-qPCR was conducted according to the manufacturer's protocol with iQ™ SYBR® Green Supermix (#170-8882, Bio-Rad Laboratories, Hercules, CA, USA) and CFX96 Real-Time PCR Detection System combined with CFX Manager software (Bio-Rad Laboratories).

In Study II, PicoGreen (Quant-iT™ PicoGreen™ dsDNA Assay Kit, Thermo Scientific) was used for normalization. In Study IV, the efficiency corrected $2^{-\Delta\Delta Ct}$ method was utilized in data analysis and the relative expression was normalized

against a suitable housekeeping gene (*36b4)*. Sequences of the self-designed primers and Bio-Rad Prime PCR™ Assay IDs are listed in Table 2.

4.7.2.2 Extracellular vesicles (IV)

The miScript II RT Kit (#218161, Qiagen) was used for the cDNA synthesis of the EV extracted miRNAs according to the manufacturer's instructions. Briefly, 12 µl of the isolated EV RNA was used for reverse transcription using 5x miScript HiFlex buffer. For the RT-qPCR, 1 µl of the non-diluted EV cDNA was used. The RT-qPCR protocol was identical as previously described (Karvinen et al. 2020). The $2^{-\Delta Cq}$ equation, where ΔCq is the target Cq-value – housekeeping Cq-value, was used for data normalization and evaluation of the relative expressions. The miR primers (miScript Primer Assay, Qiagen) are listed in Table 2.

TABLE 2 Primers used for the quantitative real-time PCR.

Transcript	**Sequence, 5´- 3´**	**Bio-Rad PrimePCR™ Assay ID**	**Study**
INHIBINβA	F: GCTCAGACAGCTCTTACCACA		II
	R: AGCAAATTCTCTTTCTGGTCCC		
GDF8	F: TGGTCATGATCTTGCTGTAACC		II
	R: CTTGACCTCTAAAAACGGATTCA		
GDF11	F: ACCACCGAGACCGTCATTAG		II
	R: AGGGCTGCCATCTGTCTG		
ACVR2B		qHsaCID0016227	II
FOLLISTATIN		qHsaCID0014487	II
36b4	F: GGCCCTGCACTCTCGCTTTC		IV
	R: TGCCAGGACGCGCTTGT		
Gdf8	F: AAGATGGGCTGAATCCCTTT		II
	R: GCAGTCAAGCCCCAAAGTCTC		
Gdf11	F: CGTCACATCCGTATCCGTTC		II
	R: AAAGGATGCAGCCCCTCAG		
InhibinβA	F: GAACGGGTATGTGGAGATAG		II
	R: TGAAATAGACGGATGGTGAC		
Tceal7	F: TTGTGGCAAGGAGAAGAGAAG		IV
	R: TGAAATTGCCTTCCAGTCGC		
Acvr2b		qMmuCID0015599	II
Cxcl1		qMmuCED0003898	IV
Cxcl5		qMmuCED0003886	IV
Follistatin		qMmuCID0022360	II
Scml4		qMmuCED0050877	IV
miR		**miScript Primer Assay ID**	**Study**
cel-miR-39-3p		MS00019789	IV
miR-1-3p		MS00008358	IV
miR-133a-3p		MS00031423	IV

F, forward sequence; R, reverse sequence

4.7.3 Sample preparation and RNA sequencing (IV)

Before the RNA sequencing libraries were prepared, genomic DNA was eliminated using dsDNase enzyme (EN0771, Thermo Scientific) after which the RNA concentration and integrity were measured with TapeStation (Agilent Technologies, Santa Clara, CA, USA). The libraries were created using QuantSeq 3´ mRNA-Seq Library Prep Kit for Ion Torrent (012.24A, Lexogen, Greenland, NH, USA) according to the manufacturer's protocols. To add the adapter sequences and generate enough material for sequencing, the libraries were amplified with the maximal number of cycles recommended (17 cycles) by the manufacturer. All the other steps were conducted according to the manufacturer's instructions.

Next, the DNA concentrations were measured using Qubit dsDNA HS Assay Kit (Invitrogen) followed by pooling of the barcoded libraries in equimolar concentrations (5 ng per sample). For the purification of the pool, 1.2x sparQ PureMag Beads (QuantaBio, Beverly, MA, USA) was used before running the samples on a High Sensitivity D1000 Screen Tape (Agilent Technologies) to verify the quality and the molarity of the samples. This step was followed by emulsion PCR run on OneTouch2 instrument with Ion PGM™ Hi-Q™ OT2 Kit (Life Technologies, Carslbad CA USA), following the protocol for 400-bp template according to the manufacturer's protocol to bind the template to Ion Sphere Particles. Finally, the Ion Sphere Particles were loaded into an Ion 318 v2 BC chip to be sequenced by an Ion Torrent Personal Genome Machine using Ion PGM™ Hi-Q™ View Sequencing Kit (Life Technologies).

4.7.4 RNA sequencing data analyses (IV)

The sequencing data analyses were conducted using Chipster software (https://chipster.csc.fi/). First, the quality of the two distinct runs of the same samples was analyzed using multiQC for many FASTQ files followed by combining of the files per sample from runs 1 and 2. Next, the reads were aligned to the genome using STAR for single end reads and HTSeq was used to count the number of aligned reads per gene. The differentially expressed genes (DEG) in different conditions were obtained using edgeR. From this step onwards, the data were analyzed using Gene Set Enrichment Analysis (GSEA) together with the fgsea R-package as previously described (Graber et al. 2021). The Molecular Signatures Database (https://gsea-mgsigdb.org) was used to obtain the databases needed for the GSEA analyses.

4.8 Protein analyses

4.8.1 Protein extraction (I-III)

Skeletal muscle (tibialis anterior) and cell lysates were homogenized in an ice-cold buffer containing 20 mM HEPES (pH 7.4), 1 mM EDTA, 5 mM EGTA, 10

mM $MgCl_2$, 100 mM β-glycerophosphate, 1 mM Na_3VO_4, 2 mM (muscles) or 1 mM (cell lysates) DTT, 1% NP-40 (muscles) or 1% TritonX-100 (cell lysates) and 3% Halt™ Protease and Phosphatase Inhibitor Cocktail (#1861280, Thermo Scientific). In Study I, following the homogenization muscle samples were agitated with vortex for 30 minutes at 4 °C prior to centrifugation for 10 minutes at 10 000 *g* at 4 °C. In studies II to IV, the cell homogenates were centrifuged for 5 minutes at 500 *g* (II, optimal to study protein synthesis) or for 10 minutes at 13 000 *g* (III, optimal for common signaling analyses). Supernatants were stored at -80 °C. In Study II, protein synthesis was analyzed using surface sensing of translation (SUnSET) method (Schmidt et al. 2009) in which puromycin was added to a final concentration of 1 μM 30 minutes prior to the cell lysis (Pekkala et al. 2015). Total protein content of the homogenates was measured by the Bicinchoninic Acid Protein Assay Kit (Pierce Biotechnology, Rockford, USA), with an automated KoneLab (I-II) or Indiko plus (III) analyzer (Thermo Scientific).

4.8.2 Western blotting (I-IV)

Skeletal muscle (30 μg) or cell (7-10 μg) homogenates were solubilized in Laemmli sample buffer containing 5% β-mercaptoethanol and the samples were heated at 95 °C for 10 minutes to denature the proteins. Due to the identical study design, protein homogenates extracted for Study III were also analyzed in Study IV. Criterion TGX (I) or Criterion TGX Stain-Free (II-IV) precast 4–20% gradient gels were used to separate proteins by SDS-PAGE in Criterion electrophoresis cell (Bio-Rad Laboratories, Hercules, CA, USA). The proteins were transferred to the PVDF membrane using Criterion blotter on ice at 4 °C (I) or when stain-free technology was used for the normalization (II-IV), the gels were activated under UV-light before blotting using Trans-Blot® Turbo™ Transfer System (II-IV) (BioRad Laboratories). After transfer, Ponceau S (I) or stain free (II-IV) images were obtained using ChemiDoc XRS or ChemiDoc MP device (Bio-Rad Laboratories), respectively. This step was followed by 2-hour blocking of the membranes in 5% non-fat dry milk (or for p-Smad3 in 5% bovine serum albumin, BSA) in Tris-buffered saline (TBS) with 0.1% Tween-20 (TBS-T) at RT. The primary antibodies (Table 3) were diluted in TBS-T containing 2.5% non-fat dry milk or 2.5% BSA (p-Smad3) and the membranes were probed overnight at 4 °C in gentle rocking. The next day, after TBS-T washes, the membranes were incubated with horseradish peroxidase-conjugated secondary antibodies (Jackson ImmunoResearch Laboratories, PA, USA) for 1 hour at RT followed by final TBS-T washes. For protein visualization, enhanced chemiluminescence (SuperSignal west femto maximum sensitivity substrate; Pierce Biotechnology) was used and the proteins were imaged using ChemiDoc XRS (I) or ChemiDoc MP (II-IV) device (Bio-Rad Laboratories). Proteins were quantified (band intensity × volume) with Quantity One software version 4.6.3 (I) or Image Lab software version 6.0 (II-IV) (Bio-Rad Laboratories). In Study I, GAPDH and Ponceau S were used as loading controls and the results were normalized to their mean value. In studies II to IV, a stain-free image was used as a loading control and the results were normalized by dividing the intensity of the analyzed band by the intensity of the whole stain-free lane.

TABLE 3 Primary antibodies used in Western blot.

Antibody	Manufacturer	Cat. No.	Dilution	Study
GAPDH	Abcam	ab9485	1:10 000	I
p-Smad 3 (Ser423/Ser425)	Abcam	ab52903	1:1000	II
Smad 3	Abcam	ab40854	1:1000	II
p-p38 (Thr180/Tyr182)	CST	4511	1:1000	II, III
p38	CST	9212	1:1000	II, III
p-ACC (Ser79)	CST	3661	1:2000	III
p-Akt (Ser473)	CST	9271	1:1000	II
Akt	CST	4691	1:1000	II
p-AMPK (Thr172)	CST	2531	1:1000	III
ATGL	CST	2138	1:1500	I
p-C/EBPβ (Thr235)	CST	3084	1:1000	II
C/EBPβ	CST	3082	1:1000	II
p-ERK1/2 (Thr202/Tyr204)	CST	9101	1:1000	II, III
ERK1/2	CST	9102	1:1000	II, III
p-HSL (Ser660)	CST	4126	1:1000	I
HSL	CST	4017	1:1000	I
p-NF-κB (Ser536)	CST	3033	1:1000	IV
p-SAPK/JNK1/2 (Thr183/Tyr185)	CST	4668	1:1000	II, III
SAPK/JNK1/2	CST	9252	1:1000	II, III
p-STAT3 (Tyr705)	CST	9145	1:1000	II
STAT3	CST	9139	1:1000	II
MF 20 concentrate	DSHB	AB 2147781	1:3000	IV
Follistatin	LSBio	LS-B14665	1:1000	II

ACC, acetyl-CoA carboxylase; Akt, Akt kinase/protein kinase B; AMPK, AMP-activated protein kinase; ATGL, adipose triglyceride lipase; Cat. No, catalogue number; C/EBPβ, CCAAT-enhancer-binding proteins; CST, Cell signaling Technology; ERK1/2, extracellular signal-regulated protein kinases 1/2; GAPDH, glyceraldehyde 3-phosphate dehydrogenase; HSL, hormone sensitive lipase; LSBio, Lifespan Biosciences; NB, Novus Biologicals; p, phosphorylated; SAPK/JNK1/2, stress-activated protein kinase/c-Jun N-terminal kinase 1/2; Smad3, mothers against decapentaplegic homolog 3; STAT3, signal transducer and activator of transcription 3.

4.8.3 Enzyme activity analysis (III)

In Study III, lactate dehydrogenase enzyme activity from the cell culture media was measured by lactate dehydrogenase assay kit (#981906 Thermo Scientific) according to the manufacturer's protocols with an automated Indiko plus analyzer (Thermo Scientific).

4.8.4 Cytokine analyses (III)

A multiplex cytokine assay (#115549MS, Q-Plex Mouse 4-plex Cytokine Panel, Quansys Biosciences, North West, UT, USA) and IL-6 Mouse ELISA Kit (#KMC0061, Thermo Scientific) were conducted according to the manufacturer's protocols. The cytokines and their detection limits in the 4-plex assay were IL-1β

(12.41 pg/ml), IL-6 (2.90 pg/ml), tumor necrosis factor α (3.40 pg/ml), and interferon γ (5.40 pg/ml). In IL-6 assay, the detection limit was < 3 pg/ml.

4.9 Lipid analyses

4.9.1 Triacylglycerol extraction (I)

The muscle triacylglycerol extraction was conducted as previously described (Bruce et al. 2007). Briefly, the muscle samples were pulverized using liquid nitrogen and a ~20 mg subsample was homogenized in 2:1 (v/v) chloroform-methanol solution on ice followed by mixing in rotatory shaker for 20 minutes at RT. After addition of 0.9% NaCl, the samples were centrifuged for 10 minutes at 382 *g* at RT. The lower phase was collected and evaporated at 70 °C using SpeedVac Concentrator (Thermo Scientific). The resulting lipid pellet was dissolved into absolute ethanol. The triacylglycerol concentration was measured by a Triglyceride kit (#981786, Thermo Scientific) using an automated KoneLab analyzer (Thermo Scientific).

4.10 Statistical analyses

In all studies, the statistical analyses were performed with IBM SPSS Statistics, version 24–26 for Windows (SPSS, Chicago, IL, USA) and the level of significance was set at $P < 0.05$ unless stated otherwise. The data were tested for normality (Shapiro-Wilk test) and equality of variances (Levene's test) when suitable. The data are expressed as means ± SEM unless stated otherwise.

Study I: Differences in the metabolites were analyzed after Benjamini-Hochberg corrected false discovery rate (FDR) corrections for multiple testing and the detected differences were considered significant when FDR < 0.05 and fold change (FC) > |1.2|. The multiple group comparisons from the tumor-bearing mice groups were performed by Holm-Bonferroni corrected *t*-tests or a non-parametric Mann-Whitney *U*-test depending on normal distribution of the variables. The comparisons of two groups (C26+PBS vs. CTRL or CTRL vs. tumor-bearing groups pooled) were performed by using a two-tailed unpaired Student's *t*-test or non-parametric Mann-Whitney *U*-test depending on normal distribution of the variables. In cases lacking the sACVR2B-Fc administration effect, pooling of the tumor-bearing mice (referred as C26-effect) was justified. Pearson correlation coefficient was used to study correlations.

Study II: For the statistical evaluation, a two-tailed paired or unpaired Student's *t*-test or Mann Whitney *U*-test were used depending on normal distribution of the variables. In cases lacking myostatin effect, pooling of the groups was conducted.

Studies III–IV: In the case of metabolomics (III), enzyme activity analysis (III), cell lysate RT-qPCR (III–IV), and Western blot (III–IV), the interaction and main effects were analyzed using the two-way multivariate analysis of variance (two-way MANOVA), while multivariate Tukey's test was used for group comparisons. In the case of miRNA RT-qPCR, a Mann Whitney *U*-test was used to analyze group comparisons and the effects of EL-EPS and media glucose content (IV). In Study IV, extreme outliers in RT-qPCR analyses were removed based on Grubbs' test (https://graphpad.com). Correlations were analyzed with Spearman's correlation coefficient (III). For the analyses of the differentially expressed genes (DEG), the significance was set, using Benjamini-Hochberg procedure, at FDR < 0.05 for multiple comparisons and FC > |1.2| (IV).

5 RESULTS

5.1 The effects of cachexia and blockade of myostatin and activins (I)

5.1.1 Skeletal muscle metabolome

This study was a part of a larger project which showed that, along with improving survival, the blockade of myostatin and activins by the soluble ACVR2B-Fc (sACVR) administration reversed the C26 cancer-induced skeletal muscle atrophy and restored protein synthesis level, while the tumor mass remained unaffected by the sACVR (Nissinen et al. 2018).

The MS-based metabolomics resulted in the identification of 219 individual metabolites in total from both skeletal muscle and serum. These 156 metabolites were detected in more than 30% of the animals, thus approving them for the further analyses from both data sets. In the skeletal muscle, the C26 cancer alone (C26 + PBS vs. CTRL) and the C26 effect (i.e., C26 pool vs. CTRL) resulted in 23 and 39 significantly altered metabolites, respectively, of which 19 metabolites were shared among the groups (Figure 6A). The C26 cancer induced changes in six biologically functional groups including 1) amino acids and their derivatives, 2) energy metabolism related metabolites, 3) amides and amines, 4) nucleotides, 5) vitamins and hormones and 6) others (C26 effect, Figure 6B). Overall, the effect of the C26 cancer on the studied metabolites was more pronounced than the sACVR administration effect (sACVR pool vs. C26 + PBS), especially in amino acids and energy metabolism related metabolites (Figure 6C-D). That being said, increased sACVR effect was observed in nine and decreased effect in three metabolites (Figure 6E).

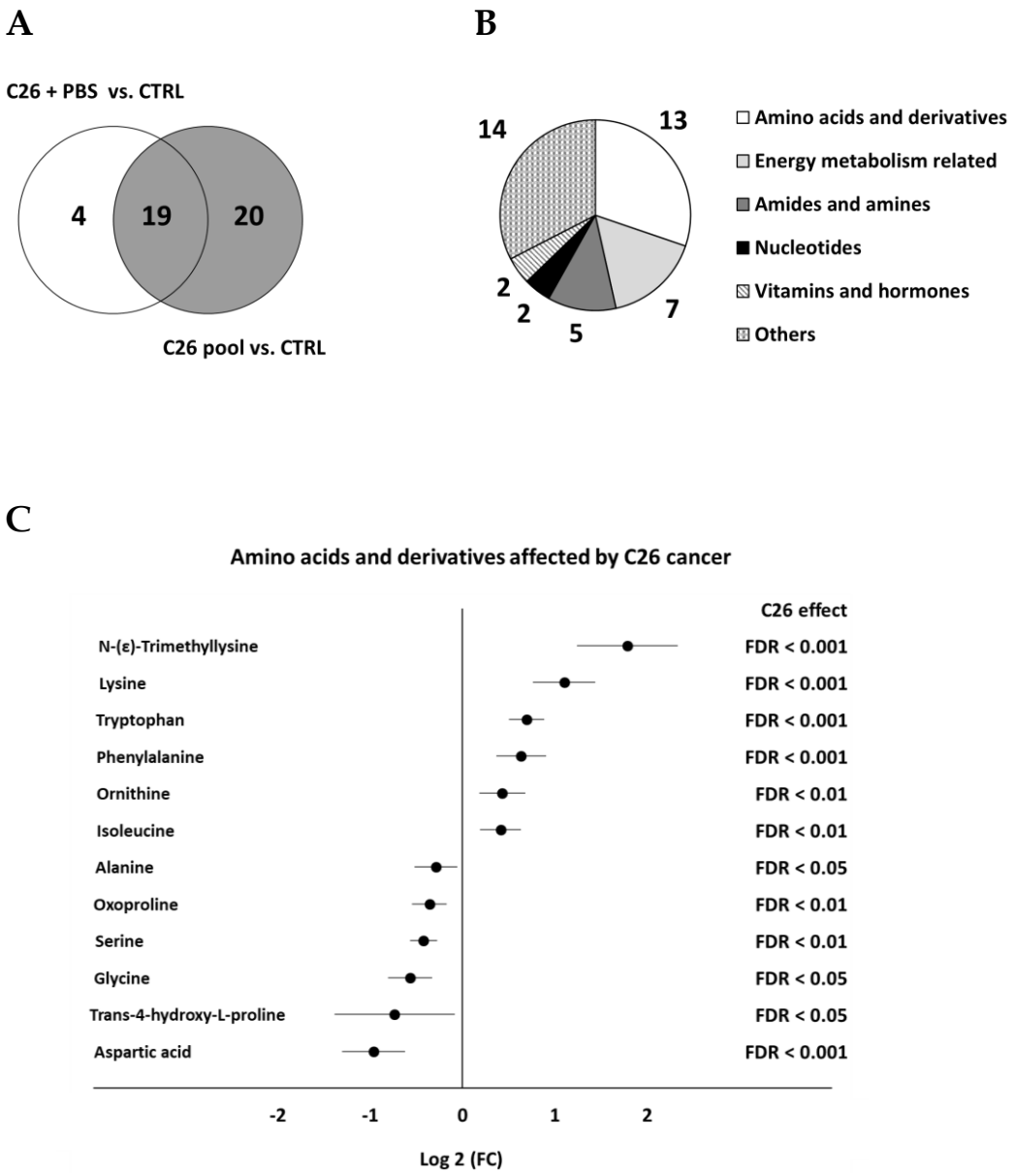

FIGURE 6 The effects of C26 cancer on skeletal muscle metabolome. *Continued on the next page.*

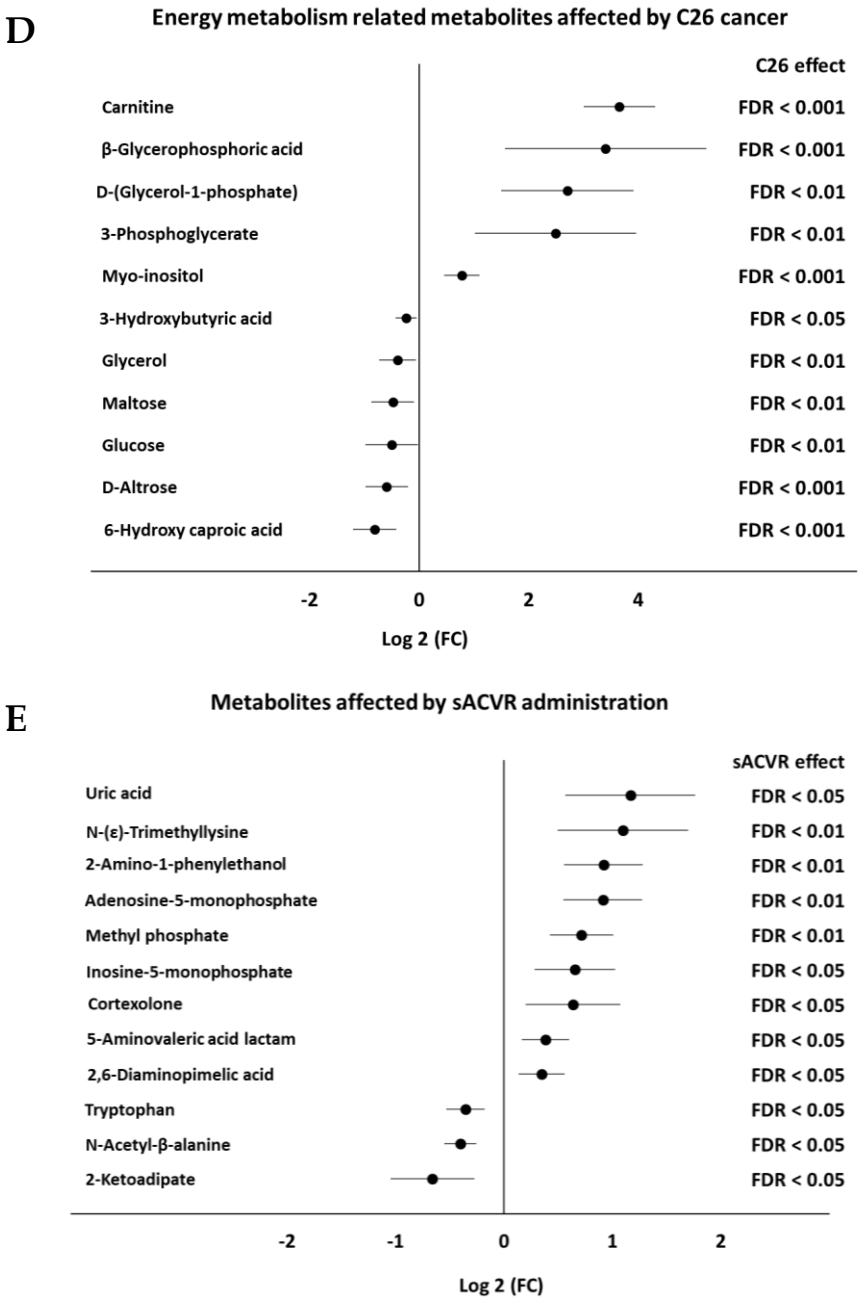

FIGURE 6 The effects of C26 cancer on skeletal muscle metabolome. (A) Venn graph of the altered metabolites. (B) Biologically functional groups affected by the C26 cancer. Forest plots of the skeletal muscle (C) amino acids and related derivatives and (D) energy metabolism related metabolites altered in C26 cancer. Forest plot of the (E) metabolites altered by the sACVR administration (sACVR pool vs. C26 + PBS). Data are presented as logarithmically transformed fold changes (Log 2 FC) and 95% confidence intervals are calculated using a *t*-test–based formula. Group differences were analyzed with false discovery rate-corrected Student's *t*-test. The N sizes are in parenthesis: CTRL (15), C26 + PBS (13), C26 + sACVR/b (7), and C26 + sACVR/c (13). sACVR, soluble activin receptor type 2B; sACVR/b, sACVR administration before C26 injection; sACVR/c, sACVR administration before and after C26 injection.

5.1.2 Skeletal muscle lipid metabolism

Because the C26 cancer affected metabolites related to lipid metabolism (e.g., fatty acid transporter carnitine and glycerol derivatives), the present study examined whether the lipid content in the skeletal muscle was affected as well. In agreement with the metabolomics, the triacylglycerol content was lower in the skeletal muscle (C26 effect, $P < 0.01$), while the protein content of the adipose triglyceride lipase (ATGL) and phosphorylated hormone sensitive lipase (HSL) were higher (Figure 7).

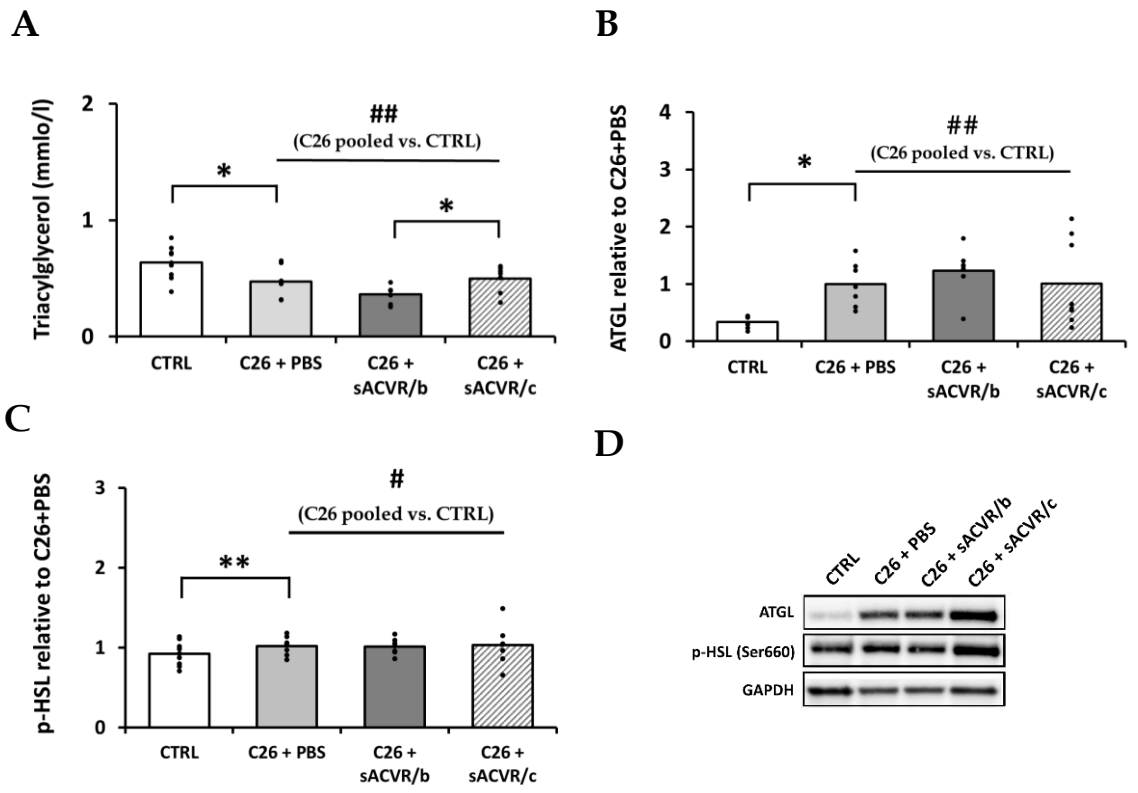

FIGURE 7 Lipid metabolism in the skeletal muscle was affected by the C26 cancer. (A) Triacylglycerol concentration in gastrocnemius. (B) Adipose triglyceride lipase (ATGL) and (C) phosphorylated hormone sensitive lipase (HSL) in tibialis anterior. (D) Representative blots. In A-B, the values are presented as normalized to C26 + PBS = 1. * and ** = $P < 0.05$ and $P < 0.01$, respectively. # and ## = C26 pooled vs. CTRL, $P < 0.05$ and $P < 0.01$, respectively. Student's *t*-test was used to analyze C26 + PBS vs. CTRL and C26 pool vs. CTRL. Individual comparisons were analyzed by Holm-Bonferroni-corrected Student's *t*-test. The N sizes are in parenthesis: CTRL (9), C26 + PBS (7), C26 + sACVR/b (7), and C26 + sACVR/c (8). sACVR, soluble activin receptor type 2B; sACVR/b, sACVR administration before C26 injection; sACVR/c, sACVR administration before and after C26 injection.

5.1.3 Serum metabolome

Besides skeletal muscle, the serum metabolomes of the mice were examined to verify whether the C26 cancer effect also overruled the sACVR effect on a systemic level. In parallel to the skeletal muscle, serum analysis demonstrated that the C26 effect sis dominate the changes in the blood metabolome even more than it did in the skeletal muscle. The C26 cancer alone and the C26 effect resulted in 13 and 20 significantly altered metabolites, respectively, while no sACVR effects were observed (Figure 8A). The altered metabolites belonged to (1) fatty acids and energy sources, (2) amino acids and (3) others (Figure 8B), the C26 cancer mainly decreasing their content (Figure 8C–D).

Finally, to examine whether any of the identified metabolites would correlate with the loss of body mass and thus would possibly act as a marker of cachexia and muscle atrophy, Pearson correlation analyses were conducted. The results demonstrated that the loss of body mass within the last two days prior to sample collection correlated strongly with skeletal muscle ($r = -0.837$, $P < 0.001$) and serum phenylalanine ($r = -0.899$, $P < 0.001$) contents (Figure 8E).

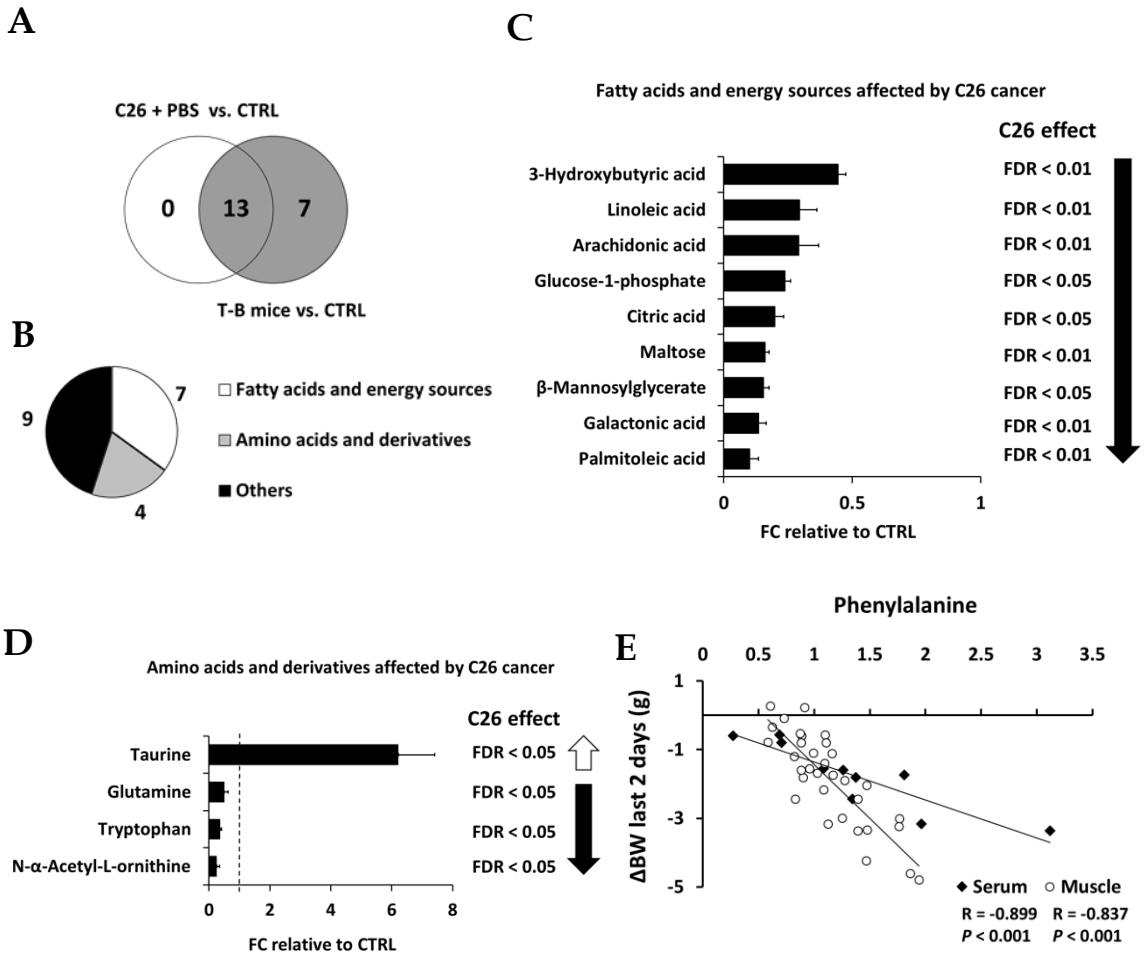

FIGURE 8 The effects of the C26 cancer on serum metabolome. (A) Venn graph of the altered metabolites. (B) Biologically functional groups affected by the C26 cancer. Fold changes (FC) of the serum (C) fatty acids and energy sources and (D) amino acids and derivatives in C26 cancer (C26 pool vs. CTRL). In the figures, CTRL = 1 (dashed line in D) and only the FC of the tumor-bearing (T-B) mice is shown. Arrows depict the direction of the change relative to CTRL. In A–C, false discovery rate (FDR)-corrected Student's *t*-test was used. (D) Pearson correlation between muscle and serum phenylalanine and loss of body mass (ΔBM) in tumor-bearing mice within the last 2 days before tissue collection. The N sizes for serum in A–D were as follows: CTRL (N = 15), C26 + PBS (N = 13), C26 + sACVR (N = 13). In E, muscle N sizes were as follows: C26 + PBS (N = 13), C26 + sACVR/b (N = 7) and sACVR/c (N = 13). sACVR, soluble activin receptor type 2B; sACVR/b, sACVR administration before C26 injection; sACVR/c, sACVR administration before and after C26 injection.

5.2 Direct effects of myostatin on muscle cells (II)

5.2.1 Signaling pathways

This study was conducted as a continuum of the *in vivo* cancer experiments. The aim was to develop an *in vitro* model to study the direct effects of myostatin and other ACVR ligands on skeletal muscle cells at a molecular level. The focus was on myostatin because it is a well-known regulator of muscle size and may act as a tumorkine, thus promoting muscle atrophy.

Differentiated murine C2C12 cells were used as an *in vitro* model of skeletal muscle. However, because the chosen method created a culture of cells in distinct differentiation stages, the effects of 100 ng/µl myostatin administration on both myoblasts and myotubes to analyze whether the observed responses were dependent on the differentiation stage were examined. Analysis of the canonical (Smad-dependent, Smad3) and non-canonical (Smad-independent, MAPKs) signaling pathways demonstrated that myostatin had (1) greater effects on myoblasts than on myotubes and that (2) short-term exposure was more effective to upregulate Smad-dependent and Smad-independent pathways than long-term exposure was (Table 4). In contrast, the co-culture of the C26 cancer cells and C2C12 myoblasts and myotubes as an in vitro model of tumorkine burden on skeletal muscle resulted in similar responses to canonical, non-canonical and inflammatory (signal transducer and activator of transcription 3 and CCAAT-enhancer-binding proteins) signaling independent of the differentiation stage (Table 4).

To increase the understanding of how the C2C12 myoblast differentiation is regulated and whether this could affect the responsiveness of the cells to myostatin, the mRNA expression of common ACVR ligands, their receptor (ACVR2B) and follistatin, an endogenous blocker of myostatin, were analyzed. Endogenous levels of ACVR ligands and follistatin were increased, while ACVR2B expression remained unaltered in myotubes (Table 4). Furthermore, the protein content of follistatin increased in the C2C12 myotubes in comparison to myoblasts (Figure 9).

Next, human CHQ myoblasts and myotubes were exposed to myostatin to investigate whether the reduced effects on Smad3 and MAPKs signaling were cell line and origin specific. In the CHQ cells, the responsiveness was maintained in both differentiation stages and in contrast to the C2C12 cells, the mRNA of the ACVR ligands and follistatin as well as protein content of follistatin remained unaltered during differentiation (Table 4, Figure 9). Myostatin administration had no effect on follistatin protein content in either cell line (Figure 9).

TABLE 4 The effects of the short- (2 h) and long-term (24 h) myostatin administration on C2C12 and CHQ myoblasts (MB) and myotubes (MT). The effects of 24-hour co-culture of C2C12 MB and MT with C26 cells is depicted as C26. Due to the lack of significant changes in total protein contents, they are not presented in the table. For statistical analyses, a two-tailed paired or unpaired Student's *t*-test or Mann Whitney *U*-test were used. N = 6–8 per group in protein and N = 3 per group in mRNA experiments. ↑, ↑ ↑ and ↑ ↑ ↑ = $P < 0.05$, $P < 0.01$ and $P < 0.001$, respectively.

Protein	C2C12 MB	C2C12 MT	CHQ MB	CHQ MT
p-p38	2h: ↑↑	2h: ↑, C26: ↓	2h: ↑↑	2h: ↑
p-ERK1/2	2h: ↑	-	2h: ↑	24h: ↑↑
p-SAPK/JNK1/2	2h: ↑↑	-	2h: ↑	24h: ↑↑
p-C/EBPβ	2h: ↑↑, C26: ↑	C26: ↑↑	-	-
p-Smad3	2h: ↑↑↑, C26: ↓	2h: ↑↑, C26: ↓	2h: ↑↑	2h: ↑↑, 24h: ▲
p-STAT3	2h: ↑↑↑, C26: ↑↑↑	2h: ↑↑, C26: ↑↑	24h: ↑↑↑	-
Follistatin*		↑↑↑		↔
mRNA				
*Acvr2b**		↔		↔
*Follistatin**		↑		↔
*Gf8**		↑↑↑		▼
*Gdf11**		↑↑↑		↔
*InhibinβA**		↑↑↑		↓↓

ACVR2B, activin type 2B receptor; C/EBPβ, CCAAT-enhancer-binding proteins; ERK1/2, extracellular signal-regulated protein kinase 1/2; GDF8; myostatin/growth differentiation factor 8; GDF11, growth differentiation factor 11; InhibinβA, activin A; NA, not analyzed; p, phosphorylated; SAPK/JNK1/2, stress-activated protein kinase/c-Jun N-terminal kinase 1/2; STAT3, signal transducer and activator of transcription 3; * = myotubes vs. myoblasts; ▲ = increasing trend; ▼= decreasing trend; -, unaltered result.

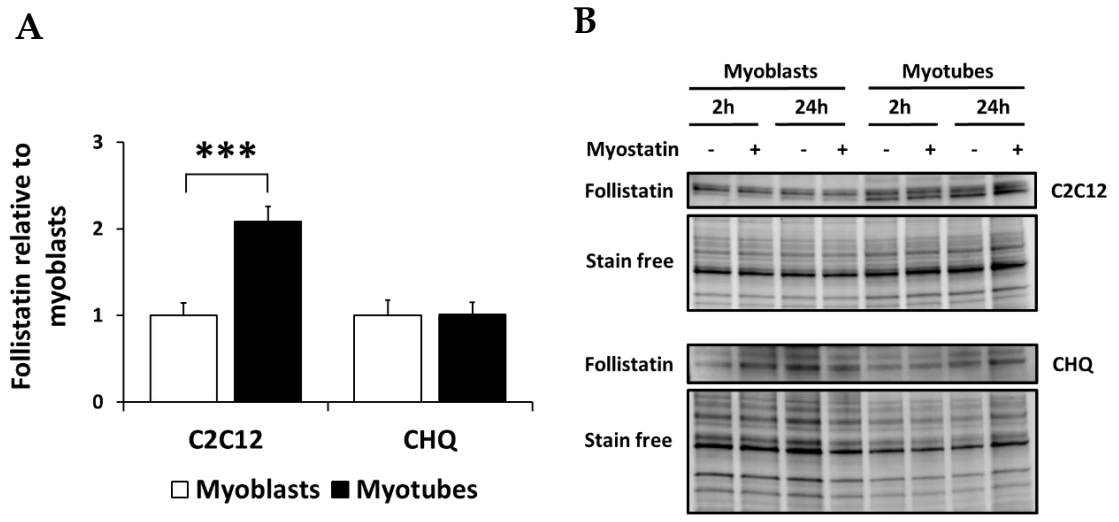

FIGURE 9 (A) Follistatin protein content in the C2C12 and CHQ myoblasts and myotubes. In A, the values are normalized to myoblasts = 1. (B) Representative blots. *** = $P < 0.001$. Due to the lack of myostatin effect, control (-) and myostatin (+) samples were pooled, resulting in N = 12 per group. Student's *t*-test was used for statistical analyses.

5.3 Contraction-induced changes on muscle cell metabolism (III, IV)

5.3.1 Validation of the C2C12 myotube contraction protocol

The murine C2C12 myotubes were used as an *in vitro* model of increased physical activity (exercise-like contracted myotubes) and inactivity (non-contracted myotubes) to compare the changes at the molecular level as well as in signaling pathways between conditions that promote disease progression/atrophy (studies I & II) or health/cell-cell crosstalk (studies III & IV). Chronic low-frequency exercise-like electrical pulse stimulation (EL-EPS) was applied to the C2C12 myotubes (1 Hz, 12 V, 2 ms) and the contractions were visualized under a bright-field microscope. The analyses of the common exercise-induced changes, such as increased phosphorylation of AMPK and ACC as well as IL-6 secretion (Nikolić et al. 2017) demonstrated that our pilot experiments reproduced similar physiological changes as *in vivo* exercise (Figure 10A-C). Based on the medium lactate dehydrogenase activity as a marker of possible sarcolemma damage, the applied EL-EPS had no adverse effects on the cell viability, while the cells grown under high glucose conditions may be more viable. Thus, only pooled results are presented (Figure 10D).

5.3.2 Myotube and medium metabolome

The C2C12 myotube and media as well as cell-free media metabolomes were analyzed after the EL-EPS using highly quantitative ^{1}H-NMR-based metabolomics. The cells were grown under high and low glucose conditions to examine the effect of nutrient availability on the myotube metabolism, signaling pathways and exerkine secretion during physical activity and inactivity. Overall, 39 and 37 metabolites were identified from the cells and the media, respectively, of which 37 and 34 were detected in > 50% of the samples, thus meeting the reporting threshold for further analyses (Figure 11A). Of these, 24 metabolites were identified from both the cells and the media. The analyzed metabolites belonged to four biologically functional groups including (1) energy-related metabolites, (2) short and branched chain fatty acids (S/BCFAs) and ketone bodies, (3) amino acids and related derivatives, and (4) vitamins and others (Figure 11A). Importantly, the EL-EPS had no effects on the cell-free media metabolome (Figure 11B).

Of the energy metabolism-related metabolites, EL-EPS enhanced the utilization of glucose and phosphocreatine as inferred from their decreased contents in the media and in the cells, respectively (Figure 11C-D). Glycolysis was enhanced during the EL-EPS based on the increased lactate production and secretion (Figure 11F). Additionally, the content of acetate, a potential fuel source during exercise (Hargreaves & Spriet 2020) was increased in the cells and in the media, while the ketone body 3-hydroxybutyrate increased in the media after the EL-EPS (Figure 11E, G).

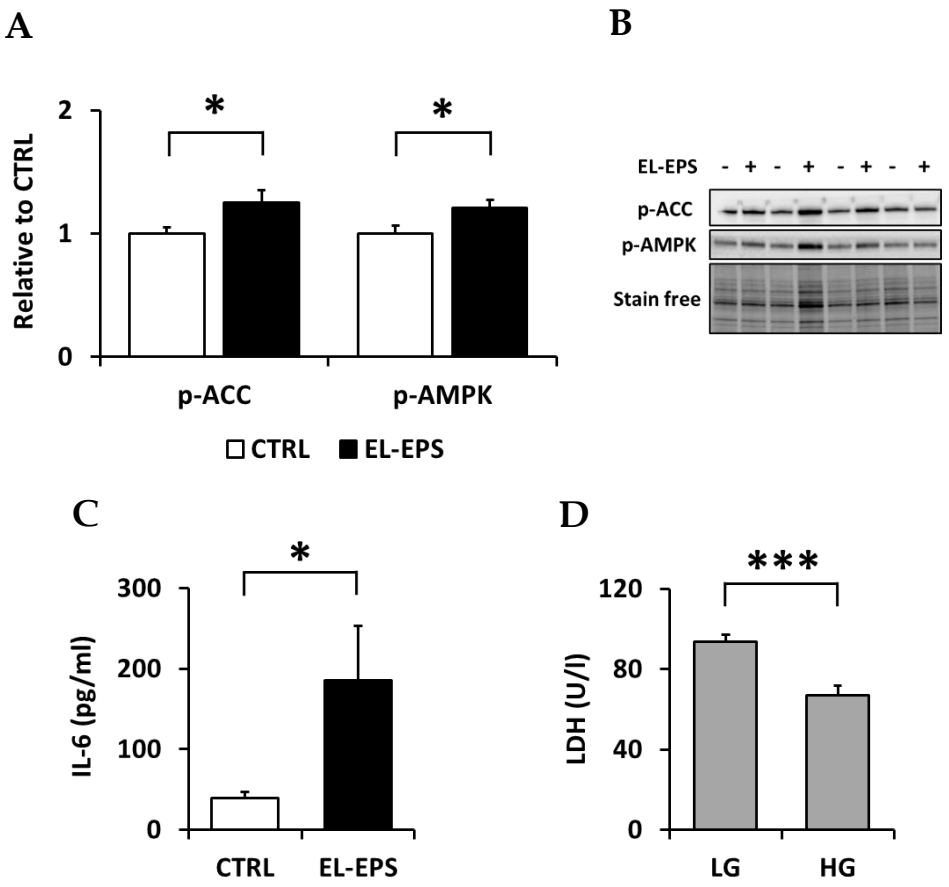

FIGURE 10 The results from the C2C12 pilot experiments using low-frequency exercise-like electrical pulse stimulation (EL-EPS) protocol. (A) Phosphorylated ACC and AMPK. In A, the values are presented as normalized to CTRL = 1. N = 7 per group. -, CTRL; +, EL-EPS. (B) Representative blots. (C) Interleukin-6 (IL-6) medium content, N = 4 per group. (D) Lactate dehydrogenase (LDH) enzyme activity from the C2C12 media. Due to the lack of EL-EPS effect, stimulated and non-stimulated samples were pooled, N = 12 per group. Statistical analyses were conducted as follows, in A and D Student's *t*-test. In B, Mann-Whitney *U*–test was used. * = $P < 0.05$ and *** = $P < 0.001$. In A–C, a high glucose media was used, while in D low and high glucose media (LG and HG, respectively) were used.

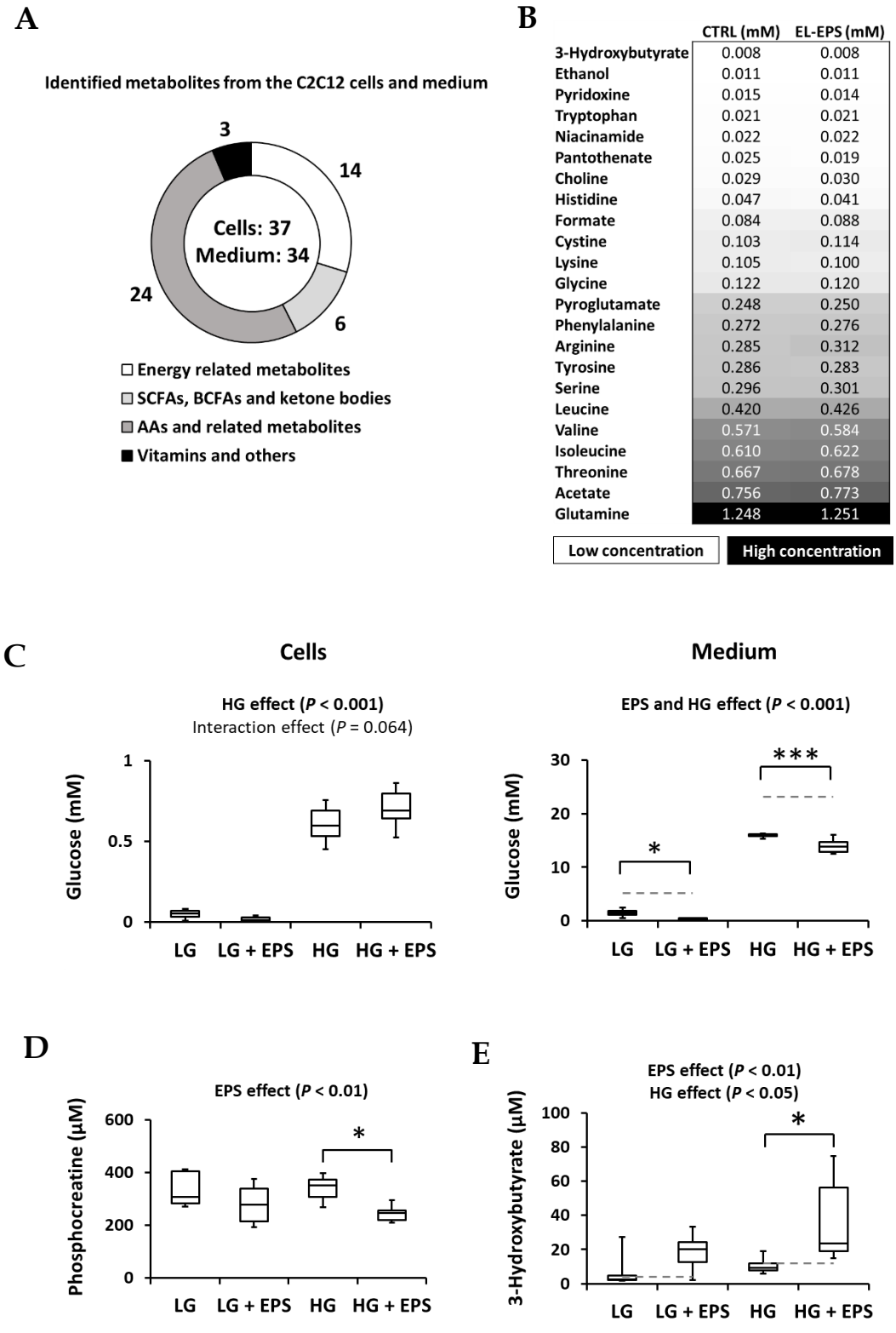

FIGURE 11 The effects of exercise-like electrical pulse stimulation (EL-EPS) on myotube and media metabolomes. *Continued on the next page.*

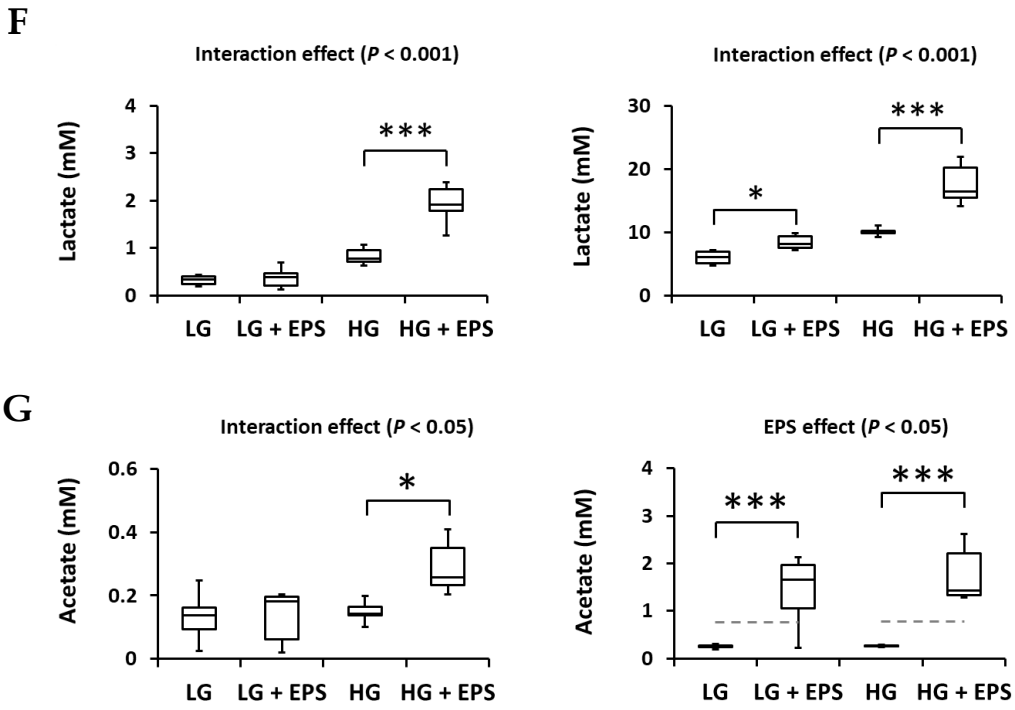

FIGURE 11 The effects of exercise-like electrical pulse stimulation (EL-EPS) on myotube and media metabolomes. (A) The number and biological groups of identified metabolites. (B) Heat map of the metabolites identified from the non-stimulated (CTLR) and stimulated (EL-EPS) cell-free fresh media controls. The low (LG) and high (HG) glucose samples were pooled except for glucose and myo-inositol due to their distinct concentrations between the media and thus they are not presented in the heat map. (C) Glucose, (D) phosphocreatine, (E) 3-hydroxybutyrate, (F) lactate and (G) acetate contents in the cells and/or in the media. For the analysis of the EL-EPS and media glucose content (EPS and HG effects, respectively) and their interaction effect, the two-way MANOVA was used. The group comparisons were analyzed with multivariate Tukey's test. * = $P < 0.05$ and *** = $P < 0.001$. N = 6–8 per group.

Interestingly, the intra- and extracellular content of the branched chain fatty acids (BCFA) were increased after the EL-EPS independent of the media glucose availability (Figure 12A-B). The BCFAs (2-methylbutyrate, isobutyrate and isovalerate) originate from the catabolism of branched chain amino acids (BCAA), which were also increased in the myotubes after the EL-EPS (Figure 12A-B). In agreement with the observed increases in other biological groups, amino acids other than BCAA were also increased in the myotubes after the EL-EPS (Figure 13A-B). Overall, the effect of EL-EPS on detected amino acids in the myotubes and media were greater than the effect of media glucose content.

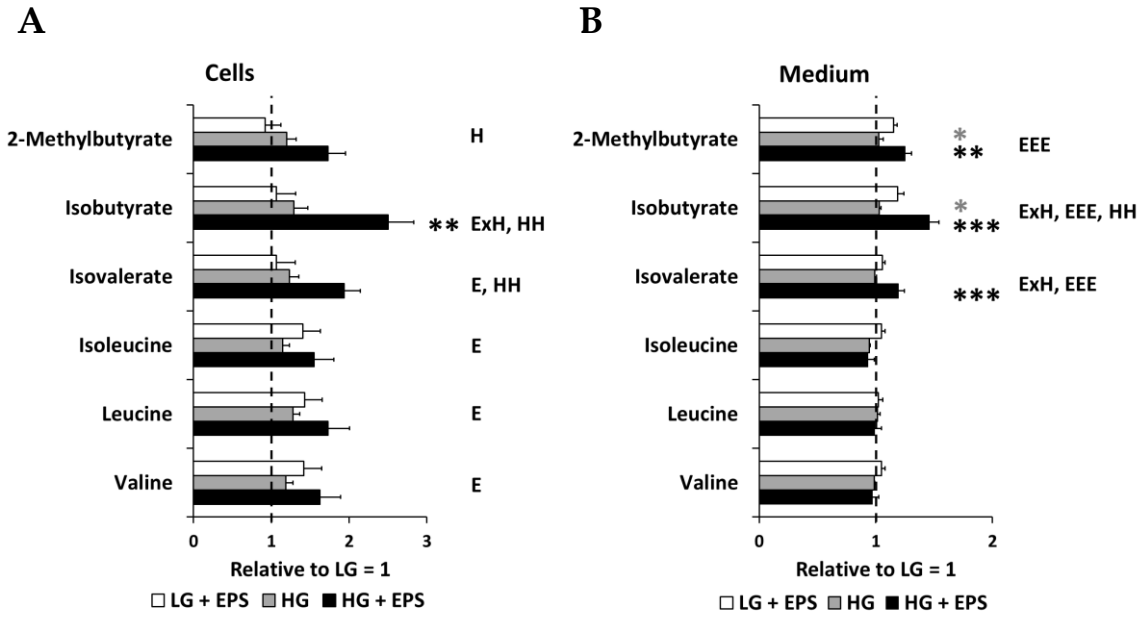

FIGURE 12 Branched chain fatty acids and branched chain amino acids (A) in the myotubes and (B) in the media. Data are presented as fold changes relative to low glucose (LG), which is set as 1 (dashed line). Gray stars represent multivariate Tukey's *t*-test, LG + EPS vs. LG and black stars represent HG + EPS vs. HG. * = P < 0.05, ** = P < 0.01, *** = P < 0.001, respectively. The two-way MANOVA results of the EL-EPS, media glucose content and their interaction effect are presented as letters (E, H and ExH, respectively). One letter = P < 0.05, two letters = P < 0.01 and three letters = P < 0.001. HG = high glucose, N = 6–8 per group.

Intracellular metabolism of the common exercise-inducible markers, the phosphorylation of SAPK/JNK1/2, but not the other MAPKs (p-p38 and p-ERK1/2, data not shown) as well as secretion of IL-6 were increased after the EL-EPS independent of the glucose availability (Figure 14A-C). In contrast, oleate oxidation was higher in high glucose conditions, while EL-EPS further decreased it in these highly glycolytic C2C12 cells (Figure 14D).

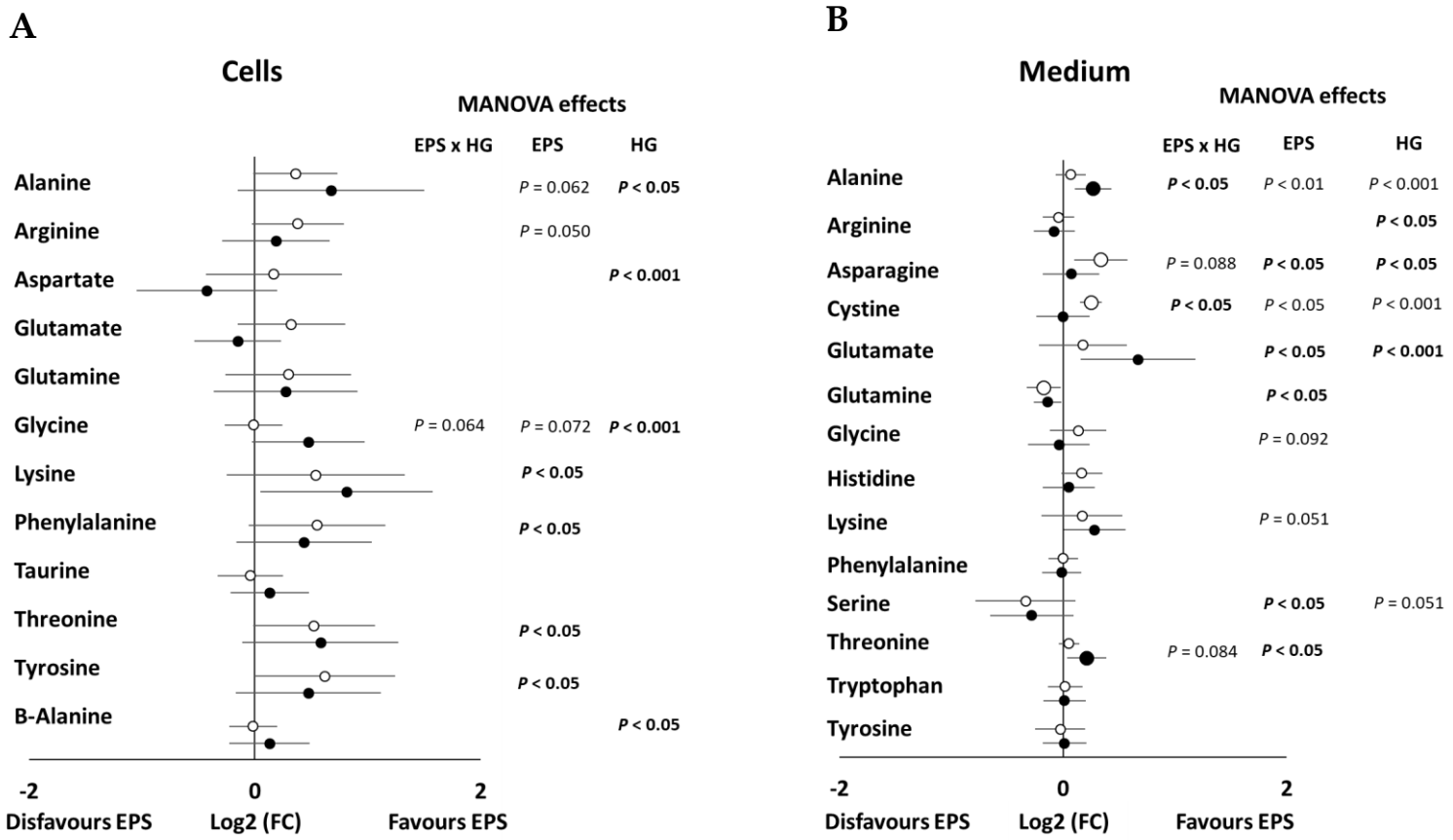

FIGURE 13 Forest plots of the amino acids (A) in the myotubes and (B) in the media. The data are presented as logarithmically transformed fold changes (Log2 FC). The 95% confidence intervals are presented as error bars of the analyzed groups (LG and LG + EPS or HG and HG + EPS). The two-way MANOVA, i.e., EL-EPS effect (EPS) and glucose effect (HG), as well as interaction effect (EPS x HG) are presented on the right. Open circles = low glucose samples, black circles = high glucose samples. Larger circles represent significant group comparisons analyzed by multivariate Tukey's test. N = 6–8 per group.

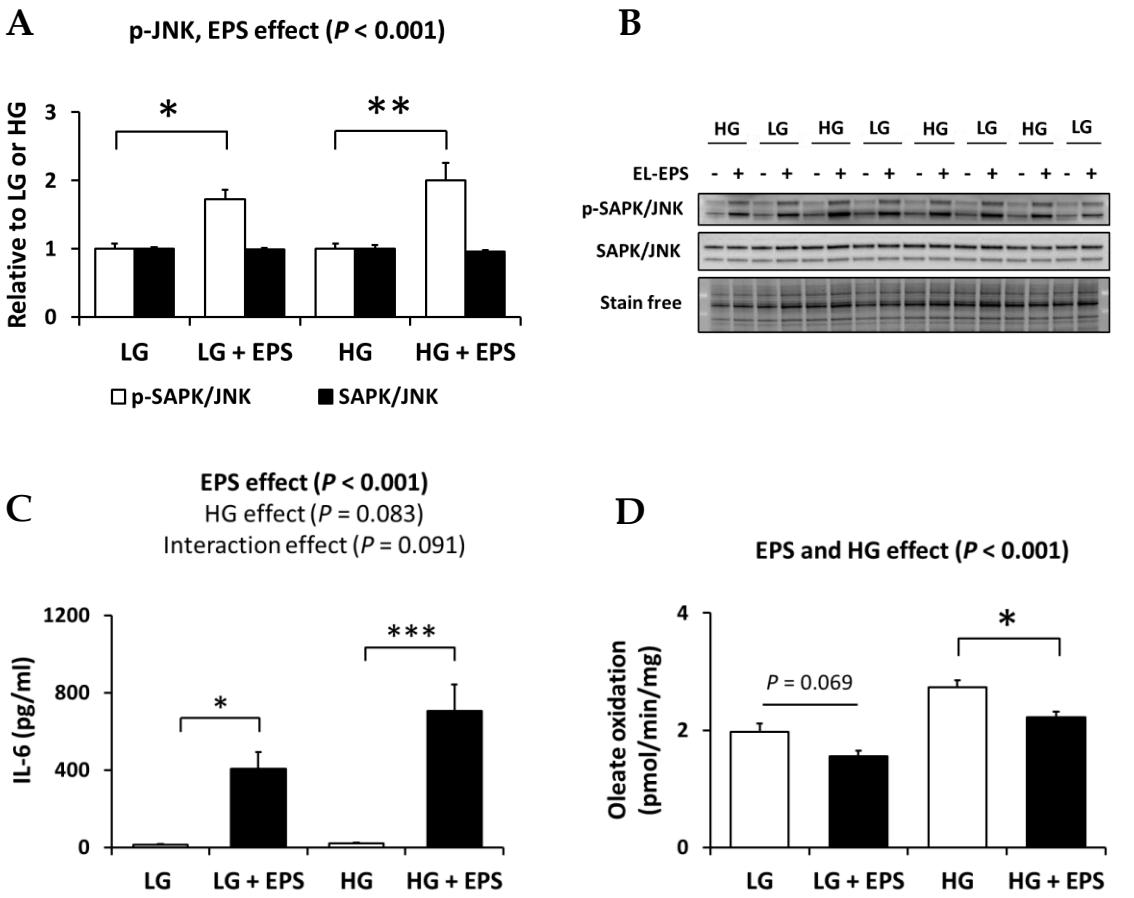

FIGURE 14 The effects of exercise-like electrical pulse stimulation (EL-EPS) on signaling pathways and exerkine secretion. (A) Phosphorylated stress-activated protein kinase/c-Jun N-terminal kinase (SAPK/JNK)1/2 and total SAPK/JNK1/2. (B) Representative blots. (C) Interleukin-6 (IL-6) concentration in the media. (D) Oleate oxidation measured as $^{3}H_2O$ released to the media. In A, the values are presented as normalized to LG or HG = 1. The two-way MANOVA was used to analyze main effects, i.e., EL-EPS effect (EPS) and glucose effect (HG), as well as interaction effect (EPS x HG). The group comparisons were analyzed by Tukey's test. In A–C, N = 6 per group. In D, N = 8–10 per group. * = P < 0.05, *** = P < 0.001, respectively. LG, low glucose; HG, high glucose; -, no EL-EPS; +, EL-EPS.

5.3.3 Myotube transcriptome

The analysis of the C2C12 myotube transcriptome was conducted as a continuum of the metabolomics study. The experimental procedures were identical between the two studies.

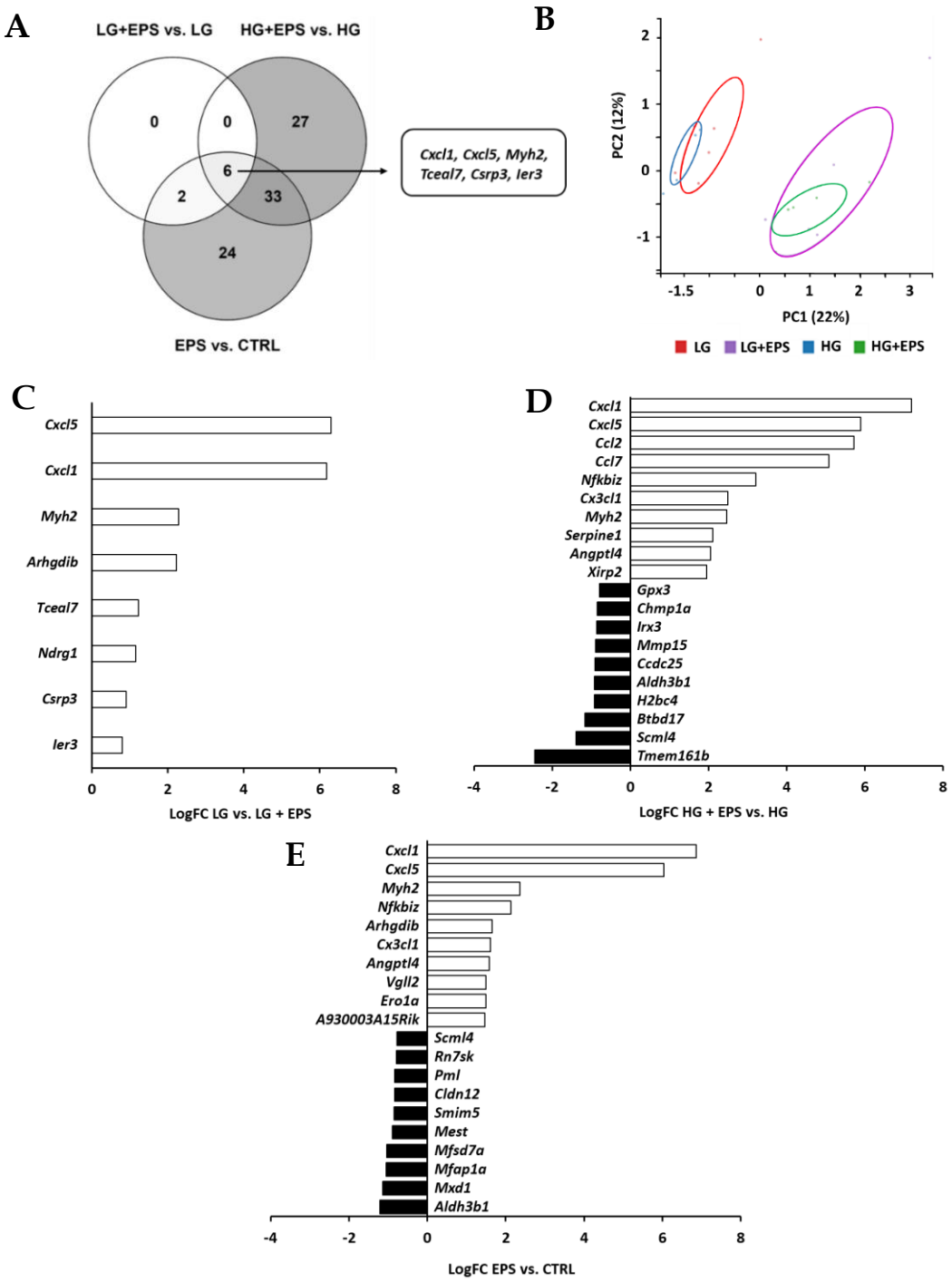

FIGURE 15 The effects of exercise-like electrical pulse stimulation (EL-EPS) on the C2C12 transcriptome. (A) Venn graph of the differentially expressed genes (DEGs). (B) The principal component (PC) analysis score plot normalized by min max without transform or scaling. The top 8–10 up- and downregulated DEGs in (C) low and (D) high glucose conditions (LG and HG, respectively) as well as (E) in response to the EL-EPS (pool of EPS vs. CTRL). In the figures, false discovery rate (FDR) < 0.05 and logarithmically transformed fold change (LogFC) > $|1.2|$. N = 5 per group. The Visualization and Integration of Metabolomics Experiments software https://viime.org (Choudhury et al. 2020) was utilized for the illustration of the PCA score plot.

The average number of reads per sample was 346 191, resulting, on average, in 255 387 genes per sample. Overall, 15 273 transcripts were identified from the C2C12 myotubes. Of these, using rather stringent criteria (FDR < 0.05 for multiple testing and FC > |1.2|), 8 and 66 differentialy expressed genes (DEGs) were identified from the low and high conditions in response to the EL-EPS, respectively (Figure 15A). The stimulation effect alone (pool of the stimulated vs. non-stimulated samples, i.e., EPS vs. CTRL) resulted in 65 DEGs. Furthermore, six DEGs were shared between these three comparisons (*Cxcl1*, *Cxcl5*, *Myh2*, *Tceal7*, *Csrp3* and *Ier3*). The principal component analysis demonstrated a clear separation between the stimulated and the non-stimulated groups, but less separation between the high and low glucose conditions (Figure 15B). The top 8–10 most altered DEGs in each condition are presented in Figure 15C–E. Under the low glucose condition, all of the eight DEGs were upregulated, while under the high glucose condition 50 DEGs were upregulated and 16 downregulated. The EL-EPS effect resulted in 50 upregulated and 15 downregulated DEGs.

The RNA-seq results were further validated by analysing the expression of the few of the most up- and downregulated genes by RT-qPCR. The results demonstrate that the expressions of *Cxcl1*, *Cxcl5* and *Tceal7* were increased and *Scml4* almost significanlty decreased, as was shown by the RNA-seq (Figure 16).

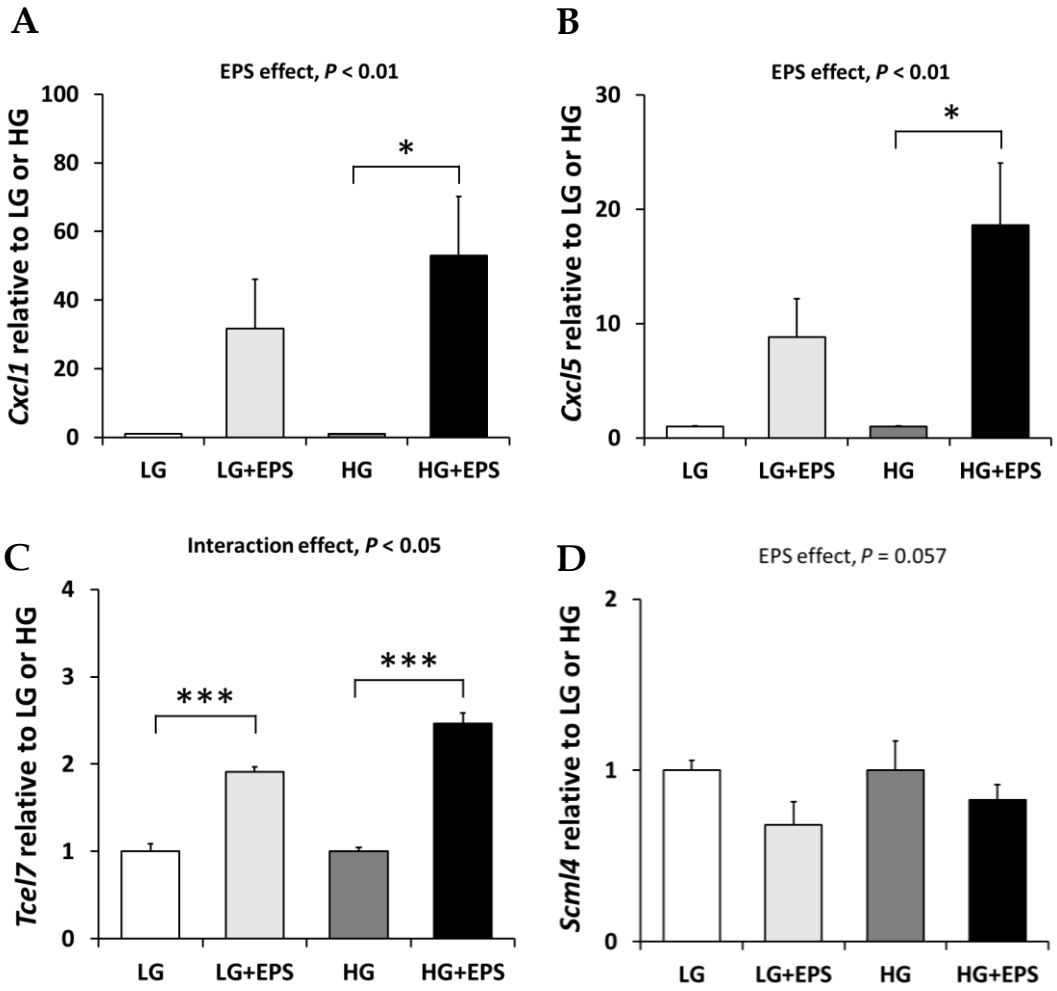

FIGURE 16 The effects of exercise-like electrical pulse stimulation (EL-EPS) on the expression of (A) *Cxcl1*, (B) *Tceal7*, (C) *Cxcl5* and (D) *Scml4*. The data are presented as normalized to low (LG) or high (HG) glucose = 1. For the analysis of the EL-EPS and media glucose effect (EPS and HG effects, respectively) and their interaction effect, the two-way MANOVA was used. The group comparisons were analyzed with multivariate Tukey's test. * = P < 0.05 and *** = P < 0.001, respectively. N = 3–4 per group.

The bioinformatic searches were conducted using Gene Set Enrichment Analysis together with fgsea R-package as previously described (Graber et al. 2021). These analyses were conducted with three different databases, Gene Ontology Biological Processes, Kyoto Encyclopedia of Genes and Genomes and Reactome. Independent of the database used and the comparison analyzed, the pathways related to the structural components and contractility as well as cytokine and other inflammatory responses were among the most frequently identified (Table 5, EPS vs. CTRL presented).

TABLE 5 The top 3 most up- and downregulated pathways in the myotubes in response to exercise-like electrical pulse stimulation (EL-EPS, EPS pool vs. CTRL). Bold = muscle structure and contractile pathway, italics = cytokine and inflammatory responsive pathway. ↑ = positive normalized enrichment score (NES), i.e., upregulated pathway, ↓ = negative NES, i.e., downregulated pathway. GOBP, Gene Ontology Biological Processes; KEGG, Kyoto Encyclopedia of Genes and Genomes; R, Reactome. N = 10 per group, false discovery rate (FDR) < 0.05 and FC > |1.2|.

	Pathway	FDR	NES	
GOBP	**Muscle Filament Sliding**	0.000	2.62	↑
	Actin Mediated Cell Contraction	0.000	2.25	↑
	Myeloid Leukocyte Migration	0.000	2.22	↑
	Retina Morphogenesis in Camera Type Eye	0.010	-2.01	↓
	Multivesicular Body Organization	0.012	-2.01	↓
	Neural Retina Development	0.026	-1.92	↓
KEGG	**Cardiac Muscle Contraction**	0.001	2.03	↑
	ECM Receptor Interaction	0.001	1.99	↑
	Chemokine Signaling Pathway	0.000	1.97	↑
	Pathogenic Escherichia Coli Infection	0.041	-1.75	↓
	Adherens Junction	0.049	-1.62	↓
	Axon Guidance	0.041	-1.59	↓
R	*Chemokine Receptors Bind Chemokines*	0.000	2.47	↑
	Striated Muscle Contraction	0.000	2.47	↑
	Class A 1 Rhodopsin Like Receptors	0.000	2.37	↑
	Autophagy	0.035	-1.67	↓

Notably, the number of the upregulated pathways was greater than the number of downregulated pathways. Related to upregulated inflammatory signaling in the transcriptome, the phosphorylation of NF-κB was also increased after the EL-EPS (Figure 17A). Of the contractile proteins, myosin heavy chain 1 content remained unaltered (Figure 17B).

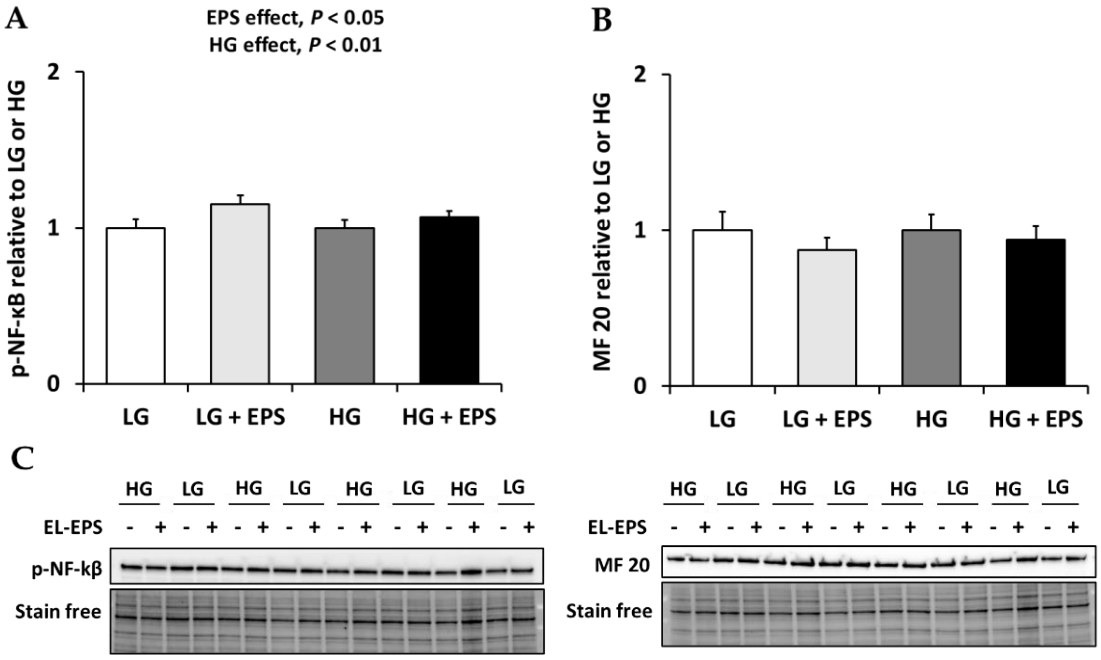

FIGURE 17 Effects of exercise-like electrical pulse stimulation (EL-EPS) on (A) phosphorylated nuclear factor (NF)-κB and (B) myosin heavy chain 1 (MF 20). (C) Representative blots. The data is presented as normalized to low (LG) or high (HG) glucose = 1. For the analysis of the EL-EPS and media glucose content (EPS and HG effects, respectively) and their interaction effect, the two-way MANOVA was used. The group comparisons were analyzed with multivariate Tukey's test. -, no EL-EPS; +, EL-EPS. N = 6 per group.

5.3.4 Extracellular vesicles containing miRNAs

To validate the suitability of EL-EPS model to study intercellular crosstalk, the EVs were collected from the cell culture media from the stimulated and non-stimulated myotubes. Verification of the successful EV extraction was conducted by nanoparticle tracking analysis and electron microscopy at the EV Core at the University of Helsinki, Finland. The results showed that the used protocol was able to extract the EVs and that the particles detected were the expected (~ 100 nm) size (Figure 18).

Next, the RNA was extracted from the collected EVs to analyze their miRNA content. This was conducted to evaluate whether similar contraction-induced changes occur in the EV content *in vitro* as does after *in vivo* exercise. For this analysis, two common myomiRNAs, miR-1 and miR-133a, were selected based on the previous studies demonstrating their increased content in the circulating EVs after exercise (Vechetti et al. 2021; Zhou et al. 2020). The expression of miR-1-3p was increased in response to EL-EPS, and although miR-133a-3p expression was also increased by several folds, this was non-significant due to high variation (Figure 19).

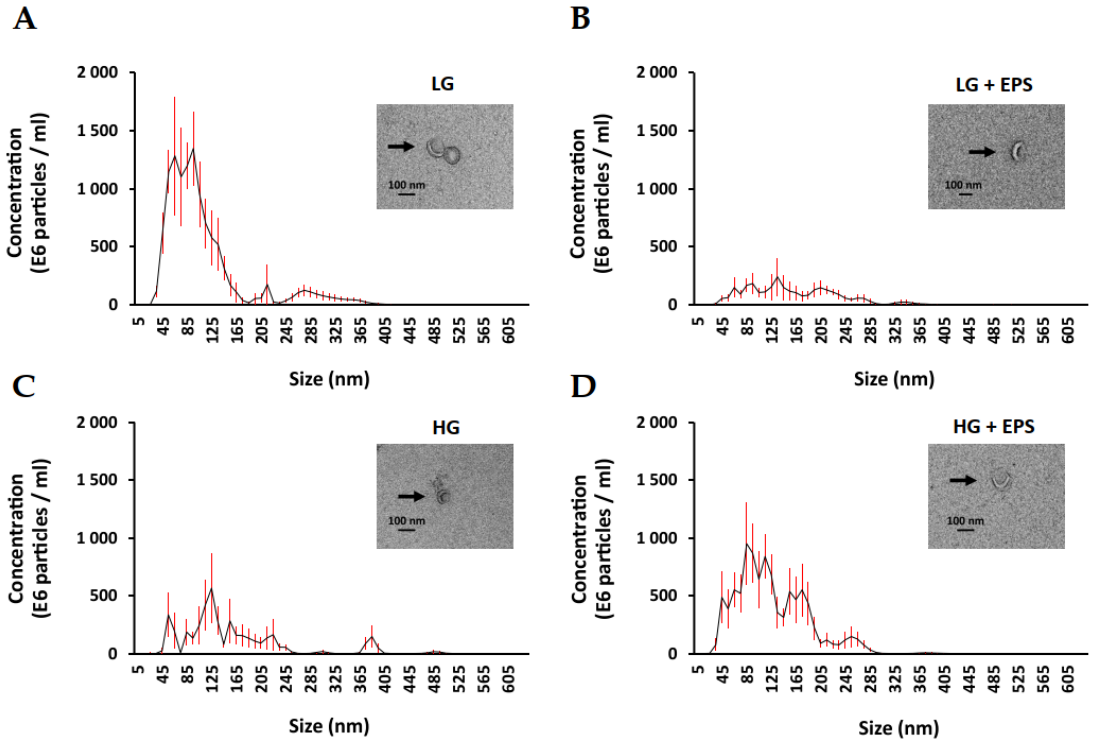

FIGURE 18 The validation of extracellular vesicle (EV) extraction the from the C2C12 cell media by nanoparticle analysis (NTA) and electron microscopy (EM). (A, B) Low and (C, D) high glucose (LG and HG, respectively) samples without (A, C) and with (B, D) exercise-like electrical pulse stimulation (EPS). Histograms present the concentration of the particles from the NTA analysis and the red error bars depict standard error of mean. Corresponding EM images are shown on the right and black arrows point to the representative EVs. N = 1 per group.

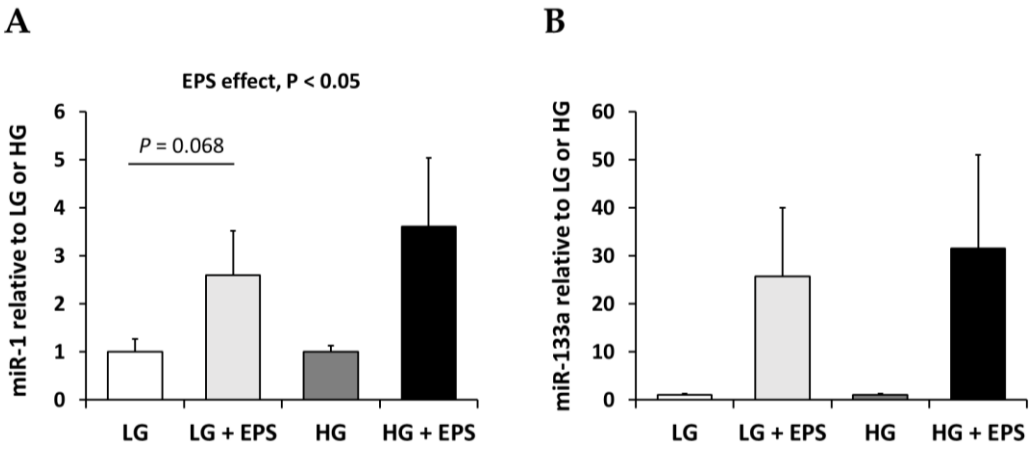

FIGURE 19 The contents of (A) miR-1-3p and (B) miR-133a-3p in the C2C12 cell-derived extracellular vesicles. For the analysis of the main exercise-like electrical pulse stimulation (EPS) and media glucose (HG) effects and the group comparisons, Mann Whitney *U*-test was used. The values are presented as normalized to low (LG) or high (HG) glucose = 1. N = 5–6 per group.

6 DISCUSSION

The purpose of this dissertation was to study the effects of changes in skeletal muscle size and muscle contractions on skeletal muscle physiology, metabolism and secretome. Skeletal muscle atrophy was modelled by C26 cancer cachexia and blockade of ACVR ligands was used as a model to prevent muscle wasting Exercise-like electrical pulse stimulation of the skeletal muscle cells was used as an *in vitro* exercise mimetic to analyze intra- and extracellular changes induced by the myotube contractions.

The main findings of this dissertation were as follows:

1. Muscle wasting and myotube contractions had various differences in their effects, such as increased phenylalanine levels in cachexia and enhanced branched chain fatty acid metabolism in exercise. However, they also induced rather similar changes in a few amino acids and energy metabolism intermediates. (I, III)

2. The cancer-induced pertubations on the skeletal muscle metabolism as well as serum metabolites remained largely unaffected by the blocking of ACVR ligands (e.g., myostatin and activins), highlighting the dominant effects of cachexia on the studied markers. (I)

3. *In vitro*, myostatin promoted signaling via atrophy-related Smad-dependent and Smad-independent pathways. The differentiation of the murine C2C12, but not human CHQ myogenic cell line into myotubes reduced the effects of myostatin, thus suggesting cell line and differentiation state specific responses to myostatin. (II)

4. Higher nutrient (i.e., glucose) availability in the C2C12 myotubes augmented the metabolite responses to the EL-EPS. Instead, some of the measured changes in signaling, exerkine secretion and fatty acid oxidation were less affected by the glucose availability after EL-EPS. Increased

production and secretion of acetate and branched chain fatty acids suggests that they may act as putative exerkines. (III)

5. Similar to metabolomics, higher nutrient availability augmented the transcriptional responses of the C2C12 myotubes to the EL-EPS. Biological processes mostly affected by the EL-EPS at the level of transcription included contractile ability and inflammatory/cytokine response. Similar to *in vivo* exercise, the packing of especially miR-1 was increased to the extracellular vesicles in response to EL-EPS independent of glucose availability. (IV)

This was to the best of my knowledge the first study (1) to analyze skeletal muscle and serum metabolomes after blocking myostatin and activins with sACVR2B-Fc in C26 tumor-bearing mice, (2) to compare the effects of myostatin on two skeletal muscle cell lines (murine and human) in distinct differentation stages as well as to analyze (3) the metabolomes of both C2C12 myotubes and media, (4) myotube transcriptome and (5) extracellular vesicle miRNA content after EL-EPS under variable nutritional conditions.

6.1 Metabolomic responses to cancer cachexia and myotube contractions

In vivo and *in vitro* metabolomics were used to analyze the effects of different physiological conditions on skeletal muscle metabolism (intracellular effects) and serum/cell culture media (extracellular effects). Because two different methods, MS and ^{1}H-NMR, were used to conduct the metabolomics, the analyzed metabolites differed in composition and in number between the studies I and III. Indeed, while MS identifies more metabolites also with low abundance, ^{1}H-NMR detects highly abundant metabolites very quantitatively (Marshall & Powers 2017). However, regardless of the method being used (MS in the study I or ^{1}H-NMR in the study III), the groups with similar biological functions and nature were identified intra- and extracellularly.

Cancer cachexia dominated the changes in skeletal muscle and serum metabolomes over the effects of reversal of muscle atrophy by blocking ACVR ligands such as myostatin and activins. The results suggest that although this approach is known to improve survival (Nissinen et al. 2018; Zhou et al. 2010), the metabolite level changes in the studied tissues may not explain this finding. Furthermore, probably many of the observed cancer-induced effects on skeletal muscle metabolism were not directly due to the altered skeletal muscle mass. In agreement with the results from our cachectic model, the blockade of myostatin and activins has been shown to have only minor effects on the metabolite levels in the skeletal muscle and serum of healthy mice (Barreto et al. 2017; O'Connell et al. 2019).

In vitro, the exercise-mimicking contractions of the C2C12 myotubes resulted in expected metabolic changes, such as increased glycolysis (Nikolić et al. 2017), while unexpected findings were also reported. Identification of acetate and BCAA catabolism-related intermediates as putative exerkines was a novel observation similar to the fact that the changes in the metabolite profiles were augmented under high glucose conditions. Notably, the EL-EPS had no effect on cell viability or cell-free media composition. Next, the following sections focus on a few of the main biological groups affected by cancer cachexia and/or EL-EPS.

Intermediates of energy metabolism. Impaired energy metabolism and malnutrition are hallmarks of cancer cachexia. A previously reported decrease in food intake in these same C26 tumor-bearing mice was accompanied by simultaneous loss of fats (Nissinen et al. 2018) and intramuscular triglycerides, and the metabolite level changes found in this study supported these results. Indeed, although the C26-tumor bearing may develop hyperlipidemia and hyperglycemia (Der-Torossian et al. 2013a), skeletal muscle and serum contents of multiple glucose- and lipid-derived metabolites were decreased similarly as previously reported (Cui et al. 2019b; Der-Torossian et al. 2013b; Pin et al. 2019). These results show that the cancer-mediated energy crisis is detectable also at the metabolite level. As a result of the reduced energy source content, carbon flow through the TCA cycle (i.e., TCA cycle flux) might have been compromised in the C26 tumor-bearing mice (Der-Torossian et al. 2013b; Pin et al. 2019). Indeed, cancer cachexia can lead to mitochondrial dysfunction and impaired ATP production in the skeletal muscle (Porporato 2016). To maintain the TCA cycle flux during cancer cachexia, amino acids, such as glutamine, glutamate, and BCAAs have been suggested to replenish the TCA cycle intermediates via anaplerosis (Cui et al. 2019b; Pin et al. 2019). It is possible that this might have occurred also in the present work.

To validate whether the myotube contractions induce expected metabolic responses, glycolysis markers including glucose and lactate are commonly analyzed from the myotube media after EL-EPS (Nikolić et al. 2017). To the best of my knowledge, the present dissertation is the first to analyze contraction-induced changes on both muscle cell and media metabolome. Previously, Hoshino and colleagues have analyzed myotube metabolome in response to EL-EPS (Hoshino et al. 2020). Thus, comparison to the existing *in vitro* literature is restricted. However, it seems that the selected EL-EPS parameters affect the myotube metabolome based on the distinct responses reported after low (1 Hz) and high (20 Hz) frequency protocols in the C2C12 myotubes (Hoshino et al. 2020). Furthermore, duration of the EL-EPS also affects the observed changes in the myotube metabolome. Indeed, the 24-hour low-frequency EL-EPS used in this dissertation resulted in significant changes to the myotube metabolism, while no changes were observed after 1-hour low-frequency EL-EPS (Hoshino et al. 2020). This is not unexpected because *in vivo* exercise intensity and duration also affect the metabolomic responses (Sakaguchi et al. 2019; Schranner et al. 2020).

The C2C12 myotubes are glycolytic in nature (Burch et al. 2010) and they rely on anaerobic ATP production, especially during the 24-hour low-frequency

EL-EPS based on the increased production and secretion of lactate in this study. This might reduce the need of carbon flow through the TCA cycle during EL-EPS and lead to accumulation of the TCA cycle intermediates in the myotubes similarly as previously reported (Hoshino et al. 2020). Cancer cachexia also appeared to decrease carbon flow through the TCA cycle. Despite the same outcome, the reason is different. Cancer-induced downregulation of the TCA cycle was likely due to a lack of energetic substrates, while during EL-EPS glycolysis and lactate production provide enough ATP to maintain contractions, thus reducing the need for complete TCA cycles. *In vivo*, the circulating TCA cycle intermediates have been shown to be increased after exercise where they might take part in intercellular communication (Maurer et al. 2021). Unfortunately, the ^{1}H-NMR spectroscopy was probably not sensitive enough to detect these molecules from the C2C12 media.

Further comparisons of the present *in vitro* EL-EPS media results to the previous *in vivo* biofluid (serum, plasma, saliva and urine) findings after exercise (Sakaguchi et al. 2019; Schranner et al. 2020) demonstrated similarities between the studied metabolomes. The main groups affected after *in vivo* exercise included substrates, intermediates, and the products of especially energy-related metabolism, including amino acid-related and lipid-derived metabolites as well as the TCA cycle intermediates (Sakaguchi et al. 2019; Schranner et al. 2020) similarly as reported in this dissertation. However, although changes in the blood metabolome after acute bouts of exercise have been reported to be time dependent, the work presented here focused on the rapid post-stimulation–induced changes. Based on the presented *in vitro* results and previous *in vivo* findings (Contrepois et al. 2020), it seems that despite the model studied, the metabolites that rapidly change after EL-EPS and exercise include energetic metabolites such as lactate, pyruvate, and TCA cycle intermediates.

Amino acids. Amino acids were among the best represented groups identified by both MS and ^{1}H-NMR. Based on the increased intracellular amino acid content in both models, cancer cachexia and EL-EPS may have promoted protein breakdown and/or amino acid recycling. However, protein breakdown is chronically elevated during cancer cachexia (Penna et al. 2019) and protein synthesis is decreased (Nissinen et al. 2018), while during exercise protein breakdown is elevated acutely and protein synthesis is greater than protein breakdown, thus leading to positive protein balance over time (Tipton et al. 2018). These factors highlight the differences between the two opposing conditions.

Due to the cancer cachexia–induced skeletal muscle atrophy and despite its reversal by blocking myostatin and activins (Nissinen et al. 2018), the contents of many glycogenic amino acids were decreased in the skeletal muscle of the tumor-bearing mice in agreement with previous reports (Cui et al. 2019b; Der-Torossian et al. 2013b). Of the aromatic amino acids, phenylalanine content in the skeletal muscle and serum were increased and indeed, the metabolism of this amino acid is reported to be altered in cancer patients (Cala et al. 2018; Scioscia et al. 1998). In my dissertation, a strong correlation between skeletal muscle as well as serum phenylalanine contents with the loss of body mass. This suggests that

phenylalanine could act as a biomarker of muscle atrophy and/or cachexia as suggested by others as well (Miller et al. 2019). Further, high serum phenylalanine levels in colorectal cancer patients have been associated with systemic inflammation and muscle wasting (Sirniö et al. 2019). Related to inflammation, the reason for the enhanced phenylalanine release could be the cancer-induced synthesis of liver acute phase response proteins, which contain relatively more aromatic amino acids than contractile proteins (Reeds et al. 1993). Thus, excessive proteolysis in the skeletal muscle is needed to support liver protein synthesis (Reeds et al. 1993). Indeed, it was previously shown in these same C26 tumor-bearing mice that hepatic protein synthesis as well as acute phase response were increased in tumor-bearing mice (Nissinen et al. 2018). These findings further support the hypothesis that muscle-derived aromatic amino acids could be used for synthesis of the acute phase response proteins.

Similar to *in vivo* exercise (Tipton et al. 2018), the chronic low-frequency EL-EPS promoted amino acid recycling, which was observed as increased intracellular content of almost all of the identified amino acids (e.g., BCAAs and aromatic amino acids). Hoshino and colleagues demonstrated that some of the identified amino acids were increased, while others were decreased in the C2C12 myotubes after 1-hour EL-EPS (Hoshino et al. 2020). *In vivo* exercise has been shown to target amino acids and especially the BCAAs in the skeletal muscle (Klein et al. 2020) as observed here *in vitro*.

During cachexia and EL-EPS, amino acids were less affected in the serum and in the media, respectively, than in the skeletal muscle or myotubes. However, previous studies have reported that cancer cachexia alters serum amino acid profile (Sirniö et al. 2019; Miller et al. 2019; Yang et al. 2018), partly depending of the progression state of the disease (Sirniö et al. 2019). *In vitro*, metabolite contents in the cell-containing and cell-free media were evaluated after EL-EPS to roughly estimate the uptake and release ratio of the metabolites. The results suggested that alanine, asparagine, cystine, glutamate, glycine, histidine, lysine and tryptophan were probably released into the media, while glutamine, serine and tyrosine were taken up by the cells during EL-EPS. In some cases, media glucose content affected these responses. The observed results are in agreement with *in vivo* exercise, which has been shown to increase the content of many amino acids in the skeletal muscle interstitial fluid after acute exercise (Zhang et al. 2018), while in other biofluids the results were more versatile (Schranner et al. 2020). Additionally, *in vivo* exercise has been reported to lower the circulating glutamine levels (Pedersen et al. 2020). The appeared increase in serine uptake during EL-EPS may be important to maintain anabolic processes in the cells (Ly et al. 2020). Further studies are needed to confirm these results using kinetic tracer methods, such as fluxomics (i.e., analysis of dynamic metabolite turnover) (Hui et al. 2020). Also, more time-course studies are needed to track metabolite level changes and myotube recovery after EL-EPS to better understand myotube metabolism in response to contractions. This is important for the future studies aiming to apply EL-EPS on the same myotubes on consecutive days.

Ketone bodies and branched/short chain fatty acids. An interesting group of metabolites related to BCAAs were their breakdown intermediates, branched chain fatty acids (BCFA) that were elevated after EL-EPS both in the cells and in the media. This is in agreement with the previous *in vivo* studies reporting other BCAA catabolites from different biofluids after exercise (Contrepois et al. 2020; Klein et al. 2020; Schranner et al. 2020). That being said, the present studies were, to the best of my knowledge, the first to show that these metabolites originated from the contracting skeletal muscle cells. Furthermore, the culturing of the C2C12 myotubes in BCAA-free media blocked BCFA production and release after EL-EPS, which further support the theory that the BCFAs originated from the BCAA catabolism (Study III).

Acetate is a short chain fatty acid that can act as an alternative energy source during exercise (Hargreaves & Spriet 2020) and indeed, increased intra- and extracellular content of acetate were observed. In addition, 3-hydroxybutyrate, a common ketone body that can also act as an energy source was increased in the media after EL-EPS, suggesting its release from the cells. These fuel sources may originate from excessive glycolysis because acetate can originate from pyruvate via enzymatic and non-enzymatic pathways and hyperactive glucose metabolism (Liu et al. 2018). Additionally, acetyl-CoA can be converted to acetate probably via acyl-CoA thioesterases (Tillander et al. 2014). Instead, 3-hydroxybutyrate, which may originate from lipolysis and fatty acid oxidation, has been found from the skeletal muscle interstitial fluid after exercise although it commonly originates from the liver (Zhang et al. 2018). Further, increased blood 3-hydroxybutyrate content has been reported after exercise (Schranner et al. 2020). Although acetate and 3-hydroxybutyrate were identified as putative exerkines, this hypothesis needs to be further validated.

To summarize, firstly, although it seems that the effects through which blocking myostatin and activins improves survival may include effects on skeletal muscle, this outcome probably cannot be explained by the metabolite-level changes in the skeletal muscle or serum. Indeed, because reversal of skeletal muscle wasting was not able to counteract the cancer-induced effects on metabolism, these factors might not have been regulated by the changes in the skeletal muscle mass to begin with. Most likely, the improvements at the multi-organ level sum up into a better outcome (Hulmi et al. 2021) but this needs to be addressed in the future studies. Secondly, the intra- and extracellular metabolic changes in the C2C12 myotubes after the EL-EPS demonstrate that this exercise-mimicking *in vitro* model is suitable to study contraction-induced changes in skeletal muscle cells. The effects of EL-EPS on myotube and media metabolome are currently an underappreciated topic warranting more research especially under distinct stimulation protocols and nutritional conditions. Finally, although these two very distinct physiological conditions affected metabolites of the similar biological groups, including amino acids and intermediates of energy metabolism, unique changes among the conditions demonstrate that their molecular mechanisms differ fundamentally.

6.2 Transcriptional changes in differentiating and contracting myotubes

Differentiating myotubes. Differentiation of the skeletal muscle cells have been shown to upregulate the expression of different TGF-β family members and their blocker, follistatin (Artaza et al. 2002; Moran et al. 2002; Ríos et al. 2001; Rossi et al. 2010), similarly as reported in this dissertation. Interestingly, compared to murine C2C12 myotubes, these transcriptional changes induced by the myotube differentiation were minor in the human CHQ cells, which may be due to metabolic differences between the cell lines (Abdelmoez et al. 2020). Members of the TGF-β family are known to regulate muscle and myotube metabolism not only in atrophy but also in normal conditions. For example, myostatin acts in a paracrine manner to regulate proliferation and cell survival of the myoblasts (Ríos et al. 2001), while exogenous myostatin prevents normal myotube formation possibly by downregulating the expression of mediators of skeletal muscle development and myogenesis and by interfering with the mTORC1 signaling rather than promoting atrophy (Trendelenburg et al. 2009). Similarly, activin A inhibits proliferation and differentiation of the myotubes, thus affecting myogenesis (Bloise et al. 2018). In contrast to the TGF-β members, follistatin promotes myogenic differentiation and force generation in the C2C12 cells (Ikeda et al. 2017). The results of the present work support the evidence that endogenous TGF-β members regulate differentiation of the C2C12 cells, while in CHQ cells they might have a smaller role. Overall, endogenic and exogenic TGF-β members as well as their endogenous binding proteins such as follistatin may have distinct effects on myotube differentiation in various skeletal muscle cell lines and more studies are warranted to address this issue.

Contracting myotubes. Overall, the most upregulated pathways were related to myotube contraction as well as cytokine and other inflammatory responses similarly as reported by others (Fukushima et al. 2021). The expression of sarcomeric genes including myosin heavy chain isoforms were upregulated by the EL-EPS in agreement with some (Fukushima et al. 2021; Lambernd et al. 2012) but not all (Marš et al. 2020) of the studies. Upregulation of different myosin heavy chain isoforms is most likely related to the fact that myotube cultures always contain cells that are in variable differentiation stages (Wright et al. 2014) and that EL-EPS may induce differentiation of the myoblasts into myotubes (Kawahara et al. 2006). Furthermore, the changes in the expression of the contractile genes may also support reorganization of the skeletal muscle architecture including cytoskeleton and sarcomere modifications that are needed for the myotube contractions (Fujita et al. 2007; Lambernd et al. 2012).

Similar to *in vivo* exercise (Kramer & Goodyear 2007), the cytokine and/or inflammatory responses to the EL-EPS is a prominent finding demonstrated widely at the level of transcription (Fukushima et al. 2021; Scheler et al. 2013; Sidorenko et al. 2018), translation (Laurens et al. 2020b; Raschke et al. 2013) and secretion (Farmawati et al. 2013; Miyatake et al. 2016; Nedachi et al. 2009). In

agreement to many of these reports, the results presented in this dissertation demonstrated upregulated expression of various chemokines, which are mediators of the intercellular communication. Indeed, chemokines are shown to enhance muscle repair and recovery after exercise by promoting macrophage infiltration into the skeletal muscle (Catoire & Kersten 2015). Infiltrated macrophages regulate processes related to inflammation, satellite cells and cytokines that may possibly contribute to muscle growth (Walton et al. 2019). In *in vitro* models, elevated media content of chemokines has been associated with C2C12 myoblast migration and differentiation in response to the EL-EPS (Miyatake et al. 2016; Nedachi et al. 2009), while monocyte chemoattraction may be promoted by chemokine release (Miyatake et al. 2016). Additionally, upregulated expression of macrophage migration inhibitory factor (*Mif*) was observed after the EL-EPS in the present work. Previous studies have suggested that MIF is a putative pro-inflammatory myokine that regulates both inflammatory response as well as skeletal muscle regeneration after damage (Reimann et al. 2010).

Contracting myotube-derived EVs and miRNAs. Previously *in vivo* studies have analyzed EV miRNA profiles in response to exercise and they have reported that, for example, miR-1, miR-21, miR-126, miR-133a, miR-146a and miR-206 could act as potential biomarkers of exercise (Mooren et al. 2014; Russell & Lamon 2015; Soplinska et al. 2020; Vechetti et al. 2021).

In agreement with these studies, increased EV content of two myomiRNAs, miR-1-3p and possibly miR-133a-3p in response to EL-EPS was observed here. This suggests that also myotube contractions may induce similar changes in the EVs as found previously in *in vivo* exercise. However, our results from the representative samples measuring EV number were inconsistent. *In vivo* exercise has been shown to increase the number of circulating EVs (Whitham et al. 2018), while a similar increase was observed only in the HG condition. Regardless, the levels of the studied miRNAs increased in response to EL-EPS independent of glucose availability. This suggests that the abundancy of the miRNAs, yet not necessarily the number of EVs, increased in response to EL-EPS. Notably, utilization of the *in vitro* exercise model verifies that the EVs observed in this work indeed originate from the contracting myotubes. Furthermore, serum-free cell culture conditions excluded the possibility of co-isolation of, for example, high-density lipoproteins (Simonsen 2017), thus enabling analysis of the EVs alone.

Since the cultured skeletal muscle cells differentiate at variable rates, it is worth noting that both myoblasts and myotubes release EVs and that the myotube-derived EVs may promote myoblast differentiation (Rome et al. 2019). Indeed, the studied miRNAs have been shown to regulate differentiation of the C2C12 cells (Zhang et al. 2014). For example, miR-1 promotes myogenesis and miR-133a proliferation (Chen et al. 2006) and they are involved in the development of human skeletal muscle (Koutsoulidou et al. 2011). This suggests that myotube contractions possibly promote processes that inhibit proliferation and enhance differentiation, at least in the C2C12 cells. Furthermore, miR-1 has been shown to regulate mitochondrial metabolism (Silver et al. 2018; Rodrigues et al. 2021), while miR-133a has proven to have an important role in the regulation of

the skeletal muscle adaptations to exercise (Nie et al. 2016), highlighting the role of these miRNAs in mediating responses to exercise.

Besides the preliminary examinations of the contraction-induced effects in the EV number and miRNA content presented in this dissertation, further studies are warranted to better understand the role of EV-mediated effects in auto- and paracrine as well as endocrine manner in response to EL-EPS. In addition, in this dissertation only a few exercise-responsive miRNAs were analyzed, but in the future more profound methods, such as miRNA sequencing are needed to gain a more comprehensive view of these potential exerkines. Finally, it remains to be fully elucidated what are the mechanisms through which miRNAs are selectively packed into the EVs and how intercellular communication is mediated by the EVs in response to exercise.

6.3 Signaling pathways in skeletal muscle cells

Signaling in response to myostatin and C26 cell conditioned media. The myostatin enhanced canonical (i.e., Smad) and non-canonical (e.g., MAPK) signaling in the skeletal muscle cells were in agreement with the existing literature (Schmierer & Hill 2007; Weiss & Attisano 2013). However, these results seemed to be dependent on the cell line used, the differentiation stage of the cells and partly on the time-point studied. Interestingly, follistatin gene expression and protein content were increased in the C2C12 but not in the CHQ cells during differentiation, which may partly explain the distinct responses of the cell lines because follistatin is an endogenous blocker of myostatin, activin A and GDF11 (Amthor et al. 2004; Lee & McPherron 2001; Schneyer et al. 2008). Besides canonical and non-canonical signaling, myostatin administration and co-culture of the C26 cancer and muscle cells affected inflammatory pathways. Myostatin enhanced inflammatory signaling more in the myoblasts than in the myotubes, while the co-culture induced similar inflammatory responses independent of the differentiation stage. These results thus suggest that the effects of the tumorkine pool are more pronounced than those of the myostatin alone. In the CHQ cell line, both myoblasts and myotubes responded to myostatin administration and the effects of myostatin were observed after short- and long-term incubation.

Together the results suggest that the C2C12 cell line is not an ideal model to study the direct effects of myostatin and possibly other TGF-β family members on skeletal muscle metabolism. However, more studies are needed to reveal the underlying mechanisms that block myostatin effects in the C2C12 cells and the role of follistatin in this response needs to be validated.

Signaling in response to myotube contractions. In addition to atrophic stimuli, MAPK signaling is enhanced also after variable conditions including exercise (Kramer & Goodyear 2007). In agreement, EL-EPS increased phosphorylation of SAPK/JNK1/2 similarly as previous *in vitro* (Nikolić et al. 2017) and exercise studies *in vivo* (Kramer & Goodyear 2007) have shown. This pathway has been reported to be activated during intensive exercise (Kramer & Goodyear 2007)

and concordantly, the EL-EPS enhanced lactate production. This suggests that although being a low-frequency protocol, the applied EL-EPS resembled intensive exercise in the C2C12 cells. Indeed, utilization of the primary human skeletal muscle cells in EL-EPS studies could provide a more realistic and individualized model to examine the metabolic responses of myotube contractions induced by different types of EL-EPS.

Exercise is also known to transiently affect inflammatory pathways (Kramer & Goodyear 2007). In agreement, the EL-EPS enhanced IL-6 secretion from the contracting skeletal muscle cells, which is one of the most common findings in exercise studies (Fiuza-Luces et al. 2013; Nikolić et al. 2017). The expression of IL-6 is regulated via NF-κB signaling (Brasier 2010), which indeed was phosphorylated more after EL-EPS. Similarly, IL-6 is also regulated by lactate (Hojman et al. 2019), which was also increased after EL-EPS. Thus, despite lacking normal microenvironment and other physiological factors, the contracting myotubes produce many of the key responses to contractions as has been reported after *in vivo* exercise.

Together, based on the increased signaling via MAPKs and inflammatory pathways, both tumorkine load (myostatin and C26 conditioned media) and myotube contractions (EL-EPS) affected many similar processes. However, similarly as in the case of increased protein breakdown and/or amino acid recycling, the two approaches will have distinct long-term effects on skeletal muscle metabolism. Tumorkines mimic tumor-burden, which has been reported to promote chronic inflammation and lead to dysregulated skeletal muscle metabolism (Tsoli & Robertson 2013). Instead, exercise-induced inflammatory response in the skeletal muscle has been associated with important adaptation processes including muscle repair and regeneration (Peake et al. 2017). Finally, cancer cachexia is a chronic condition that continuously promotes skeletal muscle atrophy and other catabolic processes together with the tumorkines. Instead, EL-EPS induces acute and transient responses to the studied metabolites, many of which return close to the baseline during rest (Hoshino et al. 2020) similar *to in vivo* exercise (Sakaguchi et al. 2019). These fundamental differences between myostatin/tumorkine-induced or myotube contraction-induced inflammatory signaling highlight the differences between the studied models. The major factor between these processes is their chronic (tumorkines) and acute (EL-EPS) effects on myotube metabolism.

6.4 Effects of nutrient availability on contraction-induced responses in myotubes

Nutrition is a critical factor that regulates metabolism during and after *in vivo* exercise (Hargreaves & Spriet 2020). Indeed, exercise-induced processes, including metabolic effects, transcription and signaling pathways are regulated by macronutrient intake *in vivo* (Hawley et al. 2018). However, the number of studies

directly investigating the effects of nutritional state on the responses of myotube contractions is small (Farmawati et al. 2013; Fukushima et al. 2021), which demonstrates that this area of research has remained understudied.

The C2C12 cells are routinely cultured in high (4.5 g/l) glucose containing media, while EL-EPS has been applied on myotubes in high and low (1.0 g/l) glucose conditions. The problem is that only a few C2C12 studies (e.g., four out of 28 articles reviewed by Nikolić and colleagues (Nikolić et al. 2017)) have clearly reported the glucose content used during EL-EPS. In non-stimulated C2C12 cells, higher glucose availability upregulated glycolytic phenotype in comparison to low glucose conditions, thus demonstrating the importance of addressing the effect of nutritional availability also during EL-EPS (MacDonald et al. 2020). The work presented in this dissertation aimed to elucidate this issue by analyzing contraction-induced responses of the C2C12 myotubes grown under high and low glucose conditions at the levels of transcription, translation, metabolites and signaling.

In vivo, greater metabolic disturbances in response to exercise are thought to induce greater adaptations in the skeletal muscle. One strategy to augment these responses has been to restrict carbohydrate intake and to exercise under a glycogen-depleted state (Hawley et al. 2018). Interestingly, higher media glucose and thus presumably higher glycogen content (Farmawati et al. 2013) during *in vitro* EL-EPS augmented metabolite and gene expression responses (omics), while other analyses including cytokine secretion, signaling pathways, oleate oxidation and EV miRNA packing were less affected by the glucose availability. This seemingly contradictory result may be explained at least in part by the cell viability evaluated by the media lactate dehydrogenase activity. Indeed, lower activity of this enzyme suggests that the myotubes grown under high glucose conditions might be more viable and thus metabolically more active because under low glucose conditions, intra- and extracellular glucose was almost diminished. This might have affected the metabolic capacity of the myotubes grown under low glucose conditions and yield lower metabolite level responses to EL-EPS. This was the case also based on the transcriptomics. Together, the lower glucose availability might have compromised the contraction-induced responses and adaptations in the myotubes based on the lesser effects on the omics, at least after the 24-hour EL-EPS. Interestingly, lower glucose availability did not promote unique EL-EPS responses based on the analyzed markers. Instead, responses remained either unaltered or they were affected to a lesser extent than in high glucose conditions at both the metabolite and gene expression levels. Other cellular processes, such as signaling and the media exerkines, were overall less affected by glucose availability, tending to suggest that cell viability may not be at the only mechanism explaining enhanced metabolome and transcriptome responses to EL-EPS. The reason for the more distinct differences in omics could be due to higher sensitivity of the ^{1}H-NMR and RNA sequencing methods than that of the Western blot.

It is important to understand more broadly how nutrient availability affects myotube metabolism so that the *in vitro* EL-EPS model would even better mimic

in vivo exercise conditions. Although this dissertation provided a starting point for the research of this topic, more work is needed to examine the effects of myotube nutrient availability on metabolism after for example short-term and high-frequency simulation protocols. Additionally, more studies are needed that would analyze myotube recovery after EL-EPS under variable nutritional conditions. Especially in these cases nutrition availability might play a big role in myotube adaptations.

6.5 Strengths and limitations

One of the main strengths of this dissertation was the utilization of many *in vivo* and *in vitro* approaches to study the skeletal muscle physiology and mediators of intercellular communication under distinct health and nutritional conditions that are known to affect skeletal muscle size and metabolic homeostasis.

More specifically, the experimental cancer and blockade of ACVR ligands (e.g., myostatin and activins) provided a systemic model to study how the changes in skeletal muscle size affect metabolomic responses (I). The lack of a group of healthy mice administered with a blockade of myostatin and activins is one limitation of this set-up. However, previous studies have shown that the effects of blocking myostatin and activins in healthy mice had only minor effects on the skeletal muscle and serum metabolomes (Barreto et al. 2017; O'Connell et al. 2019). It remains unclear, however, how well these preclinical observations could be scaled up to a human population and thus caution is needed when interpreting the results. Analysis of the direct myostatin effects on two different skeletal muscle cell lines (II) provided valuable insights for other researchers aiming to develop an *in vitro* skeletal muscle atrophy model. Indeed, the origin-specific characteristics as well as myotube maturation are critical factors that need to be addressed in future studies examining the effects of myostatin and possibly other TGF-β family members on skeletal muscle cells. Our unsuccessful attempts to measure follistatin concentration from the cell culture media is a limitation. Although transcriptional and translational analyses demonstrated that follistatin increased during the differentiation of the C2C12 cells, it acts as a myostatin blocker in the circulation. For this reason, it remains to be determined whether follistatin could explain why the C2C12 cells are not an ideal model to study the effects of myostatin, or even possibly other TGF-β family members, on the skeletal muscle cells.

The studies III and IV focused on the *in vitro* exercise model. Regarding these two studies, one strength of this dissertation was to examine the effects of myotube contractions with two different omics-methods including metabolomics (III) and transcriptomics (IV). The media composition (i.e., supplements) can affect metabolomics (Daskalaki et al. 2018; Lagziel et al. 2020), transcriptomics (Fukushima et al. 2021; MacDonald et al. 2020) and even extraction of the EVs (Simonsen 2017). For this reason, conducting the EL-EPS experiments under serum-free conditions to prevent for example co-isolation of serum-containing

high-density lipoproteins during EV extraction (Simonsen 2017) was a strength of the study. Analysis of the cell-free samples demonstrated that EL-EPS had no effects on the media metabolome and that the BCFAs originate from the C2C12 cells. However, although this allowed us also to robustly assess the metabolite uptake and release during EL-EPS (Study III), further studies are needed to examine dynamic metabolite turnover using isotope tracers, such as fluxomics (Hui et al. 2020).

To exclude the electrode-mediated changes on the media metabolites, the metabolome of the cell-free media controls with and without stimulation (i.e., no cells/no power and no cells/power) was analyzed as previously recommended (Nikolić et al. 2017). However, electrode-mediated effects on EVs were not analyzed. This is important to be elucidated in future studies because it is possible that some particles including EVs, which have been shown to bind to plasticware (Evtushenko et al. 2020), might attach to the carbon electrodes during EL-EPS. Thus, future EL-EPS studies that examine EVs should include electrodes in the control wells as well.

Although intercellular communication was analyzed by administration of the EL-EPS conditioned media to hepatocytes (Study III, data not presented in the thesis due to the minor changes) and by analyzing the EV miRNA content, these were preliminary efforts to model contraction-induced intercellular communication *in vitro*. More research is needed to better understand which less studied media components (e.g., metabolites and EVs) mediate the contraction-induced health benefits of exercise and how they recognize the target cells. Additionally, a broader analysis of the EV miRNAs would have provided a more comprehensive understanding of how the contracting myotubes mediate intercellular communication in response to EL-EPS. Moreover, although myotube transcriptome was examined, the used method did not enable simultaneous analysis of both mRNA and miRNA and the first was selected for the analysis. Because miRNAs also respond to exercise in the skeletal muscle (Vechetti et al. 2021) and they regulate translation, analysis of the myotube containing miRNAs would have been a good addition to the present work.

The selected *in vitro* EL-EPS model *per se* has obvious strengths, such as the ability to exclusively examine skeletal muscle cells intra- and extracellularly. However, the limitations include the lack of innervation, circulation and contact with the connective tissue proteins. In the EL-EPS studies, inclusion of suitable controls and proper cleaning of the carbon electrodes is particularly important because electrode-mediated changes have been reported (Evers-van Gogh et al. 2015). Utilization of single pulses during EL-EPS do not ideally represent contractile activity of the skeletal muscle *in vivo* and instead periodic batches of pulses have been recommended (Vepkhvadze et al. 2021). Additionally, because different skeletal muscle cell lines have their species origin-specific characteristics that affect their contractility and metabolism (Abdelmoez et al. 2020), caution should be taken when comparing the C2C12 myotube EL-EPS responses to another cell line or scaling up to *in vivo* comparisons, especially in humans. Notably, the suitability of the immortalized C2C12 cell line, which originates from the

1970s (Yaffe & Saxel 1977) has been questioned in muscle research due to the selection pressure as well as requirements of contact inhibition and serum withdrawal for myotube maturation (Rodgers & Ward 2021). Finally, similar to many previous studies, the samples in this dissertation were collected immediately after the EL-EPS, while more time-points for sample harvesting after the EL-EPS would be needed. This is because many of the exercise-induced changes can be rapid and transient (e.g., cytokine secretion bursts (Shirasaki et al. 2014) and miRNA responses (Russell et al. 2013) or, on the other hand, delayed (e.g., increased myotube size (Tarum et al. 2017)).

The combination of the concepts from Studies I to IV would have tied the muscle wasting and exercise models together better from the perspective of this dissertation. Indeed, myostatin, for example, prevents myonuclear accumulation (i.e., myotube formation) in the C2C12 cells, while the rest period after EL-EPS promotes myonuclear accumulation (Kneppers et al. 2018). It remains to be established whether, for example, myostatin effects during EL-EPS could be diminished and whether follistatin, for instance, could be related to this phenomenon. That being said, EL-EPS has been shown to counteract the effects of other muscle wasting-promoting factors, such as doxorubicin-mediated atrophy (Guigni et al. 2019). These studies highlight the flexibility of the EL-EPS model – it can be used not only to study the effects of myotube contractions *per se*, but it can also be combined with research topics that are related to variable health conditions.

6.6 Future directions

The findings presented in this dissertation and in previous studies suggest that although blocking ACVR ligands and the maintenance of skeletal muscle mass might be important for better survival during experimental cancer cachexia, the underlying mechanisms are not completely understood. It remains to be elucidated what the role of skeletal muscle is in the tissue crosstalk during cancer cachexia and what these mediators could be. Although metabolites did not provide clear answers, other *in vivo* and *in vitro* models, methods and/or omics-approaches could be able to reveal these mediators and processes that make skeletal muscle possibly an important tissue for survival, as has been claimed.

Besides blocking myostatin and activins, other methods to prevent and/or reverse cancer-induced skeletal muscle wasting are needed. Although exercise has been shown to improve many cancer-induced metabolic perturbations (Raun et al. 2021), the metabolite level changes in these situations are less clear. It has been reported that exercise had only minor effects on the serum metabolites in breast cancer patients, although exercise still improved their diagnosis (Febvey-Combes et al. 2021). Additionally, it has been shown that exercise may limit tumor growth (Lu et al. 2018), which could have beneficial effects on the whole-body metabolism as well. An alternative approach to study the effects of exercise on skeletal muscle metabolism during cancer is to apply EL-EPS on myotubes under tumorkine load. However, *in vitro* models, such as organ-on-a-chip or

tissue-on-a-chip models that are being developed rapidly, could provide feasible opportunities to study intercell communication in different conditions, including cancer and exercise. Additionally, the EL-EPS model will most likely shift from 2D culturing towards 3D models, which better resemble *in vivo* conditions. Indeed, 3D EL-EPS models have already been successfully established (Hernández-Albors et al. 2019; Mestre et al. 2018; Nakamura et al. 2021) and hopefully a combination of this method with other improvements developed in the *in vitro* field will result in an optimal model to study not only muscle cell metabolism but also intercellular communication.

Of the mediators of the intercellular communication during EL-EPS, omics have focused mainly on proteomics and transcriptomics, while metabolomics and analysis of the EVs and their content have been underappreciated. These provide an interesting topic for the future studies. For example, labeled tracers and fluxomics could provide a novel approach to better understand contraction-induced changes in the myotubes and intercellular communication in different conditions. Thus far, the EL-EPS protocols are not strictly categorized to mimic either endurance or resistance exercise, although accumulating evidence shows that muscle hypertrophy can also be achieved by *in vitro* contractions. Development in this area in the future could provide a tool to study more widely different types of exercise, their similarities and differences as well as effects on other tissues at a whole-body level. This could reduce the need for *in vivo* studies, which, however, would still be needed to validate the *in vitro* results.

Although murine C2C12 myotubes have their advantages in EL-EPS studies, such as reliable and reproducible contractility, in the future more research will most likely be conducted with primary human myotubes. This approach has, of course, limitations, such as the lifespan of the cells extracted from the skeletal muscle biopsies, but on the other hand, primary human myotubes provide better understanding of the individual responses to exercise. Indeed, EL-EPS could also be used to, for example, determine the genetic ability of people to respond to exercise (i.e., low vs. high responders (Mann et al. 2014)), which could lead to the development of more individualized exercise programs. Furthermore, primary human myotubes not only provide great opportunities to study donor-specific characteristics in healthy populations but also in patients with various diseases that target skeletal muscle. Indeed, there are already studies analyzing donor-specific differences with EL-EPS in, for example, diabetic and/or obese populations (Al-Bayati et al. 2019; Feng et al. 2015; Lim et al. 2018; Løvsletten et al. 2020; Park et al. 2019) but other conditions beyond impaired glucose- and/or lipid-handling are recommended.

7 MAIN FINDINGS AND CONCLUSIONS

The main findings and conclusions of this dissertation are summarized as follows:

1. The experimental C26 cancer had greater effects on the skeletal muscle and serum metabolomes than the blockade of myostatin and activins, altough the latter was previously shown to improve survival from cancer and to reverse muscle atrophy. This suggests that cancer-induced effects on metabolites were not direcly associated with altered skeletal muscle mass or survival. Of the individual metabolites, phenylalanine was identified as a potential marker of muscle atrophy. (I)

2. Cell-line specific differences in the C2C12 and CHQ myotube maturation can greatly affect their responses to myostatin. Indeed, the observed changes in the canonical and non-canonical pathways were more pronounced in the C2C12 myoblasts and in the myotubes, while similar responses were observed in the CHQ cells independent of the differentiation stage. The results suggest that the widely used C2C12 cell line might not be ideal to study the effects of myostatin and perhaps other ACVR ligands. (II)

3. Higher media glucose content during EL-EPS amplified the metabolite responses of the C2C12 myotubes. For example, lactate, acetate, BCFAs and TCA cycle intermediates were increased more under high glucose conditions. Importantly, EL-EPS had no effects on cell viability or cell-free media metabolome thus suggesting that the observed changes were derived from intact skeletal muscle cells. Finally, the BCAA catabolites, acetate and 3-hydroxybutyrate were identified as putative exerkines warranting further research. (III)

4. The effects of EL-EPS on the C2C12 myotube transcriptome were more pronounced under high glucose conditions. Potentially, activators of transcription might have been overrun by the repressors in low glucose

conditions. These differentially expressed genes were related to processes including myotube contraction and cytokine/inflammatory response independent of the media glucose availability. Increased packing of the exercise-responsive miRNAs into the EVs released from the myotubes demonstrated that besides analysis of intracellular changes, EL-EPS can be potentially utilized to study intercellular communication through miRNAs. (IV)

YHTEENVETO (SUMMARY IN FINNISH)

Luurankolihasten merkitys arjessa on suuri, sillä tämä hyvin mukautumiskykyinen kudos muodostaa lähes 40% kehon kokonaispainosta. Sen lisäksi, että luurankolihakset mahdollistavat liikkumisen, ne osallistuvat energia-aineenvaihduntaan ja kudosten väliseen vuorovaikutukseen. Riippuen luurankolihaksen saamista signaaleista, se pystyy joko pienentämään tai suurentamaan kokoaan säätelemällä proteiinisynteesiä ja proteiinien hajotusta.

Monet tilanteet, kuten ikääntyminen, vähäinen ravinnonsaanti ja alhainen fyysinen aktiivisuus sekä erilaiset taudit, kuten syövät ja niihin usein liittyvä kakeksia, edistävät luurankolihasten katoa. Heikentynyt lihasvoima ja -massa haittaavat toimintakykyä ja ovat riskitekijöitä kohonneelle kuolleisuudelle ja heikommalle lääkevasteelle esimerkiksi syövässä. Tästä syystä on tärkeää ymmärtää, mitkä tekijät tilanteen aiheuttavat ja miten lihaskatoa voisi ehkäistä.

Yleisimpiä lihaskatoa edistäviä tekijöitä ovat esimerkiksi myostatiini ja aktiviinit. Nämä tekijät ovat tärkeitä lihaskoon säätelijöitä ja niiden määrän lisääntyminen kakeksiassa aiheuttaa useita ei-toivottuja muutoksia luurankolihaksissa ja koko elimistössä. Kakeksiaa on tutkittu usein erilaisilla syöpämalleilla koeeläin-asetelmissa. Toimiva lihassolumalli tarjoaisi kuitenkin mahdollisuuden tutkia myostatiinin ja aktiviinien sekä niiden estämisen suoria vaikutuksia luurankolihakseen ilman eettisiä ongelmia. Muun muassa tämän vuoksi uusien solumallien kehittäminen on tärkeää.

Farmakologisten tekijöiden, kuten myostatiinin ja aktiviinien toiminnan ehkäisijöiden lisäksi luurankolihaksen massaa voi kasvattaa ja ylläpitää liikunnan ja terveellisten elintapojen avulla. On ajateltu, että useat liikunnan aikaansaamat terveyshyödyt ja -vaikutukset voivat olla seurausta supistuvan lihaksen erittämistä säätelytekijöistä. Näitä tekijöitä kutsutaan ekserkiineiksi. Ekserkiinit voivat vaikuttaa lihakseen, sen läheisiin tai jopa kaukaisiin kudoksiin muuttaen niiden aineenvaihduntaa terveyttä edistäväksi. Vaikka ekserkiinejä onkin tutkittu jo jonkin aikaa, läheskään kaikkien ekserkiinien vaikutuksista tai kohdekudoksista ei ole tietoa. Tämän vuoksi ekserkiinejä tulee tutkia lisää.

Ihmisillä tehtävä lihas- ja liikuntatutkimus ei ole ongelmatonta, sillä yleisesti kerätyt näytteet, kuten verinäytteet sisältävät tekijöitä muistakin kuin lihassoluista. Tällöin ei voida olla täysin varmoja siitä, mistä tutkitut molekyylit ovat peräisin. Tämän vuoksi on tärkeää hyödyntää liikuntaa mallintavia lihassoluasetelmia. Kasvatetut ja erilaistetut lihassolut supistuvat lihaksen tavoin, kun niiden kasvatusliuokseen johdetaan sähköimpulsseja. Tutkimalla lihassolujen sisäistä aineenvaihduntaa ja niiden kasvatusliuokseen erittämiä tekijöitä, voidaan olla varmoja molekyylien alkuperästä ja lihassupistuksen aiheuttamista muutoksista niiden pitoisuuksissa.

Tämän väitöskirjatyön tarkoituksena oli tutkia lihaskoon säätelyyn osallistuvien tekijöiden, kuten myostatiinin ja aktiviininien, vaikutuksia luurankolihaksen aineenvaihduntaan ja signalointiin lihaskadossa ja -kasvussa hyödyntäen hiiri- ja/tai lihassolumallia. Lihaskato estettiin liukoisella kasvutekijäreseptorilla, joka sitoo vapaana olevan myostatiinin ja aktiviinit itseensä. Näin ne eivät voi

vaikuttaa negatiivisesti luurankolihakseen tai muihin kudoksiin. Tiedetäänkin, että tarpeeksi pitkä altistus tälle kasvutekijäreseptorille kasvattaa lihasmassaa. Liikunnankaltaisella sähköstimulaatiolla mallinettiin lihassupistusten aikaansaamia fysiologisia muutoksia ja tutkittiin molekyylitasolla mitä muutoksia lihasten supistelu aiheuttaa lihassolujen sisällä (solun sisäinen aineenvaihdunta) ja niiden ulkopuolella (lihassolujen erittämät tekijät).

Tämän väitöskirjan tulosten perusteella havaittiin, että syövän aiheuttama lihaskato muutti merkittävästi erilaisten aineenvaihduntatuotteiden ja signaalireitin proteiinien pitoisuuksia ja aktiivisuuksia niin luurankolihaksessa kuin veressä. Lisäksi, vaikka luurankolihaksen kato estettiin liukoisella kasvutekijäreseptorilla, se ei palauttanut näiden molekyylien pitoisuuksia normaalille tasolle. Näyttääkin siltä, että syövän vaikutus luurankolihaksen ja veren molekyyleihin on suurempi kuin itse lihaskoon vaikutus.

Jotta lihaskatoa aiheuttavia tekijöitä ja niiden suoria vaikutuksia lihaksen aineenvaihduntaan voidaan tutkia mekanistisemmalla tasolla, hiirikokeen jälkeen siirryttiin solukokeisiin. Tässä työssä myostatiinin aiheuttamia vasteita lihaksessa tutkittiin käyttämällä hiiri- ja ihmisperäistä lihassolulinjaa sekä erilaistumattomia ja erilaistuneita lihassoluja. Syöpäsolujen erittämien tekijöiden vaikutuksia tutkittiin kasvattamalla syöpä- ja lihassoluja yhdessä. Tulokset osoittivat, että yleisesti käytetyn hiiren lihassolulinjan erilaistuminen vähensi havaittuja vasteita myostatiinille, kun taas samaa ei havaittu ihmisen lihassolulinjalla. Syöpäsolujen vaikutukset hiiren lihassolulinjaan olivat samanlaisia erilaistumattomien ja erilaistuneiden solujen välillä. Nämä tulokset tarjoavat tärkeää tietoa solulinjojen erilaisuuksista ja käyttömahdollisuuksista erilaisissa koeasetelmissa.

Lihassolujen liikunnankaltaiset supistukset saivat aikaan sekä odotettuja että odottamattomia muutoksia niin molekyylien pitoisuuksissa kuin geenien ilmentymisessä. Eniten muuttuneisiin reitteihin kuuluivat riippumatta käytetystä mittausmenetelmästä energia-aineenvaihduntaan, lihassolujen supistuskykyyn sekä solujen ja kudosten väliseen vuorovaikutukseen osallistuvat tekijät. Ravitsemuksen roolia liikunnan aikana mallinnettiin kasvattamalla lihassoluja korkea- tai matalaglukoosisessa kasvatusliuoksessa. Tulokset osoittivat, että vasteet sekä molekyyli- että geenitasoilla olivat suurempia silloin, kun lihassoluilla oli enemmän glukoosia, eli polttoainetta, käytettävissään.

Tämän väitöskirjan tulokset osoittivat, että niin eläin- kuin solukokeilla on paikkansa lihas- ja liikuntatutkimuksessa. Saadut tulokset lisäävät solutason ymmärrystä lihaksen ja lihassolujen vasteista erilaisiin fysiologisiin muutoksiin. Näitä menetelmiä hyödyntämällä voidaan tutkia niin lihassolujen sisäistä aineenvaihduntaa kuin sitä, mikä on lihaksesta peräisin olevien säätelytekijöiden rooli kudosten välisessä vuorovaikutuksessa.

REFERENCES

Aas, V., Torblå, S., Andersen, M. H., Jensen, J., & Rustan, A. C. (2002). Electrical stimulation improves insulin responses in a human skeletal muscle cell model of hyperglycemia. *Annals of the New York Academy of Sciences*, *967*(1), 506–515.

Abdelmoez, A. M., Sardón Puig, L., Smith, J. A. B., Gabriel, B. M., Savikj, M., Dollet, L., Chibalin, A. V, Krook, A., Zierath, J. R., & Pillon, N. J. (2020). Comparative profiling of skeletal muscle models reveals heterogeneity of transcriptome and metabolism. *American Journal of Physiology-Cell Physiology*, *318*(3), C615–C626.

Al-Bayati, A., Brown, A., & Walker, M. (2019). Impaired enhancement of insulin action in cultured skeletal muscle cells from insulin resistant type 2 diabetic patients in response to contraction using electrical pulse stimulation. *Journal of Diabetes and Its Complications*, *33*(12), 107412.

Amthor, H., Macharia, R., Navarrete, R., Schuelke, M., Brown, S. C., Otto, A., Voit, T., Muntoni, F., Vrbova, G., Partridge, T., Zammit, P., Bunger, L., & Patel, K. (2007). Lack of myostatin results in excessive muscle growth but impaired force generation. *Proceedings of the National Academy of Sciences*, *104*(6), 1835–1840.

Amthor, H., Nicholas, G., McKinnell, I., Kemp, C. F. F., Sharma, M., Kambadur, R., & Patel, K. (2004). Follistatin complexes Myostatin and antagonises Myostatin-mediated inhibition of myogenesis. *Developmental Biology*, *270*(1), 19–30.

Argilés, J. M., Busquets, S., Stemmler, B., & López-Soriano, F. J. (2014). Cancer cachexia: understanding the molecular basis. *Nature Reviews Cancer*, *14*(11), 754–762.

Argilés, J. M., López-Soriano, F. J., Stemmler, B., & Busquets, S. (2019). Therapeutic strategies against cancer cachexia. *European Journal of Translational Myology*, *29*(1).

Artaza, J. N., Bhasin, S., Mallidis, C., Taylor, W., Ma, K., & Gonzalez-Cadavid, N. F. (2002). Endogenous expression and localization of myostatin and its relation to myosin heavy chain distribution in C2C12 skeletal muscle cells. *Journal of Cellular Physiology*, *190*(2), 170–179.

Atherton, P. J., & Smith, K. (2012). Muscle protein synthesis in response to nutrition and exercise. *The Journal of Physiology*, *590*(5), 1049–1057.

Ato, S., Kido, K., Miyake, T., Yokokawa, T., & Fujita, S. (2017). The Effect of Acute Resistance Exercise On Muscle Protein Synthesis in Atrophied Rat Skeletal Muscle After Unloading. *The FASEB Journal*, *31*, 1022.7.

Attaix, D., & Baracos, V. E. (2010). MAFbx/Atrogin-1 expression is a poor index of muscle proteolysis. *Current Opinion in Clinical Nutrition and Metabolic Care*, *13*(3), 223–224.

Ballarò, R., Costelli, P., & Penna, F. (2016). Animal models for cancer cachexia. *Current Opinion in Supportive and Palliative Care*, *10*(4), 281–287.

Barlow, J., Carter, S., & Solomon, T. P. J. (2018). Probing the effect of physiological

concentrations of IL-6 on insulin secretion by INS-1 832/3 insulinoma cells under diabetic-like conditions. *International Journal of Molecular Sciences*, *19*(7), 1924.

Barlow, J., & Solomon, T. P. J. (2019). Conditioned media from contracting skeletal muscle potentiates insulin secretion and enhances mitochondrial energy metabolism of pancreatic beta-cells. *Metabolism*, *91*, 1–9.

Barreto, R., Kitase, Y., Matsumoto, T., Pin, F., Colston, K. C., Couch, K. E., O'Connell, T. M., Couch, M. E., Bonewald, L. F., & Bonetto, A. (2017). ACVR2B/Fc counteracts chemotherapy-induced loss of muscle and bone mass. *Scientific Reports*, *7*(1), 1–13.

Bloise, E., Ciarmela, P., Dela Cruz, C., Luisi, S., Petraglia, F., & Reis, F. M. (2018). Activin a in mammalian physiology. *Physiological Reviews*, *99*(1), 739–780.

Bodine, S. C., & Baehr, L. M. (2014). Skeletal muscle atrophy and the E3 ubiquitin ligases MuRF1 and MAFbx/atrogin-1. *American Journal of Physiology-Endocrinology and Metabolism*, *307*(6), E469–E484.

Brasier, A. R. (2010). The nuclear factor- B-interleukin-6 signalling pathway mediating vascular inflammation. *Cardiovascular Research*, *86*(2), 211–218.

Brooks, G. A. (2020). Lactate as a fulcrum of metabolism. *Redox Biology*, *35*, 101454.

Brown, S. C., Beurg, M., Grouselle, M., Koenig, J., Krueger, S., Lucy, J. A., & Georgescauld, D. (1995). Spatial and temporal distribution of [Ca2] i in normal human myotubes. A fura-2 imaging study. *European Journal of Cell Biology*, *66*(4), 382–388.

Browne, G. J., & Proud, C. G. (2002). Regulation of peptide-chain elongation in mammalian cells. *European Journal of Biochemistry*, *269*(22), 5360–5368.

Bruce, C. R., Brolin, C., Turner, N., Cleasby, M. E., van der Leij, F. R., Cooney, G. J., & Kraegen, E. W. (2007). Overexpression of carnitine palmitoyltransferase I in skeletal muscle in vivo increases fatty acid oxidation and reduces triacylglycerol esterification. *American Journal of Physiology-Endocrinology and Metabolism*, *292*(4), E1231–E1237.

Burch, N., Arnold, A.-S., Summermatter, S., Santos, G. B. S., Christe, M., Boutellier, U., Toigo, M., & Handschin, C. (2010). Electric pulse stimulation of cultured murine muscle cells reproduces gene expression changes of trained mouse muscle. *PloS One*, *5*(6), e10970.

Burks, T. N., & Cohn, R. D. (2011). Role of TGF-β signaling in inherited and acquired myopathies. *Skeletal Muscle*, *1*(1), 19.

Cala, M. P., Agulló-Ortuño, M. T., Prieto-García, E., González-Riano, C., Parrilla-Rubio, L., Barbas, C., Díaz-García, C. V., García, A., Pernaut, C., & Adeva, J. (2018). Multiplatform plasma fingerprinting in cancer cachexia: a pilot observational and translational study. *Journal of Cachexia, Sarcopenia and Muscle*, *9*(2), 348–357.

Carter, S., & Solomon, T. P. J. (2019). In vitro experimental models for examining the skeletal muscle cell biology of exercise: the possibilities, challenges and future developments. *Pflügers Archiv-European Journal of Physiology*, *471*(3), 413–429.

Castets, P., Lin, S., Rion, N., Di Fulvio, S., Romanino, K., Guridi, M., Frank, S.,

Tintignac, L. A., Sinnreich, M., & Rüegg, M. A. (2013). Sustained activation of mTORC1 in skeletal muscle inhibits constitutive and starvation-induced autophagy and causes a severe, late-onset myopathy. *Cell Metabolism*, *17*(5), 731–744.

Catoire, M., & Kersten, S. (2015). The search for exercise factors in humans. *The FASEB Journal*, *29*(5), 1615–1628.

Chaweewannakorn, C., Nyasha, M. R., Chen, W., Sekiai, S., Tsuchiya, M., Hagiwara, Y., Bouzakri, K., Sasaki, K., & Kanzaki, M. (2020). Exercise-evoked intramuscular neutrophil-endothelial interactions support muscle performance and GLUT4 translocation: a mouse gnawing model study. *The Journal of Physiology*, *598*(1), 101–122.

Chen, J.-F., Mandel, E. M., Thomson, J. M., Wu, Q., Callis, T. E., Hammond, S. M., Conlon, F. L., & Wang, D.-Z. (2006). The role of microRNA-1 and microRNA-133 in skeletal muscle proliferation and differentiation. *Nature Genetics*, *38*(2), 228–233.

Chen, W., Nyasha, M. R., Koide, M., Tsuchiya, M., Suzuki, N., Hagiwara, Y., Aoki, M., & Kanzaki, M. (2019). In vitro exercise model using contractile human and mouse hybrid myotubes. *Scientific Reports*, *9*(1), 11914.

Choudhury, R., Beezley, J., Davis, B., Tomeck, J., Gratzl, S., Golzarri-Arroyo, L., Wan, J., Raftery, D., Baumes, J., & O'Connell, T. M. (2020). Visualization and integration of metabolomics experiments. *Journal of Open Source Software*, *5*(54), 2410.

Christensen, C. S., Christensen, D. P., Lundh, M., Dahllöf, M. S., Haase, T. N., Velasquez, J. M., Laye, M. J., Mandrup-Poulsen, T., & Solomon, T. P. J. (2015). Skeletal muscle to pancreatic β-cell cross-talk: the effect of humoral mediators liberated by muscle contraction and acute exercise on β-cell apoptosis. *The Journal of Clinical Endocrinology & Metabolism*, *100*(10), E1289–E1298.

Contrepois, K., Wu, S., Moneghetti, K. J., Hornburg, D., Ahadi, S., Tsai, M.-S., Metwally, A. A., Wei, E., Lee-McMullen, B., & Quijada, J. V. (2020). Molecular choreography of acute exercise. *Cell*, *181*(5), 1112-1130. e16.

Cotton, T. R., Fischer, G., Wang, X., McCoy, J. C., Czepnik, M., Thompson, T. B., & Hyvönen, M. (2018). Structure of the human myostatin precursor and determinants of growth factor latency. *The EMBO Journal*, *37*(3), 367–383.

Cui, P., Huang, C., Guo, J., Wang, Q., Liu, Z., Zhuo, H., & Lin, D. (2019a). Metabolic profiling of tumors, sera, and skeletal muscles from an orthotopic murine model of gastric cancer associated-cachexia. *Journal of Proteome Research*, *18*(4), 1880–1892.

Cui, P., Shao, W., Huang, C., Wu, C.-J., Jiang, B., & Lin, D. (2019b). Metabolic derangements of skeletal muscle from a murine model of glioma cachexia. *Skeletal Muscle*, *9*(1), 3.

Daskalaki, E., Pillon, N. J., Krook, A., Wheelock, C. E., & Checa, A. (2018). The influence of culture media upon observed cell secretome metabolite profiles: The balance between cell viability and data interpretability. *Analytica Chimica Acta*, *1037*, 338–350.

De Gasperi, R., Hamidi, S., Harlow, L. M., Ksiezak-Reding, H., Bauman, W. A., & Cardozo, C. P. (2017). Denervation-related alterations and biological activity of miRNAs contained in exosomes released by skeletal muscle fibers. *Scientific Reports*, *7*(1), 1–11.

Der-Torossian, H., Asher, S. A., Winnike, J. H., Wysong, A., Yin, X., Willis, M. S., O'Connell, T. M., & Couch, M. E. (2013a). Cancer cachexia's metabolic signature in a murine model confirms a distinct entity. *Metabolomics*, *9*(3), 730–739.

Der-Torossian, H., Gourin, C. G., & Couch, M. E. (2012). Translational implications of novel findings in cancer cachexia: the use of metabolomics and the potential of cardiac malfunction. *Current Opinion in Supportive and Palliative Care*, *6*(4), 446–450.

Der-Torossian, H., Wysong, A., Shadfar, S., Willis, M. S., McDunn, J., & Couch, M. E. (2013b). Metabolic derangements in the gastrocnemius and the effect of Compound A therapy in a murine model of cancer cachexia. *Journal of Cachexia, Sarcopenia and Muscle*, *4*(2), 145–155.

Derynck, R., & Budi, E. H. (2019). Specificity, versatility, and control of TGF-β family signaling. *Science Signaling*, *12*(570), eaav5183.

Derynck, R., & Zhang, Y. E. (2003). Smad-dependent and Smad-independent pathways in TGF-β family signalling. *Nature*, *425*(6958), 577.

Ding, H., Zhang, G., Sin, K. W. T., Liu, Z., Lin, R., Li, M., & Li, Y. (2017). Activin A induces skeletal muscle catabolism via p38β mitogen-activated protein kinase. *Journal of Cachexia, Sarcopenia and Muscle*, *8*(2), 202–212.

Dschietzig, T. B. (2014). Myostatin—from the mighty mouse to cardiovascular disease and cachexia. *Clinica Chimica Acta*, *433*, 216–224.

Düsterhöft, S., & Pette, D. (1990). Effects of electrically induced contractile activity on cultured embryonic chick breast muscle cells. *Differentiation*, *44*(3), 178–184.

Edom, F., Mouly, V., Barbet, J. P., Fiszman, M. Y., & Butler-Browne, G. S. (1994). Clones of human satellite cells can express in vitro both fast and slow myosin heavy chains. *Developmental Biology*, *164*(1), 219–229.

Egan, B., & Zierath, J. R. (2013). Exercise metabolism and the molecular regulation of skeletal muscle adaptation. *Cell Metabolism*, *17*(2), 162–184.

Elkina, Y., von Haehling, S., Anker, S. D., & Springer, J. (2011). The role of myostatin in muscle wasting: an overview. *Journal of Cachexia, Sarcopenia and Muscle*, *2*(3), 143.

Elsner, P., Grunnet, N., & Quistorff, B. (2003). Effects of electrostimulation on glycogenolysis in cultured rat myotubes. *Pflügers Archiv*, *447*(3), 356–362.

Evans, W. J., Morley, J. E., Argilés, J., Bales, C., Baracos, V., Guttridge, D., Jatoi, A., Kalantar-Zadeh, K., Lochs, H., & Mantovani, G. (2008). Cachexia: a new definition. *Clinical Nutrition*, *27*(6), 793–799.

Evers-van Gogh, I. J. A., Alex, S., Stienstra, R., Brenkman, A. B., Kersten, S., & Kalkhoven, E. (2015). Electric pulse stimulation of myotubes as an in vitro exercise model: cell-mediated and non-cell-mediated effects. *Scientific Reports*, *5*, 10944.

Evtushenko, E. G., Bagrov, D. V., Lazarev, V. N., Livshits, M. A., & Khomyakova, E. (2020). Adsorption of extracellular vesicles onto the tube walls during storage in solution. *PLoS One*, *15*(12), e0243738.

Farmawati, A., Kitajima, Y., Nedachi, T., Sato, M., Kanzaki, M., & Nagatomi, R. (2013). Characterization of contraction-induced IL-6 up-regulation using contractile C2C12 myotubes. *Endocrine Journal*, *60*(2), 137–147.

Fearon, K. C. H., Glass, D. J., & Guttridge, D. C. (2012). Cancer cachexia: mediators, signaling, and metabolic pathways. *Cell Metabolism*, *16*(2), 153–166.

Fearon, K., Strasser, F., Anker, S. D., Bosaeus, I., Bruera, E., Fainsinger, R. L., Jatoi, A., Loprinzi, C., MacDonald, N., & Mantovani, G. (2011). Definition and classification of cancer cachexia: an international consensus. *The Lancet Oncology*, *12*(5), 489–495.

Febvey-Combes, O., Jobard, E., Rossary, A., Pialoux, V., Foucaut, A.-M., Morelle, M., Delrieu, L., Martin, A., Caldefie-Chézet, F., Touillaud, M., Berthouze, S. E., Boumaza, H., Elena-Herrmann, B., Bachmann, P., Trédan, O., Vasson, M.-P., & Fervers, B. (2021). Effects of an exercise and nutritional intervention on circulating biomarkers and metabolomic profiling during adjuvant treatment for localized breast cancer: Results from the PASAPAS feasibility randomized controlled trial. *Integrative Cancer Therapies*, *20*, 1534735420977666.

Feng, Y. Z., Nikolić, N., Bakke, S. S., Kase, E. T., Guderud, K., Hjelmesæth, J., Aas, V., Rustan, A. C., & Thoresen, G. H. (2015). Myotubes from lean and severely obese subjects with and without type 2 diabetes respond differently to an in vitro model of exercise. *American Journal of Physiology-Cell Physiology*, *308*(7), C548–C556.

Fiuza-Luces, C., Garatachea, N., Berger, N. A., & Lucia, A. (2013). Exercise is the real polypill. *Physiology*, *28*(5), 330–358.

Forterre, A., Jalabert, A., Chikh, K., Pesenti, S., Euthine, V., Granjon, A., Errazuriz, E., Lefai, E., Vidal, H., & Rome, S. (2014). Myotube-derived exosomal miRNAs downregulate Sirtuin1 in myoblasts during muscle cell differentiation. *Cell Cycle*, *13*(1), 78–89.

Fujita, H., Nedachi, T., & Kanzaki, M. (2007). Accelerated de novo sarcomere assembly by electric pulse stimulation in C2C12 myotubes. *Experimental Cell Research*, *313*(9), 1853–1865.

Fujiwara, Y., Kobayashi, T., Chayahara, N., Imamura, Y., Toyoda, M., Kiyota, N., Mukohara, T., Nishiumi, S., Azuma, T., & Yoshida, M. (2014). Metabolomics evaluation of serum markers for cachexia and their intra-day variation in patients with advanced pancreatic cancer. *PloS One*, *9*(11), e113259.

Fukushima, T., Takata, M., Kato, A., Uchida, T., Nikawa, T., & Sakakibara, I. (2021). Transcriptome analyses of in vitro exercise models by Clenbuterol supplementation or electrical pulse stimulation. *Applied Sciences*, *11*(21), 10436.

Furuichi, Y., Manabe, Y., Takagi, M., Aoki, M., & Fujii, N. L. (2018). Evidence for acute contraction-induced myokine secretion by C2C12 myotubes. *PloS One*,

13(10), e0206146.

Gallagher, I. J., Jacobi, C., Tardif, N., Rooyackers, O., & Fearon, K. (2016). Omics/systems biology and cancer cachexia. *Seminars in Cell & Developmental Biology*, *54*, 92–103.

Gamer, L. W., Wolfman, N. M., Celeste, A. J., Hattersley, G., Hewick, R., & Rosen, V. (1999). A novel BMP expressed in developing mouse limb, spinal cord, and tail bud is a potent mesoderm inducer in Xenopus embryos. *Developmental Biology*, *208*(1), 222–232.

Ge, X., McFarlane, C., Vajjala, A., Lokireddy, S., Ng, Z. H., Tan, C. K., Tan, N. S., Wahli, W., Sharma, M., & Kambadur, R. (2011). Smad3 signaling is required for satellite cell function and myogenic differentiation of myoblasts. *Cell Research*, *21*(11), 1591–1604.

Gingras, A.-C., Raught, B., & Sonenberg, N. (1999). eIF4 initiation factors: effectors of mRNA recruitment to ribosomes and regulators of translation. *Annual Review of Biochemistry*, *68*(1), 913–963.

Giskeødegård, G. F., Madssen, T. S., Euceda, L. R., Tessem, M., Moestue, S. A., & Bathen, T. F. (2019). NMR-based metabolomics of biofluids in cancer. *NMR in Biomedicine*, *32*(10), e3927.

Goldstein, M. S. (1961). Humoral nature of the hypoglycemic factor of muscular work. *Diabetes*, *10*, 232–234.

Graber, T. G., Maroto, R., Thompson, J., Widen, S., Man, Z., Pajski, M. L., & Rasmussen, B. B. (2021). Skeletal muscle transcriptome alterations related to physical function decline in older mice. *BioRxiv*.

Graham, Z. A., De Gasperi, R., Bauman, W. A., & Cardozo, C. P. (2017). Recombinant myostatin reduces highly expressed microRNAs in differentiating C2C12 cells. *Biochemistry and Biophysics Reports*, *9*, 273–280.

Gray, A. M., & Mason, A. J. (1990). Requirement for activin A and transforming growth factor--beta 1 pro-regions in homodimer assembly. *Science*, *247*(4948), 1328–1330.

Guigni, B. A., Fix, D. K., Bivona, J. J., Palmer, B. M., Carson, J. A., & Toth, M. J. (2019). Electrical stimulation prevents doxorubicin-induced atrophy and mitochondrial loss in cultured myotubes. *American Journal of Physiology-Cell Physiology*, *317*(6), C1213–C1228.

Han, H. Q., Zhou, X., Mitch, W. E., & Goldberg, A. L. (2013). Myostatin/activin pathway antagonism: molecular basis and therapeutic potential. *The International Journal of Biochemistry & Cell Biology*, *45*(10), 2333–2347.

Han, Y.-Q., Ming, S.-L., Wu, H.-T., Zeng, L., Ba, G., Li, J., Lu, W.-F., Han, J., Du, Q.-J., & Sun, M.-M. (2018). Myostatin knockout induces apoptosis in human cervical cancer cells via elevated reactive oxygen species generation. *Redox Biology*, *19*, 412–428.

Hardee, J. P., Counts, B. R., & Carson, J. A. (2019). Understanding the role of exercise in cancer cachexia therapy. *American Journal of Lifestyle Medicine*, *13*(1), 46–60.

Hargreaves, M., & Spriet, L. L. (2020). Skeletal muscle energy metabolism during exercise. *Nature Metabolism*, 1–12.

Harrison, C. A., Al-Musawi, S. L., & Walton, K. L. (2011). Prodomains regulate the synthesis, extracellular localisation and activity of TGF-β superfamily ligands. *Growth Factors*, *29*(5), 174–186.

Hawley, J. A., Lundby, C., Cotter, J. D., & Burke, L. M. (2018). Maximizing cellular adaptation to endurance exercise in skeletal muscle. *Cell Metabolism*, *27*(5), 962–976.

Hernández-Albors, A., Castaño, A. G., Fernández-Garibay, X., Ortega, M. A., Balaguer, J., & Ramón-Azcón, J. (2019). Microphysiological sensing platform for an in-situ detection of tissue-secreted cytokines. *Biosensors and Bioelectronics: X*, *2*, 100025.

Hiam, D., & Lamon, S. (2020). Circulating microRNAs: let's not waste the potential. *American Journal of Physiology-Cell Physiology*, *319*(2), C313–C315.

Hoffman, N. J. (2017). Omics and exercise: global approaches for mapping exercise biological networks. *Cold Spring Harbor Perspectives in Medicine*, *7*(10), a029884.

Hoffmann, C., & Weigert, C. (2017). Skeletal muscle as an endocrine organ: The role of myokines in exercise adaptations. *Cold Spring Harbor Perspectives in Medicine*, *7*(11), a029793.

Hojman, P., Brolin, C., Nørgaard-Christensen, N., Dethlefsen, C., Lauenborg, B., Olsen, C. K., Åbom, M. M., Krag, T., Gehl, J., & Pedersen, B. K. (2019). IL-6 release from muscles during exercise is stimulated by lactate-dependent protease activity. *American Journal of Physiology-Endocrinology and Metabolism*, *316*(5), E940–E947.

Hong, S., Zhou, W., Fang, B., Lu, W., Loro, E., Damle, M., Ding, G., Jager, J., Zhang, S., & Zhang, Y. (2017). Dissociation of muscle insulin sensitivity from exercise endurance in mice by HDAC3 depletion. *Nature Medicine*, *23*(2), 223.

Hoshino, D., Kawata, K., Kunida, K., Hatano, A., Yugi, K., Wada, T., Fujii, M., Sano, T., Ito, Y., & Furuichi, Y. (2020). Trans-omic analysis reveals ROS-dependent pentose phosphate pathway activation after high-frequency electrical stimulation in C2C12 myotubes. *Iscience*, *23*(10), 101558.

Hu, F., Li, N., Li, Z., Zhang, C., Yue, Y., Liu, Q., Chen, L., Bilan, P. J., & Niu, W. (2018). Electrical pulse stimulation induces GLUT4 translocation in a Rac-Akt-dependent manner in C2C12 myotubes. *FEBS Letters*, *592*(4), 644–654.

Huang, Z., Chen, D., Zhang, K., Yu, B., Chen, X., & Meng, J. (2007). Regulation of myostatin signaling by c-Jun N-terminal kinase in C2C12 cells. *Cellular Signalling*, *19*(11), 2286–2295.

Huang, Z., Chen, X., & Chen, D. (2011). Myostatin: a novel insight into its role in metabolism, signal pathways, and expression regulation. *Cellular Signalling*, *23*(9), 1441–1446.

Huh, J. Y. (2018). The role of exercise-induced myokines in regulating metabolism. *Archives of Pharmacal Research*, *41*(1), 14–29.

Hui, S., Cowan, A. J., Zeng, X., Yang, L., TeSlaa, T., Li, X., Bartman, C., Zhang, Z., Jang, C., & Wang, L. (2020). Quantitative fluxomics of circulating metabolites. *Cell Metabolism*, *32*(4), 676-688. e4.

Hulmi, J. J., Nissinen, T. A., Penna, F., & Bonetto, A. (2021). Targeting the activin

receptor signaling to counteract the multi-systemic complications of cancer and its treatments. *Cells*, *10*(3), 516.

Hulmi, J. J., Oliveira, B. M., Silvennoinen, M., Hoogaars, W. M. H., Ma, H., Pierre, P., Pasternack, A., Kainulainen, H., & Ritvos, O. (2013). Muscle protein synthesis, mTORC1/MAPK/Hippo signaling, and capillary density are altered by blocking of myostatin and activins. *American Journal of Physiology-Endocrinology and Metabolism*, *304*(1), E41–E50.

Hulmi, J. J., Walker, S., Ahtiainen, J. P., Nyman, K., Kraemer, W. J., & Häkkinen, K. (2012). Molecular signaling in muscle is affected by the specificity of resistance exercise protocol. *Scandinavian Journal of Medicine & Science in Sports*, *22*(2), 240–248.

Ikeda, K., Ito, A., Imada, R., Sato, M., Kawabe, Y., & Kamihira, M. (2017). In vitro drug testing based on contractile activity of C2C12 cells in an epigenetic drug model. *Scientific Reports*, *7*, 44570.

Ishiuchi, Y., Sato, H., Tsujimura, K., Kawaguchi, H., Matsuwaki, T., Yamanouchi, K., Nishihara, M., & Nedachi, T. (2018). Skeletal muscle cell contraction reduces a novel myokine, chemokine (CXC motif) ligand 10 (CXCL10): potential roles in exercise-regulated angiogenesis. *Bioscience, Biotechnology, and Biochemistry*, *82*(1), 97–105.

Jackman, R. W., Floro, J., Yoshimine, R., Zitin, B., Eiampikul, M., El-Jack, K., Seto, D. N., & Kandarian, S. C. (2017). Continuous release of tumor-derived factors improves the modeling of cachexia in Muscle cell culture. *Frontiers in Physiology*, *8*, 738.

Jorgenson, K. W., Phillips, S. M., & Hornberger, T. A. (2020). Identifying the structural adaptations that drive the mechanical load-induced growth of skeletal muscle: A scoping review. *Cells*, *9*(7), 1658.

Kahn, B. B., Alquier, T., Carling, D., & Hardie, D. G. (2005). AMP-activated protein kinase: ancient energy gauge provides clues to modern understanding of metabolism. *Cell Metabolism*, *1*(1), 15–25.

Kainulainen, H., Hulmi, J. J., & Kujala, U. M. (2013). Potential role of branched-chain amino acid catabolism in regulating fat oxidation. *Exercise and Sport Sciences Reviews*, *41*(4), 194–200.

Kaivo-Oja, N., Mottershead, D. G., Mazerbourg, S., Myllymaa, S., Duprat, S. S., Gilchrist, R. B., Groome, N. P., Hsueh, A. J., & Ritvos, O. (2005). Adenoviral gene transfer allows Smad-responsive gene promoter analyses and delineation of type I receptor usage of transforming growth factor-β family ligands in cultured human granulosa luteal cells. *The Journal of Clinical Endocrinology & Metabolism*, *90*(1), 271–278.

Karvinen, S., Sievänen, T., Karppinen, J. E., Hautasaari, P., Bart, G., Samoylenko, A., Vainio, S. J., Ahtiainen, J. P., Laakkonen, E. K., & Kujala, U. M. (2020). MicroRNAs in extracellular vesicles in sweat change in response to endurance exercise. *Frontiers in Physiology*, *11*, 676.

Kawahara, Y., Yamaoka, K., Iwata, M., Fujimura, M., Kajiume, T., Magaki, T., Takeda, M., Ide, T., Kataoka, K., Asashima, M., & Yuge, L. (2006). Novel electrical stimulation sets the cultured myoblast contractile function to 'On.'

Pathobiology, *73*(6), 288–294.
Kim, S. G., Buel, G. R., & Blenis, J. (2013). Nutrient regulation of the mTOR complex 1 signaling pathway. *Molecules and Cells*, *35*(6), 463–473.
Klein, D. J., McKeever, K. H., Mirek, E. T., & Anthony, T. G. (2020). Metabolomic response of equine skeletal muscle to acute fatiguing exercise and training. *Frontiers in Physiology*, *11*, 110.
Kneppers, A., Verdijk, L., de Theije, C., Corten, M., Gielen, E., van Loon, L., Schols, A., & Langen, R. (2018). A novel in vitro model for the assessment of postnatal myonuclear accretion. *Skeletal Muscle*, *8*(1), 4.
Kostidis, S., Addie, R. D., Morreau, H., Mayboroda, O. A., & Giera, M. (2017). Quantitative NMR analysis of intra-and extracellular metabolism of mammalian cells: A tutorial. *Analytica Chimica Acta*, *980*, 1–24.
Koutsoulidou, A., Mastroyiannopoulos, N. P., Furling, D., Uney, J. B., & Phylactou, L. A. (2011). Expression of miR-1, miR-133a, miR-133b and miR-206 increases during development of human skeletal muscle. *BMC Developmental Biology*, *11*(1), 34.
Kramer, H. F., & Goodyear, L. J. (2007). Exercise, MAPK, and NF-κB signaling in skeletal muscle. *Journal of Applied Physiology*, *103*(1), 388–395.
Lagziel, S., Gottlieb, E., & Shlomi, T. (2020). Mind your media. *Nature Metabolism*, 1–4.
Lambernd, S., Taube, A., Schober, A., Platzbecker, B., Görgens, S. W., Schlich, R., Jeruschke, K., Weiss, J., Eckardt, K., & Eckel, J. (2012). Contractile activity of human skeletal muscle cells prevents insulin resistance by inhibiting pro-inflammatory signalling pathways. *Diabetologia*, *55*(4), 1128–1139.
Langley, B., Thomas, M., Bishop, A., Sharma, M., Gilmour, S., & Kambadur, R. (2002). Myostatin inhibits myoblast differentiation by down-regulating MyoD expression. *Journal of Biological Chemistry*, *277*(51), 49831–49840.
Laplante, M., & Sabatini, D. M. (2009). mTOR signaling at a glance. *Journal of Cell Science*, *122*(20), 3589–3594.
Laplante, M., & Sabatini, D. M. (2012). mTOR signaling in growth control and disease. *Cell*, *149*(2), 274–293.
Laurens, C., Bergouignan, A., & Moro, C. (2020a). Exercise-released myokines in the control of energy metabolism. *Frontiers in Physiology*, *11*.
Laurens, C., Parmar, A., Murphy, E., Carper, D., Lair, B., Maes, P., Vion, J., Boulet, N., Fontaine, C., Marquès, M., Larrouy, D., Harant, I., Thalamas, C., Montastier, E., Caspar-Bauguil, S., Bourlier, V., Tavernier, G., Grolleau, J.-L., Bouloumié, A., … Moro, C. (2020b). Growth and differentiation factor 15 is secreted by skeletal muscle during exercise and promotes lipolysis in humans. *JCI Insight*, *5*(6), e131870.
Lee, J. H., & Jun, H.-S. (2019). Role of myokines in regulating skeletal muscle Mass and function. *Frontiers in Physiology*, *10*, 42.
Lee, S.-J., & Glass, D. J. (2011). Treating cancer cachexia to treat cancer. *Skeletal Muscle*, *1*(1), 1–5.
Lee, S.-J., & McPherron, A. C. (2001). Regulation of myostatin activity and muscle growth. *Proceedings of the National Academy of Sciences*, *98*(16), 9306–9311.

Lee, S.-J., Reed, L. A., Davies, M. V, Girgenrath, S., Goad, M. E. P., Tomkinson, K. N., Wright, J. F., Barker, C., Ehrmantraut, G., & Holmstrom, J. (2005). Regulation of muscle growth by multiple ligands signaling through activin type II receptors. *Proceedings of the National Academy of Sciences*, *102*(50), 18117–18122.

Lessard, S. J., MacDonald, T. L., Pathak, P., Han, M. S., Coffey, V. G., Edge, J., Rivas, D. A., Hirshman, M. F., Davis, R. J., & Goodyear, L. J. (2018). JNK regulates muscle remodeling via myostatin/SMAD inhibition. *Nature Communications*, *9*(1), 3030.

Lewis, G. D., Farrell, L., Wood, M. J., Martinovic, M., Arany, Z., Rowe, G. C., Souza, A., Cheng, S., McCabe, E. L., Yang, E., Shi, X., Deo, R., Roth, F. P., Asnani, A., Rhee, E. P., Systrom, D. M., Semigran, M. J., Vasan, R. S., Carr, S. A., … Gerszten, R. E. (2010). Metabolic signatures of exercise in human plasma. *Science Translational Medicine*, *2*(33), 33ra37.

Li, L.-J., Ma, J., Li, S.-B., Chen, X.-F., & Zhang, J. (2019). Electric pulse stimulation inhibited lipid accumulation on C2C12 myotubes incubated with oleic acid and palmitic acid. *Archives of Physiology and Biochemistry*, 1–7.

Li, Z., Yue, Y., Hu, F., Zhang, C., Ma, X., Li, N., Qiu, L., Fu, M., Chen, L., & Yao, Z. (2018). Electrical pulse stimulation induces GLUT4 translocation in C2C12 myotubes that depends on Rab8A, Rab13, and Rab14. *American Journal of Physiology-Endocrinology and Metabolism*, *314*(5), E478–E493.

Lim, S., Chaves, A., Zheng, D., & Houmard, J. (2018). Increases in insulin signaling following electrical pulse stimulation are blunted in myotubes derived from severely obese individuals with or without type 2 diabetes. *The FASEB Journal*, *32*, 603.18.

Ling, N., Ying, S.-Y., Ueno, N., Shimasaki, S., Esch, F., Hotta, M., & Guillemin, R. (1986). Pituitary FSH is released by a heterodimer of the β-subunits from the two forms of inhibin. *Nature*, *321*(6072), 779–782.

Liu, L., Zhang, Y., Liu, T., Ke, C., Huang, J., Fu, Y., Lin, Z., Chen, F., Wu, X., & Chen, Q. (2021). Pyrroloquinoline quinone protects against exercise-induced fatigue and oxidative damage via improving mitochondrial function in mice. *The FASEB Journal*, *35*(4), e21394.

Liu, X., Cooper, D. E., Cluntun, A. A., Warmoes, M. O., Zhao, S., Reid, M. A., Liu, J., Lund, P. J., Lopes, M., & Garcia, B. A. (2018). Acetate production from glucose and coupling to mitochondrial metabolism in mammals. *Cell*, *175*(2), 502-513. e13.

Lombardi, G., Sanchis-Gomar, F., Perego, S., Sansoni, V., & Banfi, G. (2016). Implications of exercise-induced adipo-myokines in bone metabolism. *Endocrine*, *54*(2), 284–305.

Loumaye, A., de Barsy, M., Nachit, M., Lause, P., van Maanen, A., Trefois, P., Gruson, D., & Thissen, J. (2017). Circulating Activin A predicts survival in cancer patients. *Journal of Cachexia, Sarcopenia and Muscle*, *8*(5), 768–777.

Lovett, J. A. C., Durcan, P. J., & Myburgh, K. H. (2018). Investigation of circulating extracellular vesicle microRNA following two consecutive bouts of muscle-damaging exercise. *Frontiers in Physiology*, *9*, 1149.

Løvsletten, N. G., Rustan, A. C., Laurens, C., Thoresen, G. H., Moro, C., & Nikolić, N. (2020). Primary defects in lipid handling and resistance to exercise in myotubes from obese donors with and without type 2 diabetes. *Applied Physiology, Nutrition, and Metabolism*, *45*(2), 169–179.

Lowe, R., Shirley, N., Bleackley, M., Dolan, S., & Shafee, T. (2017). Transcriptomics technologies. *PLoS Computational Biology*, *13*(5), e1005457.

Lu, M., Sanderson, S. M., Zessin, A., Ashcraft, K. A., Jones, L. W., Dewhirst, M. W., Locasale, J. W., & Hsu, D. S. (2018). Exercise inhibits tumor growth and central carbon metabolism in patient-derived xenograft models of colorectal cancer. *Cancer & Metabolism*, *6*(1), 14.

Ly, C. H., Lynch, G. S., & Ryall, J. G. (2020). A metabolic roadmap for somatic stem cell fate. *Cell Metabolism*, *31*(6), 1052–1067.

Ma, X. M., & Blenis, J. (2009). Molecular mechanisms of mTOR-mediated translational control. *Nature Reviews Molecular Cell Biology*, *10*(5), 307.

MacDonald, T. L., Pattamaprapanont, P., Pathak, P., Fernandez, N., Freitas, E. C., Hafida, S., Mitri, J., Britton, S. L., Koch, L. G., & Lessard, S. J. (2020). Hyperglycaemia is associated with impaired muscle signalling and aerobic adaptation to exercise. *Nature Metabolism*, *2*(9), 902–917.

Mann, T. N., Lamberts, R. P., & Lambert, M. I. (2014). High responders and low Responders: Factors associated with individual variation in response to standardized training. *Sports Medicine*, *44*(8), 1113–1124.

Marotta, M., Bragós, R., & Gómez-Foix, A. M. (2004). Design and performance of an electrical stimulator for long-term contraction of cultured muscle cells. *BioTechniques*, *36*(1), 68–73.

Marš, T., Miš, K., Meznarič, M., Prpar Mihevc, S., Vid, J., Haugen, F., Rogelj, B., Raustan, A. C., Thoresen, G. H., Pirkmajer, S., & Nikolić, N. (2020). Innervation and electrical pulse stimulation–in vitro effects on human skeletal muscle cells. *Applied Physiology, Nutrition, and Metabolism*, *ja*.

Marshall, D. D., & Powers, R. (2017). Beyond the paradigm: Combining mass spectrometry and nuclear magnetic resonance for metabolomics. *Progress in Nuclear Magnetic Resonance Spectroscopy*, *100*, 1–16.

Massagué, J., Seoane, J., & Wotton, D. (2005). Smad transcription factors. *Genes and Development*, *19*(23), 2783–2810.

Matsakas, A., Macharia, R., Otto, A., Elashry, M. I., Mouisel, E., Romanello, V., Sartori, R., Amthor, H., Sandri, M., Narkar, V., & Patel, K. (2012). Exercise training attenuates the hypermuscular phenotype and restores skeletal muscle function in the myostatin null mouse. *Experimental Physiology*, *97*(1), 125–140.

Matsakas, A., Mouisel, E., Amthor, H., & Patel, K. (2010). Myostatin knockout mice increase oxidative muscle phenotype as an adaptive response to exercise. *Journal of Muscle Research and Cell Motility*, *31*(2), 111–125.

Maurer, J., Hoene, M., & Weigert, C. (2021). Signals from the circle: Tricarboxylic acid cycle intermediates as myometabokines. *Metabolites*, *11*(8), 474.

McPherron, A. C., Lawler, A. M., & Lee, S.-J. (1997). Regulation of skeletal muscle mass in mice by a new TGF-p superfamily member. *Nature*, *387*(6628), 83.

McPherron, A. C., Lawler, A. M., & Lee, S.-J. (1999). Regulation of anterior/posterior patterning of the axial skeleton by growth/differentiation factor 11. *Nature Genetics*, *22*(3), 260–264.

Melzer, K. (2011). Carbohydrate and fat utilization during rest and physical activity. *E-SPEN, the European e-Journal of Clinical Nutrition and Metabolism*, *6*(2), e45–e52.

Mestre, R., Patiño, T., Barceló, X., Anand, S., Pérez-Jiménez, A., & Sánchez, S. (2018). Force modulation and adaptability of 3D-bioprinted biological actuators based on skeletal muscle tissue. *Advanced Materials Technologies*, 1800631.

Miller, J., Alshehri, A., Ramage, M. I., Stephens, N. A., Mullen, A. B., Boyd, M., Ross, J. A., Wigmore, S. J., Watson, D. G., & Skipworth, R. J. E. (2019). Plasma metabolomics identifies lipid and amino acid markers of weight loss in patients with upper gastrointestinal cancer. *Cancers*, *11*(10), 1594.

Miyatake, S., Bilan, P. J., Pillon, N. J., & Klip, A. (2016). Contracting C2C12 myotubes release CCL2 in an NF-κB-dependent manner to induce monocyte chemoattraction. *American Journal of Physiology-Endocrinology and Metabolism*, *310*(2), E160–E170.

Mooren, F. C., Viereck, J., Krüger, K., & Thum, T. (2014). Circulating microRNAs as potential biomarkers of aerobic exercise capacity. *American Journal of Physiology-Heart and Circulatory Physiology*, *306*(4), H557–H563.

Moran, J. L., Li, Y., Hill, A. A., Mounts, W. M., & Miller, C. P. (2002). Gene expression changes during mouse skeletal myoblast differentiation revealed by transcriptional profiling. *Physiological Genomics, 10*(2), 103-111.

Mouisel, E., Relizani, K., Mille-Hamard, L., Denis, R., Hourdé, C., Agbulut, O., Patel, K., Arandel, L., Morales-Gonzalez, S., Vignaud, A., Garcia, L., Ferry, A., Luquet, S., Billat, V., Ventura-Clapier, R., Schuelke, M., & Amthor, H. (2014). Myostatin is a key mediator between energy metabolism and endurance capacity of skeletal muscle. *American Journal of Physiology-Regulatory, Integrative and Comparative Physiology*, *307*(4), R444–R454.

Murphy, R. M., Watt, M. J., & Febbraio, M. A. (2020). Metabolic communication during exercise. *Nature Metabolism*, *2*(9), 805–816.

Nakamura, T., Takagi, S., Okuzaki, D., Matsui, S., & Fujisato, T. (2021). Hypoxia transactivates cholecystokinin gene expression in 3D-engineered muscle. *Journal of Bioscience and Bioengineering*, *132*(1), 64–70.

Nakashima, M., Toyono, T., Akamine, A., & Joyner, A. (1999). Expression of growth/differentiation factor 11, a new member of the BMP/TGFβ superfamily during mouse embryogenesis. *Mechanisms of Development*, *80*(2), 185–189.

Nandi, D., Tahiliani, P., Kumar, A., & Chandu, D. (2006). The ubiquitin-proteasome system. *Journal of Biosciences*, *31*(1), 137–155.

Naumann, K., & Pette, D. (1994). Effects of chronic stimulation with different impulse patterns on the expression of myosin isoforms in rat myotube cultures. *Differentiation*, *55*(3), 203–211.

Nedachi, T., Fujita, H., & Kanzaki, M. (2008). Contractile C2C12 myotube model

for studying exercise-inducible responses in skeletal muscle. *American Journal of Physiology-Endocrinology and Metabolism*, *295*(5), E1191–E1204.

Nedachi, T., Hatakeyama, H., Kono, T., Sato, M., & Kanzaki, M. (2009). Characterization of contraction-inducible CXC chemokines and their roles in C2C12 myocytes. *American Journal of Physiology-Endocrinology and Metabolism*, *297*(4), E866–E878.

Newman, J. C., & Verdin, E. (2014). β-hydroxybutyrate: much more than a metabolite. *Diabetes Research and Clinical Practice*, *106*(2), 173–181.

Nie, Y., Sato, Y., Wang, C., Yue, F., Kuang, S., & Gavin, T. P. (2016). Impaired exercise tolerance, mitochondrial biogenesis, and muscle fiber maintenance in miR-133a–deficient mice. *The FASEB Journal*, *30*(11), 3745–3758.

Nikolić, N., Görgens, S. W., Thoresen, G. H., Aas, V., Eckel, J., & Eckardt, K. (2017). Electrical pulse stimulation of cultured skeletal muscle cells as a model for in vitro exercise - possibilities and limitations. *Acta Physiologica*, *220*(3), 310–331.

Nikolić, N., Skaret Bakke, S., Tranheim Kase, E., Rudberg, I., Flo Halle, I., Rustan, A. C., Thoresen, G., & Aas, V. (2012). Electrical pulse stimulation of cultured human skeletal muscle cells as an in vitro model of exercise. *PLoS ONE*, *7*(3), e33203.

Nissinen, T. A., Hentilä, J., Penna, F., Lampinen, A., Lautaoja, J. H., Fachada, V., Holopainen, T., Ritvos, O., Kivelä, R., & Hulmi, J. J. (2018). Treating cachexia using soluble ACVR2B improves survival, alters mTOR localization, and attenuates liver and spleen responses. *Journal of Cachexia, Sarcopenia and Muscle*, *9*(3), 514–529.

O'Connell, T. M., Ardeshirpour, F., Asher, S. A., Winnike, J. H., Yin, X., George, J., Guttridge, D. C., He, W., Wysong, A., & Willis, M. S. (2008). Metabolomic analysis of cancer cachexia reveals distinct lipid and glucose alterations. *Metabolomics*, *4*(3), 216.

O'Connell, T. M., Pin, F., Couch, M. E., & Bonetto, A. (2019). Treatment with soluble activin receptor type IIB alters metabolic response in chemotherapy-induced cachexia. *Cancers*, *11*(9), 1222.

Ogasawara, R., Jensen, T. E., Goodman, C. A., & Hornberger, T. A. (2019). Resistance exercise-induced hypertrophy: a potential role for rapamycin-insensitive mTOR. *Exercise and Sport Sciences Reviews*, *47*(3), 188–194.

Oliver, S. G., Winson, M. K., Kell, D. B., & Baganz, F. (1998). Systematic functional analysis of the yeast genome. *Trends in Biotechnology*, *16*(9), 373–378.

Otto, A., & Patel, K. (2010). Signalling and the control of skeletal muscle size. *Experimental Cell Research*, *316*(18), 3059–3066.

Park, S., Turner, K. D., Zheng, D., Brault, J. J., Zou, K., Chaves, A. B., Nielsen, T. S., Tanner, C. J., Treebak, J. T., & Houmard, J. A. (2019). Electrical pulse stimulation induces differential responses in insulin action in myotubes from severely obese individuals. *The Journal of Physiology*, *597*(2), 449–466.

Peake, J. M., Della Gatta, P., Suzuki, K., & Nieman, D. C. (2015). Cytokine expression and secretion by skeletal muscle cells: regulatory mechanisms and exercise effects. *Exercise Immunology Review*, *21*(2), 8–25.

Peake, J. M., Neubauer, O., Della Gatta, P. A., & Nosaka, K. (2017). Muscle damage and inflammation during recovery from exercise. *Journal of Applied Physiology*, *122*(3), 559–570.

Pedersen, B. K., Akerstrom, T. C. A., Nielsen, A. R., & Fischer, C. P. (2007). Role of myokines in exercise and metabolism. *Journal of Applied Physiology*, *103*(3), 1093–1098.

Pedersen, B. K., & Saltin, B. (2015). Exercise as medicine - evidence for prescribing exercise as therapy in 26 different chronic diseases. *Scandinavian Journal of Medicine & Science in Sports*, *25*, 1–72.

Pedersen, K. S., Gatto, F., Zerahn, B., Nielsen, J., Pedersen, B. K., Hojman, P., & Gehl, J. (2020). Exercise-mediated lowering of glutamine availability suppresses tumor growth and attenuates muscle wasting. *Iscience*, 100978.

Pekkala, S., Wiklund, P., Hulmi, J. J., Pöllänen, E., Marjomäki, V., Munukka, E., Pierre, P., Mouly, V., Mero, A., & Alén, M. (2015). Cannabinoid receptor 1 and acute resistance exercise–In vivo and in vitro studies in human skeletal muscle. *Peptides*, *67*, 55–63.

Penna, F., Ballarò, R., Beltrà, M., De Lucia, S., García Castillo, L., & Costelli, P. (2019). The skeletal muscle as an active player against cancer cachexia. *Frontiers in Physiology*, *10*, 41.

Penna, F., Costamagna, D., Fanzani, A., Bonelli, G., Baccino, F. M., & Costelli, P. (2010). Muscle wasting and impaired myogenesis in tumor bearing mice are prevented by ERK inhibition. *PloS One*, *5*(10), e13604.

Philip, B., Lu, Z., & Gao, Y. (2005). Regulation of GDF-8 signaling by the p38 MAPK. *Cellular Signalling*, *17*(3), 365–375.

Piccirillo, R. (2019). Exercise-induced myokines with therapeutic potential for muscle wasting. *Frontiers in Physiology*, *10*, 287.

Pillon, N. J., Gabriel, B. M., Dollet, L., Smith, J. A. B., Puig, L. S., Botella, J., Bishop, D. J., Krook, A., & Zierath, J. R. (2020). Transcriptomic profiling of skeletal muscle adaptations to exercise and inactivity. *Nature Communications*, *11*(1), 1–15.

Pin, F., Barreto, R., Couch, M. E., Bonetto, A., & O'Connell, T. M. (2019). Cachexia induced by cancer and chemotherapy yield distinct perturbations to energy metabolism. *Journal of Cachexia, Sarcopenia and Muscle*, *10*(1), 140–154.

Porporato, P. E. (2016). Understanding cachexia as a cancer metabolism syndrome. *Oncogenesis*, *5*(2), e200.

Pourteymour, S., Eckardt, K., Holen, T., Langleite, T., Lee, S., Jensen, J., Birkeland, K. I., Drevon, C. A., & Hjorth, M. (2017). Global mRNA sequencing of human skeletal muscle: Search for novel exercise-regulated myokines. *Molecular Metabolism*, *6*(4), 352–365.

Puhka, M., Nordberg, M. E., Valkonen, S., Rannikko, A., Kallioniemi, O., Siljander, P., & Af Hällström, T. M. (2017). KeepEX, a simple dilution protocol for improving extracellular vesicle yields from urine. *European Journal of Pharmaceutical Sciences*, *98*, 30–39.

Rabinowitz, J. D., & White, E. (2010). Autophagy and metabolism. *Science*, *330*(6009), 1344–1348.

Raschke, S., Eckardt, K., Holven, K. B., Jensen, J., & Eckel, J. (2013). Identification and validation of novel contraction-regulated myokines released from primary human skeletal muscle cells. *PloS One*, *8*(4), e62008.

Raschke, S., & Eckel, J. (2013). Adipo-Myokines: Two Sides of the Same Coin—Mediators of Inflammation and Mediators of Exercise. *Mediators of Inflammation*, *2013*, 1–16.

Raun, S. H., Buch-Larsen, K., Schwarz, P., & Sylow, L. (2021). Exercise—A Panacea of Metabolic Dysregulation in Cancer: Physiological and Molecular Insights. *International Journal of Molecular Sciences*, *22*(7), 3469.

Reeds, P. J., Kurpad, A., Opekun, A., Jahoor, F., Wong, W. W., & Klein, P. D. (1993). Acute phase and transport protein synthesis in stimulated infection in undernourished men using uniformly labelled Spirulina Platensis. *International Atomic Energy Agency*, 21.

Reimann, J., Schnell, S., Schwartz, S., Kappes-Horn, K., Dodel, R., & Bacher, M. (2010). Macrophage migration inhibitory factor in normal human skeletal muscle and inflammatory myopathies. *Journal of Neuropathology & Experimental Neurology*, *69*(6), 654–662.

Reimann, L., Wiese, H., Leber, Y., Schwäble, A. N., Fricke, A. L., Rohland, A., Knapp, B., Peikert, C. D., Drepper, F., & van der Ven, P. F. M. (2017). Myofibrillar Z-discs are a protein phosphorylation hot spot with protein kinase C (PKCα) modulating protein dynamics. *Molecular & Cellular Proteomics*, *16*(3), 346–367.

Ren, D., Song, J., Liu, R., Zeng, X., Yan, X., Zhang, Q., & Yuan, X. (2021). Molecular and Biomechanical Adaptations to Mechanical Stretch in Cultured Myotubes. *Frontiers in Physiology*, *12*.

Ríos, R., Carneiro, I., Arce, V. M., & Devesa, J. (2001). Myostatin regulates cell survival during C2C12 myogenesis. *Biochemical and Biophysical Research Communications*, *280*(2), 561–566.

Rodgers, B. D., & Ward, C. W. (2021). Myostatin/Activin receptor ligands in muscle and the development status of attenuating drugs. *Endocrine Reviews*, bnab030.

Rodgers, B. D., Wiedeback, B. D., Hoversten, K. E., Jackson, M. F., Walker, R. G., & Thompson, T. B. (2014). Myostatin stimulates, not inihibits, C2C12 myoblast proliferation. *Endocrinology*, *155*(3), 670–675.

Rodrigues, A. C., Spagnol, A. R., Frias, F. de T., de Mendonça, M., Araújo, H. N., Guimarães, D., Silva, W. J., Bolin, A. P., Murata, G. M., & Silveira, L. (2021). Intramuscular Injection of miR-1 Reduces Insulin Resistance in Obese Mice. *Frontiers in Physiology*, *12*, 676265.

Rodriguez, J., Vernus, B., Chelh, I., Cassar-Malek, I., Gabillard, J.-C., Sassi, A. H., Seiliez, I., Picard, B., & Bonnieu, A. (2014). Myostatin and the skeletal muscle atrophy and hypertrophy signaling pathways. *Cellular and Molecular Life Sciences*, *71*(22), 4361–4371.

Rome, S., Forterre, A., Bouzakri, K., & Mizgier, M. L. (2019). Skeletal muscle-released extracellular vesicles: State of the art. *Frontiers in Physiology*, *10*, 929.

Romijn, J. A., Coyle, E. F., Sidossis, L. S., Gastaldelli, A., Horowitz, J. F., Endert,

E., & Wolfe, R. R. (1993). Regulation of endogenous fat and carbohydrate metabolism in relation to exercise intensity and duration. *American Journal of Physiology-Endocrinology And Metabolism*, *265*(3), E380–E391.

Rossi, S., Stoppani, E., Gobbo, M., Caroli, A., & Fanzani, A. (2010). L6E9 myoblasts are deficient of myostatin and additional TGF-? Members are candidates to developmentally control their fiber formation. *BioMed Research International*, *2010*, 326909.

Russell, A. P., & Lamon, S. (2015). Exercise, skeletal muscle and circulating microRNAs. In *Progress in Molecular Biology and Translational Science* (pp. 471–496).

Russell, A. P., Lamon, S., Boon, H., Wada, S., Güller, I., Brown, E. L., Chibalin, A. V., Zierath, J. R., Snow, R. J., Stepto, N., Wadley, G. D., & Akimoto, T. (2013). Regulation of miRNAs in human skeletal muscle following acute endurance exercise and short-term endurance training. *The Journal of Physiology*, *591*(18), 4637–4653.

Safdar, A., Saleem, A., & Tarnopolsky, M. A. (2016). The potential of endurance exercise-derived exosomes to treat metabolic diseases. *Nature Reviews Endocrinology*, *12*(9), 504.

Safdar, A., & Tarnopolsky, M. A. (2018). Exosomes as mediators of the systemic adaptations to endurance exercise. *Cold Spring Harbor Perspectives in Medicine*, *8*(3), a029827.

Sakaguchi, C. A., Nieman, D. C., Signini, E. F., Abreu, R. M., & Catai, A. M. (2019). Metabolomics-based studies assessing exercise-induced alterations of the human metabolome: A systematic review. *Metabolites*, *9*(8), 164.

Sancak, Y., Bar-Peled, L., Zoncu, R., Markhard, A. L., Nada, S., & Sabatini, D. M. (2010). Ragulator-Rag complex targets mTORC1 to the lysosomal surface and is necessary for its activation by amino acids. *Cell*, *141*(2), 290–303.

Sartori, R., Hagg, A., Zampieri, S., Armani, A., Winbanks, C. E., Viana, L. R., Haidar, M., Watt, K. I., Qian, H., Pezzini, C., Zanganeh, P., Turner, B. J., Larsson, A., Zanchettin, G., Pierobon, E. S., Moletta, L., Valmasoni, M., Ponzoni, A., Attar, S., … Sandri, M. (2021a). Perturbed BMP signaling and denervation promote muscle wasting in cancer cachexia. *Science Translational Medicine*, *13*(605), eaay9592.

Sartori, R., Romanello, V., & Sandri, M. (2021b). Mechanisms of muscle atrophy and hypertrophy: implications in health and disease. *Nature Communications*, *12*(1), 330.

Sartori, R., Schirwis, E., Blaauw, B., Bortolanza, S., Zhao, J., Enzo, E., Stantzou, A., Mouisel, E., Toniolo, L., Ferry, A., Stricker, S., Goldberg, A. L., Dupont, S., Piccolo, S., Amthor, H., & Sandri, M. (2013). BMP signaling controls muscle mass. *Nature Genetics*, *45*(11), 1309–1318.

Scheler, M., Irmler, M., Lehr, S., Hartwig, S., Staiger, H., Al-Hasani, H., Beckers, J., Hrabé de Angelis, M., Häring, H.-U., & Weigert, C. (2013). Cytokine response of primary human myotubes in an in vitro exercise model. *American Journal of Physiology-Cell Physiology*, *305*(8), C877–C886.

Schmidt, E. K., Clavarino, G., Ceppi, M., & Pierre, P. (2009). SUnSET, a

nonradioactive method to monitor protein synthesis. *Nature Methods*, *6*(4), 275.

Schmierer, B., & Hill, C. S. (2007). TGFβ–SMAD signal transduction: molecular specificity and functional flexibility. *Nature Reviews Molecular Cell Biology*, *8*(12), 970–982.

Schneyer, A. L., Sidis, Y., Gulati, A., Sun, J. L., Keutmann, H., & Krasney, P. A. (2008). Differential antagonism of activin, myostatin and growth and differentiation factor 11 by wild-type and mutant follistatin. *Endocrinology*, *149*(9), 4589–4595.

Schnyder, S., & Handschin, C. (2015). Skeletal muscle as an endocrine organ: PGC-1α, myokines and exercise. *Bone*, *80*, 115–125.

Schranner, D., Kastenmüller, G., Schönfelder, M., Römisch-Margl, W., & Wackerhage, H. (2020). Metabolite concentration changes in humans after a bout of exercise: a systematic review of exercise metabolomics studies. *Sports Medicine-Open*, *6*(1), 11.

Schultz, E., & Lipton, B. H. (1982). Skeletal muscle satellite cells: Changes in proliferation potential as a function of age. *Mechanisms of Ageing and Development*, *20*(4), 377–383.

Scioscia, K. A., Snyderman, C. H., & Wagner, R. (1998). Altered serum amino acid profiles in head and neck cancer. *Nutrition and Cancer*, *30*(2), 144–147.

Severinsen, M. C. K., & Pedersen, B. K. (2020). Muscle–organ crosstalk: The emerging roles of myokines. *Endocrine Reviews*, *41*(4), 594–609.

Shainberg, A., & Burstein, M. (1976). Decrease of acetylcholine receptor synthesis in muscle cultures by electrical stimulation. *Nature*, *264*(5584), 368.

Shirasaki, Y., Yamagishi, M., Suzuki, N., Izawa, K., Nakahara, A., Mizuno, J., Shoji, S., Heike, T., Harada, Y., & Nishikomori, R. (2014). Real-time single-cell imaging of protein secretion. *Scientific Reports*, *4*, 4736.

Sidorenko, S., Klimanova, E., Milovanova, K., Lopina, O. D., Kapilevich, L. V, Chibalin, A. V, & Orlov, S. N. (2018). Transcriptomic changes in C2C12 myotubes triggered by electrical stimulation: Role of Ca2+i-mediated and Ca2+i-independent signaling and elevated [Na+]i/[K+]i ratio. *Cell Calcium*, *76*, 72–86.

Silver, J., Wadley, G., & Lamon, S. (2018). Mitochondrial regulation in skeletal muscle: A role for non-coding RNAs? *Experimental Physiology*, *103*(8), 1132–1144.

Simonsen, J. B. (2017). What are we looking at? Extracellular vesicles, lipoproteins, or both? *Circulation Research*, *121*(8), 920–922.

Sirniö, P., Väyrynen, J. P., Klintrup, K., Mäkelä, J., Karhu, T., Herzig, K.-H., Minkkinen, I., Mäkinen, M. J., Karttunen, T. J., & Tuomisto, A. (2019). Alterations in serum amino-acid profile in the progression of colorectal cancer: Associations with systemic inflammation, tumour stage and patient survival. *British Journal of Cancer*, *120*(2), 238–246.

Son, Y. H., Lee, S.-M., Lee, S. H., Yoon, J. H., Kang, J. S., Yang, Y. R., & Kwon, K.-S. (2019). Comparative molecular analysis of endurance exercise in vivo with electrically stimulated in vitro myotube contraction. *Journal of Applied*

Physiology, *127*(6), 1742–1753.
Soplinska, A., Zareba, L., Wicik, Z., Eyileten, C., Jakubik, D., Siller-Matula, J. M., De Rosa, S., Malek, L. A., & Postula, M. (2020). MicroRNAs as biomarkers of systemic changes in response to endurance exercise—A comprehensive review. *Diagnostics*, *10*(10), 813.
Spriet, L. L. (2014). New insights into the interaction of carbohydrate and fat metabolism during exercise. *Sports Medicine*, *44*(1), 87–96.
Stephens, N. A., Skipworth, R. J., & Fearon, K. C. (2008). Cachexia, survival and the acute phase response. *Current Opinion in Supportive & Palliative Care*, *2*(4), 267–274.
Stojan, G., & Christopher-Stine, L. (2015). Metabolic, drug-induced, and other noninflammatory myopathies. In *Rheumatology* (pp. 1255–1263).
Tamura, K., Goto-Inoue, N., Miyata, K., Furuichi, Y., Fujii, N. L., & Manabe, Y. (2020). Effect of treatment with conditioned media derived from C2C12 myotube on adipogenesis and lipolysis in 3T3-L1 adipocytes. *PloS One*, *15*(8), e0237095.
Tamura, Y., Kouzaki, K., Kotani, T., & Nakazato, K. (2020). Electrically stimulated contractile activity-induced transcriptomic responses and metabolic remodeling in C2C12 myotubes: twitch vs. tetanic contractions. *American Journal of Physiology-Cell Physiology*, *319*(6), C1029–C1044.
Tarum, J., Folkesson, M., Atherton, P. J., & Kadi, F. (2017). Electrical pulse stimulation: an in vitro exercise model for the induction of human skeletal muscle cell hypertrophy. A proof-of-concept study. *Experimental Physiology*, *102*(11), 1405–1413.
Thelen, M. H. M., Simonides, W. S., & Hardeveld, C. van. (1997). Electrical stimulation of C2C12 myotubes induces contractions and represses thyroid-hormone-dependent transcription of the fast-type sarcoplasmic-reticulum Ca2 -ATPase gene. *Biochemical Journal*, *321*(3), 845–848.
Thorley, M., Duguez, S., Mazza, E. M. C., Valsoni, S., Bigot, A., Mamchaoui, K., Harmon, B., Voit, T., Mouly, V., & Duddy, W. (2016). Skeletal muscle characteristics are preserved in hTERT/cdk4 human myogenic cell lines. *Skeletal Muscle*, *6*(1), 43.
Tillander, V., Nordström, E. A., Reilly, J., Strozyk, M., Van Veldhoven, P. P., Hunt, M. C., & Alexson, S. E. H. (2014). Acyl-CoA thioesterase 9 (ACOT9) in mouse may provide a novel link between fatty acid and amino acid metabolism in mitochondria. *Cellular and Molecular Life Sciences*, *71*(5), 933–948.
Tipton, K. D., Hamilton, D. L., & Gallagher, I. J. (2018). Assessing the role of muscle protein breakdown in response to nutrition and exercise in humans. *Sports Medicine*, *48*(S1), 53–64.
Townson, S. A., Martinez-Hackert, E., Greppi, C., Lowden, P., Sako, D., Liu, J., Ucran, J. A., Liharska, K., Underwood, K. W., Seehra, J., Kumar, R., & Grinberg, A. V. (2012). Specificity and structure of a high affinity Activin Receptor-like Kinase 1 (ALK1) signaling complex. *Journal of Biological Chemistry*, *287*(33), 27313–27325.
Trendelenburg, A. U., Meyer, A., Rohner, D., Boyle, J., Hatakeyama, S., & Glass,

D. J. (2009). Myostatin reduces Akt/TORC1/p70S6K signaling, inhibiting myoblast differentiation and myotube size. *American Journal of Physiology-Cell Physiology*, *296*(6), C1258–C1270.

Trovato, E., Di Felice, V., & Barone, R. (2019). Extracellular vesicles: delivery vehicles of myokines. *Frontiers in Physiology*, *10*, 522.

Tseng, Y.-C., Kulp, S. K., Lai, I.-L., Hsu, E.-C., He, W. A., Frankhouser, D. E., Yan, P. S., Mo, X., Bloomston, M., Lesinski, G. B., Marcucci, G., Guttridge, D. C., Bekaii-Saab, T., & Chen, C.-S. (2015). Preclinical investigation of the novel histone deacetylase inhibitor AR-42 in the treatment of cancer-induced cachexia. *Journal of the National Cancer Institute*, *107*(12), djv274.

Tsoli, M., & Robertson, G. (2013). Cancer cachexia: malignant inflammation, tumorkines, and metabolic mayhem. *Trends in Endocrinology & Metabolism*, *24*(4), 174–183.

Vale, W., Rivier, J., Vaughan, J., McClintock, R., Corrigan, A., Woo, W., Karr, D., & Spiess, J. (1986). Purification and characterization of an FSH releasing protein from porcine ovarian follicular fluid. *Nature*, *321*(6072), 776–779.

Valero-Breton, M., Warnier, G., Castro-Sepulveda, M., Deldicque, L., & Zbinden-Foncea, H. (2020). Acute and chronic effects of high frequency electric pulse stimulation on the Akt/mTOR pathway in human primary myotubes. *Frontiers in Bioengineering and Biotechnology*, *8,* 565679.

Vechetti, I. J., Valentino, T., Mobley, C. B., & McCarthy, J. J. (2021). The role of extracellular vesicles in skeletal muscle and systematic adaptation to exercise. *The Journal of Physiology*, *599*(3), 845–861.

Vepkhvadze, T. F., Vorotnikov, A. V, & Popov, D. V. (2021). Electrical stimulation of cultured myotubes in vitro as a model of skeletal muscle activity: Current state and future prospects. *Biochemistry (Moscow)*, *86*(5), 597–610.

Verzola, D., Barisione, C., Picciotto, D., Garibotto, G., & Koppe, L. (2019). c. *Kidney International*, *95*(3), 506–517.

Vettore, L., Westbrook, R. L., & Tennant, D. A. (2019). New aspects of amino acid metabolism in cancer. *British Journal of Cancer*, 1–7.

Wackerhage, H., Schoenfeld, B. J., Hamilton, D. L., Lehti, M., & Hulmi, J. J. (2019). Stimuli and sensors that initiate skeletal muscle hypertrophy following resistance exercise. *Journal of Applied Physiology*, *126*(1), 30–43.

Walker, R. G., McCoy, J. C., Czepnik, M., Mills, M. J., Hagg, A., Walton, K. L., Cotton, T. R., Hyvönen, M., Lee, R. T., & Gregorevic, P. (2018). Molecular characterization of latent GDF8 reveals mechanisms of activation. *Proceedings of the National Academy of Sciences*, *115*(5), E866–E875.

Walton, R. G., Kosmac, K., Mula, J., Fry, C. S., Peck, B. D., Groshong, J. S., Finlin, B. S., Zhu, B., Kern, P. A., & Peterson, C. A. (2019). Human skeletal muscle macrophages increase following cycle training and are associated with adaptations that may facilitate growth. *Scientific Reports*, *9*(1), 969.

Wang, H., & Wang, B. (2016). Extracellular vesicle microRNAs mediate skeletal muscle myogenesis and disease. *Biomedical Reports*, *5*(3), 296–300.

Warren, S. (1932). The immediate causes of death in cancer. *The American Journal of the Medical Sciences*, *184 (5)*, 610–615.

Watt, M. J., & Cheng, Y. (2017). Triglyceride metabolism in exercising muscle. *Biochimica et Biophysica Acta (BBA)-Molecular and Cell Biology of Lipids*, *1862*(10), 1250–1259.

Wehrle, U., Düsterhöft, S., & Pette, D. (1994). Effects of chronic electrical stimulation on myosin heavy chain expression in satellite cell cultures derived from rat muscles of different fiber-type composition. *Differentiation*, *58*(1), 37–46.

Weigert, C., Hoene, M., & Plomgaard, P. (2019). Hepatokines—a novel group of exercise factors. *Pflügers Archiv - European Journal of Physiology*, *471*(3), 383–396.

Weigert, C., Lehmann, R., Hartwig, S., & Lehr, S. (2014). The secretome of the working human skeletal muscle—A promising opportunity to combat the metabolic disaster? *PROTEOMICS-Clinical Applications*, *8*(1–2), 5–18.

Weiss, A., & Attisano, L. (2013). The TGFbeta superfamily signaling pathway. *Wiley Interdisciplinary Reviews: Developmental Biology*, *2*(1), 47–63.

Westheimer, F. H. (1987). Why nature chose phosphates. *Science*, *235*(4793), 1173–1178.

Whitham, M., & Febbraio, M. A. (2016). The ever-expanding myokinome: discovery challenges and therapeutic implications. *Nature Reviews Drug Discovery*, *15*(10), 719–729.

Whitham, M., Parker, B. L., Friedrichsen, M., Hingst, J. R., Hjorth, M., Hughes, W. E., Egan, C. L., Cron, L., Watt, K. I., & Kuchel, R. P. (2018). Extracellular vesicles provide a means for tissue crosstalk during exercise. *Cell Metabolism*, *27*(1), 237–251.

Winbanks, C. E., Chen, J. L., Qian, H., Liu, Y., Bernardo, B. C., Beyer, C., Watt, K. I., Thomson, R. E., Connor, T., Turner, B. J., McMullen, J. R., Larsson, L., McGee, S. L., Harrison, C. A., & Gregorevic, P. (2013). The bone morphogenetic protein axis is a positive regulator of skeletal muscle mass. *Journal of Cell Biology*, *203*(2), 345–357.

Wolfe, R. R. (2006). The underappreciated role of muscle in health and disease. *The American Journal of Clinical Nutrition*, *84*(3), 475–482.

Wolfman, N. M., McPherron, A. C., Pappano, W. N., Davies, M. V, Song, K., Tomkinson, K. N., Wright, J. F., Zhao, L., Sebald, S. M., & Greenspan, D. S. (2003). Activation of latent myostatin by the BMP-1/tolloid family of metalloproteinases. *Proceedings of the National Academy of Sciences*, *100*(26), 15842–15846.

Wright, C. R., Brown, E. L., Della-Gatta, P. A., Ward, A. C., Lynch, G. S., & Russell, A. P. (2014). G-CSF does not influence C2C12 myogenesis despite receptor expression in healthy and dystrophic skeletal muscle. *Frontiers in Physiology*, *5*, 170.

Wullschleger, S., Loewith, R., & Hall, M. N. (2006). TOR signaling in growth and metabolism. *Cell*, *124*(3), 471–484.

Yaffe, D., & Saxel, O. R. A. (1977). Serial passaging and differentiation of myogenic cells isolated from dystrophic mouse muscle. *Nature*, *270*(5639), 725–727.

Yáñez-Mó, M., Siljander, P. R.-M., Andreu, Z., Bedina Zavec, A., Borràs, F. E., Buzas, E. I., Buzas, K., Casal, E., Cappello, F., Carvalho, J., Colás, E., Cordeiro-da Silva, A., Fais, S., Falcon-Perez, J. M., Ghobrial, I. M., Giebel, B., Gimona, M., Graner, M., Gursel, I., … De Wever, O. (2015). Biological properties of extracellular vesicles and their physiological functions. *Journal of Extracellular Vesicles*, *4*(1), 27066.

Yang, Q., Zhao, J., Hao, J., Li, B., Huo, Y., Han, Y., Wan, L., Li, J., Huang, J., & Lu, J. (2018). Serum and urine metabolomics study reveals a distinct diagnostic model for cancer cachexia. *Journal of Cachexia, Sarcopenia and Muscle*, *9*(1), 71–85.

Yang, W., Chen, Y., Zhang, Y., Wang, X., Yang, N., & Zhu, D. (2006). Extracellular signal–regulated kinase 1/2 mitogen-activated protein kinase pathway is involved in myostatin-regulated differentiation repression. *Cancer Research*, *66*(3), 1320–1326.

Yusof, H. M., Ab-Rahim, S., Suddin, L. S., Saman, M. S. A., & Mazlan, M. (2018). metabolomics profiling on different stages of colorectal cancer: A systematic review. *The Malaysian Journal of Medical Sciences: MJMS*, *25*(5), 16.

Zhang, J., Bhattacharyya, S., Hickner, R. C., Light, A. R., Lambert, C. J., Gale, B. K., Fiehn, O., & Adams, S. H. (2018). Skeletal muscle interstitial fluid metabolomics at rest and associated with an exercise bout: application in rats and humans. *American Journal of Physiology-Endocrinology and Metabolism*, *316*(1), E43–E53.

Zhang, L., Rajan, V., Lin, E., Hu, Z., Han, H. Q., Zhou, X., Song, Y., Min, H., Wang, X., & Du, J. (2011). Pharmacological inhibition of myostatin suppresses systemic inflammation and muscle atrophy in mice with chronic kidney disease. *The FASEB Journal*, *25*(5), 1653–1663.

Zhang, X., Zuo, X., Yang, B., Li, Z., Xue, Y., Zhou, Y., Huang, J., Zhao, X., Zhou, J., Yan, Y., Zhang, H., Guo, P., Sun, H., Guo, L., Zhang, Y., & Fu, X.-D. (2014). MicroRNA directly enhances mitochondrial translation during muscle differentiation. *Cell*, *158*(3), 607–619.

Zhang, Y., Wei, Y., Liu, D., Liu, F., Li, X., Pan, L., Pang, Y., & Chen, D. (2017). Role of growth differentiation factor 11 in development, physiology and disease. *Oncotarget*, *8*(46), 81604.

Zhao, Y., Li, N., Li, Z., Zhang, D., Chen, L., Yao, Z., & Niu, W. (2018). Conditioned medium from contracting skeletal muscle cells reverses insulin resistance and dysfunction of endothelial cells. *Metabolism*, *82*, 36–46.

Zhou, Q., Shi, C., Lv, Y., Zhao, C., Jiao, Z., & Wang, T. (2020). Circulating microRNAs in Response to Exercise Training in Healthy Adults. *Frontiers in Genetics*, 11, 256.

Zhou, X., Wang, J. L., Lu, J., Song, Y., Kwak, K. S., Jiao, Q., Rosenfeld, R., Chen, Q., Boone, T., & Simonet, W. S. (2010). Reversal of cancer cachexia and muscle wasting by ActRIIB antagonism leads to prolonged survival. *Cell*, *142*(4), 531–543.

Zhu, C., Mouly, V., Cooper, R. N., Mamchaoui, K., Bigot, A., Shay, J. W., Di Santo, J. P., Butler-Browne, G. S., & Wright, W. E. (2007). Cellular senescence in

human myoblasts is overcome by human telomerase reverse transcriptase and cyclin-dependent kinase 4: consequences in aging muscle and therapeutic strategies for muscular dystrophies. *Aging Cell*, *6*(4), 515–523.
Zi, Z., Chapnick, D. A., & Liu, X. (2012). Dynamics of TGF-β/Smad signaling. *FEBS Letters*, *586*(14), 1921–1928.

ORIGINAL PUBLICATIONS

I

MUSCLE AND SERUM METABOLOMES ARE DYSREGULATED IN COLON-26 TUMOR-BEARING MICE DESPITE AMELIORATION OF CACHEXIA WITH ACTIVIN RECEPTOR TYPE 2B LIGAND BLOCKADE

by

Lautaoja, J.H., Lalowski, M., Nissinen, T.A., Hentilä, J., Shi, Y., Ritvos, O., Cheng, S. & Hulmi, J.J. (2019).

American Journal of Physiology-Endocrinology and Metabolism, 316(5), E852–E865

https://doi.org/10.1152/ajpendo.00526.2018

Am J Physiol Endocrinol Metab 316: E852–E865, 2019.
First published March 12, 2019; doi:10.1152/ajpendo.00526.2018.

RESEARCH ARTICLE | *Translational Physiology*

Muscle and serum metabolomes are dysregulated in colon-26 tumor-bearing mice despite amelioration of cachexia with activin receptor type 2B ligand blockade

Juulia H. Lautaoja,[1] Maciej Lalowski,[2] Tuuli A. Nissinen,[1] Jaakko Hentilä,[1] Yi Shi,[3] Olli Ritvos,[4] Sulin Cheng,[3,5,6] and Juha J. Hulmi[1,4]

[1]*Faculty of Sport and Health Sciences, Neuromuscular Research Center, University of Jyväskylä, Jyväskylä, Finland;* [2]*Meilahti Clinical Proteomics Core Facility, HiLIFE, Faculty of Medicine, Biochemistry and Developmental Biology, University of Helsinki, Helsinki, Finland;* [3]*The Key Laboratory of Systems Biomedicine, Ministry of Education, Shanghai Center for Systems Biomedicine, Shanghai Jiao Tong University, Minhang District, Shanghai, China;* [4]*Department of Physiology, Faculty of Medicine, University of Helsinki, Helsinki, Finland;* [5]*Exercise, Health and Technology Center, Department of Physical Education, and Exercise Translational Medicine Center, Shanghai Jiao Tong University, Minhang District, Shanghai, China; and* [6]*Faculty of Sport and Health Sciences, University of Jyväskylä, Jyväskylä, Finland*

Submitted 4 December 2018; accepted in final form 26 February 2019

Lautaoja JH, Lalowski M, Nissinen TA, Hentilä J, Shi Y, Ritvos O, Cheng S, Hulmi JJ. Muscle and serum metabolomes are dysregulated in colon-26 tumor-bearing mice despite amelioration of cachexia with activin receptor type 2B ligand blockade. *Am J Physiol Endocrinol Metab* 316: E852–E865, 2019. First published March 12, 2019; doi:10.1152/ajpendo.00526.2018.—Cancer-associated cachexia reduces survival, which has been attenuated by blocking the activin receptor type 2B (ACVR2B) ligands in mice. The purpose of this study was to unravel the underlying physiology and novel cachexia biomarkers by use of the colon-26 (C26) carcinoma model of cancer cachexia. Male BALB/c mice were subcutaneously inoculated with C26 cancer cells or vehicle control. Tumor-bearing mice were treated with vehicle (C26+PBS) or soluble ACVR2B either before (C26+sACVR/b) or before and after (C26+sACVR/c) tumor formation. Skeletal muscle and serum metabolomics analysis was conducted by gas chromatography-mass spectrometry. Cancer altered various biologically functional groups representing *1*) amino acids, *2*) energy sources, and *3*) nucleotide-related intermediates. Muscle metabolomics revealed increased content of free phenylalanine in cancer that strongly correlated with the loss of body mass within the last 2 days of the experiment. This correlation was also detected in serum. Decreased ribosomal RNA content and phosphorylation of a marker of pyrimidine synthesis revealed changes in nucleotide metabolism in cancer. Overall, the effect of the experimental C26 cancer predominated over blocking ACVR2B ligands in both muscle and serum. However, the level of methyl phosphate, which was decreased in muscle in cancer, was restored by sACVR2B-Fc treatment. In conclusion, experimental cancer affected muscle and blood metabolomes mostly independently of blocking ACVR2B ligands. Of the affected metabolites, we have identified free phenylalanine as a promising biomarker of muscle atrophy or cachexia. Finally, the decreased capacity for pyrimidine nucleotide and protein synthesis in tumor-bearing mice opens up new avenues in cachexia research.

cancer; C26; myostatin; phenylalanine; ribosome

INTRODUCTION

Cancer cachexia is a life-threatening condition associated with skeletal muscle wasting with or without adipose tissue loss and with systemic inflammation, reduced tolerance to anticancer treatments, and reduced survival (5, 17, 31, 46). Depending on the type and stage of cancer, 50–80% of all cancer patients are affected by cachexia (20, 56). To date, there is no cure for cachexia, highlighting the complexity of this life-threatening condition.

Cachexia evokes multiple changes in muscle metabolism affecting the balance of, for example, amino acids, carbohydrates, and lipids (13, 14, 44). During cachexia, proteolysis especially of myofibrillar proteins increases (1), thus providing amino acids for energy production via the tricarboxylic acid (TCA) cycle in the muscle (14). Concurrently, released amino acids can, for example, promote the synthesis of the hepatic acute-phase response proteins (48). During cachexia, decreased energy and growth signaling as well as increased content of cytokines such as myostatin/activins downregulate the activity of the mechanistic target of rapamycin (mTOR) (30, 38, 43), which is one of the most important regulators of protein, nucleotide, and lipid synthesis. Organs interact during cachexia, such as when a tumor releases "tumorkines", which may negatively alter the normal function of muscle and other tissues. Activins and myostatin are negative regulators of muscle mass that can be secreted from the tumor, among other tumorkines (58). They are ligands of the activin receptors type 2A and 2B (ACVR2A/B) (67). Blocking of ACVR2 ligands by soluble activin receptor type 2B (sACVR2B-Fc) has been reported by us (43), and by others (67) to improve survival in C26 experimental cancer.

In recent years, omics approaches have become more popular in an attempt to reveal the major contributors to as well as the cause of cachexia (23). Mice bearing colon-26 (C26) carcinoma demonstrate reduced body, muscle and fat mass, decreased muscle strength and physical activity, and feed intake, as well as increases in the markers of inflammation and protein degradation (42, 43), and are thus thought to be a

Address for reprint requests and other correspondence: J. Hulmi, Faculty of Sport and Health Sciences, Neuromuscular Research Center, University of Jyväskylä, Rautpohjankatu 8, Jyväskylä 40014, Finland (e-mail: juha.hulmi@jyu.fi).

suitable preclinical model for cancer cachexia (42). Previous studies using experimental C26 cancer models have reported changes in metabolites such as amino acids, intermediates of the TCA cycle, and markers of oxidative stress in skeletal muscle (14, 57). Furthermore, metabolome of serum and/or urine has previously been analyzed in other catabolic conditions causing muscle wasting, such as human cancer cachexia (21, 65), aging (19, 24), and muscle denervation (55). Yang et al. (65) demonstrated in humans that the contents of carnosine, leucine, and phenyl acetate in serum were altered during cachexia and that the content of these markers could be used to identify risk populations. Tseng et al. (57) showed that alterations in muscle metabolome were partially reversed by a histone deacetylase inhibitor that prevented cancer cachexia. Whether this also occurs with activin receptor ligand blocking has not been addressed.

We and others (32, 43, 67) have previously demonstrated that sACVR2B-Fc administration improved survival in experimental C26 cancer cachexia, but the molecular mechanisms remain unknown. The primary aim of the present study was to assess the effects of experimental C26 cancer cachexia on skeletal muscle and serum metabolomes and whether the metabolomes are altered by administration of sACVR2B-Fc ligand blocker. Furthermore, we aimed to find novel biomarkers of cancer cachexia that could also be used to predict survival or the severity of cachexia.

MATERIALS AND METHODS

Animals

Male BALB/c mice (Charles River Laboratories, Sulzfeld, Germany), aged 5–6 wk, were housed under standard conditions (temperature 22°C, 12:12-h light-dark cycle) with free access to water and food pellets (R36; 4% fat, 55.7% carbohydrate, 18.5% protein, 3 kcal/g; Labfor, Stockholm, Sweden). The treatment of animals was in accordance with the European Convention for the Protection of Vertebrate Animals used for experimental and other scientific purposes. The protocols were approved by the National Animal Experiment Board, and all the experiments were carried out in accordance with the guidelines of that committee (permit no. ESAVI/10137/04.10.07/2014) and following the ethical standards laid down in the 1964 Declaration of Helsinki and its later amendments.

Tumor Cell Culture

C26 cells were maintained as previously described (43).

Experimental Design

The mice were randomized into four groups matched by body mass and subcutaneously inoculated with 5×10^5 C26 cancer cells in 100 μl of phosphate-buffered saline (PBS) or an equal volume of vehicle control (PBS) into the intrascapular region, as reported earlier (43). Healthy controls (CTRL, $n = 9$) were administered vehicle (PBS), and the C26 tumor-bearing mice with vehicle (C26+PBS, $n = 7$) or sACVR2B-Fc (5 mg/kg in ~100 μl PBS ip), either only before (C26+sACVR/b, $n = 7$) or both before and after tumor formation (C26+sACVR/c, $n = 8$). The mice were treated with PBS or sACVR2B-Fc every fourth day, except the C26+sACVR/b group was treated with the vehicle from *day 5* after cancer cell injection. This first experiment was repeated with the following groups (*experiment 2*): CTRL, C26+PBS, and C26+sACVR/c to increase n size for further metabolomic analyses to amount to $n = 15$ in CTRL, $n = 13$ in C26+PBS, and $n = 13$ in C26+sACVR/c. The study design is presented in Fig. 1.

Tissue Collection

At the end of both experiments, the mice were anaesthetized with an intraperitoneal injection of ketamine and xylazine mixture, and euthanized by cardiac puncture followed by cervical dislocation, as reported earlier (43). The mice were euthanized 11 and 13 days after the cancer cell inoculation in *experiments 1* and *2*, respectively, to represent the onset of cachexia. Muscle samples were weighed and snap-frozen in liquid nitrogen, while the blood was collected in serum collection tubes and centrifuged at 2,000 *g* for 10 min (Biofuge 13, Heraeus). Subcutaneous white adipose tissue (scWAT) samples were stored at −80°C until use.

Production of Soluble ACVR2B

Production and purification of the sACVR2B-Fc recombinant protein was conducted in house, as previously described (28). In brief, the ectodomain of human ACVR2B and human IgG1 Fc domain (ACVR2B-Fc) were fused and expressed in Chinese hamster ovary cells, yielding a similar but not identical protein as originally reported by Lee et al. (34).

Sample Preparation for Metabolomics

Muscle. Gastrocnemius muscles were homogenized by grinding (Jingxin Science, Guangzhou, China) for 2 min. Then, metabolites were extracted by methanol-chloroform-water (1:2.5:1, vol/vol/vol) solvent, mixed on a rotator for 1 min, and kept at −20°C for 20 min. The supernatant of the centrifugation at 15,000 *g* for 10 min at 4°C was vacuum dried (Huamei, Shanghai, China) at room temperature. After the addition of methoxyamine (15 mg/ml in pyridine; Adamas,

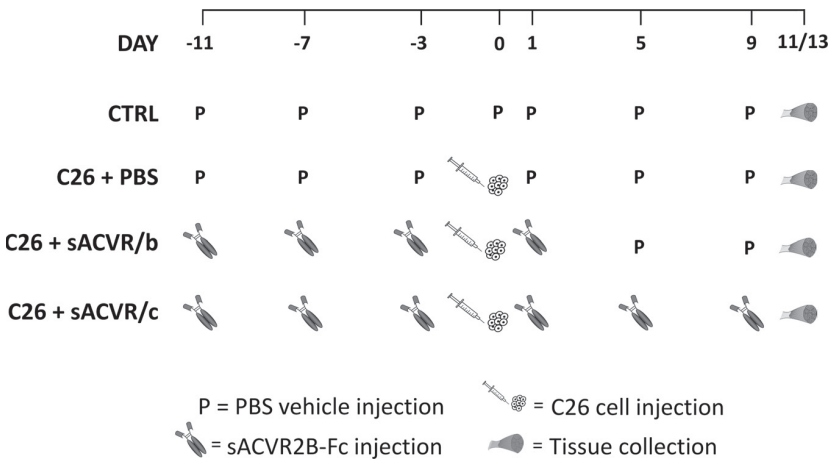

Fig. 1. Schematic presentation of the study design. Mice were randomized into 4 groups: healthy controls (CTRL, $n = 9$) and 3 groups of colon-26 (C26) tumor-bearing mice treated with PBS vehicle (C26 + PBS, $n = 7$) or soluble activin receptor 2B (sACVR2B)-Fc only before (C26 + sACVR/b, $n = 7$) or both before and after tumor formation (C26 + sACVR/c, $n = 8$). Mice were treated every 4th day, and tissues were collected on *day 11*. Experiment was replicated ($n = 5–6$ per group) without the C26 + sACVR/b group to increase n size. Tissues were collected when growth of the tumor and loss of body mass reached the levels in the first experiment (on *day 13*).

Beijing, China), samples were mixed for 10 min and shaken at 30°C for 90 min. Finally, *N*,*O*-bis(trimethylsilyl)trifluoroacetamide (BSTFA), with 1% trimethylchlorosilane (TMCS; Supelco, *Bellefonte, PA*) was added and samples shaken at 70°C for 60 min.

Serum. Metabolites from serum were extracted with methanol-chloroform (3:1, vol/v) by mixing for 1 min on a rotor and keeping the samples at −20°C for 20 min. From this step onward, the sample preparation procedure was identical to the one used for muscle.

Gas Chromatography/Time-of-Flight-Mass Spectrometry Analysis

Gas chromatography/time-of-flight-mass spectrometry (GC/TOF-MS) analysis was performed using an Agilent 6890 gas chromatography system coupled with a Pegasus III Time-of-Flight mass spectrometer. A DB-5-ms capillary column (30 m × 0.25 mm, 0.25 μm; Agilent J&W Scientific, Folsom, CA) was used to separate the trimethylsilylated (TMS) sample. Helium was used as a carrier gas at a constant flow rate of 1 ml/min. The injector temperature was set at 270°C. The GC oven temperature was initially set at 90°C for 0.5 min and then raised to 180°C at a rate of 10°C, to 240°C at a rate of 5°C, to 290°C at a rate of 25°C, and finally held at 290°C for 9 min. The temperature of transfer line and ion source was set at 270°C and 220°C, respectively. The mass spectrometry data were acquired with electron impact ionization (70 eV) at full scan mode (*m/z* 30–600). The dwell time for each scan was set at a rate of 10 spectra per second and the solvent delay at 7 min. The samples were injected in randomized order.

Data Analysis

The acquired MS data from GC/TOF-MS were analyzed by ChromaTOF software (v. 4.34; LECO, St Joseph, MI). Briefly, after alignment with the Statistic Compare component, the .csv files were generated with three-dimension data sets that included sample information, retention time-*m/z*, and peak intensities. The internal standards were used for data quality control (reproducibility). After removal of internal standards and known false-positive peaks, such as those caused by mechanical noise, column bleed, and the BSTFA derivatization procedure, the peaks representing the same metabolite were combined. The data sets were normalized using the sum intensities of peaks in each sample.

Metabolite Identification

Metabolites with both multivariate and univariate statistical significance (VIP >1.0 and $P < 0.05$) were annotated with the aid of available reference standards, NIST 11 standard mass spectral databases, and the Fiehn databases linked to ChromaTOF software. The similarity of metabolite identification in the sample compared with reference standards reaching more than 70% was considered positive identification. We detected 219 metabolites from the skeletal muscle and serum, of which 156 from both met the reporting threshold (i.e., metabolite was detected in >30% of the animals). All differentially expressed compounds in the treated groups were selected by comparing the compounds in the treated group with the control, using the multivariate statistical method and Wilcoxon-Mann-Whitney test.

Ingenuity Pathway Analysis

Further bioinformatics searches were performed with Ingenuity software after the false discovery rate (FDR) correction with altered metabolites based on FDR < 0.05 and fold change (FC) > |1.2|.

Sample Processing for Protein Analysis

Tibialis anterior muscle and scWAT were homogenized and treated with proper inhibitors as previously described (29) but with a slight modification. The muscle and scWAT homogenates were centrifuged at 10,000 *g* for 10 min or 12,000 *g* for 20 min, respectively, and the total protein content was measured with the BCA Protein Assay Kit (Pierce Biotechnology, Rockford, IL), with an automated KoneLab analyzer (Thermo Scientific, Vantaa, Finland).

Western Blotting

Muscle homogenates were solubilized in Laemmli sample buffer and heated at 95°C for 10 min to denature proteins. Samples containing 30 μg of proteins were separated by SDS-PAGE in a Criterion electrophoresis cell (Bio-Rad Laboratories, Hercules, CA) and transferred to PVDF membranes using the Trans-Blot Turbo Transfer System (Bio-Rad Laboratories). Membranes were blocked in Tris-buffered saline (TBS) with 0.1% Tween-20 (TBS-T) containing 5% nonfat dry milk and incubated overnight at 4°C with primary antibodies. Membranes were then washed in TBS-T and incubated with secondary antibody (horseradish peroxidase-conjugated anti-rabbit or anti-mouse IgG; Jackson ImmunoResearch Ely, UK) for 1 h at room temperature, followed by a washing in TBS-T. Proteins were visualized by enhanced chemiluminescence (SuperSignal west femto maximum sensitivity substrate; Pierce Biotechnology) using a ChemiDoc MP device (Bio-Rad Laboratories) and quantified (band intensity × volume) with Image Laboratory software (v. 6.0, Bio-Rad Laboratories). For muscle samples, GAPDH and Ponceau S were used as loading controls, and the results were normalized to their mean value. The quantification of GAPDH normalized to Ponceau S was similar among the groups, indicating that GAPDH protein content remained stable under the experimental conditions. scWAT results were normalized to Ponceau S only. The antibodies used in this study are listed in the Supplemental materials [https://doi.org/10.6084/m9.figshare.7756583].

RNA and DNA Extraction, cDNA Synthesis, and RT-qPCR

An RNeasy Plus Universal Mini Kit (73404, QIAGEN) with QIAzol Lysis Reagent (1023537, QIAGEN) was used to extract RNA from scWAT and gastrocnemius muscle, and the DNeasy Blood & Tissue kit (69504, QIAGEN) was used to extract DNA from the latter, all according to the manufacturer's instructions. For cDNA synthesis, iScript Advanced cDNA kit for RT-qPCR (no. 172-5038, Bio-Rad Laboratories) was used. Real-time qPCR was conducted according to the manufacturer's protocol with iQ SYBR Green Supermix (no. 170-8882, Bio-Rad Laboratories) and the CFX96 Real-Time PCR Detection System combined with CFX Manager software (Bio-Rad Laboratories). Efficiency-corrected $\Delta\Delta C_T$ method was utilized in data analysis. Among the tested housekeeping genes (*Tbp*, *Rn18S*, *Gapdh*, and *36B4*), *36B4* was chosen for skeletal muscle and *Tbp* for scWAT normalization because they were unaffected by the treatments ($P > 0.169$ and $P > 0.186$, respectively) and due to their lowest variation between the groups. The primers used in this study are listed in the Supplemental materials [https://doi.org/10.6084/m9.figshare.7756583].

Enzyme Activity Analyzes

From the gastrocnemius muscle, the activity of alanine aminotransferase (ALT) was measured by ALT/GPT Kit (Thermo Scientific), aspartate aminotransferase (AST) by AST/GOT Kit (Thermo Scientific), and xanthine oxidase (XO) by Xanthine Oxidase Activity Assay Kit (Sigma-Aldrich). The activity of 3-hydroxyacyl-CoA dehydrogenase (β-HAD) was measured as previously described (16). The enzyme activities were analyzed according to the manufacturers' protocols using an automated KoneLab measuring device (Thermo Scientific). The enzyme activity results were normalized against total protein content.

Triacylglycerol Extraction

Triacylglycerol from gastrocnemius muscle was extracted by using similar method as demonstrated earlier (8). Briefly, pulverized muscle sample was further homogenized into a chloroform-methanol (2:1)

solution, and the organic phase was evaporated with a vacuum evaporator. To dissolve the dried triacylglycerol, absolute ethanol was used, and the concentration was measured with a triglyceride kit (Thermo Scientific) using an automated KoneLab measuring device (Thermo Scientific).

Statistical Analysis.

For the omics analysis, changes in metabolites were considered significant when FDR < 0.05 and FC $> |1.2|$. For analysis of proteins, transcripts, and lipids, data were checked for normality and equality of variances by using a Shapiro-Wilk test and Levene's test, respectively. Following that, multiple group comparisons for the tumor-bearing groups were conducted by Holm-Bonferroni corrected *t*-tests or nonparametric Mann-Whitney *U*-test, when appropriate. For two-group comparisons (C26+PBS vs. CTRL or CTRL vs. tumor-bearing groups pooled), a two-tailed unpaired Student's *t*-test or nonparametric Mann-Whitney *U*-test was used. Pooling the tumor-bearing mice (referred as C26 effect) was justified in those cases in which the sACVR2B-Fc administration had no effect. Pearson's correlation coefficient was used to analyze correlations. Katiska/Himmeli software [http://www.finndiane.fi/software/katiska/] used in a GNU Octave programing environment was used to present the correlation network among tumor-bearing mice (37). Statistical analyses were performed with IBM SPSS Statistics, v. 24 for Windows (SPSS, Chicago, IL). The level of significance in these analyses was set at $P < 0.05$. Data are expressed as means ± SE if not mentioned otherwise.

RESULTS

We (43) previously demonstrated with these same mice that C26 cancer decreased both skeletal muscle and body mass and that these were prevented by sACVR2B-Fc treatment.

Experimental Cancer Has a More Significant Effect on Skeletal Muscle Metabolome Than Prevention of Muscle Wasting by Blocking ACVR2B Ligands

We studied the effects of the experimental C26 cancer on skeletal muscle metabolome by employing GC/TOF-MS. In vehicle-treated mice (C26+PBS vs. CTRL), C26 cancer alone resulted in alteration of 23 metabolites, of which 10 increased and 13 decreased at the level of FDR < 0.05 and FC $> |1.2|$ (Fig. 2*A*). Heat map clustering of 23 altered metabolites in C26+PBS vs. CTRL demonstrated the dominant effect of C26 cancer cachexia over sACVR2B-Fc administration on skeletal muscle metabolome (Fig. 2B). As an exception to this dominant effect of cancer, we observed that the decrease of methyl phosphate detected in vehicle-treated tumor-bearing mice was restored by both sACVR2B-Fc administration protocols (Fig. 3*A*). Metabolites that were significantly increased by sACVR2B-Fc administration in tumor-bearing mice without restoring the effect toward CTRL level included 2,6-diaminopimelic, 2-amino-1-phenylethanol, 5-aminovaleric acid lactam, adenosine-5-monophosphate, cortexolone, inosine-5-monophosphate, *n*-(ε)-trimethyllysine, tryptophan, and uric acid. Metabolites that were decreased by sACVR2B-Fc administration encompassed 2-ketoadipate, asparagine, and *N*-acetyl-β-alanine. These sACVR-effects vs. C26+PBS group are presented in Fig. S1 [All Supplemental material is available at: https://doi.org/10.6084/m9.figshare.7756583], except the alterations in the levels of methyl phosphate, tryptophan, and uric acid that are presented in Figs. 3*A*, 4*A*, and Fig. 6*D*, respectively.

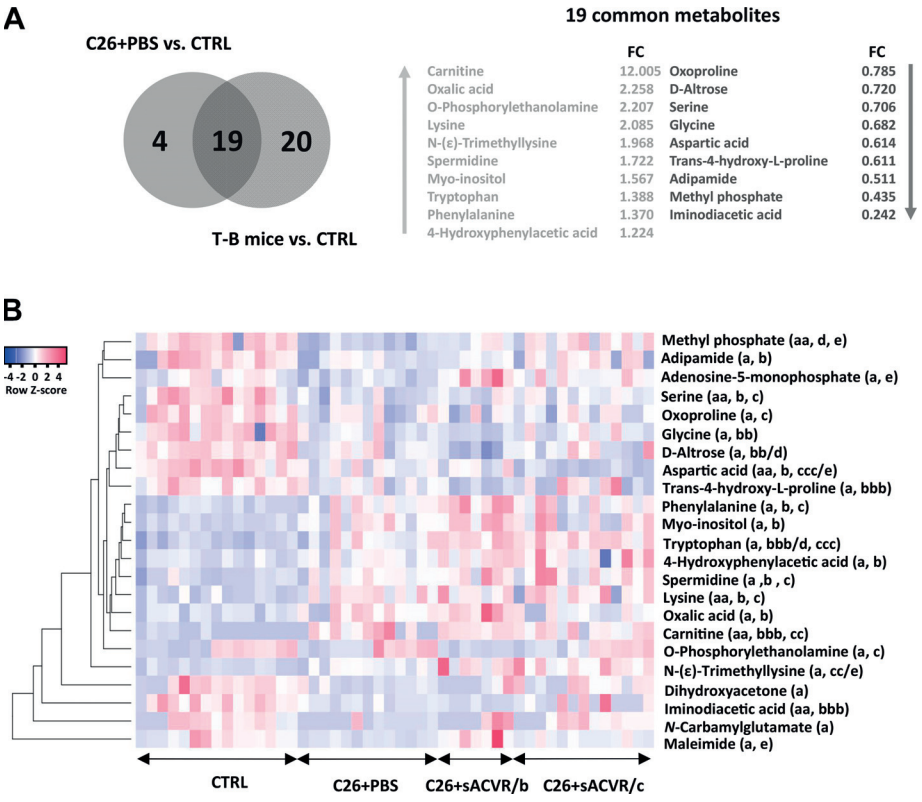

Fig. 2. Venn diagram and heat map visualization of altered metabolites in skeletal muscle. C26, colon-26 cancer; CTRL, control mice; PBS, vehicle; sACVRB, soluble activin receptor 2B; sACVR2B/b, C26 + sACVR2B before tumor formation; sACVR2B/c, C26 + before and after tumor formation; FC, fold change; FDR, false discovery rate. *A*: C26 + PBS vs. CTRL group comparison resulted in 23 altered metabolites, of which 19 were common with the pool of the tumor-bearing mice (T-B mice) vs. CTRL. The latter comparison resulted in 39 altered metabolites. Arrows point to direction of change based on their fold change (FC) values in C26 + PBS vs. CTRL comparison. *B*: heat map of 23 altered metabolites in C26 + PBS vs. CTRL comparison. Representing significances of comparisons, a = PBS vs. CTRL, b = sACVR/b vs. CTRL, c = sACVR/c vs. CTRL, d = sACVR/b vs. C26+PBS, and e = sACVR/c vs. C26+PBS. Single letter , false discovery rate (FDR) $<$ 0.05, 2 letters FDR < 0.01, and 3 letters FDR < 0.001 (in all, FC $> |1.2|$). Group sizes were: CTRL ($n = 15$), C26 + PBS ($n = 13$), C26 + sACVR/b ($n = 7$), and C26 + sACVR/c ($n = 13$). Group comparisons were analyzed with FDR-corrected Student's *t*-test.

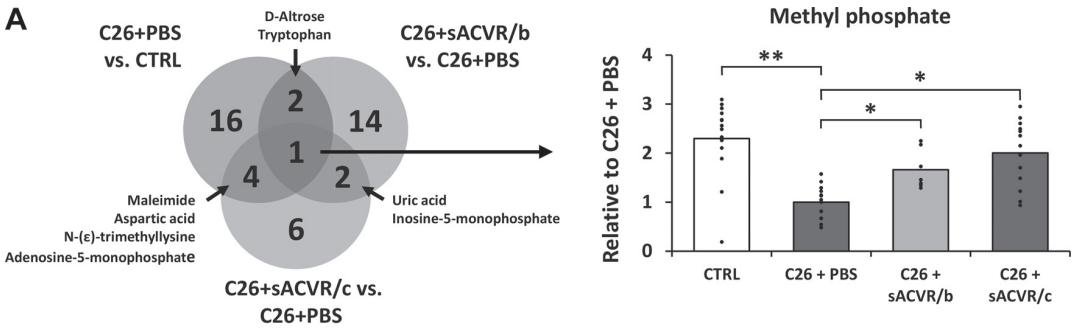

B

C26+PBS vs. CTRL	FC
Carnitine	12.005
Oxalic acid	2.258
O-Phosphorylethanolamine	2.207
Lysine	2.085
N-(ε)-Trimethyllysine	1.968
Spermidine	1.722
Myo-inositol	1.567
Tryptophan	1.388
Phenylalanine	1.370
4-Hydroxyphenylacetic acid	1.224
Oxoproline	0.785
D-Altrose	0.720
Serine	0.706
Adenosine-5-monophosphate	0.697
Glycine	0.682
Aspartic acid	0.614
Trans-4-hydroxy-L-proline	0.611
Adipamide	0.511
Methyl Phosphate	0.435
Dihydroxyacetone	0.316
N-Carbamylglutamate	0.288
Maleimide	0.263
Iminodiacetic acid	0.242

C26+sACVR/c vs. C26+PBS	FC
D-(glycerol 1-phosphate)	4.397
Uric acid	2.962
Maleimide	2.269
N-(ε)-Trimethyllysine	2.127
Methyl Phosphate	2.002
Adenosine-5-monophosphate	1.613
Inosine-5-monophosphate	1.465
Ornithine	1.298
2'-Hydroxyacetophenone	0.778
Aspartic acid	0.579
Acetanilide	0.569
Nicotinoylglycine	0.567
Asparagine	0.540

C26+sACVR/c vs. C26+sACVR/b	FC
Palmitic acid	2.340
Stearic acid	2.322
Allantoic acid	0.769
Cis-2-hydroxycinnamic acid	0.352

C26+sACVR/b vs. C26+PBS	FC
Uric acid	4.107
2-Amino-1-phenylethanol	2.936
Inosine-5-monophosphate	1.969
Malonic acid	1.895
Farnesal	1.686
Methyl Phosphate	1.660
2,6-Diaminopimelic acid	1.514
Uracil	1.497
Thymine	1.482
Hypoxanthine	1.432
Allantoic acid	1.424
Tryptophan	1.306
3-Hydroxybutyric acid	0.736
N-Acetyl-β-alanine	0.696
D-Altrose	0.550
Glucose	0.511
Palmitic acid	0.312
Naringenin	0.309
Stearic acid	0.266

Fig. 3. *A*: Venn diagram of group comparisons relative to the C26+PBS group. C26, colon-26 cancer; CTRL, control mice; PBS, vehicle; sACVRB, soluble activin receptor 2B; sACVR2B/b, C26 + sACVR2B before tumor formation; sACVR2B/c, C26 + before and after tumor formation; FC, fold change; FDR, false discovery rate. Methyl phosphate was the only common metabolite to be altered among all comparisons. *B*: significantly altered metabolites among each group comparison. * and ** = FDR < 0.05 and < 0.01, respectively (in all, FC $> |1.2|$). Group sizes were: CTRL ($n = 15$), C26 + PBS ($n = 13$), C26 + sACVR/b ($n = 7$), and C26 + sACVR/c ($n = 13$). Group comparisons were analyzed with FDR-corrected Student's *t*-test.

In addition, compared with the C26+PBS group, the continued blocking of ACVR2B ligands (C26+sACVR/c) altered 13 metabolites, of which eight increased and five decreased (Fig. 3). The discontinued treatment (C26+sACVR/b) altered 19 metabolites, of which 12 increased and seven decreased (Fig. 3). These two comparisons (C26+sACVR/c vs. C26+PBS and C26+sACVR/b vs. C26+PBS) shared three common metabolites with each other, whereas five and three altered metabolites were shared with C26+PBS vs. CTRL comparison, respectively (Fig. 3). Comparison of the two sACVR2B-Fc-administered groups yielded four metabolites differing between the treatments (Fig. 3*B*). The most altered metabolites were distributed among various biological groups, such as amino acids, energy sources, and nucleotide-related intermediates (Table S2). Our correlation network analysis using Katiska software revealed links between metabolites responding similarly to cancer or sACVR2B-Fc administration (Fig. S2).

Experimental Cancer Disturbs the Homeostasis of Skeletal Muscle Amino Acids

Among the 20 amino acids commonly found in contractile proteins, 15 were detected by GC/TOF-MS. Of those, eight were affected in the tumor-bearing mice (Fig. 4*A*). More specifically, the contents of aspartic acid, serine, glycine, serine, tryptophan, lysine, and phenylalanine were altered by cancer alone, whereas alanine and isoleucine were altered only when tumor-bearing mice were pooled (Fig. 4*A*). To identify possible markers of cachexia in the skeletal muscle, we examined the correlations of metabolites with body mass loss within the last 2 days before tissue collection. A particularly strong negative correlation of phenylalanine was observed, namely, the more phenylalanine level increased, the more body mass decreased in the tumor-bearing mice ($r = -0.873$, $P < 0.001$; Fig. 4*B*). More than 60 other significant correlations of examined variables in the tumor-bearing mice relative to the body mass change were observed within the last 2 days (Table S3). This effect may have been due to decreased muscle protein synthesis in tumor-bearing mice as demonstrated by puromycin incorporation (43). Indeed, in the current study, the phenylalanine level also correlated negatively with muscle protein synthesis (Fig. S3). Concurrently, alanine and aspartic acid levels decreased in the tumor-bearing mice, which prompted us to scrutinize the corresponding enzymatic activities. We observed that the activity of aspartate aminotransferase (AST) significantly decreased, whereas alanine aminotransferase (ALT) was nonsignificantly decreased ($P = 0.054$) in the tumor-bearing mice (Fig. 4, *C* and *D*). L-Glutamate, a product of both enzymes, remained unchanged, as did pyruvate, a product of ALT (Fig. 4*A*). Next, we examined pathways of the altered metabolites by use of the Ingenuity Pathway Analysis (IPA) software (data not shown). Based on the IPA algorithms,

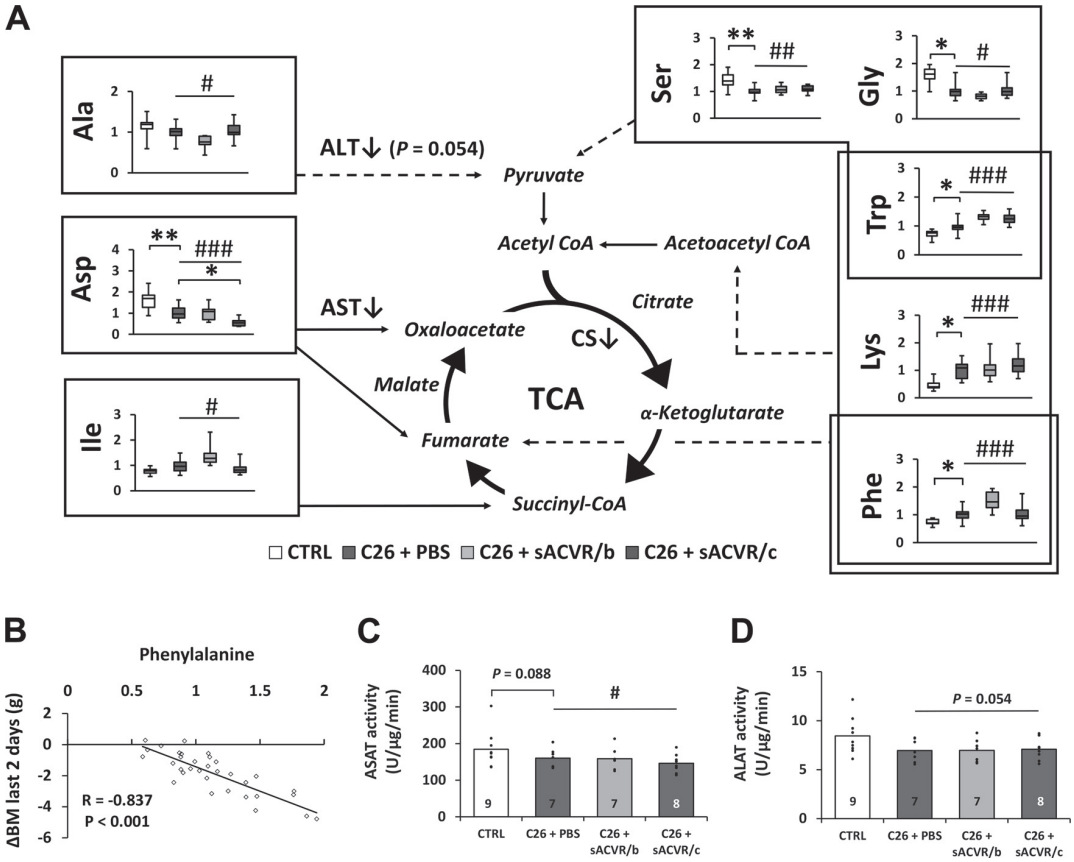

Fig. 4. Amino acid homeostasis was disturbed in tumor-bearing mice. C26, colon-26 cancer; CTRL, control mice; PBS, vehicle; sACVRB, soluble activin receptor 2B; sACVR2B/b, C26 + sACVR2B before tumor formation; sACVR2B/c, C26 + before and after tumor formation; FC, fold change; FDR, false discovery rate; CS, citrate synthase activity, reported in Ref. 43. *A*: levels of alanine (Ala), aspartic acid (Asp), serine (Ser), and glycine (Gly) decreased in skeletal muscle during cachexia, whereas levels of lysine (Lys), isoleucine (Ile), and aromatic amino acids phenylalanine (Phe) and tryptophan (Trp) increased. Note that asparagine and tryptophan displayed sACVR (sACVR2B-Fc-administered mice pooled) vs. C26 + PBS effect, FDR < 0.05 and FC $> |1.2|$. Among these amino acids, Ile and Asp (61) may be in part related to the TCA cycle in skeletal muscle, possibly also other amino acids in cancer cachexia (marked by dashed lines). TCA cycle intermediates written in cursive were not detected by gas chromatography/time-of-flight-mass spectrometry. Presented box plots are depicted as C26+PBS = 1. * and ** = FDR < 0.05 and FDR < 0.01, respectively. #, ##, and ### = C26 effect, FDR < 0.05, < 0.01, and < 0.001, respectively, with FC $> |1.2|$ in all. *B*: Pearson correlation between muscle Phe and loss of body mass (ΔBM) within the last 2 days before tissue collection in tumor-bearing mice. Enzyme activities of aspartate aminotransferase (AST; *C*) and alanine aminotransferase (ALT; *D*). In *A* and *B*, CTRL ($n = 15$), C26 + PBS ($n = 13$), C26 + sACVR/b ($n = 7$), and C26 + sACVR/c ($n = 13$); in *C* and *D*, group sizes are presented in bar graphs. Group comparisons were analyzed with FDR-corrected Student's *t*-test (*A*) or nonparametric Mann-Whitney *U*-test (*C* and *D*).

glycine and serine/glycine biosynthesis pathways were suggested to be decreased in tumor-bearing mice, explained by lowered glycine and serine contents. Moreover, upstream analysis revealed sirolimus (rapamycin) as an upstream regulator in the tumor-bearing mice, which may in part be related to previously published alterations in mechanistic target of rapamycin (mTOR) signaling (43).

Ribosomal RNA and a Marker of Nucleotide Synthesis Decreased in Experimental C26 Cancer With Only a Minor Effect of Blocking ACVR2B Ligands

We (43) previously reported lowered protein synthesis and mTOR-signaling in skeletal muscle of the tumor-bearing mice, which led us to further examine protein synthesis capacity. We observed a nonsignificant decrease in the RNA content of the skeletal muscle in tumor-bearing mice (C26+PBS vs. CTRL, $P = 0.061$; C26 effect, $P = 0.078$; Fig. 5*A*). There was also a significant decrease in 28S ribosomal RNA (Fig. 5*B*), whereas in 18S ribosomal RNA this difference did not reach statistical significance (C26 effect, $P = 0.151$; Fig. 5*C*). At this time point, 45S pre-RNA and DNA content remained unchanged (Fig. 5, *D* and *E*).

We also observed changes in other markers of nucleotide metabolism in the skeletal muscle. Interestingly, when sACVR2B-Fc treatment was discontinued, the contents of uracil, thymine, and their breakdown products hypoxanthine and uric acid increased (Fig. 6, *A–D*). To verify whether there was a change in de novo nucleotide synthesis, we analyzed CAD complex (carbamoyl phosphate synthetase 2, aspartate transcarbamylase, and dihydroorotase), which consists of the following enzymes: glutamine amidotransferase, carbamoyl-phosphate synthetase, aspartate transcarbamoylase, and dihydroorotase. The phosphorylation of CAD-Ser^{1859} is regulated by mTOR complex 1 (mTORC1) via S6K1 (4, 49) to activate the initiation of pyrimidine synthesis. We observed that both phosphorylated CAD-Ser^{1859} and total CAD decreased in the

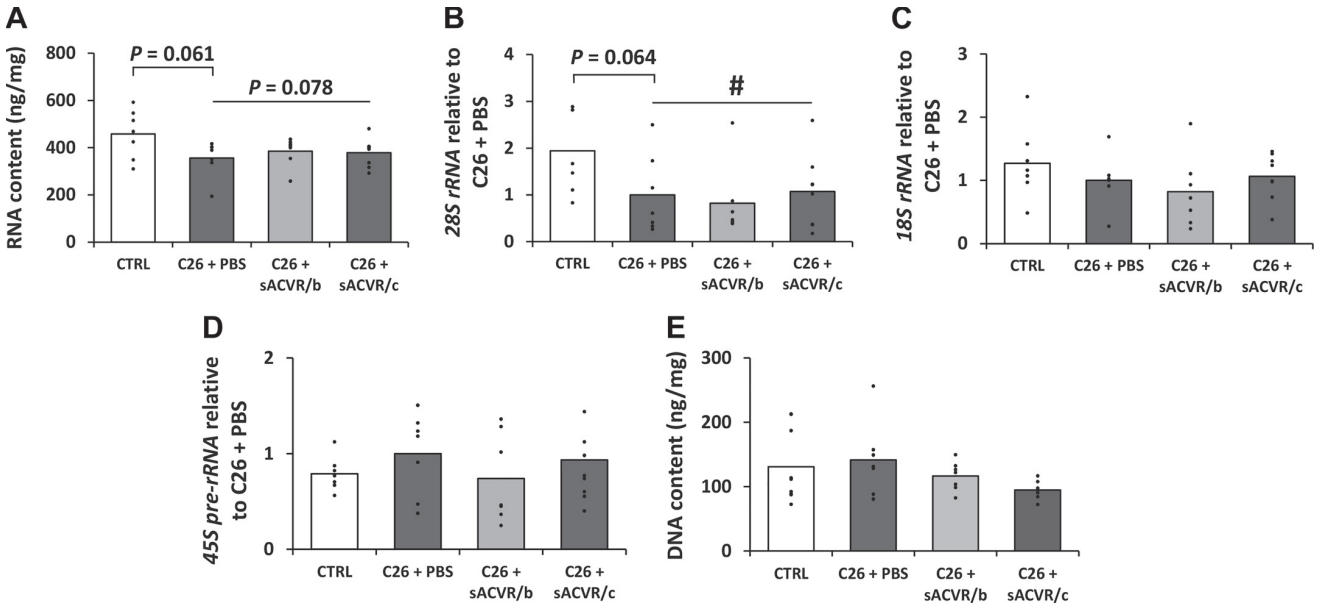

Fig. 5. Markers of ribosomal RNA content and protein synthesis capacity. C26, colon-26 cancer; CTRL, control mice; PBS, vehicle; sACVRB, soluble activin receptor 2B; sACVR2B/b, C26 + sACVR2B before tumor formation; sACVR2B/c, C26 + before and after tumor formation; FC, fold change; FDR, false discovery rate. *A*: skeletal muscle RNA content. Among ribosomal RNAs, 28S RNA content decreased in tumor-bearing mice (*B*), whereas 18S RNA demonstrated a nonsignificant decrease (*C*). 45S pre-RNA (*D*) and DNA content (*E*) remained unaltered in skeletal muscle. # = C26 effect, $P < 0.05$. CTRL vs. C26 + PBS and CTRL vs. C26 pooled were analyzed with Student's *t*-test (*A* and *E*) or nonparametric Mann-Whitney *U*-test (*B–D*). In *A* and *B*, group sizes were: CTRL ($n = 8$–9), C26 + PBS ($n = 7$), C26 + sACVR/b ($n = 7$), and C26 + sACVR/c ($n = 8$). Differences among C26 tumor-bearing mice were analyzed with Holm-Bonferroni-corrected Student's *t*-test (*A* and *E*) or nonparametric Mann-Whitney *U*-test (*B–D*).

tumor-bearing mice independently of treatment, suggesting a decrease in nucleotide synthesis capacity in experimental cancer (Fig. 6, *E–G*). The activity of XO, the end point enzyme of pyrimidine breakdown pathway, remained unaltered; yet a nonstatistical decrease in cancer condition alone was observed (C26+PBS vs. CTRL, $P = 0.068$; Fig. 6*H*).

Triacylglycerol Concentration Decreased and Lipase Content Increased in Skeletal Muscle of Tumor-Bearing Mice Without the Effect of Blocking ACVR2B Ligands

We found that triacylglycerol concentration decreased in the skeletal muscle of the tumor-bearing mice (Fig. 7*A*). This observation was supported by a concurrent increase in the content of the adipose triglyceride lipase (ATGL, Fig. 7*B*) and phosphorylated HSL-Ser^{660} (active lipase form) as well as total HSL (Fig. 7, *C* and *E*). We also observed an increase in the free fatty acid (FFA) transporter carnitine in the tumor-bearing mice (Fig. 7*F*). Interestingly, in tumor-bearing mice, carnitine correlated with body mass change within the last 2 days (pool of tumor-bearing mice $r = -0.431$, $P = 0.012$), meaning that the more carnitine increased, the larger was the body mass loss (Table S3). The activity of β-HAD, a β-oxidation enzyme, was nonsignificantly ($P = 0.099$) decreased in the cancer condition alone (Fig. 7*G*).

The Majority of Altered Metabolites Decreased in Serum of Tumor-Bearing Mice

We further investigated whether the effect of experimental C26 cancer predominated over ACVR2B ligand blocking in the serum as well. In vehicle-treated mice (C26+PBS vs. CTRL), C26 cancer alone resulted in the alteration of 13 metabolites, all of which decreased in their abundance (Fig. 8 and Table S4). No altered metabolites were detected amid sACVR2B-Fc and the vehicle-treated tumor-bearing mice (FDR > 0.168). In serum, most of the altered metabolites encompassed FFAs that were decreased in tumor-bearing mice (Fig. 8 and Table S4) at the time point when the fat mass was already at a very low level (Fig. 9*A*). However, the decrease in serum lipids was in line with the lipid-related findings from skeletal muscle, which demonstrated that C26-induced cancer cachexia also governs metabolic changes in the serum of the tumor-bearing mice independently of the ACVR2B ligand blocking.

To discover possible biomarkers of cachexia in the serum, we examined correlations of metabolites to body mass loss within the last 2 days before tissue collection. Similarly to skeletal muscle, in the tumor-bearing mice serum phenylalanine correlated negatively (i.e., the more phenylalanine increased, the more body mass decreased in all tumor-bearing mice) with the body mass change within the last 2 days ($r = -0.899$, $P < 0.001$). Furthermore, multiple other amino acids behaved in a way similar to that observed for phenylalanine in serum, for example, tyrosine ($r = -0.907$, $P < 0.001$), methionine ($r = -0.870$, $P = 0.001$), and lysine ($r = -0.843$, $P = 0.002$). For other significant correlations in the serum of tumor-bearing mice relative to body mass change within the last 2 days, see Table S5 and Fig. S4.

Browning of Subcutaneous Fat Was Not Observed in Tumor-Bearing Mice Independently of Treatment

Finally, to complement the metabolomic analyses, we tested whether scWAT browning (12, 46) was induced in experimen-

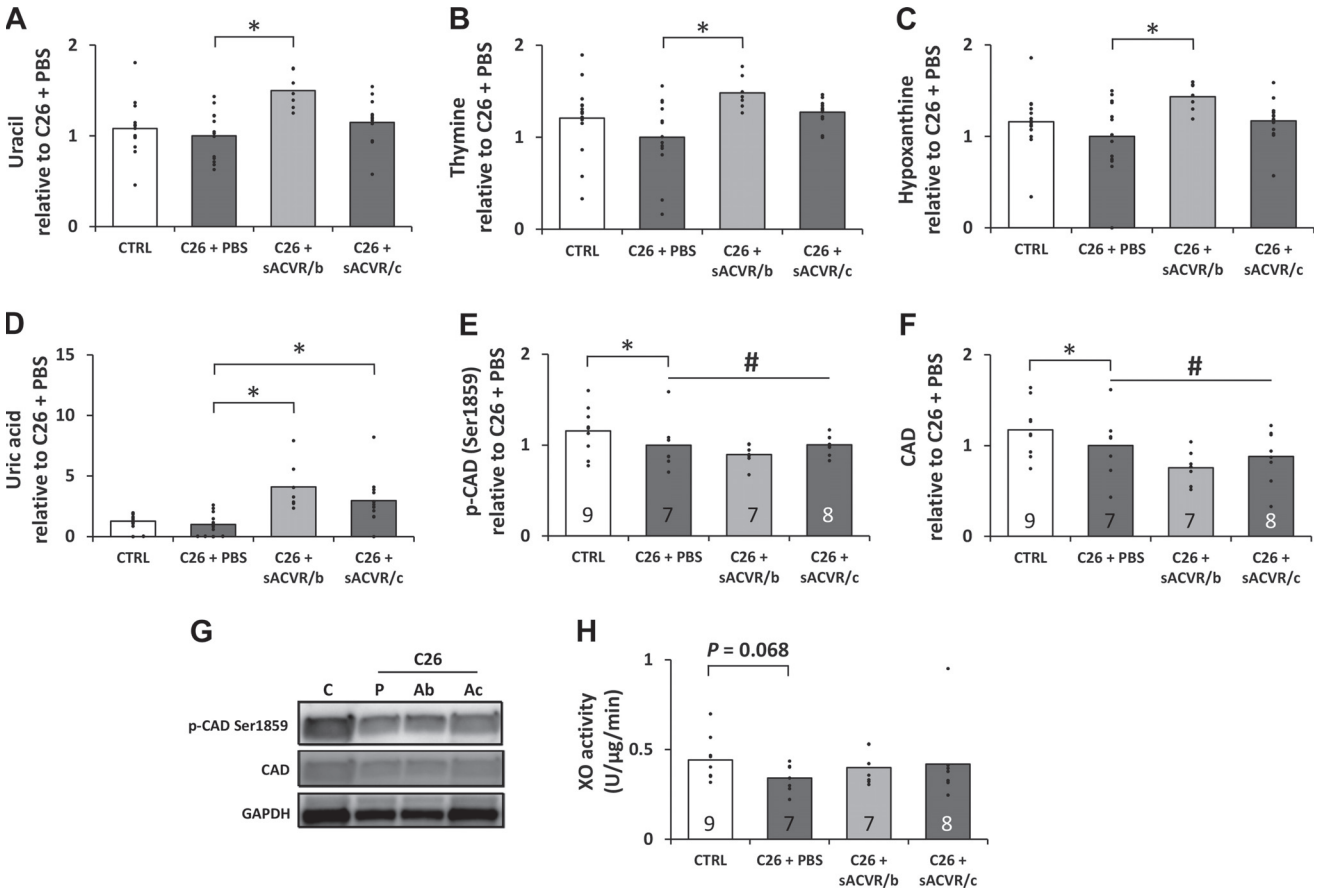

Fig. 6. Metabolites related to nucleotide metabolism and pyrimidine synthesis capacity. C26, colon-26 cancer; CTRL, control mice; PBS, vehicle; sACVRB, soluble activin receptor 2B; sACVR2B/b, C26 + sACVR2B before tumor formation; sACVR2B/c, C26 + before and after tumor formation; FC, fold change; FDR, false discovery rate. In C26 + sACVR/b group (*A*) free uracil, (*B*) free thymine, and the breakdown product of the purine nucleotides (*C*) hypoxanthine increased compared with the C26+PBS group. Another breakdown product of purine nucleotides, (*D*) uric acid increased in both sACVR2B-Fc administered groups vs. C26 + PBS. In *A–D*, * = FDR < 0.05, FC $> |1.2|$. (*E*) Phosphorylation of CAD (p-CAD-Ser^{1859}) and (*F*) total CAD decreased in tumor-bearing mice independently of treatment. *G*: representative blots: C = CTRL, *P* = C26 + PBS, Ab = C26 + sACVR/b, Ac = C26 + sACVR/c. In *E* and *F*, * = $P < 0.05$, # = C26 effect, $P < 0.05$. *H*: enzyme activity of xanthine oxidase (XO). In *A–D*, group sizes were: CTRL ($n = 15$), C26 + PBS ($n = 13$), C26 + sACVR/b ($n = 7$), and C26 + sACVR/c ($n = 13$); in *E–H*, group sizes are presented in bar graphs. In *A–D*, group comparisons were analyzed with FDR-corrected Student's *t*-test. CTRL vs. C26 + PBS and CTRL vs. C26 pooled were analyzed with Student's *t*-test and differences among C26 tumor-bearing mice (*E–H*) with Holm-Bonferroni-corrected Student's *t*-tests.

tal cancer and whether it was affected by ACVR2B ligand blocking. We also examined whether scWAT browning could in part explain the decrease in scWAT mass in tumor-bearing mice (Fig. 9*A*) and serum FFA levels (Fig. 8). Even though the gene expression of PR domain-containing 16 (Prdm16), a modulator of scWAT browning, increased in the tumor-bearing mice (Fig. 9*B*), the most common scWAT browning marker uncoupling protein-1 decreased in the scWAT of the tumor-bearing mice. This decrease was independent of the treatment utilized at the mRNA and protein levels (Fig. 9, *C* and *D*).

DISCUSSION

In this study, we have identified a few possible biomarkers of cachexia, or muscle atrophy. However, most of the changes in metabolites in cachexia were not affected by the sACVR2B-Fc administration, which indicates that the contribution of the experimental cachexia to skeletal muscle and serum metabolome is much more prominent than the effect of blocking ACVR2B ligands, even though the latter alleviated cachexia (43). We (43) earlier demonstrated that the tumor-bearing mice treated with sACVR2B-Fc had improved survival, but the present results suggest that this may be only weakly associated with the studied metabolomic changes during the onset of cachexia. Furthermore, the current results imply that muscle protein and nucleotide synthesis capacity decreases during cachexia. Further studies are needed to investigate the importance of this finding, considering that we had previously observed a decrease in muscle protein synthesis in these tumor-bearing mice (43).

As mentioned, almost all metabolic changes in skeletal muscle were explained by the cancer condition, but the treatment protocols utilized in this study produced only minor effects on the affected metabolome. However, the administration of sACVR2B-Fc reversed the cancer-induced decrease of methyl phosphate especially when the treatment was continued, almost to the level demonstrated by healthy mice. Little is known about the importance and function of this metabolite, but it seems to be related to the metabolism of purines and

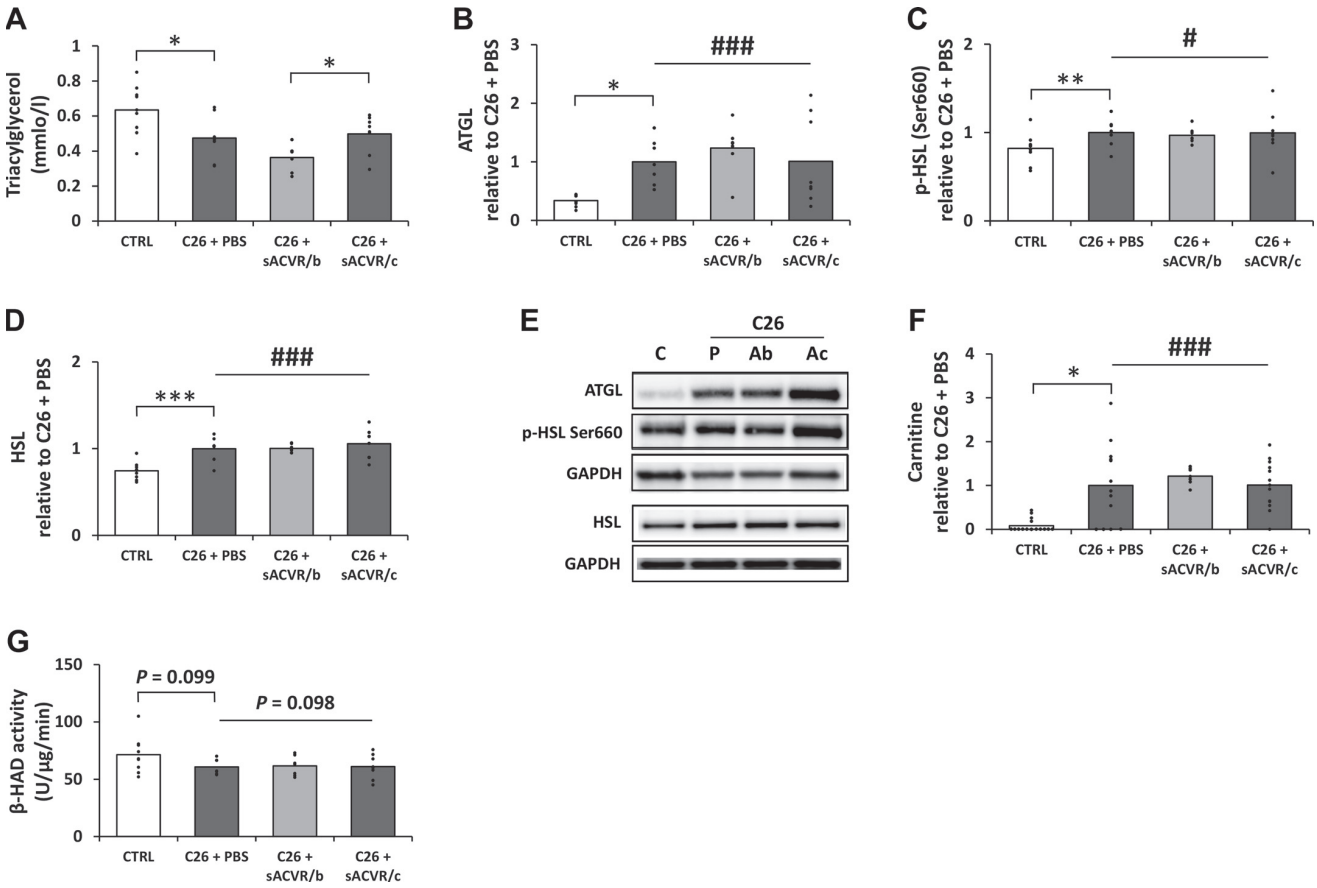

Fig. 7. Cancer alters lipid metabolism in skeletal muscle. C26, colon-26 cancer; CTRL, control mice; PBS, vehicle; sACVRB, soluble activin receptor 2B; sACVR2B/b, C26 + sACVR2B before tumor formation; sACVR2B/c, C26 + before and after tumor formation; FC, fold change; FDR, false discovery rate. Muscle triacylglycerol concentration decreased (*A*), whereas levels of lipases adipose triglyceride lipase (ATGL; *B*) and phosphorylated (*C*) and total hormone-sensitive lipase (HSL; *D*) increased in tumor-bearing mice. *E*: representative blots: C = CTRL, *P* = C26 + PBS, Ab = C26 + sACVR/b, Ac = C26 + sACVR/c. Carnitine (*F*) and 3-hydroxyacyl-CoA dehydrogenase (β-HAD; *G*) enzyme activity. *, **, and *** = $P < 0.05$, $P < 0.01$, and $P < 0.001$, respectively; #, ##, and ### = C26 effect, $P < 0.05$, $P < 0.01$, and $P < 0.001$, respectively. In *A–E* and *G*, group sizes were as follows: CTRL ($n = 9$), C26 + PBS ($n = 7$), C26 + sACVR/b ($n = 7$), and C26 + sACVR/c ($n = 8$); in *F*, CTRL ($n = 15$), C26 + PBS ($n = 13$), C26 + sACVR/b ($n = 7$), and C26 + sACVR/c ($n = 13$). CTRL vs. C26+PBS and CTRL vs. C26 pooled were analyzed with Student's *t*-test and differences among C26 tumor-bearing mice by Holm-Bonferroni-corrected Student's *t*-test (*A–E* and *G*). *F*: group comparisons were analyzed with FDR-corrected Student's *t*-test.

pyrimidines (7). Our correlation network analysis using the Katiska software revealed a few metabolites that demonstrated a similar response to cancer and its treatment. The analysis suggests a possible functional link between methyl phosphate and some of these metabolites. In addition, both sACVR2B-Fc administration protocols resulted in a miniscule recovery in the level of *n*-carbamylglutamate that was decreased by cancer. Oral *n*-carbamylglutamate administration has previously been used as a treatment in, for example, diseases causing hyperammonemia (9, 66), to enhance nitrogen excretion, and to improve antioxidant status in liver and plasma (11) as well as in the intestine (64). Thus, the effect of dietary *n*-carbamylglutamate administration in cancer cachexia should be addressed in the future. In addition to these results, we identified few metabolites responsive to the blocking of ACVR2B ligands in tumor-bearing mice (FDR < 0.05 and FC $> |1.2)$ that presented no recovering effect toward control level. Pooling of the sACVR groups resulted in alterations in multiple metabolites including: 2,6-diaminopimelic, 2-amino-1-phenylethanol, 2-ketoadipate, 5-aminovaleric acid lactam, adenosine-5-monophosphate, asparagine, cortexolone, inosine-5-monophosphate, *N*-(ε)-trimethyllysine, *N*-acetyl-β-alanine, tryptophan, and uric acid (Fig. S1). In addition, we demonstrated that the continued and discontinued sACVR2B-Fc administration protocols resulted in different metabolic responses, which are presented in Fig. 3*B*. Understanding the physiological importance of these alterations requires more dedicated research in the future.

Similar to previous findings (14, 57), we also observed that amino acid homeostasis was disturbed in skeletal muscle during cachexia. The levels of ketogenic amino acid lysine and gluconeogenic and ketogenic amino acids phenylalanine and tryptophan increased in the tumor-bearing mice. Free phenylalanine level correlated in both skeletal muscle and serum with the body mass loss. This may, in part, be due to decreased muscle protein synthesis reported earlier (43), as it correlated, in the present study with the phenylalanine content in the muscle. This result also supports the previous finding demonstrating a relationship between decreased muscle protein synthesis and increased phenylalanine content in the muscle (45). These results taken together, free phenylalanine could be a

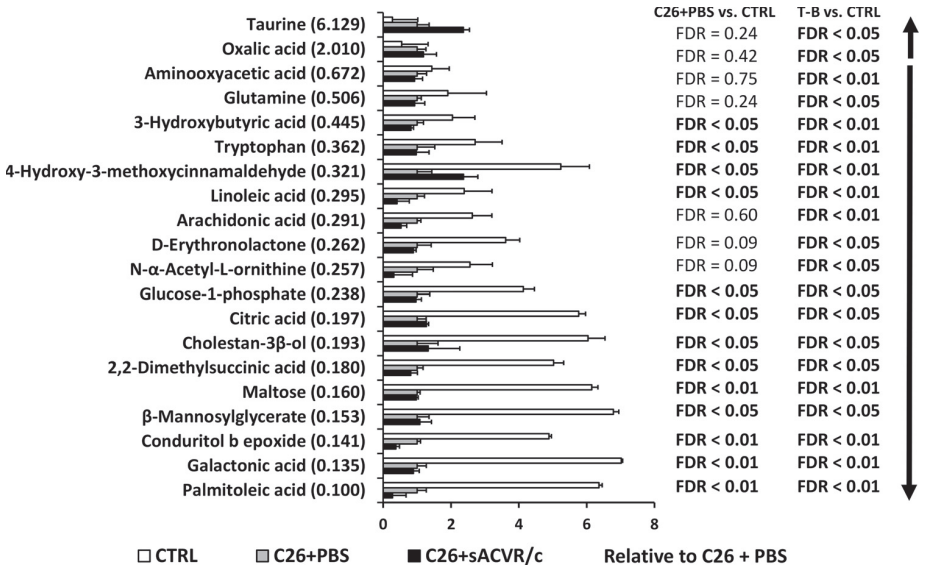

Fig. 8. In the serum metabolome, C26 cancer dominated the alterations in metabolites over blocking activin receptor ligands. C26, colon-26 cancer; CTRL, control mice; PBS, vehicle; sACVRB, soluble activin receptor 2B; sACVR2B/b, C26 + sACVR2B before tumor formation; sACVR2B/c, C26 + before and after tumor formation; FDR, false discovery rate. Cancer altered the level of 13 metabolites in C26 + PBS vs. CTRL, whereas pooling of tumor-bearing groups (T-B mice) vs. CTRL revealed alteration of 20 metabolites. FC values of the T-B vs. CTRL comparison are presented in brackets; FDR values of group comparisons are shown on the *right*. Arrows present direction of change; significant FDR values are in boldface. Group sizes were: CTRL (n = 15), C26 + PBS (n = 13), and C26 + sACVR/c (n = 13). Group comparisons were analyzed with FDR-corrected Student's t-test.

biomarker of muscle loss and reduced protein synthesis in skeletal muscle. However, in these same mice, the markers of protein degradation were found to be increased, accompanied by loss of fat (43). Thus, we cannot exclude the possibility that elevated phenylalanine may also reflect the protein degradation in addition to the altered protein synthesis. Considering that body mass loss at this time point correlated strongly with survival (Cox regression analysis $B = 0.902$, $P < 0.001$) in another group of mice (43), biomarkers related to body mass loss, reported in the current study could also predict survival. The increase in the content of phenylalanine and another aromatic amino acid, tryptophan, in the muscle of the tumor-

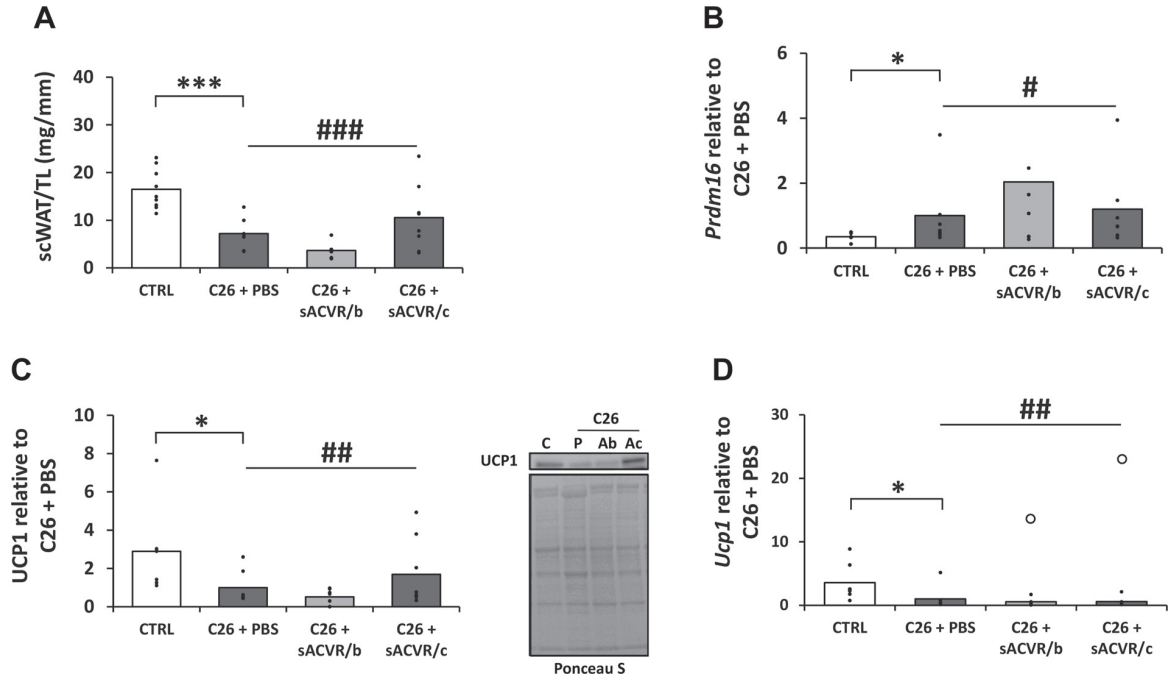

Fig. 9. White adipose tissue (WAT) browning may not explain the decreased fat mass. C26, colon-26 cancer; CTRL, control mice; PBS, vehicle; sACVRB, soluble activin receptor 2B; sACVR2B/b, C26 + sACVR2B before tumor formation; sACVR2B/c, C26 + before and after tumor formation. *A*: subcutaneous (sc)WAT mass normalized to tibia length (TL) in mm decreased in cancer independently of treatment. *Prdm16* mRNA level increased (*B*), whereas UCP1 protein decreased (*C*) in cancer. Representative blot: C = CTRL, *P* = C26 + PBS, Ab = C26 + sACVR/b, Ac = C26 + sACVR/c. *D*: *Ucp1* mRNA level decreased in tumor-bearing mice. Open circles represent outliers included in statistical analyses but excluded from group mean values. * and *** = $P < 0.05$ and < 0.001, respectively; # and ### = C26 effect vs. CTRL, $P < 0.05$, and < 0.001, respectively. Group sizes were: CTRL (n = 6–9), C26 + PBS (n = 7), C26 + sACVR/b (n = 5–7), and C26 + sACVR/c (n = 6–8). CTRL vs. C26 + PBS and CTRL vs. C26 pooled were analyzed with Student's t-test (*A* and *C*) or nonparametric Mann-Whitney U-test (*B* and *D*). Differences among C26 tumor-bearing mice were analyzed with Holm-Bonferroni-corrected Student's t-test (*A* and *C*) or nonparametric Mann-Whitney U-test (*B* and *D*).

bearing mice may be due to increased proteolysis in these mice (43). Unlike contractile proteins, acute-phase proteins (APPs) are rich in aromatic amino acids, and this may lead to an excessive muscle protein breakdown to provide an adequate amount of specific amino acids for APP synthesis (48). Indeed, this theory is supported by the fact that serum tryptophan decreased, which suggests an enhanced liver uptake of aromatic amino acids for the synthesis of APPs (48), as we previously demonstrated in these same mice (43). Our current results complement the previous studies in humans that report altered phenylalanine metabolism in the blood of cancer patients (10, 52).

We observed a decrease in glycogenic amino acids (alanine, aspartic acid, serine, and glycine) in the skeletal muscle of the tumor-bearing mice. This may suggest that, as they are released during skeletal muscle proteolysis, their carbon skeletons are further directed into the TCA cycle for energy production in muscle, released into circulation, or used in other metabolic pathways (1, 14, 33, 48). Substrate delivery to the TCA cycle was probably compromised in the tumor-bearing mice, as demonstrated by the lower content of glucose, glycerol (see Table S2), and 3-hydroxybutyric acid (FDR < 0.05, FC $= 0.847$, nonsignificant), which can be directed into the TCA cycle for energy production (14). We also observed lowered enzyme activity of AST (which converts aspartic acid and α-ketoglutarate into oxaloacetate and glutamic acid) and a nonstatistically significant ($P = 0.054$) decrease in ALT (which converts alanine and α-ketoglutarate into pyruvate and glutamic acid) in the tumor-bearing mice (27). A concurrent decrease in aspartic acid and alanine content suggests that less oxaloacetate and also pyruvate is available to sustain the TCA cycle. This finding is in agreement with the previous study by Tzika et al. (59), which used a Lewis lung carcinoma cachexia model and reported a reduced ATP synthesis rate accompanied by lowered TCA cycle flux. In line with this observation, we demonstrated lowered citrate synthase activity in the skeletal muscle of these mice (43). Serum lactate content correlated with body mass loss (Suppl. Fig. S1) with a simultaneous decrease in muscle glucose content in tumor-bearing mice. The glycolysis pathway may have been induced by cancer, as detected previously (14), at least in some mice, and the extent of this may predict the severity of cancer cachexia. Regarding the metabolites of energy metabolism, the metabolomics platform used did not allow detection of all the intermediates in these pathways. This could be overcome by using another type of metabolomics platform, such as pathway-targeted metabolomic analysis utilizing capillary ion chromatography with mass spectrometry as previously demonstrated by Wang et al. (62). However, the untargeted GC-MS used in the present study offers a broader possibility to discover novel biomarkers than the targeted platforms. Other metabolomics platforms may have revealed differences not detectable with the used platform.

In support of a previous study by Der Torossian et al. (14), we also observed that amino acids derived from 3-carbon glycolytic intermediates (i.e., glycine, serine, and alanine) decreased in the muscles of the tumor-bearing mice. This occurred independently of the sACVR2B-Fc treatment. Since glycine is a precursor for glutathione synthesis, the decrease in glycine content may be related to the decline in the level of reduced glutathione that was also observed in these mice (26) and thus oxidative stress (25). Furthermore, we observed a decrease in oxoproline content (indicator of glycine/glutathione availability) in the tumor-bearing mice, which has been shown to decline in humans by restricting dietary sulfur amino acids or glycine (39). These observations further suggest that oxidative stress is increased in the tumor-bearing mice.

To date, little is known about ribosome biogenesis in cachexia. mTOR regulates ribosome biogenesis via mTORC1 by, for example, sensing the intracellular nutrient and nucleotide levels (30). In cachexia, nutrient availability decreases in part because of decreased food intake induced by the downregulated appetite (18) formerly observed in these mice (43). Recent studies suggest that increased ribosomal content may be important in some models of hypertrophy (60, 63), while total ribosome content may decrease in muscle atrophy (2, 15, 36). We observed a decrease in the content of 28S ribosomal RNA in the skeletal muscle of the tumor-bearing mice. Previously, a decrease in total RNA content in rats with Yoshida ascites hepatoma (2), and in mice with XK1 tumor (15) have been observed. Our finding was accompanied by a previously reported decrease in protein synthesis and decreased mTOR signaling in these tumor-bearing mice (43). Furthermore, the total protein content of ribosomal protein S6 itself, which is an important component of the 40S ribosome (40), decreased in cancer in these mice (43), suggesting that both RNA and protein machineries of the ribosomes are compromised in skeletal muscles during cancer cachexia. To verify whether this has any causal effect on skeletal muscle, further studies are required.

Nucleotides consisting of sugar, base, and phosphate components are the building blocks of RNA and DNA. Carbon and nitrogen skeletons of the nucleotide bases (purines and pyrimidines) originate from amino acids (glycine, aspartic acid, and glutamine) and from one-carbon metabolism (35). A decrease in muscle glycine and aspartic acid suggests that de novo synthesis of nucleotide bases may be downregulated in experimental cancer. De novo synthesis of pyrimidine bases is regulated by mTORC1 via phosphorylated S6K1 (4), the latter observed to be decreased in these tumor-bearing mice (43). Interestingly, in support of this finding, we observed, as a novel result, a decrease in phosphorylated CAD-Ser^{1859} and total CAD in the skeletal muscle of the tumor-bearing mice, an observation that further demonstrates that de novo pyrimidine synthesis may decrease in cancer. Barreto et al. (3) predicted an inhibition of nucleotide synthesis by using IPA analysis of muscle proteomics in C26-induced cachexia, and our results support this finding. Disturbed nucleic acid synthesis due to a lack of building blocks may result in downregulation of anabolic processes and ribosome biogenesis (4). However, the DNA content remained unaltered in the tumor-bearing mice. We also observed an increase in the content of free pyrimidines (uracil and thymine) but not of purines in the skeletal muscle when sACVR2B-Fc administration was discontinued before tumor formation, which may have been due to downregulated nucleotide, RNA, and DNA synthesis or increased breakdown. Interestingly, this group (sACVR/b) also had lower survival than the group in which the treatment was continued (43). XO, which is an enzyme in nucleotide breakdown, was analyzed, but it remained unaltered. Our results highlight that more research is required on nucleotide metabolism in cancer.

Lipids have been reported to accumulate in skeletal muscle in some cancer studies (12, 53). The reason why lipid accumulation in muscle was not observed in the present study may have been due to its capability to utilize lipids. This conclusion is supported by an increased protein content of phosphorylated hormone-sensitive lipase-Ser^{660}, which activates the lipase, and of adipose triglyceride lipase in skeletal muscle, which suggests that infiltrated fatty acids are hydrolyzed for energy production. Carnitine is required for transporting the long-chain fatty acids into mitochondria, where they are subsequently used in β-oxidation (6), and the observed increase of carnitine supports the hypothesis of enhanced fatty acid transportation into mitochondria as observed previously in cachexia (47). Fukawa et al. (22) demonstrated that conditioned medium from RXF393 cancer cells directly increased the content of various carnitine transporter isoforms as well as inducing lipid atrophy and β-oxidation in human muscle cells. The effective lipid usage in the skeletal muscle occurred even though the activity of the β-oxidation enzyme β-HAD did not increase in the tumor-bearing mice. A decrease in the content of 3-hydroxybutyric acid, glycerol, triacylglycerol, and glucose in the skeletal muscle as well as the depletion of adipose tissue suggest that the majority of all energy sources and derivatives are utilized for host maintenance, tumor growth, and tumor-derived changes in energy metabolism.

Almost all altered metabolites in the serum of the tumor-bearing mice decreased without any additional effect of sACVR2B-Fc administration. In agreement with the measurements of skeletal muscle metabolome, the altered metabolites in the serum were distributed among lipids, amino acids, and carbohydrates. Interestingly, the higher the content of several amino acids in the serum was, the greater was the body mass loss, which suggests that these could be markers of the severity of cachexia, a finding that complements earlier studies (41, 54, 65). All of the detected serum fatty acids decreased in the tumor-bearing mice, which is in agreement with the findings of Cala et al. (10), which demonstrated an altered blood lipid profile in cachectic patients. This is in line with the other observations of lower content of energy sources and TCA intermediates in muscle in this study as well as in the previously reported decrease in food intake in these mice (43). This may be reflected in serum fatty acids, because the food pellets contained, for example, linoleic acid, which decreased in the serum similarly to arachidonic acid, and the metabolism of these two fatty acids is closely linked (51). We also did not observe increased browning of scWAT in these mice. Recently, Rohm et al. (50) suggested that, in cancer, fat browning might not be as common or important a phenomenon related to adipose tissue wasting as was initially thought. This phenomenon, however, warrants further research because in some murine cancer studies fat browning was reported to be induced (31, 46).

Conclusion

We have shown in the present study the effects of preclinical colon-26 cancer on muscle and serum metabolomes, a response that cannot be recovered by blocking muscle loss using soluble activin receptor. Additionally, we identified free phenylalanine as a potential biomarker of muscle atrophy and/or cancer cachexia. The reported decrease in ribosome and pyrimidine nucleotide biogenesis may pave the way toward new directions in cancer cachexia research.

ACKNOWLEDGMENTS

We thank Dr. Fabio Penna for kindly providing the C26 cells. We acknowledge Arja Pasternack and Xiaobo Zhang for their valuable technical work.

GRANTS

This work was supported by the Academy of Finland (Grant No. 275922) and the Cancer Foundation of Finland.

DISCLOSURES

No conflicts of interest, financial or otherwise, are declared by the authors.

AUTHOR CONTRIBUTIONS

J.J.H conceived and designed the original research together with T.A.N while J.J.H, M.L. and J.H.L. designed the current study; T.A.N. and J.H. performed the cancer experiments; S.C. and Y.S. conducted the metabolomics measurements while M.L. and J.H.L analyzed the metabolomics data; J.H.L. conducted protein, RNA and DNA analysis as well as prepared the figures; O.R. prepared the recombinant sACVR2B-Fc protein; J.H.L, drafted the manuscript with the guidance of J.J.H and help from M.L., T.A.N. and J.H. All the authors approved the final version of the manuscript.

REFERENCES

1. **Acharyya S, Ladner KJ, Nelsen LL, Damrauer J, Reiser PJ, Swoap S, Guttridge DC.** Cancer cachexia is regulated by selective targeting of skeletal muscle gene products. *J Clin Invest* 114: 370–378, 2004. doi:10.1172/JCI200420174.
2. **Baracos VE, DeVivo C, Hoyle DH, Goldberg AL.** Activation of the ATP-ubiquitin-proteasome pathway in skeletal muscle of cachectic rats bearing a hepatoma. *Am J Physiol* 268: E996–E1006, 1995. doi:10.1152/ajpendo.1995.268.5.E996.
3. **Barreto R, Mandili G, Witzmann FA, Novelli F, Zimmers TA, Bonetto A.** Cancer and chemotherapy contribute to muscle loss by activating common signaling pathways. *Front Physiol* 7: 472, 2016. doi:10.3389/fphys.2016.00472.
4. **Ben-Sahra I, Howell JJ, Asara JM, Manning BD.** Stimulation of de novo pyrimidine synthesis by growth signaling through mTOR and S6K1. *Science* 339: 1323–1328, 2013. doi:10.1126/science.1228792.
5. **Bossola M, Marzetti E, Rosa F, Pacelli F.** Skeletal muscle regeneration in cancer cachexia. *Clin Exp Pharmacol Physiol* 43: 522–527, 2016. doi:10.1111/1440-1681.12559.
6. **Bremer J.** Carnitine in intermediary metabolism. The metabolism of fatty acid esters of carnitine by mitochondria. *J Biol Chem* 237: 3628–3632, 1962.
7. **Brown DG, Rao S, Weir TL, O'Malia J, Bazan M, Brown RJ, Ryan EP.** Metabolomics and metabolic pathway networks from human colorectal cancers, adjacent mucosa, and stool. *Cancer Metab* 4: 11, 2016. doi:10.1186/s40170-016-0151-y.
8. **Bruce CR, Brolin C, Turner N, Cleasby ME, van der Leij FR, Cooney GJ, Kraegen EW.** Overexpression of carnitine palmitoyltransferase I in skeletal muscle in vivo increases fatty acid oxidation and reduces triacylglycerol esterification. *Am J Physiol Endocrinol Metab* 292: E1231–E1237, 2007. doi:10.1152/ajpendo.00561.2006.
9. **Burlina A, Cazzorla C, Zanonato E, Viggiano E, Fasan I, Polo G.** Clinical experience with N-carbamylglutamate in a single-centre cohort of patients with propionic and methylmalonic aciduria. *Mol Genet Metab Rep* 8: 34–40, 2016. doi:10.1016/j.ymgmr.2016.06.007.
10. **Cala MP, Agulló-Ortuño MT, Prieto-García E, González-Riano C, Parrilla-Rubio L, Barbas C, Díaz-García CV, García A, Pernaut C, Adeva J, Riesco MC, Rupérez FJ, Lopez-Martin JA.** Multiplatform plasma fingerprinting in cancer cachexia: a pilot observational and translational study. *J Cachexia Sarcopenia Muscle* 9: 348–357, 2018. doi:10.1002/jcsm.12270.
11. **Cao W, Xiao L, Liu G, Fang T, Wu X, Jia G, Zhao H, Chen X, Wu C, Cai J, Wang J.** Dietary arginine and N-carbamylglutamate supplementation enhances the antioxidant statuses of the liver and plasma against oxidative stress in rats. *Food Funct* 7: 2303–2311, 2016. doi:10.1039/C5FO01194A.

12. **Das SK, Eder S, Schauer S, Diwoky C, Temmel H, Guertl B, Gorkiewicz G, Tamilarasan KP, Kumari P, Trauner M, Zimmermann R, Vesely P, Haemmerle G, Zechner R, Hoefler G.** Adipose triglyceride lipase contributes to cancer-associated cachexia. *Science* 333: 233–238, 2011. doi:10.1126/science.1198973.
13. **Der-Torossian H, Asher SA, Winnike JH, Wysong A, Yin X, Willis MS, O'Connell TM, Couch ME.** Cancer cachexia's metabolic signature in a murine model confirms a distinct entity. *Metabolomics* 9: 730–739, 2013. doi:10.1007/s11306-012-0485-6.
14. **Der-Torossian H, Wysong A, Shadfar S, Willis MS, McDunn J, Couch ME.** Metabolic derangements in the gastrocnemius and the effect of Compound A therapy in a murine model of cancer cachexia. *J Cachexia Sarcopenia Muscle* 4: 145–155, 2013. doi:10.1007/s13539-012-0101-7.
15. **Emery PW, Lovell L, Rennie MJ.** Protein synthesis measured in vivo in muscle and liver of cachectic tumor-bearing mice. *Cancer Res* 44: 2779–2784, 1984.
16. **Essén-Gustavsson B, Lindholm A.** Fiber types and metabolic characteristics in muscles of wild boars, normal and halothane sensitive Swedish landrace pigs. *Comp Biochem Physiol A Comp Physiol* 78: 67–71, 1984. doi:10.1016/0300-9629(84)90094-X.
17. **Evans WJ, Morley JE, Argilés J, Bales C, Baracos V, Guttridge D, Jatoi A, Kalantar-Zadeh K, Lochs H, Mantovani G, Marks D, Mitch WE, Muscaritoli M, Najand A, Ponikowski P, Rossi Fanelli F, Schambelan M, Schols A, Schuster M, Thomas D, Wolfe R, Anker SD.** Cachexia: a new definition. *Clin Nutr* 27: 793–799, 2008. doi:10.1016/j.clnu.2008.06.013.
18. **Ezeoke CC, Morley JE.** Pathophysiology of anorexia in the cancer cachexia syndrome. *J Cachexia Sarcopenia Muscle* 6: 287–302, 2015. doi:10.1002/jcsm.12059.
19. **Fazelzadeh P, Hangelbroek RW, Tieland M, de Groot LC, Verdijk LB, van Loon LJ, Smilde AK, Alves RD, Vervoort J, Müller M, van Duynhoven JP, Boekschoten MV.** The muscle metabolome differs between healthy and frail older adults. *J Proteome Res* 15: 499–509, 2016. doi:10.1021/acs.jproteome.5b00840.
20. **Fearon KC, Glass DJ, Guttridge DC.** Cancer cachexia: mediators, signaling, and metabolic pathways. *Cell Metab* 16: 153–166, 2012. doi:10.1016/j.cmet.2012.06.011.
21. **Fujiwara Y, Kobayashi T, Chayahara N, Imamura Y, Toyoda M, Kiyota N, Mukohara T, Nishiumi S, Azuma T, Yoshida M, Minami H.** Metabolomics evaluation of serum markers for cachexia and their intra-day variation in patients with advanced pancreatic cancer. *PLoS One* 9: e113259, 2014. doi:10.1371/journal.pone.0113259.
22. **Fukawa T, Yan-Jiang BC, Min-Wen JC, Jun-Hao ET, Huang D, Qian CN, Ong P, Li Z, Chen S, Mak SY, Lim WJ, Kanayama HO, Mohan RE, Wang RR, Lai JH, Chua C, Ong HS, Tan KK, Ho YS, Tan IB, Teh BT, Shyh-Chang N.** Excessive fatty acid oxidation induces muscle atrophy in cancer cachexia. *Nat Med* 22: 666–671, 2016. doi:10.1038/nm.4093.
23. **Gallagher IJ, Jacobi C, Tardif N, Rooyackers O, Fearon K.** Omics/systems biology and cancer cachexia. *Semin Cell Dev Biol* 54: 92–103, 2016. doi:10.1016/j.semcdb.2015.12.022.
24. **Garvey SM, Dugle JE, Kennedy AD, McDunn JE, Kline W, Guo L, Guttridge DC, Pereira SL, Edens NK.** Metabolomic profiling reveals severe skeletal muscle group-specific perturbations of metabolism in aged FBN rats. *Biogerontology* 15: 217–232, 2014. doi:10.1007/s10522-014-9492-5.
25. **Ham DJ, Murphy KT, Chee A, Lynch GS, Koopman R.** Glycine administration attenuates skeletal muscle wasting in a mouse model of cancer cachexia. *Clin Nutr* 33: 448–458, 2014. doi:10.1016/j.clnu.2013.06.013.
26. **Hentilä J, Nissinen TA, Korkmaz A, Lensu S, Silvennoinen M, Pasternack A, Ritvos O, Atalay M, Hulmi JJ.** Activin receptor ligand blocking and cancer have distinct effects on protein and redox homeostasis in skeletal muscle and liver. *Front Physiol* 9: 1917, 2019. doi:10.3389/fphys.2018.01917.
27. **Huang X, Choi Y, Im H, Yarimaga O, Yoon E, Kim H.** Aspartate aminotransferase (AST/GOT) and alanine aminotransferase (ALT/GPT) detection techniques. *Sensors (Basel)* 6: 756–782, 2006. doi:10.3390/s6070756.
28. **Hulmi JJ, Oliveira BM, Silvennoinen M, Hoogaars WM, Ma H, Pierre P, Pasternack A, Kainulainen H, Ritvos O.** Muscle protein synthesis, mTORC1/MAPK/Hippo signaling, and capillary density are altered by blocking of myostatin and activins. *Am J Physiol Endocrinol Metab* 304: E41–E50, 2013. doi:10.1152/ajpendo.00389.2012.
29. **Hulmi JJ, Silvennoinen M, Lehti M, Kivelä R, Kainulainen H.** Altered REDD1, myostatin, and Akt/mTOR/FoxO/MAPK signaling in streptozotocin-induced diabetic muscle atrophy. *Am J Physiol Endocrinol Metab* 302: E307–E315, 2012. doi:10.1152/ajpendo.00398.2011.
30. **Kim SG, Buel GR, Blenis J.** Nutrient regulation of the mTOR complex 1 signaling pathway. *Mol Cells* 35: 463–473, 2013. doi:10.1007/s10059-013-0138-2.
31. **Kir S, White JP, Kleiner S, Kazak L, Cohen P, Baracos VE, Spiegelman BM.** Tumour-derived PTH-related protein triggers adipose tissue browning and cancer cachexia. *Nature* 513: 100–104, 2014. doi:10.1038/nature13528.
32. **Benny Klimek ME, Aydogdu T, Link MJ, Pons M, Koniaris LG, Zimmers TA.** Acute inhibition of myostatin-family proteins preserves skeletal muscle in mouse models of cancer cachexia. *Biochem Biophys Res Commun* 391: 1548–1554, 2010. doi:10.1016/j.bbrc.2009.12.123.
33. **Koopman R, Caldow MK, Ham DJ, Lynch GS.** Glycine metabolism in skeletal muscle: implications for metabolic homeostasis. *Curr Opin Clin Nutr Metab Care* 20: 237–242, 2017. doi:10.1097/MCO.0000000000000383.
34. **Lee SJ, Reed LA, Davies MV, Girgenrath S, Goad ME, Tomkinson KN, Wright JF, Barker C, Ehrmantraut G, Holmstrom J, Trowell B, Gertz B, Jiang MS, Sebald SM, Matzuk M, Li E, Liang LF, Quattlebaum E, Stotish RL, Wolfman NM.** Regulation of muscle growth by multiple ligands signaling through activin type II receptors. *Proc Natl Acad Sci USA* 102: 18117–18122, 2005. doi:10.1073/pnas.0505996102.
35. **Ma EH, Jones RG.** Cell growth. (TORC)ing up purine biosynthesis. *Science* 351: 670–671, 2016. doi:10.1126/science.aaf1929.
36. **Machida M, Takeda K, Yokono H, Ikemune S, Taniguchi Y, Kiyosawa H, Takemasa T.** Reduction of ribosome biogenesis with activation of the mTOR pathway in denervated atrophic muscle. *J Cell Physiol* 227: 1569–1576, 2012. doi:10.1002/jcp.22871.
37. **Mäkinen VP, Forsblom C, Thorn LM, Wadén J, Kaski K, Ala-Korpela M, Groop PH.** Network of vascular diseases, death and biochemical characteristics in a set of 4,197 patients with type 1 diabetes (the FinnDiane Study). *Cardiovasc Diabetol* 8: 54, 2009. doi:10.1186/1475-2840-8-54.
38. **Mamane Y, Petroulakis E, LeBacquer O, Sonenberg N.** mTOR, translation initiation and cancer. *Oncogene* 25: 6416–6422, 2006. doi:10.1038/sj.onc.1209888.
39. **Metges CC, Yu YM, Cai W, Lu XM, Wong S, Regan MM, Ajami A, Young VR.** Oxoproline kinetics and oxoproline urinary excretion during glycine- or sulfur amino acid-free diets in humans. *Am J Physiol Endocrinol Metab* 278: E868–E876, 2000. doi:10.1152/ajpendo.2000.278.5.E868.
40. **Meyuhas O.** Ribosomal protein S6 phosphorylation: four decades of research. *Int Rev Cell Mol Biol* 320: 41–73, 2015. doi:10.1016/bs.ircmb.2015.07.006.
41. **Moaddel R, Fabbri E, Khadeer MA, Carlson OD, Gonzalez-Freire M, Zhang P, Semba RD, Ferrucci L.** Plasma biomarkers of poor muscle quality in older men and women from the Baltimore Longitudinal Study of Aging. *J Gerontol A Biol Sci Med Sci* 71: 1266–1272, 2016. doi:10.1093/gerona/glw046.
42. **Murphy KT, Chee A, Trieu J, Naim T, Lynch GS.** Importance of functional and metabolic impairments in the characterization of the C-26 murine model of cancer cachexia. *Dis Model Mech* 5: 533–545, 2012. doi:10.1242/dmm.008839.
43. **Nissinen TA, Hentilä J, Penna F, Lampinen A, Lautaoja JH, Fachada V, Holopainen T, Ritvos O, Kivelä R, Hulmi JJ.** Treating cachexia using soluble ACVR2B improves survival, alters mTOR localization, and attenuates liver and spleen responses. *J Cachexia Sarcopenia Muscle* 9: 514–529, 2018. doi:10.1002/jcsm.12310.
44. **O'Connell TM, Ardeshirpour F, Asher SA, Winnike JH, Yin X, George J, Guttridge DC, He W, Wysong A, Willis MS, Couch ME.** Metabolomic analysis of cancer cachexia reveals distinct lipid and glucose alterations. *Metabolomics* 4: 216–225, 2008. doi:10.1007/s11306-008-0113-7.
45. **Paddon-Jones D, Sheffield-Moore M, Cree MG, Hewlings SJ, Aarsland A, Wolfe RR, Ferrando AA.** Atrophy and impaired muscle protein synthesis during prolonged inactivity and stress. *J Clin Endocrinol Metab* 91: 4836–4841, 2006. doi:10.1210/jc.2006-0651.
46. **Petruzzelli M, Schweiger M, Schreiber R, Campos-Olivas R, Tsoli M, Allen J, Swarbrick M, Rose-John S, Rincon M, Robertson G, Zechner R, Wagner EF.** A switch from white to brown fat increases energy expenditure in cancer-associated cachexia. *Cell Metab* 20: 433–447, 2014. doi:10.1016/j.cmet.2014.06.011.

47. **Pin F, Barreto R, Couch ME, Bonetto A, O'Connell TM.** Cachexia induced by cancer and chemotherapy yield distinct perturbations to energy metabolism. *J Cachexia Sarcopenia Muscle*. 10: 140–154, 2019. doi:10.1002/jcsm.12360.
48. **Reeds PJ, Kurpad A, Opekun A, Jahoor F, Wong WW, Klein PD.** Acute phase and transport protein synthesis in stimulated infection in undernourished men using uniformly labelled Spirulina Platensis. *IAEA* 26: 21–30, 1994.
49. **Robitaille AM, Christen S, Shimobayashi M, Cornu M, Fava LL, Moes S, Prescianotto-Baschong C, Sauer U, Jenoe P, Hall MN.** Quantitative phosphoproteomics reveal mTORC1 activates de novo pyrimidine synthesis. *Science* 339: 1320–1323, 2013. doi:10.1126/science.1228771.
50. **Rohm M, Schäfer M, Laurent V, Üstünel BE, Niopek K, Algire C, Hautzinger O, Sijmonsma TP, Zota A, Medrikova D, Pellegata NS, Ryden M, Kulyte A, Dahlman I, Arner P, Petrovic N, Cannon B, Amri EZ, Kemp BE, Steinberg GR, Janovska P, Kopecky J, Wolfrum C, Blüher M, Berriel Diaz M, Herzig S.** An AMP-activated protein kinase-stabilizing peptide ameliorates adipose tissue wasting in cancer cachexia in mice. *Nat Med* 22: 1120–1130, 2016. doi:10.1038/nm.4171.
51. **Salem N Jr, Pawlosky R, Wegher B, Hibbeln J.** In vivo conversion of linoleic acid to arachidonic acid in human adults. *Prostaglandins Leukot Essent Fatty Acids* 60: 407–410, 1999. doi:10.1016/S0952-3278(99)80021-0.
52. **Scioscia KA, Snyderman CH, Wagner R.** Altered serum amino acid profiles in head and neck cancer. *Nutr Cancer* 30: 144–147, 1998. doi:10.1080/01635589809514654.
53. **Stephens NA, Skipworth RJ, Macdonald AJ, Greig CA, Ross JA, Fearon KC.** Intramyocellular lipid droplets increase with progression of cachexia in cancer patients. *J Cachexia Sarcopenia Muscle* 2: 111–117, 2011. doi:10.1007/s13539-011-0030-x.
54. **Stretch C, Aubin JM, Mickiewicz B, Leugner D, Al-Manasra T, Tobola E, Salazar S, Sutherland FR, Ball CG, Dixon E, Vogel HJ, Damaraju S, Baracos VE, Bathe OF.** Sarcopenia and myosteatosis are accompanied by distinct biological profiles in patients with pancreatic and periampullary adenocarcinomas. *PLoS One* 13: e0196235, 2018. doi:10.1371/journal.pone.0196235.
55. **Tando T, Hirayama A, Furukawa M, Sato Y, Kobayashi T, Funayama A, Kanaji A, Hao W, Watanabe R, Morita M, Oike T, Miyamoto K, Soga T, Nomura M, Yoshimura A, Tomita M, Matsumoto M, Nakamura M, Toyama Y, Miyamoto T.** Smad2/3 proteins are required for immobilization-induced skeletal muscle atrophy. *J Biol Chem* 291: 12184–12194, 2016. doi:10.1074/jbc.M115.680579.
56. **Tisdale MJ.** Mechanisms of cancer cachexia. *Physiol Rev* 89: 381–410, 2009. doi:10.1152/physrev.00016.2008.
57. **Tseng YC, Kulp SK, Lai IL, Hsu EC, He WA, Frankhouser DE, Yan PS, Mo X, Bloomston M, Lesinski GB, Marcucci G, Guttridge DC, Bekaii-Saab T, Chen CS.** Preclinical investigation of the novel histone deacetylase inhibitor AR-42 in the treatment of cancer-induced cachexia. *J Natl Cancer Inst* 107: djv274, 2015. doi:10.1093/jnci/djv274.
58. **Tsoli M, Robertson G.** Cancer cachexia: malignant inflammation, tumorkines, and metabolic mayhem. *Trends Endocrinol Metab* 24: 174–183, 2013. doi:10.1016/j.tem.2012.10.006.
59. **Tzika AA, Fontes-Oliveira CC, Shestov AA, Constantinou C, Psychogios N, Righi V, Mintzopoulos D, Busquets S, Lopez-Soriano FJ, Milot S, Lepine F, Mindrinos MN, Rahme LG, Argiles JM.** Skeletal muscle mitochondrial uncoupling in a murine cancer cachexia model. *Int J Oncol* 43: 886–894, 2013. doi:10.3892/ijo.2013.1998.
60. **von Walden F, Liu C, Aurigemma N, Nader GA.** mTOR signaling regulates myotube hypertrophy by modulating protein synthesis, rDNA transcription, and chromatin remodeling. *Am J Physiol Cell Physiol* 311: C663–C672, 2016. doi:10.1152/ajpcell.00144.2016.
61. **Wagenmakers AJ.** Protein and amino acid metabolism in human muscle. *Adv Exp Med Biol* 441: 307–319, 1998.
62. **Wang J, Christison TT, Misuno K, Lopez L, Huhmer AF, Huang Y, Hu S.** Metabolomic profiling of anionic metabolites in head and neck cancer cells by capillary ion chromatography with Orbitrap mass spectrometry. *Anal Chem* 86: 5116–5124, 2014. doi:10.1021/ac500951v.
63. **Wen Y, Alimov AP, McCarthy JJ.** Ribosome biogenesis is necessary for skeletal muscle hypertrophy. *Exerc Sport Sci Rev* 44: 110–115, 2016. doi:10.1249/JES.0000000000000082.
64. **Xiao L, Cao W, Liu G, Fang T, Wu X, Jia G, Chen X, Zhao H, Wang J, Wu C, Cai J.** Arginine, *n*-carbamylglutamate, and glutamine exert protective effects against oxidative stress in rat intestine. *Anim Nutr* 2: 242–248, 2016. doi:10.1016/j.aninu.2016.04.005.
65. **Yang QJ, Zhao JR, Hao J, Li B, Huo Y, Han YL, Wan LL, Li J, Huang J, Lu J, Yang GJ, Guo C.** Serum and urine metabolomics study reveals a distinct diagnostic model for cancer cachexia. *J Cachexia Sarcopenia Muscle* 9: 71–85, 2018. doi:10.1002/jcsm.12246.
66. **Yap S, Leong HY, Abdul Aziz F, Hassim H, Sthaneshwar P, Teh SH, Abdullah IS, Ngu LH, Mohamed Z.** N-carbamylglutamate is an effective treatment for acute neonatal hyperammonaemia in a patient with methylmalonic aciduria. *Neonatology* 109: 303–307, 2016. doi:10.1159/000443630.
67. **Zhou X, Wang JL, Lu J, Song Y, Kwak KS, Jiao Q, Rosenfeld R, Chen Q, Boone T, Simonet WS, Lacey DL, Goldberg AL, Han HQ.** Reversal of cancer cachexia and muscle wasting by ActRIIB antagonism leads to prolonged survival. *Cell* 142: 531–543, 2010. doi:10.1016/j.cell.2010.07.011.

II

DIFFERENTIATION OF MURINE C2C12 MYOBLASTS STRONGLY REDUCES THE EFFECTS OF MYOSTATIN ON INTRACELLULAR SIGNALING

by

Lautaoja, J.H., Pekkala, S., Pasternack, A., Laitinen, M., Ritvos, O. & Hulmi, J.J. (2020).

Journal of Biomolecules, 10(5), 695

https://doi.org/10.3390/biom10050695

biomolecules

MDPI

Article

Differentiation of Murine C2C12 Myoblasts Strongly Reduces the Effects of Myostatin on Intracellular Signaling

Juulia H. Lautaoja [1,*], Satu Pekkala [1], Arja Pasternack [2], Mika Laitinen [3,4], Olli Ritvos [2] and Juha J. Hulmi [1,2]

1 Faculty of Sport and Health Sciences, Neuromuscular Research Center, University of Jyväskylä, 40014 Jyväskylä, Finland; satu.p.pekkala@jyu.fi (S.P.); juha.j.t.hulmi@jyu.fi (J.J.H.)
2 Department of Physiology, Faculty of Medicine, University of Helsinki, 00290 Helsinki, Finland; arja.pasternack@helsinki.fi (A.P.); olli.ritvos@helsinki.fi (O.R.)
3 Department of Medicine, Faculty of Medicine, University of Helsinki, 00029 Helsinki, Finland; mika.laitinen@helsinki.fi
4 Department of Medicine, Helsinki University Hospital, 00029 Helsinki, Finland
* Correspondence: juulia.h.lautaoja@jyu.fi; Tel.: +358-40-805-5042

Received: 2 April 2020; Accepted: 28 April 2020; Published: 30 April 2020

Abstract: Alongside in vivo models, a simpler and more mechanistic approach is required to study the effects of myostatin on skeletal muscle because myostatin is an important negative regulator of muscle size. In this study, myostatin was administered to murine (C2C12) and human (CHQ) myoblasts and myotubes. Canonical and noncanonical signaling downstream to myostatin, related ligands, and their receptor were analyzed. The effects of tumorkines were analyzed after coculture of C2C12 and colon cancer-C26 cells. The effects of myostatin on canonical and noncanonical signaling were strongly reduced in C2C12 cells after differentiation. This may be explained by increased follistatin, an endogenous blocker of myostatin and altered expression of activin receptor ligands. In contrast, CHQ cells were equally responsive to myostatin, and follistatin remained unaltered. Both myostatin administration and the coculture stimulated pathways associated with inflammation, especially in C2C12 cells. In conclusion, the effects of myostatin on intracellular signaling may be cell line- or organism-specific, and C2C12 myotubes seem to be a nonoptimal in vitro model for investigating the effects of myostatin on canonical and noncanonical signaling in skeletal muscle. This may be due to altered expression of activin receptor ligands and their regulators during muscle cell differentiation.

Keywords: coculture; follistatin; inflammation; MAPK; myotube; skeletal muscle; Smad; tumorkine

1. Introduction

The role of myostatin (growth differentiation factor 8, GDF8), a member of the transforming growth factor-β (TGF-β) family, as a negative regulator of muscle size is well recognized (for review, see [1,2]). Myostatin is a secreted protein that is expressed mainly in the skeletal muscle and to a lesser extent in the cardiac muscle and adipose tissue [3,4]. Besides coordinating normal growth and development in a healthy state, abnormal myostatin regulation promotes muscle atrophy (for review, see [5]). Myostatin binding to the activin type 2A and 2B receptors (ACVR2A/B) inhibits anabolic processes and muscle regeneration as well as enhances catabolic signaling in the skeletal muscle [6–9]. However, blocking tumor-derived cytokines ("tumorkines"), such as activin receptor (ACVR2) ligands (e.g., activins, myostatin and GDF11 [4,10,11]), by ACVR2 antagonism has attenuated muscle atrophy and improved survival in experimental cancer [8,12]. In addition, the inhibition of myostatin alone or

myostatin and GDF11 by neutralizing antibodies has attenuated cancer cachexia in vivo and muscle atrophy in vitro [13]. Further, inhibition of myostatin and/or activins by follistatin induces muscle hypertrophy in vivo [14]. Follistatin is a circulating endogenous protein that strongly increases muscle mass and is a natural ACVR2 ligand blocker [14,15]. Myostatin signaling is inhibited when follistatin binds the C-terminal dimer of the myostatin protein, thus preventing association with ACVR2A/B [15].

Alongside in vivo models, a simpler and more mechanistic in vitro approach is required to study the effects of ACVR2 ligands on skeletal muscle. Unfortunately, the physiological responses may differ depending on the cell lines and organisms used, and thus the selection of the cell line should be made based on the research question [16]. Mouse C2C12 muscle cells are the most commonly used cellular model to mimic skeletal muscle in vitro. Various studies reporting the effects of myostatin on C2C12 proliferation and differentiation exist [17–21]. Administration of myostatin to C2C12 myoblasts has been reported to promote canonical and noncanonical signaling pathways [19,21]. Firstly, the canonical pathway is activated by myostatin binding to ACVR2A/B, which further induces the activation of activin receptor type 1B (or ALK4) or TGF-β receptor type 1 (or ALK5) to phosphorylate transcription factor Smad2/3 [22–25]. Secondly, Smad2/3 forms a complex with Smad4, which translocates into the nucleus to regulate gene expression [22–24]. Furthermore, activation of the Smad2/3 pathway promotes skeletal muscle catabolism at least via the ubiquitin–proteasome system [8,26,27]. The noncanonical pathway is responsive to the same TGF-β-related proteins, such as myostatin, that are able to promote stress and inflammation-responsive mitogen-activated protein kinases (MAPKs), such as p38 MAPK (p38), stress-activated protein kinase/c-Jun N-terminal kinases (SAPK/JNKs), and extracellular signal-regulated kinases (ERKs) [22], in vitro in C2C12 cells [28–30] and at least ERK in vivo [29,31]. For example, myostatin-induced growth inhibition of the C2C12 myoblasts was associated with p38 phosphorylation [28], while Zhang et al. reported that myostatin enhanced interleukin-6 (IL-6) production via the p38 pathway has been associated with proteolysis [32]. The kinases SAPK/JNKs and ERKs, on the other hand, have been associated with suppression of C2C12 myotube differentiation after myostatin administration [29,30].

Muscle wasting during cancer increases systemic inflammation [33,34] and inflammatory tumorkines, such as IL-6, monocyte chemoattractant protein 1 (MCP-1), and regulated on activation, normal T cell expressed and secreted (RANTES), activate transcriptional factors, such as signal transducer and activator of transcription 3 (STAT3) and CCAAT-enhancer-binding protein β (C/EBPβ) [34–37]. As a result, pathways related to muscle atrophy and expression of acute phase response proteins in the inflamed muscle are activated [34–37]. Indeed, ACVR2 ligands and other tumorkines disrupt normal skeletal muscle homeostasis during cancer [38]. The effects of tumorkines on intercellular signaling have been studied by applying cancer cell medium (conditioned medium, CM) to another cell line [39–42]. However, the Transwell® coculture system [43] is a more suitable approach to study tumorkine effects because it enables a constant supply of the tumor-derived factors from the upper compartment to another cell population in the lower compartment. Jackman et al. found that although the concentration of the tumokine called leukemia inhibitory factor was constantly higher in the colon 26 carcinoma (C26)-CM than in the lower compartment of the Transwell® system, there was a benefit of the Transwell® model in that the coculture induced a greater decrease in the C2C12 myotube diameter [41,44].

The aim of this study was to investigate whether an in vitro approach could be utilized as a tool to examine the direct effects of myostatin on canonical and noncanonical signaling in widely used murine C2C12 myoblasts and myotubes. To validate the functionality of the recombinant myostatin protein and to exclude the possibility of cell line-specific responsiveness to myostatin, we repeated the experiments with human CHQ myoblasts and myotubes derived from quadriceps muscle biopsy [45]. Finally, we cocultured the muscle and cancer cells to examine the effects of tumorkines, including ACVR2 ligands, on muscle cell homeostasis.

2. Materials and Methods

2.1. Cell Cultures

Mouse C2C12 myoblasts (American Type Culture Collection, ATCC, Manassas, VA, USA) were cultured in high glucose containing Dulbecco's Modified Eagle growth medium (GM) (DMEM, #BE12-614F, Lonza, Basel, Switzerland) supplemented with 10% (*v*/*v*) fetal bovine serum (FBS, #10270, Gibco, Rockville, MD, USA), 100 U/mL penicillin and 100 µg/mL streptomycin (P/S, #15140, Gibco), and 2 mM L-glutamine (#17-605E, Lonza). For the experiments, myoblasts were seeded on 12-well or 6-well plates (Nunclon^{TM} Delta; Thermo Fisher Scientific, Waltham, MA, USA). When the myoblasts reached 95–100% confluence, the cells were rinsed with phosphate-buffered saline (PBS) and the GM was replaced by differentiation medium (DM) containing high glucose DMEM, 5% (*v*/*v*) FBS or 2% (*v*/*v*) horse serum (HS, 12449C, Sigma-Aldrich, St. Luis, MO, USA) as indicated, 100 U/mL and 100 µg/mL P/S and 2 mM L-glutamine to promote fusion into myotubes. Fresh DM was changed every second day. Representative images of the C2C12 myoblasts and myotubes differentiated with 5% FBS DM are shown in the Supplementary Material Figure S1. Human CHQ cells, derived from quadriceps muscle biopsy of a 5-day-old infant [45], were donated by Dr. Vincent Mouyly and Dr. Eija Laakkonen. The immortalization of this cell line does not have effects on myogenic cascades or any other cellular processes except restraining senescence, which justifies the usage of the commercial immortalized C2C12 cells and primary nonimmortalized CHQ cells in the present study [46,47]. Furthermore, the thigh muscles of mice and human from which these cell lines are obtained can be functionally considered similar and thus comparable [48]. The CHQ cells were cultured in growth medium with 4:1 ratio of GlutaMAX (#61965, Gibco) and Medium 199 (#41150, Gibco) supplemented with 20% (*v*/*v*) FBS (#10270, Gibco) and 50 µg/mL gentamicin (#15750, Gibco). After reaching over 90% confluence, the differentiation of CHQ myotubes was induced by replacing GM to DM containing 4:1 GlutaMAX and Medium 199, 50 µg/mL gentamicin, and 10 µg/mL bovine insulin (#15500, Sigma-Aldrich) as previously described [49]. The CHQ DM was not replaced during the differentiation. All the muscle cell experiments independent of the cell line used were conducted at day 0–1 (myoblasts in GM) or at day 5–6 (myotubes in DM) post differentiation. Colon 26 carcinoma (C26) cells were a kind gift from Dr. Fabio Penna. The C26 cells were grown in the same GM as described for the C2C12 myoblasts. All the cell experiments were performed in a humidified environment at 37 °C and 5% CO_2.

2.2. Production and Administration of Myostatin

Recombinant myostatin protein was produced in house as described earlier for its receptor [50]. Shortly, the myostatin pro-and mature domains were amplified by PCR (prodomain 5′-TGGTCCAGTGGATCTAAATGAG-3′ and 5′-CTTTTTGGTGTGTCTGTTAC-3′, mature domain 5′-GAAGGGATTTTGGTCTTGAC-3′ and 5′-TCATGAGCACCCACAGCG-3′), and the domains were subcloned into pEFIRES-P vector. Both domains are required for the proper folding of the latent TGF-β family member precursors [51,52], and we expect myostatin to have similar requirement. This construct was co-transfected to CHO-S cells, positive cells were selected with puromycin (Thermo Fisher Scientific), and protein was produced in CD OptiCHO medium (Gibco) supplemented with 2 mM L-glutamine and grown in suspension in an orbital shaker. The protein was purified with HisTrap excel column (GE Healthcare, Chicago, IL, USA), eluted with imidazole, dialyzed against PBS, and finally concentrated with an Amicon Ultra concentrator (10,000 MWCO, Millipore, Burlington, MA, USA). Most of the purified myostatin was confirmed by western blot to be in the mature form (data not shown). To determine the activity of the myostatin preparation, HepG2 cells (purchased from ATCC) were cultured in DMEM supplemented with 10% (*v*/*v*) fetal calf serum (FCS), 2 mM L-glutamine, 100 U/mL, and 100 µg/mL P/S, 1× nonessential amino acids (Sigma-Aldrich) and 1 mM sodium-pyruvate (Sigma-Aldrich) and transfected with CAGA luciferase reporter construct as earlier with modifications [53]. The cells were stimulated with the ligand for 18 h and luciferase activity was measured with luciferase assay reagent (Promega, Madison, WI, USA). Dose-dependent activity was

detected at 10–100 ng/mL and the activity of 10 ng of myostatin was abolished dose-dependently by addition of two myostatin blockers, soluble ACVR2B and follistatin (6–600 ng/mL) (data not shown). Prior to the administration to the cells, the inactive promyostatin was heated at 95 °C for five minutes to activate the mature myostatin protein [54]. The activated mature myostatin is highly conserved among human and mouse (99% identical; one amino acid difference between these species), which justifies the usage of the same myostatin on mouse C2C12 and human CHQ cell lines [4]. Before the experiments, the wells were rinsed twice with PBS and fresh medium, depending on the differentiation state GM or DM with all supplements, was added. The final myostatin concentration used was selected to be 100 ng/mL based on our dose-dependent bioassay (data not shown) and previous reports [21,32]. The 2-h time-point was selected to show acute changes and the 24-h time-point to show more delayed or persistent changes based on previous studies [18,21,55]. All myostatin experiments (N = 3) were independently replicated (total N = 6 per group).

2.3. Transwell® Method, Coculture of C2C12 and C26 Cells

The C2C12 cells were seeded on 12-well or 6-well Transwell®plates (Costar, Corning Incorporated, Corning, NY, USA) and grown as described above; myoblasts were maintained in GM while myotubes were differentiated with 5% FBS DM. The C26 cells were grown in C2C12 GM or acclimatized for 48 h to C2C12 DM prior to the combination of the cell lines as demonstrated previously [41]. The C26 cells were seeded on the Transwell® inserts with 0.4 μm porous membrane (Costar, Corning Incorporated) and grown on a separate plate. The C26 inserts were approximately 80–90% confluent when the myoblasts were 100% confluent and the myotubes were differentiated for five days. On day 0 or 5 post C2C12 differentiation, the medium of C2C12 and C26 cells was removed, wells and inserts were rinsed with PBS, and fresh GM or DM was added to both upper and lower compartments. Then, C26 inserts were placed on C2C12 wells for 24-h coculture with myoblasts or myotubes. The time-point for the coculture experiment was chosen based on previous studies [41,56]. Coculture experiments (N = 3–4) were independently replicated once (total N = 6–8 per group).

2.4. SUnSET Method for the Analysis of Protein Synthesis, Protein Extraction, and Western Blotting

To measure the level of protein synthesis from C2C12 cells during coculture with C26 cells, the surface sensing of translation (SUnSET) method was used as demonstrated previously [28]. Briefly, puromycin was added to a final concentration of 1 μM as previously reported by us [29]. From this step forward, protein extraction was performed to all samples as follows. After the treatments, the cells were rinsed twice with cold PBS and lysed and scraped on ice in a buffer containing 20 mM HEPES (pH 7.4), 1 mM EDTA, 5 mM EGTA, 10 mM $MgCl_2$, 100 mM β-glycerophosphate, 1 mM Na_3VO_4, 1 mM DTT, 1% TritonX-100 and supplemented with protease and phosphatase inhibitors (#1861280, Thermo Fisher Scientific). After 30 min, the homogenate was centrifuged for 5 min, 500× *g* at +4 °C. Bicinchoninic Acid (BCA) Protein Assay Kit (Pierce Biotechnology, Rockford, IL, USA) was used according to manufacturers' protocol to measure the total protein content with an automated KoneLab analyzer (Thermo Fisher Scientific, Vantaa, Finland). Western blot analysis was conducted as previously described [57]. In brief, ~7 or 10 μg of protein (CHQ and C2C12, respectively) were separated by SDS-PAGE, transferred to PVDF membranes, blocked and incubated overnight with primary antibodies at 4 °C. Proteins were visualized by enhanced chemiluminescence (SuperSignal west femto maximum sensitivity substrate; Pierce Biotechnology) using a ChemiDoc MP device (Bio-Rad Laboratories, Hercules, CA, USA) and quantified with Image Lab software (version 6.0; Bio-Rad Laboratories). When stain free protein synthesis (puromycin-incorporated proteins) and ubiquitinated proteins were analyzed, the whole lane intensity was quantified. Stain free was used as a loading control and the results were normalized by dividing the intensity of the analyzed band by the intensity of the whole stain free lane. When two bands of one protein were detected, the bands were quantified together. Antibodies used in this study are presented in the Supplementary Material (Table S1).

2.5. RNA Extraction, cDNA Synthesis, and Quantitative Real-Time PCR

To extract total RNA, the cells were rinsed twice with cold PBS and lysed with TRIreagent solution according to the manufacturer´s protocol (AM9738, Thermo Fisher Scientific). The synthesis of cDNA and quantitative real-time PCR (RT-qPCR) were performed as previously described [57]. The sequences of the primers used in the study are presented in Supplementary Material (Table S2). Amplicon lengths of the amplifications using self-designed primers not published previously were analyzed and the lengths were as expected (Supplementary Material Figure S2). Detector of all double stranded DNA, PicoGreen (Quant-iT™ PicoGreen™ dsDNA Assay Kit, Thermo Fisher Scientific), was used to normalize the RT-qPCR results of both cell lines according to manufacturer´s protocol because no stable housekeeping gene was detected. For the analysis of the RT-qPCR results, 2^{-Ct} values were normalized to the PicoGreen content. The PicoGreen standard curves of both cell lines are presented in Supplementary Material Figure S3. N = 3–5 per group.

2.6. Multiplex Cytokine Assay

The conditioned medium of the C26 cells (C26-CM) for multiplex cytokine assay (Q-Plex Array 16-plex ELISA, Quansys Biosciences, Logan, UT, USA) was collected as previously described [42]. Shortly, 25 µL of undiluted, overnight serum-starved C26-CM was centrifuged and passed through a 0.22 µm filter. The cytokine assay was performed according to the manufacturer's protocol. The lower limit of detection for MCP-1 was 3.40 pg/mL and 2.15 pg/mL for RANTES. The calibrator range of the assay for both was 4.12–3000 pg/mL.

2.7. Statistical Analyses

The data were tested for normality (Shapiro–Wilk test) and equality of variances (Levene´s test) using IBM SPSS Statistics version 24 for Windows (IBM SPSS Statistics, Chicago, IL, USA). For statistical evaluation, a two tailed paired or unpaired Student´s *t*-test or Mann Whitney U-test (IBM SPSS Statistics) were used when appropriate. The results are presented as means ± SEM. The level of significance was set at $p < 0.05$. Pooling of the follistatin protein content results was justified because myostatin administration had no effect on the protein in question.

3. Results

3.1. Myostatin Had a Larger Effect on the Canonical, Noncanonical, and Inflammatory Signaling in C2C12 Myoblasts than in Myotubes

The C2C12 myoblasts differentiated into myotubes very successfully within five days as only a few cells remained as myoblasts at this time-point (Supplementary Material Figure S1). The administration of myostatin increased the phosphorylation of Smad3$^{Ser423/Ser425}$ after 2, but not after 24 h in C2C12 myoblasts ($p < 0.001$, Figure 1a,f), and this response was substantially lower in myotubes ($p < 0.01$, Figure 1a,f). On the noncanonical pathway, the 2-h myostatin administration induced phosphorylation of all MAPKs, p38$^{Thr180/Tyr182}$, SAPK/JNK1/2$^{Thr183/Tyr185}$, and ERK1/2$^{Thr202/Tyr204}$ in myoblasts ($p < 0.01$, $p < 0.01$, and $p < 0.05$, respectively, Figure 1b–d,f,g), but again, in myotubes this response was very small or lost completely (Figure 1b–d,f,g). The comparison of nontreated C2C12 myotubes to myoblasts showed a nonuniform effect of differentiation into myotubes on canonical and noncanonical signaling (Figure 1e–g). To exclude the effect of the C2C12 myotube differentiation protocol, we repeated the experiment by using another differentiation method (2% HS), demonstrating that the decreased responsiveness of the C2C12 cells to myostatin after differentiation is independent of the differentiation protocol (Supplementary Material Figure S4).

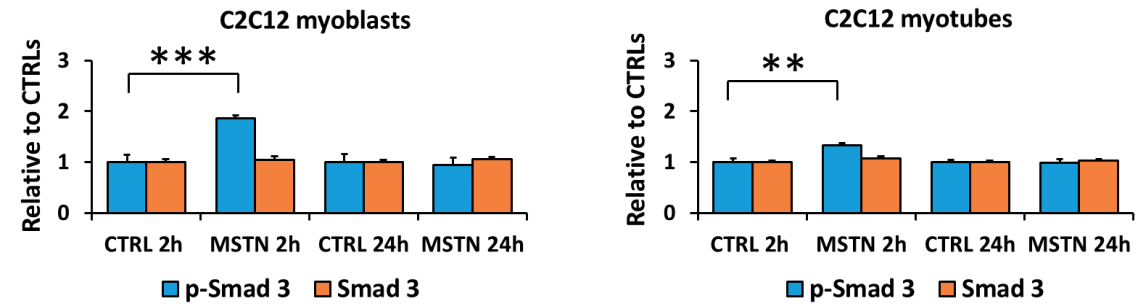

(**a**)

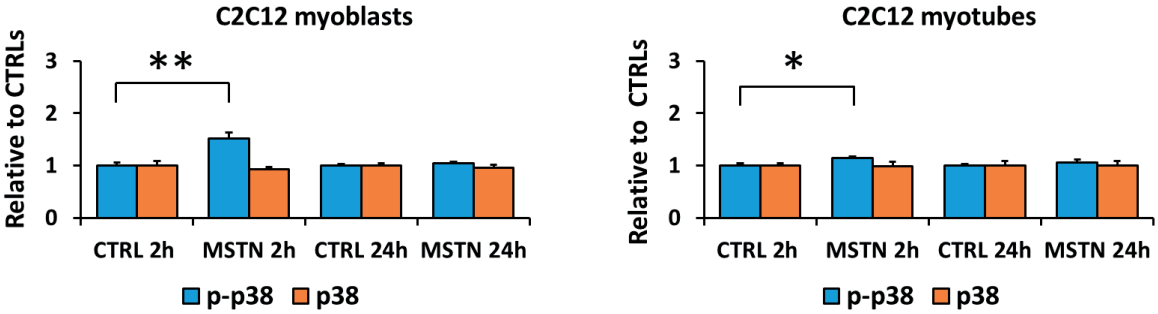

(**b**)

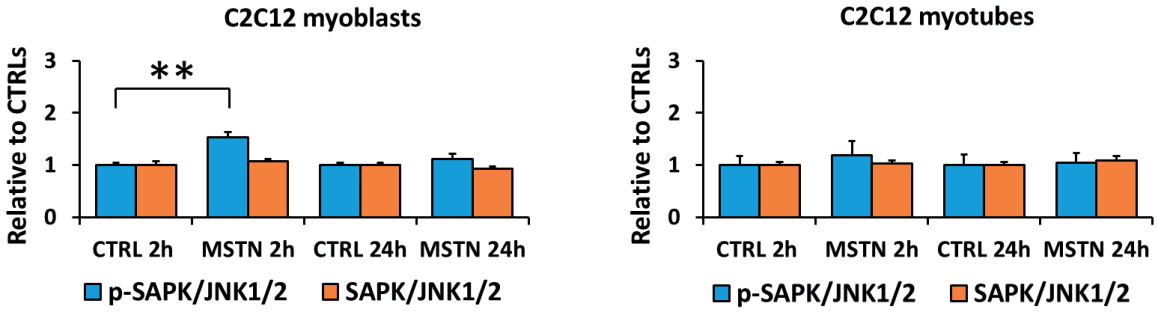

(**c**)

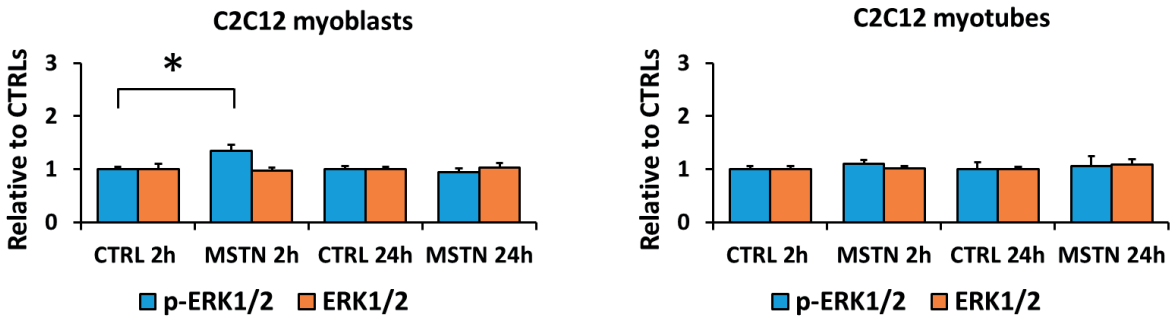

(**d**)

Figure 1. *Cont.*

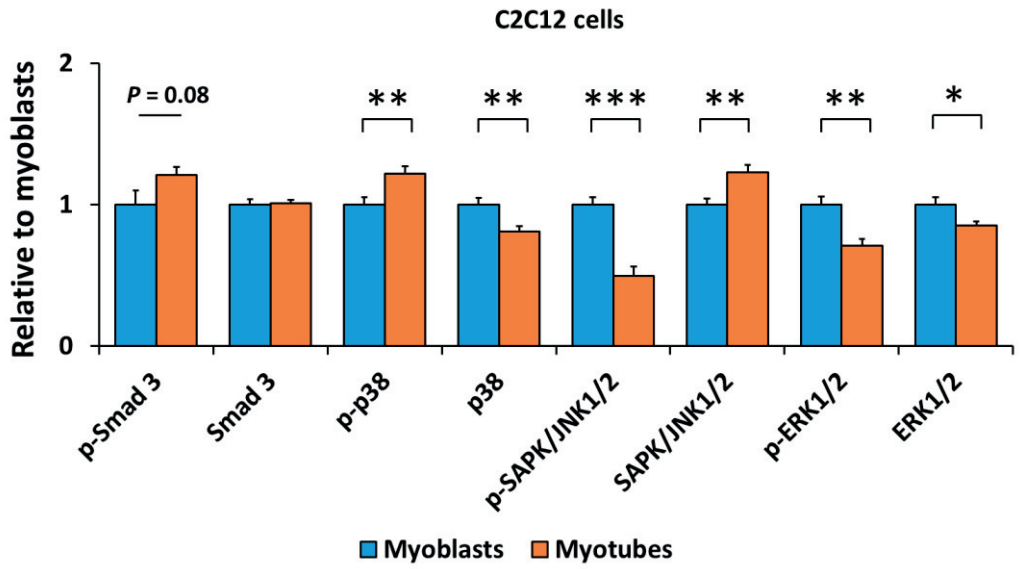

(**e**)

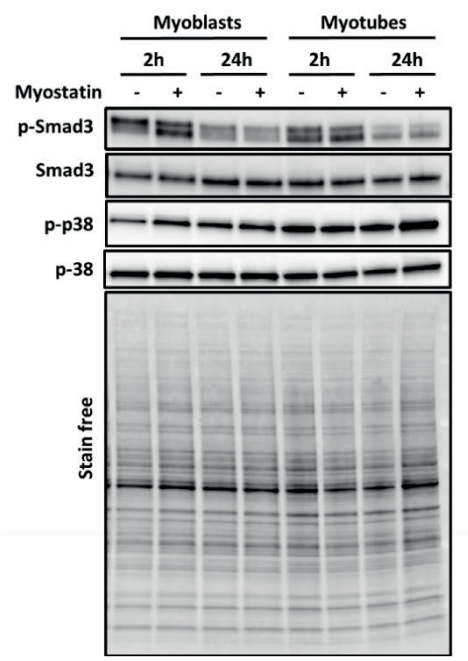

(**f**)

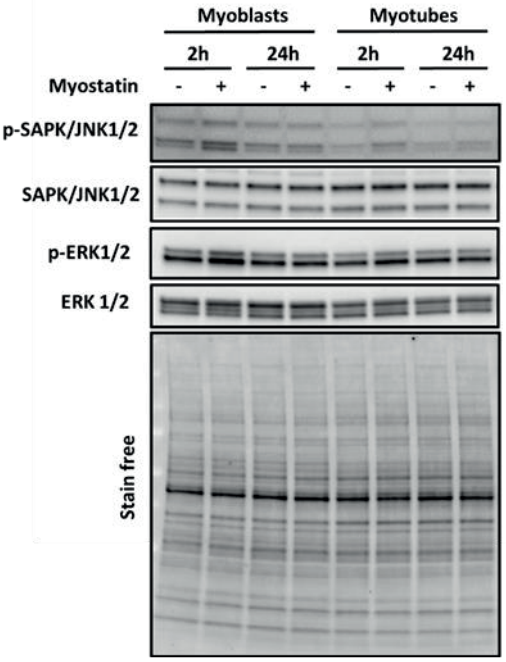

(**g**)

Figure 1. Myostatin-induced changes in the canonical (Smad3) and noncanonical (MAPKs) pathways were greater in C2C12 myoblasts than they were in myotubes. (**a**) Phosphorylated Smad3$^{Ser423/425}$ and total Smad3 in myoblasts and myotubes. (**b**) Phosphorylated p38$^{Thr180/Tyr182}$ and total p38 in myoblasts and myotubes. (**c**) Phosphorylated SAPK/JNK1/2$^{Thr183/Tyr185}$ and total SAPK/JNK1/2 in myoblast and myotubes. (**d**) Phosphorylated ERK1/2$^{Thr202/Tyr204}$ and total ERK1/2 in myoblasts and myotubes. In the figures, the values are presented as normalized to CTRL = 1. (**e**) Nontreated CTRL myoblasts and myotubes of the 2-h and 24-h time-points were pooled and the values are presented as normalized to myoblasts = 1. (**f**,**g**) Representative blots. In A–D, $N = 6$ per group. In E, $N = 12$ per group. *, **, and *** = $p < 0.05$, $p < 0.01$, and $p < 0.001$, respectively. CTRL (-) = control group, MSTN (+) = myostatin group.

The 2 h myostatin administration promoted typical inflammatory pathways in the C2C12 cells, shown by the elevated phosphorylation of STAT3^{Tyr705} in both myoblasts and myotubes ($p < 0.001$ and $p < 0.01$, respectively, Figure 2a,d) and phosphorylated C/EBPβ^{Thr235} in the myoblasts ($p < 0.01$, Figure 2b,d). When comparing the nontreated C2C12 myotubes to myoblasts, the contents of phosphorylated STAT3^{Tyr705} and total STAT3 were higher in myotubes when compared to myoblasts, whereas the opposite was true regarding the phosphorylated C/EBPβ^{Thr235} and total C/EBPβ (Figure 2c,d).

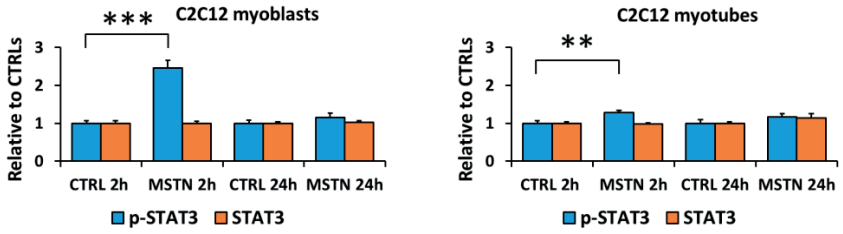

(**a**)

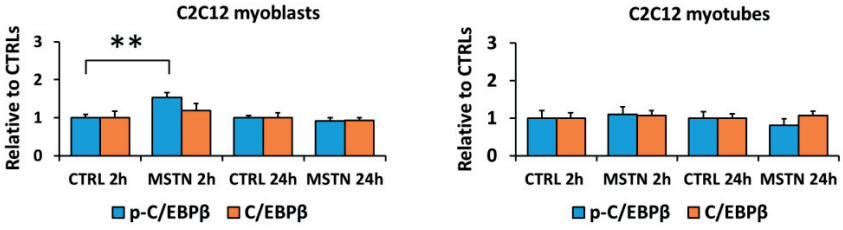

(**b**)

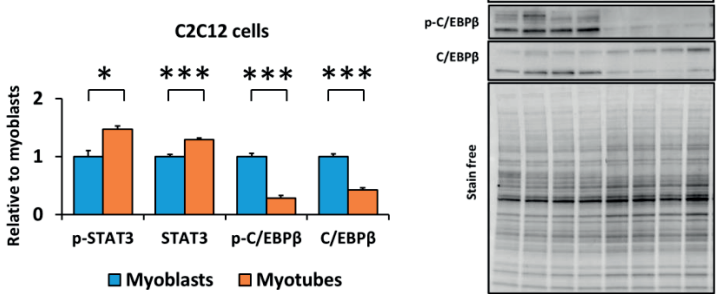

(**c**)

(**d**)

Figure 2. Myostatin administration on C2C12 cells increased inflammatory signaling in C2C12 myoblasts, whereas in myotubes the effect was very small. (**a**) Phosphorylated STAT3^{Tyr705} and total STAT3 in myoblasts and myotubes. (**b**) Phosphorylated C/EBPβ^{Thr235} and total C/EBPβ in myoblasts and myotubes. In the figures, the values are presented as normalized to CTRL = 1. (**c**) Nontreated CTRL myoblasts and myotubes of the 2-h and 24-h time-points were pooled, and the values are presented as normalized to myoblasts = 1. (**d**) Representative blots. In A–B, $N = 6$ per group. In C, $N = 12$ per group. *, **, and *** = $p < 0.05$, $p < 0.01$, and $p < 0.001$, respectively. CTRL (-) = control group, MSTN (+) = myostatin group.

3.2. The Coculture with C26 Cells Had Minor Effects on Canonical and Noncanonical Signaling in C2C12 Cells, but Increased Inflammatory Signaling Similar to the Effect of Myostatin

We previously reported that the C26 tumors express ACVR2 ligands, such as myostatin [12], and the same cell line is used in the present study. We analyzed inflammatory cytokines from the C26-CM using multiplex ELISA and found one highly (>1000 pg/mL) secreted inflammatory cytokine, MCP-1 (>3500 pg/mL), and one moderately (>100 pg/mL) secreted mediator, RANTES (>430 pg/mL), as shown by others [58]. MCP-1 and RANTES were also elevated in vivo in C26 tumor-bearing mice as we previously reported [12]. To analyze whether C26-derived tumorkines would also have more robust effects on myoblasts than they did on myotubes, we cocultured C2C12 cells in the Transwell® system with C26 cancer cells for 24 h. Interestingly, rather than activating canonical and noncanonical pathways like myostatin administration, the 24-h coculture decreased the phosphorylation of Smad3$^{Ser423/Ser425}$ in both myoblasts and myotubes ($p < 0.05$, Figure 3a,d), while the phosphorylation of p38$^{Thr180/Tyr182}$ remained unaltered in myoblasts and decreased in myotubes ($p < 0.05$, Figure 3b,e). Furthermore, after the 24-h coculture, no changes were observed in protein synthesis or in ubiquitinated proteins in C2C12 cells (Supplementary Material Figure S5). Additionally, the downstream mediators of the mechanistic target of rapamycin (mTOR) complex 1, phosphorylated S6K1/2^{Thr389} and ribosomal protein S6$^{Ser240/Ser244}$, remained also unaltered (Supplementary Material Figure S5). The phosphorylation of Akt^{Ser473} downstream to mTOR complex 2 [59] tended to decrease in myoblasts when cocultured with C26 cells ($p = 0.067$, Figure 3c–e).

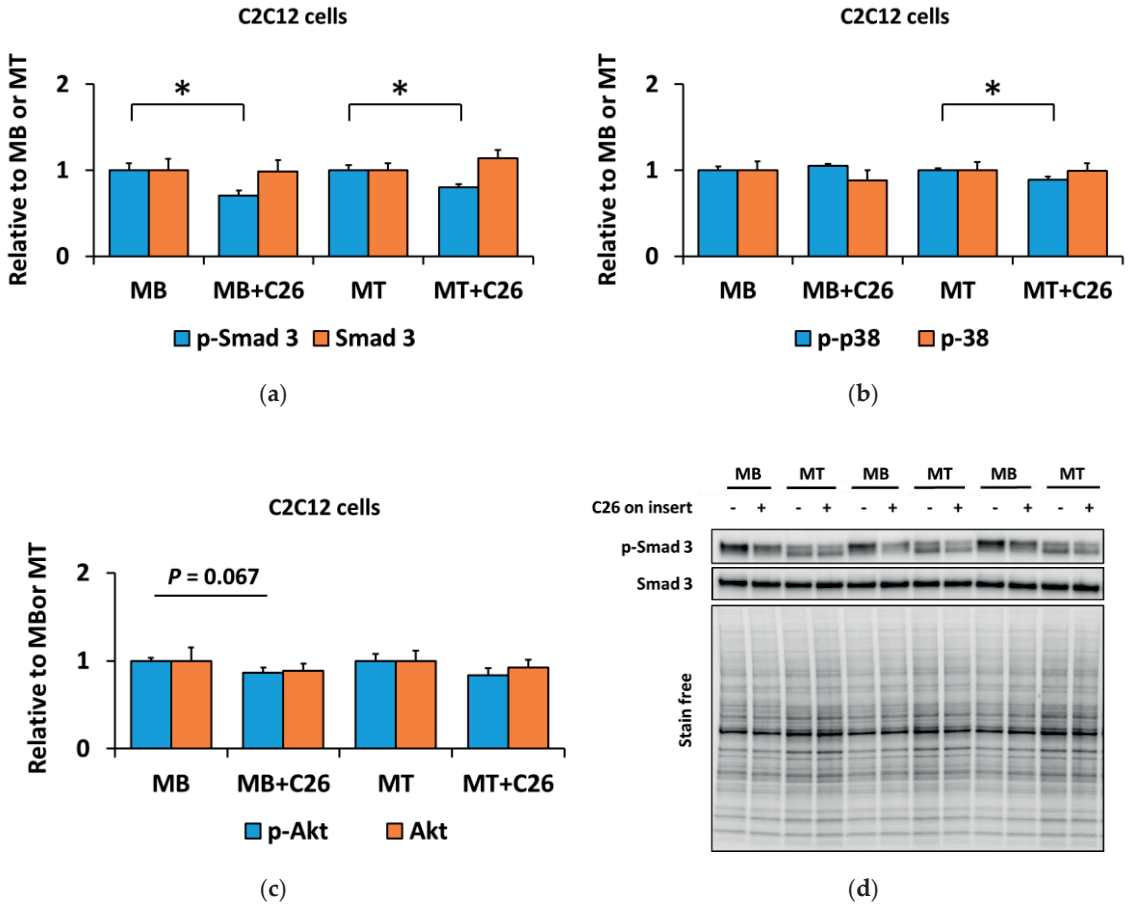

Figure 3. *Cont.*

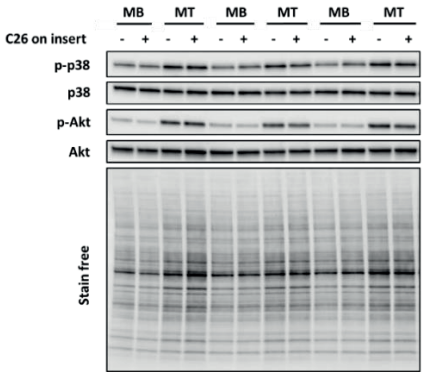

(**e**)

Figure 3. The 24-h coculture of C2C12 myoblasts (MB) and myotubes (MT) with C26 cells suppressed canonical and noncanonical signaling independent of the differentiation stage. (**a**) Phosphorylated Smad3$^{Ser423/425}$ and total Smad3. (**b**) Phosphorylated p38$^{Thr180/Tyr182}$ and total p38. (**c**) Phosphorylated Akt^{Ser473} and total Akt. In the figures, MB or MT with empty insert (-) are set as one and compared with MB or MT with C26 cells on the insert ((+), MB+C26 and MT+C26, respectively). (**d**,**e**) Representative blots. N = 6–8 per group. * = $p < 0.05$.

Similar to myostatin administration, the phosphorylation of STAT3^{Tyr705} and C/EBPβ^{Thr235} increased in both myoblasts ($p < 0.001$ and $p < 0.05$, respectively, Figure 4a–c) and myotubes ($p < 0.01$, Figure 4a–c) after the 24-h coculture with C26 cells.

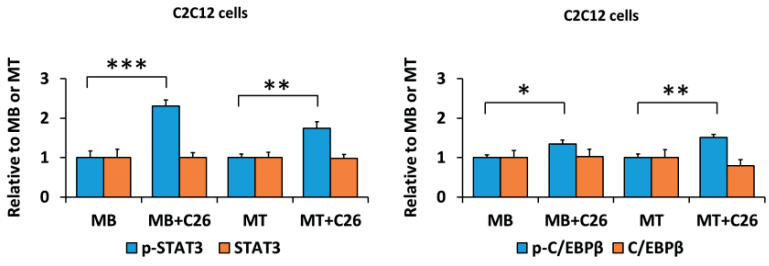

(**a**) (**b**)

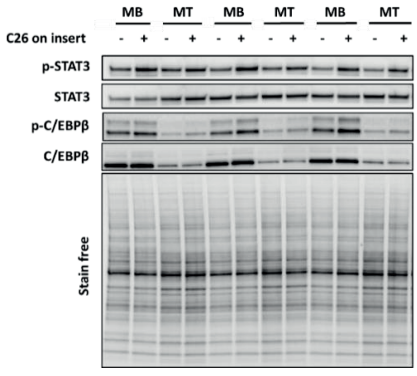

(**c**)

Figure 4. The 24-h coculture of C2C12 myoblasts (MB) and myotubes (MT) with C26 cells promotes inflammatory response independent of the differentiation stage. (**a**) Phosphorylated STAT3^{Tyr705} and total STAT3. (**b**) Phosphorylated C/EBPβ^{Thr235} and total C/EBPβ. (**c**) Representative blots. In the figures, MB or MT with empty insert (-) are set as one and compared with MB or MT with C26 cells on the insert ((+), MB+C26 and MT+C26, respectively). N = 6–8 per group. *, **, and *** = $p < 0.05$, $p < 0.01$, and $p < 0.01$, respectively.

3.3. Lower Myostatin Responsiveness in C2C12 Myotubes Was Associated with Altered Gene Expression of Myostatin Regulators

The distinct response of the C2C12 myoblasts and myotubes to myostatin suggested that the differentiation might have affected the regulation of the myostatin signaling pathway. Therefore, we analyzed the transcriptional level of the TGF-β family members and their blocker, follistatin [15], from myoblasts and myotubes. Compared to myoblasts, follistatin mRNA was increased by 20-fold (*Follistatin*, $p < 0.05$, Figure 5a) in myotubes with no changes in ACVR2B mRNA (*Acvr2b*, Figure 5b). Similar to follistatin, an increase in the mRNA of endogenous GDF11 (*Gdf11*, $p < 0.001$, Figure 5c), activin A (*InhibinβA*, $p < 0.001$, Figure 5d) and myostatin (*Gdf8*, $p < 0.001$, Figure 5e) were observed. The differentiation protocol again did not influence the results (Supplementary Material Figure S6 and Figure 5), with the exception of the unaltered myostatin level after 2% HS differentiation protocol (Supplementary Material Figure S6).

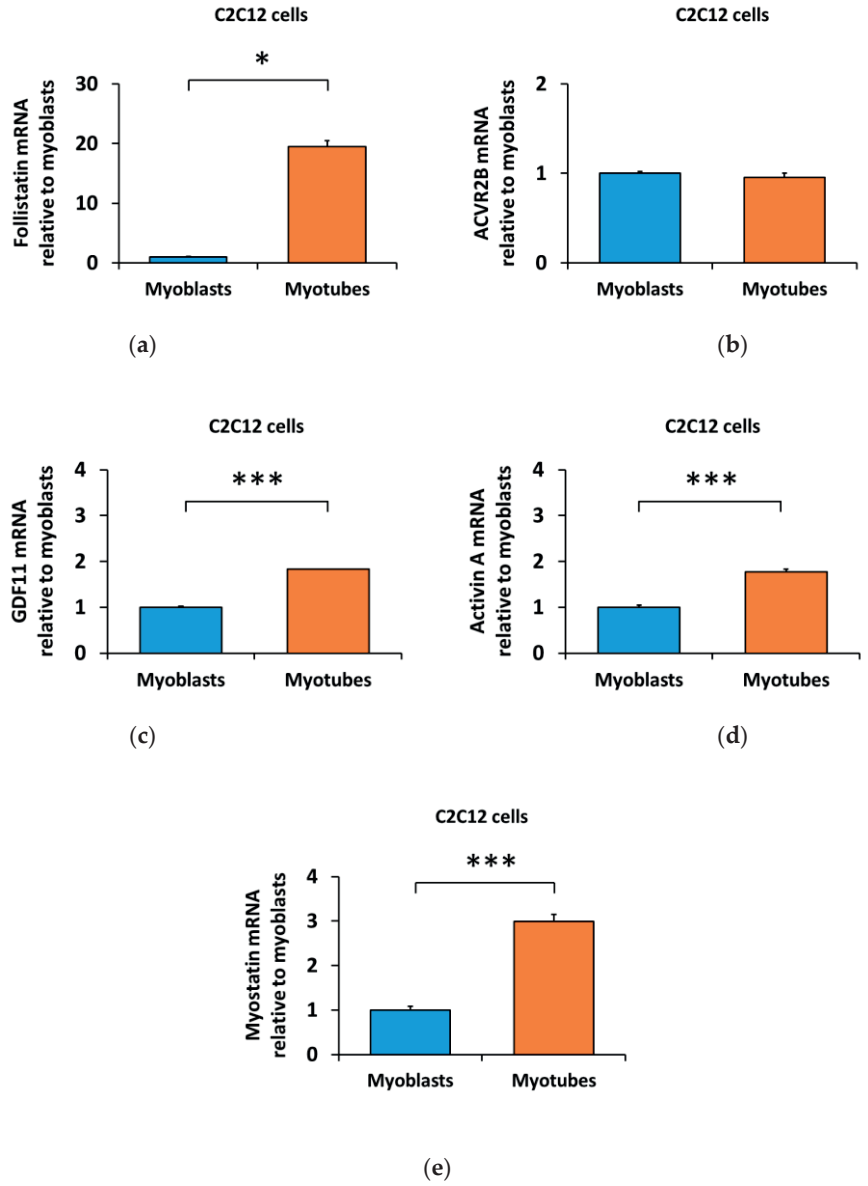

Figure 5. Differentiation of the C2C12 cells increased the mRNA level of (**a**) follistatin, while (**b**) ACVR2B remained unaltered. Of the ACVR2 ligands, (**c**) GDF11, (**d**) activin A, and (**e**) myostatin mRNAs were increased in myotubes in comparison to myoblasts. In the figures, the values are presented as normalized to myoblasts = 1. $N = 3$ per group. *, *** = $p < 0.05$ and $p < 0.001$, respectively.

Next, to validate the obtained follistatin mRNA result, we analyzed the protein content of follistatin from C2C12 cells. In agreement with the transcriptional level, follistatin protein content was increased by 2-fold in myotubes in comparison with myoblasts ($p < 0.001$, Figure 6a,b). Myostatin administration had no effect on the follistatin protein content (Figure 6a,b). Again, the effect was independent of the differentiation method (Supplementary Material Figure S7).

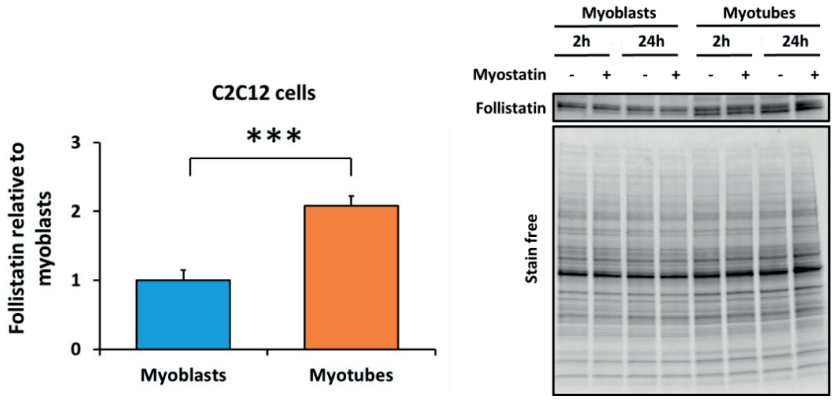

(**a**) (**b**)

Figure 6. Differentiation of the C2C12 myoblasts into myotubes increased (**a**) follistatin protein content. In the figure, the values are presented as normalized to myoblasts = 1. (**b**) Representative blot. $N = 12$ per group as control (-) and myostatin (+) samples were pooled due to lack of myostatin effect. *** = $p < 0.001$.

3.4. Human Skeletal Myotubes Are Responsive to Myostatin

We replicated the myostatin experiment using human CHQ myoblasts and myotubes to analyze whether the reduced responsiveness of the canonical and noncanonical signaling pathways to myostatin was cell-line-specific. Independent of the differentiation stage, myostatin administration to human CHQ cells increased canonical and noncanonical signaling (Figure 7a–d,f–h). In contrast to C2C12 cells with a strong and fast response in inflammatory signaling (Figure 2a,b,d), myostatin administration to CHQ cells resulted in only a minor increase in the phosphorylated $STAT3^{Tyr705}$ in myoblasts occurring after 24 h (Figure 8a,b,d). The differentiation process of CHQ myoblasts into myotubes (Figure 7e–h) was affected in a different manner than what was shown earlier in C2C12 cells (Figure 1e–g). More specifically, in C2C12 myotubes phosphorylated p38 was increased, while other phosphorylated MAPKs were decreased (Figure 1e–g), and both phosphorylated and total C/EBPβ were strongly diminished (Figure 2c,d). In contrast, in CHQ myotubes, phosphorylated p38 was decreased and most of the other phosphorylated or total MAPKs were increased (Figure 7e–h), while phosphorylated C/EBPβ was unaffected by the differentiation and total C/EBPβ was increased (Figure 8c,d). Phosphorylated STAT3 increased after differentiation (Figure 2c,d and Figure 8c,d), while Smad3 was nonresponsive to differentiation in both cell lines (Figures 1e–g and 7e–h).

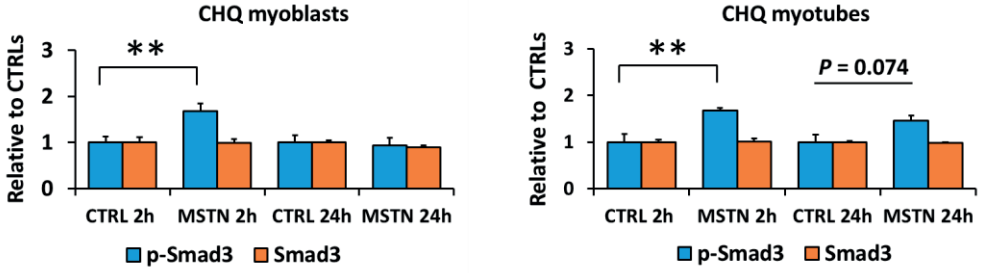

(**a**)

Figure 7. *Cont.*

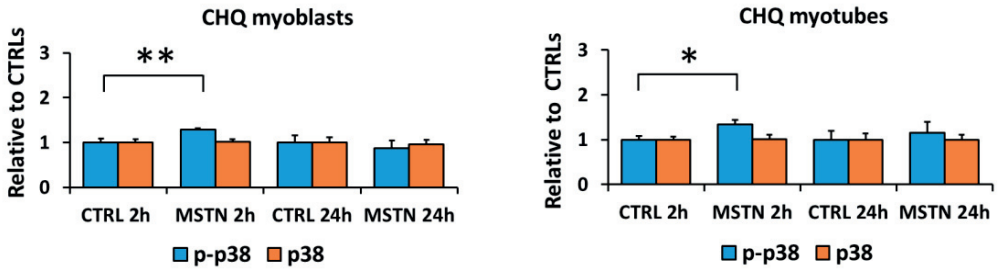

(**b**)

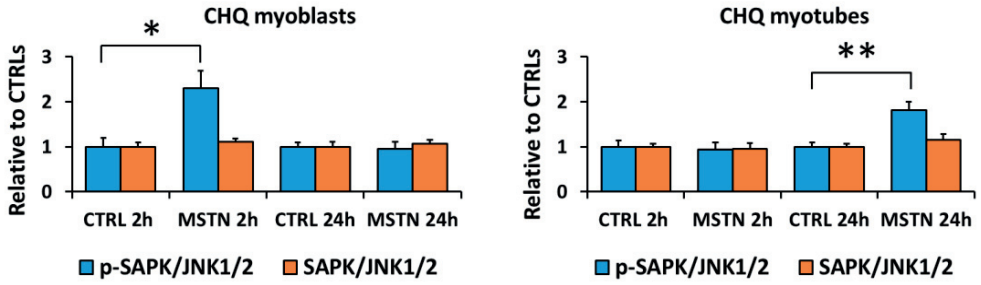

(**c**)

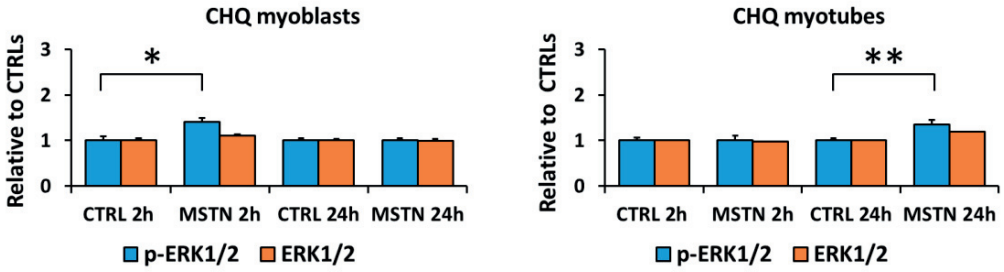

(**d**)

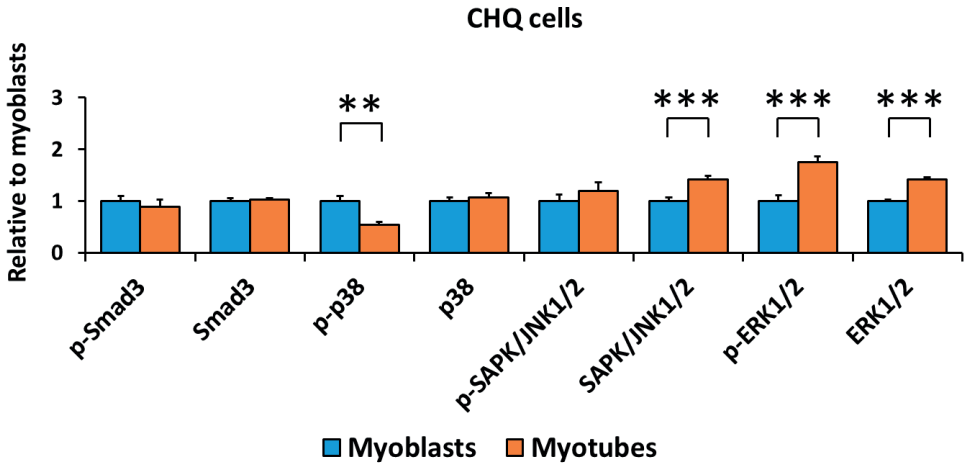

(**e**)

Figure 7. *Cont.*

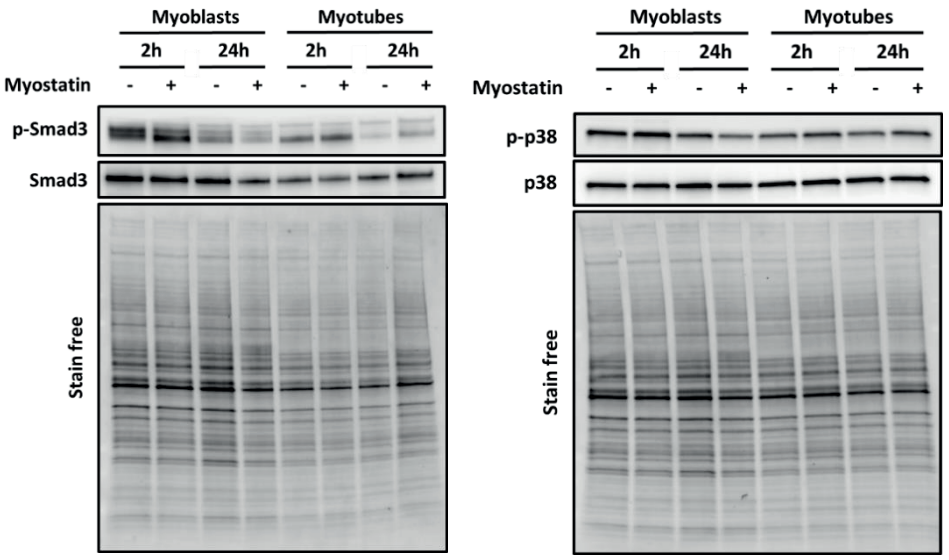

(**f**)

(**g**)

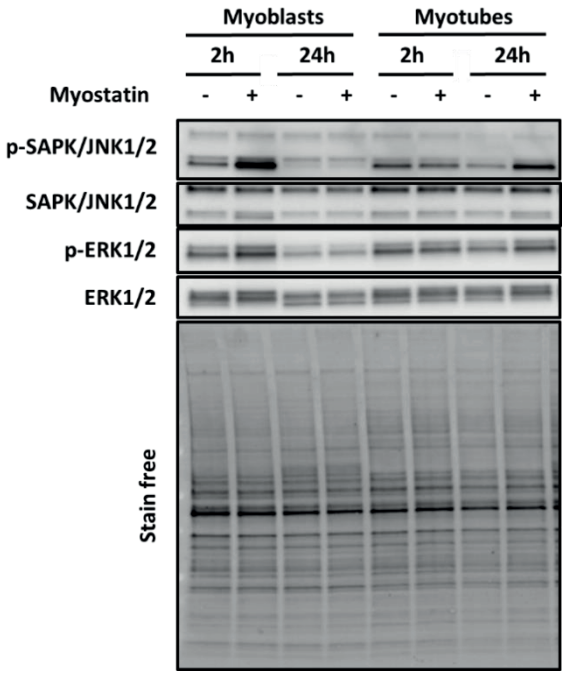

(**h**)

Figure 7. Myostatin-induced changes in the canonical (Smad3) and noncanonical (MAPKs) pathways were similar in CHQ myoblasts and myotubes**.** (**a**) Phosphorylated Smad3$^{Ser423/425}$ and total Smad3 in myoblasts and myotubes. (**b**) Phosphorylated p38$^{Thr180/Tyr182}$ and total p38 in myoblasts and myotubes. (**c**) Phosphorylated SAPK/JNK1/2$^{Thr183/Tyr185}$ and total SAPK/JNK1/2 in myoblasts and myotubes. (**d**) Phosphorylated ERK1/2$^{Thr202/Tyr204}$ and total ERK1/2 in myoblasts and myotubes. In the figures, the values are presented as normalized to CTRL = 1. (**e**) Nontreated CTRL myoblasts and myotubes of the 2-h and 24-h time-points were pooled and the values are presented as normalized to myoblasts = 1. (**f**–**h**) Representative blots. $N = 6$ per group. *, **, and *** = $p < 0.05$, $p < 0.01$, and $p > 0.001$, respectively. CTRL (-) = control group, MSTN (+) = myostatin group.

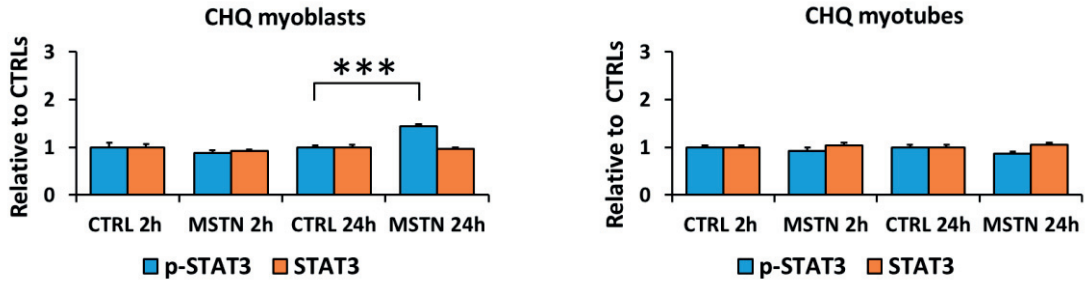

(**a**)

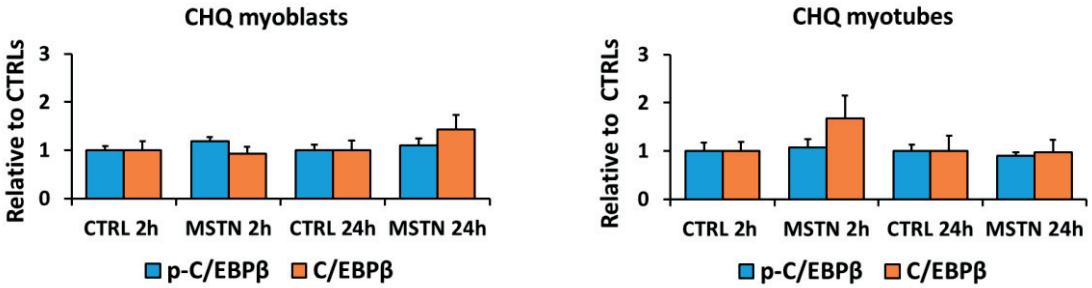

(**b**)

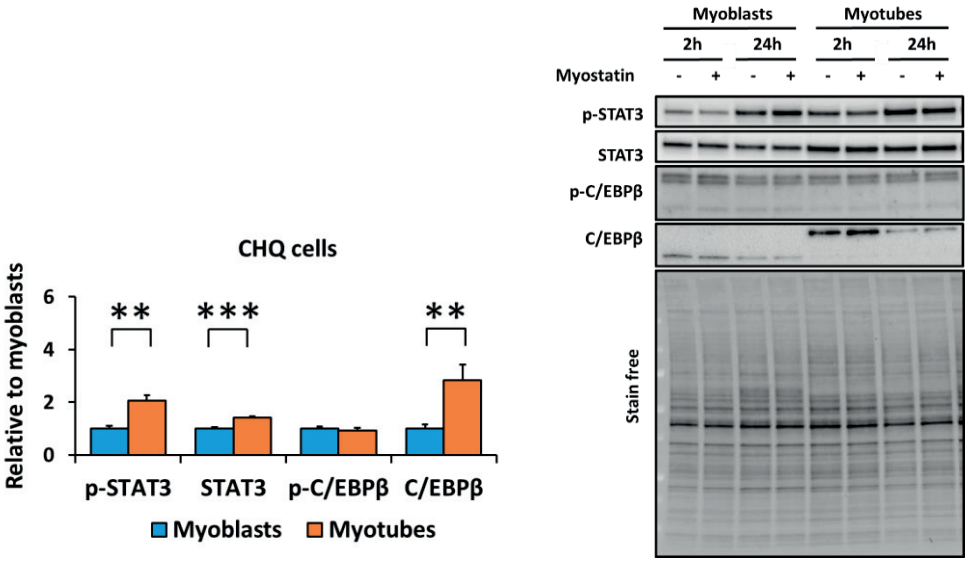

(**c**) (**d**)

Figure 8. Myostatin administration had a minor impact on inflammatory signaling in CHQ cells. (**a**) Phosphorylated STAT3^{Tyr705} and total STAT3 in myoblasts and myotubes. (**b**) Phosphorylated C/EBPβ^{Thr235} and total C/EBPβ in myoblasts and myotubes. In the figures, the values are presented as normalized to CTRL = 1. (**c**) Nontreated CTRL myoblasts and myotubes of the 2-h and 24-h time-points were pooled and the values are presented as normalized to myoblasts = 1. (**d**) Representative blots. In A–B, $N = 6$ per group. In C, $N = 12$ per group. ** and *** = $p < 0.01$ and $p < 0.001$, respectively. CTRL (-) = control group, MSTN (+) = myostatin group.

In contrast to C2C12 myotubes, the differentiation of CHQ myotubes had a smaller effect on the ACVR2 ligands and follistatin. The mRNA of follistatin (*FOLLISTATIN*), ACVR2B (*ACVR2B*), and GDF11 (*GDF11*) remained unaltered in CHQ myoblasts and myotubes, while activin A (*INHIBINβA*, $p < 0.01$) and myostatin (*GDF8*, $p = 0.073$) decreased (Figure 9a–e). Unlike in C2C12 cells, follistatin protein content remained unaltered among CHQ differentiation stages but was similarly unaffected by myostatin administration (Figure 9f,g). These results highlight the differences between C2C12 and CHQ skeletal muscle cells and their distinct ability to regulate endogenous ACVR2 ligands and their blocker, follistatin.

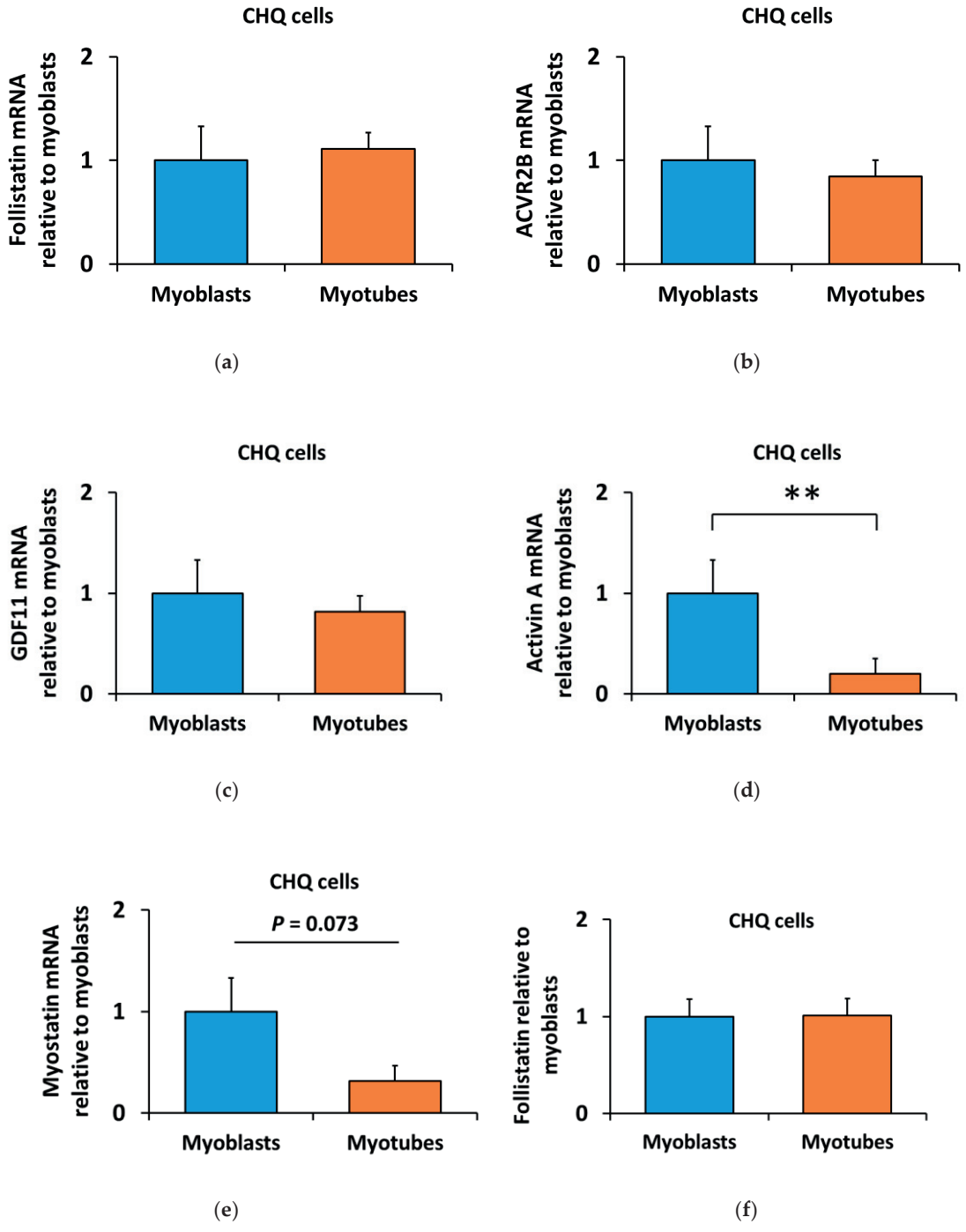

Figure 9. *Cont.*

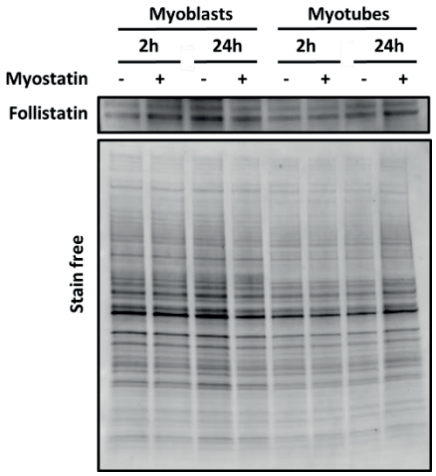

(**g**)

Figure 9. Differentiation of the CHQ cells did not alter the mRNA level of (**a**) follistatin, (**b**) ACVR2B and (**c**) GDF11. Of the ACVR2 ligands, the mRNA of (**d**) activin A and (**e**) myostatin were decreased in CHQ myotubes in comparison to myoblasts. (**f**) Differentiation of CHQ myoblasts into myotubes had no effect on follistatin protein content. (**g**) Representative blot. In the figures, the values are presented as normalized to myoblasts = 1. In A–E, N = 4–5 per group. In F, N = 12 per group as control (-) and myostatin (+) samples were pooled due to the lack of myostatin effect. ** = $p < 0.01$.

4. Discussion

In this study, we report that differentiation of C2C12 myoblasts into myotubes strongly reduced the effects of myostatin on canonical (Smad3) and noncanonical (MAPKs) signaling. Similarly, myostatin-induced phosphorylation of the inflammatory signaling proteins was greater in myoblasts than in myotubes. The inflammatory pathways, however, were similarly promoted in myoblasts and myotubes after coculture of the C2C12 cells with C26 cancer cells. This suggests that the general responsiveness to inflammation-regulating tumorkines is not reduced after differentiation. The reduced effects of myostatin in C2C12 myotubes was accompanied by enhanced expression of follistatin, an inhibitor of the TGF-β family members, and increased mRNA expression of ACVR2 ligands in C2C12 myotubes in comparison to myoblasts. Unlike in murine C2C12 cells, myostatin-induced changes in human CHQ skeletal muscle cells were mostly independent of the differentiation stage. Moreover, unlike in C2C12 cells, no changes in follistatin expression were observed while the mRNA expression of some ACVR2 ligands was even decreased in myotubes when compared to myoblasts. The reason for the lower responsiveness of the C2C12 myotubes to ACVR2 ligand myostatin may be related to the elevated follistatin content in comparison to myoblasts, because follistatin is a very strong blocker of myostatin [15]. In line with our findings, a microarray demonstrated a 50-fold increase in follistatin mRNA in C2C12 myotubes in comparison to myoblasts [60]. Rossi et al. reported that follistatin mRNA increased during differentiation in C2C12 cells, while ACVR2B mRNA expression remained unaltered [61]. Higher follistatin content in myotubes may be explained by the fact that follistatin has an important role in the myogenic differentiation and force generation for contractions in C2C12 myotubes [62]. These studies highlight the vital role of follistatin in the functionality and contractility of the C2C12 cells, which are more relevant in the myotubes than in the myoblasts.

Another possible explanation for the reduced responsiveness to myostatin in C2C12 myotubes may be the simultaneous increase in the mRNA expression of myostatin, GDF11, and activin A. Furthermore, others have previously shown that myostatin mRNA increased during C2C12 myoblast differentiation [61,63,64], and suggested that endogenous myostatin has a paracrine function as a regulator of myoblast proliferation and cell survival [63]. Similarly, activin A, another regulator of myogenesis, has also been related to the inhibition of proliferation and differentiation [23]. In the present

study, we further expand these results by showing that GDF11 mRNA increased in differentiated C2C12 myotubes. Unlike in murine cells, the differentiation of the human CHQ muscle cells did not elevate the gene expression or the protein content of follistatin or mRNA expression of ACVR2 ligands. Therefore, we speculate that this difference in ACVR2 ligands and their regulator, follistatin, between these cell models may explain different responses to myostatin. The metabolic differences of mouse C2C12, rat L6 and human skeletal muscle cell lines have been shown, and thus cell-line selection should be made based on the research question [16]. Similarly, our results suggest that C2C12 myotubes may not be the most suitable in vitro model to investigate the effects of myostatin on canonical and noncanonical signaling in skeletal muscle. However, the detailed mechanisms for the reduced myostatin response in C2C12 myotubes require further examination.

Canonical Smad signaling is a key pathway of TGF-β signaling [65]. In vivo studies have shown that myostatin induces muscle atrophy via Smad3 [66–68]. In line with our in vitro findings, Yuzawa et al. reported a greater increase in the phosphorylation of Smads after shorter (30 min) than longer (6–12 h) treatment with 300 ng/mL of myostatin in C2C12 cells [69]. Our results show that canonical signaling was increased in the C2C12 myoblasts, while this response was blunted in the myotubes. The noncanonical signaling pathway (MAPKs) has also been shown to play a role in muscle atrophy induced by the ACVR2 ligands [24,70]. We observed that myostatin administration increased the phosphorylation of all studied MAPKs in C2C12 myoblasts, while only p38 phosphorylation increased in myotubes. Therefore, similar to the canonical pathway, C2C12 myotubes lost most of their noncanonical responsiveness to myostatin during differentiation. It is possible in the C2C12 cell line that the presence of some myoblasts in the myotube culture could at least partly explain the minor remaining responsiveness to myostatin in the latter (Supplementary Material Figure S1). Our in vitro results are comparable to in vivo situation because the noncanonical signaling pathway is also responsive to myostatin in muscles in vivo. For instance, an increase in the phosphorylation of ERK1/2 in myostatin-administered mice has been reported [29], while blocking of the endogenous myostatin and activins decreased MAPK-signaling in murine muscle [50]. In contrast to our murine in vitro results, but in agreement with previous studies conducted using commercial human muscle cell lines [28,67], we observed that administration of myostatin enhanced both canonical and noncanonical signaling pathways in human CHQ myoblasts and myotubes. Interestingly, another difference between these cell lines was that differentiation of the C2C12 and CHQ myoblasts into myotubes resulted in opposite effects on MAPK-signaling, while Smad3-signaling remained unaffected after differentiation in both cell lines. However, myostatin had only a minor effect on inflammatory pathways in CHQ cells in contrast to C2C12 cells when both cell lines responded to differentiation by increased STAT-signaling and phosphorylated C/EBPβ decreased strongly only in C2C12 cells. Moreover, the effect of myostatin on inflammatory signaling was small in CHQ cells in contrast to C2C12 cells. The results suggest that the effects of myostatin may be more prominent in cell lines other than murine C2C12, and this should be taken into consideration when choosing an in vitro model for muscle research. However, in the future, time-series of the effects of myostatin on canonical and noncanonical signaling in the skeletal muscle cells should be conducted.

In recent years, a better understanding of the tissue crosstalk in diseases causing muscle atrophy, such as cancer-associated cachexia, has become important [71]. Cancers can be accompanied by tumorkine-induced inflammation [72]. Similarly, we observed in vitro that both the myostatin administration and the cancer cell coculture stimulated inflammatory pathways in C2C12 myoblasts and myotubes by increasing the phosphorylation of STAT3 and C/EBPβ, markers of increased inflammatory response [35]. However, although STAT3 has been reported to promote catabolic processes in the muscle during inflammation-induced cachexia [34], in C2C12 cells, STAT3 has been shown to regulate both proliferation and differentiation [73,74] and indeed p-STAT3 and STAT3 were elevated in myotubes when compared to myoblasts in the present study. This highlights the complexity of the interpretation of STAT3 signaling in different physiological conditions. Similarly to our study, Ding et al. reported that myostatin administration increased the phosphorylation of C/EBPβ in C2C12 myotubes [55], and they further

linked p38β-regulated C/EBPβ to catabolic processes [75]. However, the present study suggests that the C26 cell-derived tumorkines promote inflammation rather than antianabolic or catabolic signaling because no changes were observed in protein synthesis, ubiquitinated proteins, or in mTOR signaling. Similarly to STAT3, C/EBPβ may have a role in the regulation of C2C12 myoblast differentiation. Mancini et al. demonstrated that C2C12 myoblasts contained detectable levels of C/EBPβ in the early phase of differentiation into adipocytes, while C/EBPβ was not observed during differentiation into myotubes [76]. This suggests that C/EBPβ may regulate the selection of the differentiation pathway in C2C12 cells, which could explain why C/EBPβ was barely detected in myotubes in the present study. To summarize, our results indicate that the C26 cell-derived tumorkines, although they have been shown to decrease myotube size after 24-h coculture [41], seemed to have only minor effects on antianabolic and catabolic signaling at this time-point. Furthermore, time-series experiments on the tumorkine secretion kinetics during coculture in various muscle cell lines should be conducted in the future.

5. Conclusions

In this study, we investigated whether an in vitro muscle cell approach could be utilized as a tool to study the direct effects of myostatin and tumorkines on myoblasts and myotubes. The results demonstrate that the canonical and noncanonical responses to myostatin were dependent on the differentiation stage of the C2C12 cells as well as on the signaling pathway studied. The reduced myostatin responsiveness of the C2C12 myotubes could possibly be due to the endogenous regulation of the TGF-β family members and their regulators during differentiation. Importantly, the results demonstrate that the decreased effects of myostatin on canonical and noncanonical signaling were not a universal phenomenon in cell models, because the human muscle cells restrained the responsiveness to myostatin. Therefore, according to our results, C2C12 myotubes are not a recommended cell line to study the effects of myostatin and possibly other ACVR2 ligands.

Supplementary Materials: The following are available online at http://www.mdpi.com/2218-273X/10/5/695/s1, Figure S1: Representative images of the differentiated C2C12 myotubes. Table S1: Antibodies used in western blot (WB) and immunocytochemistry (ICC). Table S2: Primers used in real-time qPCR analyses. Figure S2: Amplicon lengths of the CHQ cell RT-qPCR products. Figure S3: PicoGreen normalization of the RT-qPCR results. Figure S4: Repeated 2-h C2C12 myotube experiment with alternative differentiation protocol (2% horse serum, HS). Figure S5: The coculture of C2C12 myoblasts and myotubes with C26 cancer cells. Figure S6: Protein content of follistatin in C2C12 myotubes differentiated with 2% HS.

Author Contributions: Conceptualization, J.H.L., S.P. and J.J.H.; Formal analysis, J.H.L.; Funding acquisition, S.P. and J.J.H.; Investigation, J.H.L.; Methodology, A.P., M.L. and O.R.; Project administration, J.H.L. and J.J.H.; Supervision, S.P. and J.J.H.; Validation, A.P., M.L. and O.R.; Visualization, J.H.L.; Writing—original draft, J.H.L.; Writing—review & editing, J.H.L., S.P., A.P. and J.J.H. All authors have read and agreed to the published version of the manuscript.

Funding: This work was funded by the Academy of Finland (Grant No. 308042 to S.P. and 275922 to J.J.H.).

Acknowledgments: We thank Vincent Mouyly and Eija Laakkonen for kindly providing the human CHQ skeletal muscle cells and Fabio Penna for providing the C26 cells. Bettina Hutz is thanked for staining and imaging the cells for ICC, and Anita Kopperi for guiding with the Transwell® coculture procedures. Tuuli Nissinen is thanked for suggestions regarding experimental design.

Conflicts of Interest: The authors declare no conflict of interest.

Abbreviations

ACVR2	Activin receptor type 2
ACVR2B	Activin receptor type 2B
ALK4 or 5	Activin receptor-like kinase 4 or 5
BCA	Bicinchoninic Acid
C26-CM	Colon 26 carcinoma cell conditioned medium
C/EBPβ	CCAAT-enhancer-binding protein β
DM	Differentiation medium
DMEM	Dulbecco´s modified Eagle´s medium

ERK1/2	Extracellular signal-regulated kinase 1/2
FBS	Fetal bovine serum
GDF	Growth differentiation factor
GM	Growth medium
HS	Horse serum
IL-6	Interleukin-6
MAPK(s)	Mitogen-activated protein kinase(s)
MCP-1	Monocyte chemoattractant protein-1 or CCL2
PBS	Phosphate buffered saline
P/S	Penicillin-streptomycin
RANTES	Regulated on activation, normal T cell expressed and secreted or CCL5
SAPK/JNK1/2	Stress-activated protein kinase/c-Jun N-terminal kinase 1/2
STAT3	Signal transducer and activator of transcription 3
Smad3	Small mothers against decapentaplegic 3
TGF-β	Transforming growth factor-β

References

1. Lee, S.; Reed, L.A.; Davies, M.V.; Girgenrath, S.; Goad, M.E.; Tomkinson, K.N.; Wright, J.F.; Barker, C.; Ehrmantraut, G.; Holmstrom, J. Regulation of muscle growth by multiple ligands signaling through activin type II receptors. *Proc. Natl. Acad. Sci. USA* **2005**, *102*, 18117–18122. [CrossRef] [PubMed]
2. Otto, A.; Patel, K. Signalling and the control of skeletal muscle size. *Exp. Cell Res.* **2010**, *316*, 3059–3066. [CrossRef] [PubMed]
3. Sharma, M.; Kambadur, R.; Matthews, K.G.; Somers, W.G.; Devlin, G.P.; Conaglen, J.V.; Fowke, P.J.; Bass, J.J. Myostatin, a transforming growth factor-β superfamily member, is expressed in heart muscle and is upregulated in cardiomyocytes after infarct. *J. Cell. Physiol.* **1999**, *180*, 1–9. [CrossRef]
4. McPherron, A.C.; Lawler, A.M.; Lee, S. Regulation of skeletal muscle mass in mice by a new TGF-p superfamily member. *Nature* **1997**, *387*, 83. [CrossRef]
5. Rodriguez, J.; Vernus, B.; Chelh, I.; Cassar-Malek, I.; Gabillard, J.; Sassi, A.H.; Seiliez, I.; Picard, B.; Bonnieu, A. Myostatin and the skeletal muscle atrophy and hypertrophy signaling pathways. *Cell. Mol. Life Sci.* **2014**, *71*, 4361–4371. [CrossRef]
6. Dschietzig, T.B. Myostatin—From the mighty mouse to cardiovascular disease and cachexia. *Clin. Chim. Acta* **2014**, *433*, 216–224. [CrossRef]
7. Egerman, M.A.; Glass, D.J. Signaling pathways controlling skeletal muscle mass. *Crit. Rev. Biochem. Mol. Biol.* **2014**, *49*, 59–68. [CrossRef]
8. Zhou, X.; Wang, J.L.; Lu, J.; Song, Y.; Kwak, K.S.; Jiao, Q.; Rosenfeld, R.; Chen, Q.; Boone, T.; Simonet, W.S. Reversal of cancer cachexia and muscle wasting by ActRIIB antagonism leads to prolonged survival. *Cell* **2010**, *142*, 531–543. [CrossRef]
9. Elkina, Y.; von Haehling, S.; Anker, S.D.; Springer, J. The role of myostatin in muscle wasting: An overview. *J. Cachexia Sarcopenia Muscle* **2011**, *2*, 143. [CrossRef]
10. Kingsley, D.M. The TGF-beta superfamily: New members, new receptors, and new genetic tests of function in different organisms. *Genes Dev.* **1994**, *8*, 133–146. [CrossRef]
11. Goebel, E.J.; Hart, K.N.; McCoy, J.C.; Thompson, T.B. Structural biology of the TGFβ family. *Exp. Biol. Med.* **2019**, *244*, 1530–1546. [CrossRef] [PubMed]
12. Nissinen, T.A.; Hentilä, J.; Penna, F.; Lampinen, A.; Lautaoja, J.H.; Fachada, V.; Holopainen, T.; Ritvos, O.; Kivelä, R.; Hulmi, J.J. Treating cachexia using soluble ACVR2B improves survival, alters mTOR localization, and attenuates liver and spleen responses. *J. Cachexia Sarcopenia Muscle* **2018**, *9*, 514–529. [CrossRef] [PubMed]
13. Lach-Trifilieff, E.; Minetti, G.C.; Sheppard, K.; Ibebunjo, C.; Feige, J.N.; Hartmann, S.; Brachat, S.; Rivet, H.; Koelbing, C.; Morvan, F. An antibody blocking activin type II receptors induces strong skeletal muscle hypertrophy and protects from atrophy. *Mol. Cell. Biol.* **2014**, *34*, 606–618. [CrossRef] [PubMed]
14. Iskenderian, A.; Liu, N.; Deng, Q.; Huang, Y.; Shen, C.; Palmieri, K.; Crooker, R.; Lundberg, D.; Kastrapeli, N.; Pescatore, B. Myostatin and activin blockade by engineered follistatin results in hypertrophy and improves dystrophic pathology in mdx mouse more than myostatin blockade alone. *Skelet. Muscle* **2018**, *8*, 34. [CrossRef]

15. Lee, S.; McPherron, A.C. Regulation of myostatin activity and muscle growth. *Proc. Natl. Acad. Sci. USA* **2001**, *98*, 9306–9311. [CrossRef]
16. Abdelmoez, A.M.; Sardón Puig, L.; Smith, J.A.; Gabriel, B.M.; Savikj, M.; Dollet, L.; Chibalin, A.V.; Krook, A.; Zierath, J.R.; Pillon, N.J. Comparative profiling of skeletal muscle models reveals heterogeneity of transcriptome and metabolism. *Am. J. Physiol. Cell Physiol.* **2019**, *318*, C615–C626. [CrossRef]
17. Langley, B.; Thomas, M.; Bishop, A.; Sharma, M.; Gilmour, S.; Kambadur, R. Myostatin inhibits myoblast differentiation by down-regulating MyoD expression. *J. Biol. Chem.* **2002**, *277*, 49831–49840. [CrossRef]
18. Rodgers, B.D.; Wiedeback, B.D.; Hoversten, K.E.; Jackson, M.F.; Walker, R.G.; Thompson, T.B. Myostatin stimulates, not inihibits, C2C12 myoblast proliferation. *Endocrinology* **2014**, *155*, 670–675. [CrossRef]
19. Pèrié, L.; Parenté, A.; Brun, C.; Magnol, L.; Pélissier, P.; Blanquet, V. Enhancement of C2C12 myoblast proliferation and differentiation by GASP-2, a myostatin inhibitor. *Biochem. Biophys. Rep.* **2016**, *6*, 39–46. [CrossRef]
20. Uemura, K.; Hayashi, M.; Itsubo, T.; Oishi, A.; Iwakawa, H.; Komatsu, M.; Uchiyama, S.; Kato, H. Myostatin promotes tenogenic differentiation of C2C12 myoblast cells through Smad. *FEBS Open Bio* **2017**, *7*, 522–532. [CrossRef]
21. Graham, Z.A.; De Gasperi, R.; Bauman, W.A.; Cardozo, C.P. Recombinant myostatin reduces highly expressed microRNAs in differentiating C2C12 cells. *Biochem. Biophys. Rep.* **2017**, *9*, 273–280. [CrossRef] [PubMed]
22. Burks, T.N.; Cohn, R.D. Role of TGF-β signaling in inherited and acquired myopathies. *Skelet. Muscle* **2011**, *1*, 19. [CrossRef] [PubMed]
23. Bloise, E.; Ciarmela, P.; Dela Cruz, C.; Luisi, S.; Petraglia, F.; Reis, F.M. Activin a in mammalian physiology. *Physiol Rev.* **2018**, *99*, 739–780. [CrossRef] [PubMed]
24. Derynck, R.; Zhang, Y.E. Smad-dependent and Smad-independent pathways in TGF-β family signalling. *Nature* **2003**, *425*, 577. [CrossRef]
25. Rebbapragada, A.; Benchabane, H.; Wrana, J.L.; Celeste, A.J.; Attisano, L. Myostatin signals through a transforming growth factor β-like signaling pathway to block adipogenesis. *Mol. Cell. Biol.* **2003**, *23*, 7230–7242. [CrossRef]
26. Han, H.Q.; Zhou, X.; Mitch, W.E.; Goldberg, A.L. Myostatin/activin pathway antagonism: Molecular basis and therapeutic potential. *Int. J. Biochem. Cell Biol.* **2013**, *45*, 2333–2347. [CrossRef]
27. Tisdale, M.J. Reversing cachexia. *Cell* **2010**, *142*, 511–512. [CrossRef]
28. Philip, B.; Lu, Z.; Gao, Y. Regulation of GDF-8 signaling by the p38 MAPK. *Cell. Signal.* **2005**, *17*, 365–375. [CrossRef]
29. Yang, W.; Chen, Y.; Zhang, Y.; Wang, X.; Yang, N.; Zhu, D. Extracellular Signal–Regulated Kinase 1/2 Mitogen-Activated Protein Kinase Pathway Is Involved in Myostatin-Regulated Differentiation Repression. *Cancer Res.* **2006**, *66*, 1320–1326. [CrossRef]
30. Huang, Z.; Chen, D.; Zhang, K.; Yu, B.; Chen, X.; Meng, J. Regulation of myostatin signaling by c-Jun N-terminal kinase in C2C12 cells. *Cell. Signal.* **2007**, *19*, 2286–2295. [CrossRef]
31. Penna, F.; Costamagna, D.; Fanzani, A.; Bonelli, G.; Baccino, F.M.; Costelli, P. Muscle wasting and impaired myogenesis in tumor bearing mice are prevented by ERK inhibition. *PLoS ONE* **2010**, *5*, e13604. [CrossRef]
32. Zhang, L.; Rajan, V.; Lin, E.; Hu, Z.; Han, H.Q.; Zhou, X.; Song, Y.; Min, H.; Wang, X.; Du, J. Pharmacological inhibition of myostatin suppresses systemic inflammation and muscle atrophy in mice with chronic kidney disease. *FASEB J.* **2011**, *25*, 1653–1663. [CrossRef] [PubMed]
33. Cole, C.L.; Kleckner, I.R.; Jatoi, A.; Schwarz, E.M.; Dunne, R.F. The Role of Systemic Inflammation in Cancer-Associated Muscle Wasting and Rationale for Exercise as a Therapeutic Intervention. *JCSM Clin. Rep.* **2018**, *3*, 1–19. [CrossRef]
34. Zimmers, T.A.; Fishel, M.L.; Bonetto, A. STAT3 in the systemic inflammation of cancer cachexia. *Semin. Cell Dev. Biol.* **2016**, *54*, 28–41. [CrossRef]
35. Poli, V. The role of C/EBP isoforms in the control of inflammatory and native immunity functions. *J. Biol. Chem.* **1998**, *273*, 29279–29282. [CrossRef] [PubMed]
36. Chen, W.; Gao, Q.; Han, S.; Pan, F.; Fan, W. The CCL2/CCR2 axis enhances IL-6-induced epithelial-mesenchymal transition by cooperatively activating STAT3-Twist signaling. *Tumor Biol.* **2015**, *36*, 973–981. [CrossRef] [PubMed]

37. Kovacic, J.C.; Gupta, R.; Lee, A.C.; Ma, M.; Fang, F.; Tolbert, C.N.; Walts, A.D.; Beltran, L.E.; San, H.; Chen, G. Stat3-dependent acute Rantes production in vascular smooth muscle cells modulates inflammation following arterial injury in mice. *J. Clin. Investig.* **2010**, *120*, 303–314. [CrossRef]
38. Loumaye, A.; de Barsy, M.; Nachit, M.; Lause, P.; van Maanen, A.; Trefois, P.; Gruson, D.; Thissen, J. Circulating Activin A predicts survival in cancer patients. *J. Cachexia Sarcopenia Muscle* **2017**, *8*, 768–777. [CrossRef]
39. Zhang, G.; Liu, Z.; Ding, H.; Zhou, Y.; Doan, H.A.; Sin, K.W.T.; Zhu, Z.J.; Flores, R.; Wen, Y.; Gong, X. Tumor induces muscle wasting in mice through releasing extracellular Hsp70 and Hsp. *Nat. Commun.* **2017**, *8*, 589. [CrossRef]
40. Zhang, G.; Jin, B.; Li, Y. C/EBPβ mediates tumour-induced ubiquitin ligase atrogin1/MAFbx upregulation and muscle wasting. *EMBO J.* **2011**, *30*, 4323–4335. [CrossRef]
41. Jackman, R.W.; Floro, J.; Yoshimine, R.; Zitin, B.; Eiampikul, M.; El-Jack, K.; Seto, D.N.; Kandarian, S.C. Continuous Release of Tumor-Derived Factors Improves the Modeling of Cachexia in Muscle Cell Culture. *Front. Physiol.* **2017**, *8*, 738. [CrossRef]
42. Seto, D.N.; Kandarian, S.C.; Jackman, R.W. A key role for leukemia inhibitory factor in C26 cancer cachexia. *J. Biol. Chem.* **2015**, *290*, 19976–19986. [CrossRef] [PubMed]
43. Renaud, J.; Martinoli, M. Development of an insert co-culture system of two cellular types in the absence of cell-cell contact. *JoVE J. Vis. Exp.* **2016**, e54356. [CrossRef] [PubMed]
44. Gadient, R.A.; Patterson, P.H. Leukemia inhibitory factor, Interleukin 6, and other cytokines using the GP130 transducing receptor: Roles in inflammation and injury. *Stem Cells* **1999**, *17*, 127–137. [CrossRef] [PubMed]
45. Edom, F.; Mouly, V.; Barbet, J.P.; Fiszman, M.Y.; Butler-Browne, G.S. Clones of human satellite cells can express in vitro both fast and slow myosin heavy chains. *Dev. Biol.* **1994**, *164*, 219–229. [CrossRef] [PubMed]
46. Zhu, C.; Mouly, V.; Cooper, R.N.; Mamchaoui, K.; Bigot, A.; Shay, J.W.; Di Santo, J.P.; Butler-Browne, G.S.; Wright, W.E. Cellular senescence in human myoblasts is overcome by human telomerase reverse transcriptase and cyclin-dependent kinase 4: Consequences in aging muscle and therapeutic strategies for muscular dystrophies. *Aging Cell* **2007**, *6*, 515–523. [CrossRef]
47. Thorley, M.; Duguez, S.; Mazza, E.M.C.; Valsoni, S.; Bigot, A.; Mamchaoui, K.; Harmon, B.; Voit, T.; Mouly, V.; Duddy, W. Skeletal muscle characteristics are preserved in hTERT/cdk4 human myogenic cell lines. *Skelet. Muscle* **2016**, *6*, 43. [CrossRef]
48. Charles, J.P.; Cappellari, O.; Spence, A.J.; Hutchinson, J.R.; Wells, D.J. Musculoskeletal geometry, muscle architecture and functional specialisations of the mouse hindlimb. *PLoS ONE* **2016**, *11*, e0147669. [CrossRef]
49. Pekkala, S.; Wiklund, P.; Hulmi, J.J.; Pöllänen, E.; Marjomäki, V.; Munukka, E.; Pierre, P.; Mouly, V.; Mero, A.; Alén, M. Cannabinoid receptor 1 and acute resistance exercise–In vivo and in vitro studies in human skeletal muscle. *Peptides* **2015**, *67*, 55–63. [CrossRef]
50. Hulmi, J.J.; Oliveira, B.M.; Silvennoinen, M.; Hoogaars, W.M.; Ma, H.; Pierre, P.; Pasternack, A.; Kainulainen, H.; Ritvos, O. Muscle protein synthesis, mTORC1/MAPK/Hippo signaling, and capillary density are altered by blocking of myostatin and activins. *Am. J. Physiol. Endocrinol. Metab.* **2013**, *304*, E41–E50. [CrossRef]
51. Gray, A.M.; Mason, A.J. Requirement for activin A and transforming growth factor–beta 1 pro-regions in homodimer assembly. *Science* **1990**, *247*, 1328–1330. [CrossRef]
52. Cotton, T.R.; Fischer, G.; Wang, X.; McCoy, J.C.; Czepnik, M.; Thompson, T.B.; Hyvönen, M. Structure of the human myostatin precursor and determinants of growth factor latency. *EMBO J.* **2018**, *37*, 367–383. [CrossRef] [PubMed]
53. Kaivo-Oja, N.; Mottershead, D.G.; Mazerbourg, S.; Myllymaa, S.; Duprat, S.; Gilchrist, R.B.; Groome, N.P.; Hsueh, A.J.; Ritvos, O. Adenoviral gene transfer allows Smad-responsive gene promoter analyses and delineation of type I receptor usage of transforming growth factor-β family ligands in cultured human granulosa luteal cells. *J. Clin. Endocrinol. Metab.* **2005**, *90*, 271–278. [CrossRef] [PubMed]
54. Wolfman, N.M.; McPherron, A.C.; Pappano, W.N.; Davies, M.V.; Song, K.; Tomkinson, K.N.; Wright, J.F.; Zhao, L.; Sebald, S.M.; Greenspan, D.S. Activation of latent myostatin by the BMP-1/tolloid family of metalloproteinases. *Proc. Natl. Acad. Sci. USA* **2003**, *100*, 15842–15846. [CrossRef]
55. Ding, H.; Zhang, G.; Sin, K.W.T.; Liu, Z.; Lin, R.; Li, M.; Li, Y. Activin A induces skeletal muscle catabolism via p38β mitogen-activated protein kinase. *J. Cachexia Sarcopenia Muscle* **2017**, *8*, 202–212. [CrossRef]

56. Wu, Q.; Sun, S.; Li, Z.; Yang, Q.; Li, B.; Zhu, S.; Wang, L.; Wu, J.; Yuan, J.; Wang, C. Breast cancer-released exosomes trigger cancer-associated cachexia to promote tumor progression. *Adipocyte* **2019**, *8*, 31–45. [PubMed]
57. Lautaoja, J.H.; Lalowski, M.; Nissinen, T.A.; Hentilä, J.J.; Shi, Y.; Ritvos, O.; Cheng, S.; Hulmi, J.J. Muscle and serum metabolomes are dysregulated in colon-26 tumor-bearing mice despite amelioration of cachexia with activin receptor type 2B ligand blockade. *Am. J. Physiol. Endocrinol. Metab.* **2019**, *316*, E852–E865. [CrossRef]
58. Kandarian, S.C.; Nosacka, R.L.; Delitto, A.E.; Judge, A.R.; Judge, S.M.; Ganey, J.D.; Moreira, J.D.; Jackman, R.W. Tumour-derived leukaemia inhibitory factor is a major driver of cancer cachexia and morbidity in C26 tumour-bearing mice. *J. Cachexia Sarcopenia Muscle* **2018**, *9*, 1109–1120. [CrossRef]
59. Sarbassov, D.D.; Guertin, D.A.; Ali, S.M.; Sabatini, D.M. Phosphorylation and regulation of Akt/PKB by the rictor-mTOR complex. *Science* **2005**, *307*, 1098–1101. [CrossRef]
60. Moran, J.L.; Li, Y.; Hill, A.A.; Mounts, W.M.; Miller, C.P. Gene expression changes during mouse skeletal myoblast differentiation revealed by transcriptional profiling. *Physiol. Genom.* **2002**, *10*, 103–111. [CrossRef] [PubMed]
61. Rossi, S.; Stoppani, E.; Gobbo, M.; Caroli, A.; Fanzani, A. L6E9 Myoblasts Are Deficient of Myostatin and Additional TGF-β Members Are Candidates to Developmentally Control Their Fiber Formation. *BioMed Res. Int.* **2010**, *2010*, 326909.
62. Ikeda, K.; Ito, A.; Imada, R.; Sato, M.; Kawabe, Y.; Kamihira, M. In vitro drug testing based on contractile activity of C2C12 cells in an epigenetic drug model. *Sci. Rep.* **2017**, *7*, 44570. [CrossRef]
63. Ríos, R.; Carneiro, I.; Arce, V.M.; Devesa, J. Myostatin regulates cell survival during C2C12 myogenesis. *Biochem. Biophys. Res. Commun.* **2001**, *280*, 561–566. [CrossRef]
64. Artaza, J.N.; Bhasin, S.; Mallidis, C.; Taylor, W.; Ma, K.; Gonzalez-Cadavid, N.F. Endogenous expression and localization of myostatin and its relation to myosin heavy chain distribution in C2C12 skeletal muscle cells. *J. Cell. Physiol.* **2002**, *190*, 170–179. [CrossRef] [PubMed]
65. Heldin, C.; Miyazono, K.; Ten Dijke, P. TGF-β signalling from cell membrane to nucleus through SMAD proteins. *Nature* **1997**, *390*, 465. [CrossRef] [PubMed]
66. Goodman, C.A.; McNally, R.M.; Hoffmann, F.M.; Hornberger, T.A. Smad3 induces atrogin-1, inhibits mTOR and protein synthesis, and promotes muscle atrophy in vivo. *Mol. Endocrinol.* **2013**, *27*, 1946–1957. [CrossRef] [PubMed]
67. Trendelenburg, A.U.; Meyer, A.; Rohner, D.; Boyle, J.; Hatakeyama, S.; Glass, D.J. Myostatin reduces Akt/TORC1/p70S6K signaling, inhibiting myoblast differentiation and myotube size. *Am. J. Physiol. Cell Physiol.* **2009**, *296*, C1258–C1270. [CrossRef]
68. Sartori, R.; Milan, G.; Patron, M.; Mammucari, C.; Blaauw, B.; Abraham, R.; Sandri, M. Smad2 and 3 transcription factors control muscle mass in adulthood. *Am. J. Physiol. Cell Physiol.* **2009**, *296*, C1248–C1257. [CrossRef]
69. Yuzawa, H.; Koinuma, D.; Maeda, S.; Yamamoto, K.; Miyazawa, K.; Imamura, T. Arkadia represses the expression of myoblast differentiation markers through degradation of Ski and the Ski-bound Smad complex in C2C12 myoblasts. *Bone* **2009**, *44*, 53–60. [CrossRef]
70. Ábrigo, J.; Campos, F.; Simon, F.; Riedel, C.; Cabrera, D.; Vilos, C.; Cabello-Verrugio, C. TGF-β requires the activation of canonical and non-canonical signalling pathways to induce skeletal muscle atrophy. *Biol. Chem.* **2018**, *399*, 253–264. [CrossRef]
71. Fearon, K.; Strasser, F.; Anker, S.D.; Bosaeus, I.; Bruera, E.; Fainsinger, R.L.; Jatoi, A.; Loprinzi, C.; MacDonald, N.; Mantovani, G. Definition and classification of cancer cachexia: An international consensus. *Lancet Oncol.* **2011**, *12*, 489–495. [CrossRef]
72. Tsoli, M.; Robertson, G. Cancer cachexia: Malignant inflammation, tumorkines, and metabolic mayhem. *Trends Endocrinol. Metab.* **2013**, *24*, 174–183. [CrossRef] [PubMed]
73. Sun, L.; Ma, K.; Wang, H.; Xiao, F.; Gao, Y.; Zhang, W.; Wang, K.; Gao, X.; Ip, N.; Wu, Z. JAK1–STAT1–STAT3, a key pathway promoting proliferation and preventing premature differentiation of myoblasts. *J. Cell Biol.* **2007**, *179*, 129–138. [CrossRef] [PubMed]
74. Wang, K.; Wang, C.; Xiao, F.; Wang, H.; Wu, Z. JAK2/STAT2/STAT3 are required for myogenic differentiation. *J. Biol. Chem.* **2008**, *283*, 34029–34036. [CrossRef]

75. Zhang, G.; Li, Y. p38β MAPK upregulates atrogin1/MAFbx by specific phosphorylation of C/EBPβ. *Skelet. Muscle* **2012**, *2*, 20. [CrossRef]
76. Mancini, A.; El Bounkari, O.; Norrenbrock, A.F.; Scherr, M.; Schaefer, D.; Eder, M.; Banham, A.H.; Pulford, K.; Lyne, L.; Whetton, A.D. FMIP controls the adipocyte lineage commitment of C2C12 cells by downmodulation of C/EBPalpha. *Oncogene* **2007**, *26*, 1020–1027. [CrossRef]

III

HIGHER GLUCOSE AVAILABILITY AUGMENTS THE METABOLIC RESPONSES OF THE C2C12 MYOTUBES TO EXERCISE-LIKE ELECTRICAL PULSE STIMULATION

by

Lautaoja, J.H., O´Connell, T.M., Mäntyselkä, S., Peräkylä, J., Kainulainen, H., Pekkala, S., Permi, P. & Hulmi, J.J. (2021).

American Journal of Physiology-Endocrinology and Metabolism, 321(2), E229–E245

https://doi.org/10.1152/ajpendo.00133.2021

AMERICAN JOURNAL OF PHYSIOLOGY
ENDOCRINOLOGY AND METABOLISM

Am J Physiol Endocrinol Metab 321: E229–E245, 2021.
First published June 28, 2021; doi:10.1152/ajpendo.00133.2021

RESEARCH ARTICLE

Higher glucose availability augments the metabolic responses of the C2C12 myotubes to exercise-like electrical pulse stimulation

Juulia H. Lautaoja,[1] Thomas M. O'Connell,[2]* Sakari Mäntyselkä,[1,3]* Juuli Peräkylä,[3] Heikki Kainulainen,[1] Satu Pekkala,[1]* Perttu Permi,[3,4]* and Juha J. Hulmi[1]

[1]*Faculty of Sport and Health Sciences, NeuroMuscular Research Center, University of Jyväskylä, Jyväskylä, Finland;*
[2]*Department of Otolaryngology-Head & Neck Surgery, Indiana University School of Medicine, Indianapolis, Indiana;*
[3]*Department of Biological and Environmental Science, University of Jyväskylä, Jyväskylä, Finland; and* [4]*Department of Chemistry, Nanoscience Center, University of Jyväskylä, Jyväskylä, Finland*

Abstract

The application of exercise-like electrical pulse simulation (EL-EPS) has become a widely used exercise mimetic in vitro. EL-EPS produces similar physiological responses as in vivo exercise, while less is known about the detailed metabolic effects. Routinely, the C2C12 myotubes are cultured in high-glucose medium (4.5 g/L), which may alter EL-EPS responses. In this study, we evaluate the metabolic effects of EL-EPS under the high- and low-glucose (1.0 g/L) conditions to understand how substrate availability affects the myotube response to EL-EPS. The C2C12 myotube, media, and cell-free media metabolites were analyzed using untargeted nuclear magnetic resonance (NMR)-based metabolomics. Furthermore, translational and metabolic changes and possible exerkine effects were analyzed. EL-EPS enhanced substrate utilization as well as production and secretion of lactate, acetate, 3-hydroxybutyrate, and branched-chain fatty acids (BCFAs). The increase in BCFAs correlated with branched-chain amino acids (BCAAs) and BCFAs were strongly decreased when myotubes were cultured without BCAAs suggesting the action of acyl-CoA thioesterases on BCAA catabolites. Notably, not all EL-EPS responses were augmented by high glucose because EL-EPS increased phosphorylated c-Jun N-terminal kinase and interleukin-6 secretion independent of glucose availability. Administration of acetate and EL-EPS conditioned media on HepG2 hepatocytes had no adverse effects on lipolysis or triacylglycerol content. Our results demonstrate that unlike in cell-free media, the C2C12 myotube and media metabolites were affected by EL-EPS, particularly under high-glucose condition suggesting that media composition should be considered in future EL-EPS studies. Furthermore, acetate and BCFAs were identified as putative exerkines warranting more research.

NEW & NOTEWORTHY The present study examined for the first time the metabolome of *1*) C2C12 myotubes, *2*) their growth media, and *3*) cell-free media after exercise-like electrical pulse stimulation under distinct nutritional loads. We report that myotubes grown under high-glucose conditions had greater responsiveness to EL-EPS when compared with lower glucose availability conditions and increased media content of acetate and branched-chain fatty acids suggests they might act as putative exerkines warranting further research.

acetate; branched-chain fatty acids; exerkine; metabolomics; skeletal muscle

INTRODUCTION

Adequate physical activity is known to prevent and treat many diseases, such as metabolic, cardiovascular, and musculoskeletal disorders (1). During exercise, muscles secrete molecules that can act as intra- (autocrine and paracrine) or intertissue (endocrine) signaling factors (2). These muscle-derived signaling mediators have been recently shown to promote, for instance, muscle-liver cross talk during and after exercise, which is essential for many physiological processes, such as regulation of energy metabolism during increased fuel demand (3, 4). Overall, recognition of the skeletal muscle as a secretory organ (5, 6) has opened a new research area in exercise physiology.

Pedersen et al. (7) originally named muscle-originated proteins and cytokines as myokines. Afterward, Tarnopolsky and coworkers (8) defined exerkines as myokines and other molecules, such as metabolites, extracellular vesicles, and nucleic acids, secreted from the contracting muscles [i.e., myometabokiome (9)] and other tissues. Due to the large size (30%–40% of the body mass) and great vascularization, contribution of the skeletal muscle to the secreted myokine/exerkine pool is significant (10). A number of in vivo studies have been conducted including analyses of a variety of body fluids (11–13) and muscle tissues as well as examination of

* T. M. O'Connell and S. Mäntyselkä contributed equally to this work. S. Pekkala and P. Permi contributed equally to this work.
Correspondence: J. Lautaoja (juulia.h.lautaoja@jyu.fi); J. Hulmi (juha.hulmi@jyu.fi).
Submitted 6 April 2021 / Accepted 25 May 2021; Accepted 23 June 2021

arteriovenous difference (14) to examine muscle-derived molecules during rest and exercise. However, these analyses will include molecules secreted from other organs in the body so that metabolic products of skeletal muscle cannot be specified.

To look specifically at skeletal muscle metabolism with exercise, we have used a widely adopted cell culture model to mimic in vivo exercise in vitro. This model involves treating the C2C12 myotubes with exercise-like electrical pulse stimulation [hereafter EL-EPS as recommended (15)], which has been shown to produce similar physiological responses at transcriptional, translational, and metabolic levels as in vivo exercise (for review, see Refs. 15, 16). A major benefit of the in vitro EL-EPS approach is the ability to selectively and exclusively study myotube metabolism and myotube-derived molecules.

Although nutrition is a critical factor that regulates skeletal muscle response to exercise, in vitro studies have largely overlooked the composition of the media (17). Indeed, a recent study showed that the media composition had a major effect on the analyzed metabolite profiles of different cell lines (18). Thus, to raise awareness of this aspect, we examined the effects of two media containing different amounts of glucose and EL-EPS on myotube metabolism. Because the glucose content in routine cell culture medium may differ from normal/healthy physiological range (19), it is important to determine how the metabolic functioning of myotubes after EL-EPS is affected by the glucose availability.

In the present study, we aimed to assess the effects of EL-EPS and nutritional status (glucose availability) on C2C12 myotube metabolism by conducting untargeted nuclear magnetic resonance (NMR)-based metabolomics analysis of both the cell extract and the media. To roughly estimate whether metabolite uptake or release was occurring, we also analyzed cell-free media controls. The latter was analyzed also after EL-EPS to exclude the possible direct effects of EL-EPS on the media. Altogether, our results show that the glucose availability affected a significant number of the observed metabolic changes in response to EL-EPS suggesting that nutrient availability is indeed a critical factor that should be taken into account in the future studies.

MATERIALS AND METHODS

Cell Cultures

Murine C2C12 myoblasts and human HepG2 hepatocytes were purchased from American Type Culture Collection (Manassas, VA). The myoblasts were grown and differentiated as previously described (20). Briefly, the myoblasts were seeded on 6-well plates (NunclonTM Delta; Thermo Fisher Scientific, Waltham, MA) at a density of ~12,000 cells/cm^2. The growth medium (GM) contained high-glucose (HG, 4.5 g/L) Dulbecco's modified Eagle medium (DMEM, No. BE12-614F, Lonza, Basel, Switzerland), 10% (vol/vol) fetal bovine serum (FBS, No. 10270, Gibco, Rockville, MD), 100 U/mL penicillin and 100 μg/mL streptomycin (P/S, No. 15140, Gibco), and 2 mM L-glutamine (No. 25030, Gibco). The differentiation medium (DM) contained HG DMEM supplemented with 5% (vol/vol) FBS, 100 U/mL, and 100 μg/mL P/S and 2 mM L-glutamine. The HG DM was refreshed every two days, except at *day 4* postdifferentiation the cells were acclimatized to low-glucose (LG, 1 g/L, No. BE12-707F, Lonza) DM if the following experiments were conducted in LG conditions. According to the medium provider, the only difference between the DMEMs used is the glucose content. The C2C12 experiments were conducted at *days 4–6* postdifferentiation in 2 mL of medium. The cells were tested negative for mycoplasma (MycoSPY, M020-025, Biontex Laboratories GmbH, München, Germany). The HepG2 cells were grown in HG DMEM/Glutamax medium (No. 31266, Gibco) supplemented with 10% (vol/vol) FBS and 100 U/mL and 100 μg/mL P/S. The cells were seeded on 10-cm^2 dishes (NunclonTM Delta; Thermo Fisher Scientific) at a density of ~9,000 cells/cm^2. The HepG2 cells experiments were conducted in 5 mL of serum-free (SF) and antibiotic-free medium. All the cell experiments were performed below passage number 9 (C2C12) or 12 (HepG2) in a humidified environment at 37°C and 5% CO_2.

EL-EPS Protocols for C2C12 Myotubes

Comparable low-frequency EL-EPS protocol as used in the present study has previously been reported to induce similar metabolic and translational changes as in vivo exercise (21–23). According to the studies by Nikolić et al. (16) along with visible contractions verified under a microscope (results not shown), the 24-h chronic low-frequency EL-EPS protocol (1 Hz, 2 ms, 12 V) was chosen. On *day 6* postdifferentiation, all C2C12 samples were collected immediately after the cessation of the EL-EPS.

EL-EPS for Metabolomics

On *day 5* post C2C12 differentiation, the wells were rinsed with phosphate buffered saline (PBS, No. 10010, Gibco) and serum-free (SF) HG or LG DMEM supplemented with 2 mM L-glutamine was added for 1 h (24). The medium was removed, the wells were rinsed with PBS and fresh SF HG or LG DMEM supplemented with 2 mM L-glutamine was added. The chronic low-frequency EL-EPS was applied by placing the C-Dish carbon electrodes attached to C-Pace EM machine (IonOptix Corporation, Milton, MA) to the wells. To roughly elucidate whether the cells possibly take up or release metabolites, we analyzed the metabolome of the cell-free LG and HG media supplemented with 2 mM L-glutamine. As recommended previously (18), the cell-free media were treated identical to the cell-containing samples as they were also incubated for 24 h with and without EL-EPS (i.e., no cells/no power and no cells/power), n = 3 (Supplemental Table S1 and Fig. S2; all Supplemental material is available at https://doi.org/10.6084/m9.figshare.14376413.v1).

EL-EPS for Oleate Oxidation

The cells were first acclimatized to dissolved and albumin-complexed 0.1 mM oleic acid (No. O3008, oleic acid-albumin from bovine serum, Sigma-Aldrich, St. Luis, MO) and 1 mM L-carnitine (C0158, Sigma-Aldrich) in either SF LG or HG DMEM supplemented with 2 mM L-glutamine on the *day 4* postdifferentiation. The next day, the electrodes were placed directly to the wells and EL-EPS was applied. The

measurement of oleate oxidation was carried out for 2 h at 37°C as previously described (25) with slight modifications. Briefly, at differentiation *day 6*, after 22 h of stimulation, EL-EPS was paused, the media were collected, and centrifuged for 1 min at 1,000 *g* before storing at −80°C. The cells were rinsed with PBS and fresh SF HG or LG DMEM supplemented with 2 mM L-glutamine, 0.1 mM oleic acid, 1 mM L-carnitine and 1 μCi/mL [9,10-^{3}H(N)] oleic acid (24 Ci/mmol, NET289005MC, PerkinElmer, Boston, MA) was added. The radiolabeled oleic acid was omitted from the negative controls. The EL-EPS was applied for the remaining 2 h.

Nuclear Magnetic Resonance Spectroscopy

The cell lysates and the experiment media (including cell-free controls) were collected and prepared for the ^{1}H NMR analysis as described previously (26) with slight modifications. Briefly, samples from three wells were pooled to ensure adequate metabolite concentrations per one ^{1}H NMR measurement. Media from three wells were mixed with cold methanol (600 μL of sample and 1,200 μL of methanol) and cells were scraped into 200 μL of 90% (vol/vol) 9:1 aqueous methanol/chloroform mixture. The resulting supernatants were stored at −80°C before room temperature lyophilization using vacuum concentrator (Speed Vac plus SC110 A Savant Instruments Inc., Farmingdale, NY) equipped with a vacuum pump (Vacuum pump V-700, Büchi, Flawil, Switzerland) and controller (Vacuum Controller V-850, Büchi). The experiments were replicated independently three times, total n = 6–8 per group.

The samples lyophilized at RT were reconstituted as previously described (26) with slight modifications. In brief, Na_2HPO_4-NaH_2PO_4 buffer (150 mM, pH = 7.4) in 99.8% D_2O (Acros Organics, Thermo Fisher Scientific) containing 0.5 mM 3-(trimethylsilyl) propanesulfonic-d6 acid sodium salt (DSS-d6, IS-2 Internal Standard, Chenomx, Edmonton, Canada) was used for reconstitution. The samples were placed in 3-mm round-bottom NMR sample tubes (Norell Inc., Morganton, NC) for analysis. All the NMR spectra were collected using a Bruker AVANCE III HD NMR spectrometer, operating at 800 MHz ^{1}H frequency (Bruker Corporation, MA) equipped with a cryogenically cooled ^{1}H, ^{13}C, ^{15}N triple-resonance probehead. The temperature of the samples was set at 25°C during the measurements. For the ^{1}H one-dimensional (1-D) NOESY experiments, the free induction decay (FID) was sampled with 133,926 points covering the spectral width of 16,741 Hz, using a relaxation delay of 5 s, acquisition time of 4 s, and mixing time of 0.1 s. The signal was accumulated with 128 scans. The obtained data were analyzed using Chenomx 8.5–8.6 software (Chenomx). In addition to ^{1}H 1-D spectra, heteronuclear ^{1}H-^{13}C single quantum coherence spectroscopy (HSQC) and ^{1}H-^{13}C HSQC-total correlation spectroscopy (HSQC-TOCSY), as well as homonuclear ^{1}H-^{1}H TOCSY and ^{1}H-^{1}H double quantum filtered correlation spectroscopy (DQF-COSY) two-dimensional (2-D) spectra were used to confirm the identification of the profiled metabolites. The TopSpin 4.0.9 software (Bruker Corporation) was used for processing and analysis of the 2-D spectra. The spike in-analyses of isobutyric acid (No. I1754, Sigma-Aldrich), isovaleric acid (No. 129542, Sigma-Aldrich) were included.

Oleate Oxidation

After the EL-EPS, the media were run through ion-exchange columns containing Dowex-OH-resin (pH 7, 1X8-200, Cat no. 217425, Sigma Aldrich) (25). Deionized H_2O was used to elute the $^{3}H_2O$, which originates from intracellular [9,10-^{3}H(N)] oleic acid β-oxidation that was further secreted to the media. The radioactivity was analyzed as disintegration per minute (DPM) in Optiphase HiSafe 3 scintillation cocktail (Cat. No. 1200.437, PerkinElmer) with Tri-Carb 2910 TR Liquid Scintillation Analyzer (PerkinElmer). The results were calculated using PerkinElmer equations (https://www.perkinelmer.com/fi/lab-products-and-services/application-support-knowledgebase/radiometric/radiochemical-calculations.html). The cells were washed twice with PBS and harvested for total protein content analysis as previously described (20) except for centrifugation at 13,000 *g* for 10 min at +4°C. The oleate oxidation results were normalized against total protein content and the experiments were replicated independently three times, total n = 8–10 per group.

HepG2 Hepatocyte Experiments

Normal and steatotic HepG2 hepatocytes were used in the experiments. Based on our dose-response experiment steatosis, i.e., fat accumulation, was induced by 24-h administration of 500 μM oleic acid (No. 03008, Sigma-Aldrich) in serum- and antibiotic-free conditions when compared with the nonexposed hepatocytes (Supplemental Fig. S1). The acetate (sodium acetate, CAS No. 127-09-3, Merck, Darmstadt, Germany) dose-response experiment in steatotic hepatocytes suggested that a greater dose (3 mM) that was observed in ^{1}H NMR analysis (1.5 mM) had no additional effect on intracellular triacylglycerol content over the lower dose (Supplemental Fig. S1).

The normal and steatotic hepatocytes were administered with EL-EPS-stimulated or unstimulated C2C12 conditioned medium (CM) or alternatively with or without 1.5 mM acetate. The C2C12 cells were treated as described for the HG ^{1}H NMR analysis. After EL-EPS, the media of the stimulated and unstimulated cells were collected and centrifuged for 5 min at 217 *g* RT to remove cell debris before administration on hepatocytes. In another set of experiments, 1.5 mM acetate or equivalent volume of PBS was administered on both normal and steatotic hepatocytes in serum- and antibiotic-free DMEM/Glutamax. After the 24-h incubation, triacylglycerol extraction from the hepatocytes was conducted. Briefly, the media were collected, centrifuged for 5 min at 217 *g*, RT and stored at −80°C until use. The HepG2 cells were washed and scraped into PBS, while subsamples for the measurement of total protein content were homogenized into previously described buffer (20). Next, 2:1 methanol-chloroform mixture was added to PBS-cell suspension followed by 5 min centrifugation at 724 *g*, RT. The supernatant was transferred into a new tube and chloroform, 50 mM citric acid, and H_2O were added. Methanol and chloroform phases were separated by centrifugation for 10 min at 724 *g*, RT. Chloroform phase was collected and evaporated at +70°C using SpeedVac Concentrator (Thermo Fisher Scientific). The resulting lipid pellet was dissolved into ethanol before measurement. The content of intracellular triacylglycerol as well

as glycerol and cytokines in the media were measured as described in the next two sections.

Measurement of Total Protein Content, Enzyme Activities, Triacylglycerol, and Media Glycerol Contents

Total protein content (Bicinchoninic Acid Protein Assay Kit, Pierce Biotechnology, Rockford, IL), triacylglycerol (No. 981786, Thermo Fisher Scientific), and glycerol (No. 984316, Thermo Fisher Scientific) concentrations as well as lactate dehydrogenase (LDH) (No. 981906, Thermo Fisher Scientific) and citrate synthase (CS) (No. CS0720, Sigma-Aldrich) enzyme activities were measured with an automated Konelab or Indiko plus analyzer (Thermo Fisher Scientific). All assays were conducted according to manufacturer's protocols and enzyme activities in the cells were normalized against total protein content.

4-Plex Cytokine ELISA Analyses

The C2C12 and HepG2 media were centrifuged for 1 min at 1,000 *g* or 5 min at 217 *g*, respectively, at +4°C and resulting supernatants were stored at −80°C until use. Next, 25 μL of the samples were directed to mouse [Q-Plex Mouse 4-plex Cytokine Panel (No. 115549MS, Quansys Biosciences, North West, UT)] or human 4-plex Cytokine Panel (Q-Plex Human Cytokine High Sensitivity, No. 112533HU, Quansys Biosciences) assay that were conducted according to the manufacturer's protocols. In the murine assay, the limit of detection for interleukin-1β (IL-1β) was 12.41 pg/mL, for IL-6 2.90 pg/mL, for tumor necrosis factor α (TNF-α) 3.40 pg/mL, and for interferon γ (IFN-γ) 5.40 pg/mL. In the human assay, the limit of detection for IL-4 was 0.02 pg/mL, for IL-6 0.30 pg/mL, for IL-10 2.39 pg/mL, and for IFN-γ 0.09 pg/mL.

Protein Extraction and Western Blot

The cells were harvested for Western blot and enzyme activity analysis as previously described (20) except for centrifugation at 13,000 *g* for 10 min at +4°C. The Western blot was conducted as previously described (20). Briefly, 10 μg of total protein per samples were loaded on 4%–20% Criterion TGX Stain-Free protein gels (No. 5678094, Bio-Rad Laboratories, Hercules, CA) and samples were separated by SDS-PAGE. To visualize proteins using stain-free technology, the gels were activated and the proteins were transferred to the PVDF membranes followed by blocking and overnight probing with primary antibodies at +4°C (27). Enhanced chemiluminescence (SuperSignal west femto maximum sensitivity substrate; Pierce Biotechnology, Rockford, IL) and ChemiDoc MP device (Bio-Rad Laboratories) were together used for protein visualization. Stain free (whole lane) was used as a loading control and for the normalization of the results. Primary antibodies used in the present study were purchased from Cell Signaling Technology: p38$^{Thr180/Tyr182}$ (No. 4511), p38 (No. 9212), ERK1/2$^{Thr202/Tyr204}$ (No. 9101), ERK1/2 (No. 9102), SAPK/JNK1/2$^{Thr183/Tyr185}$ (No. 4668), and SAPK/JNK1/2 (No. 9252). The horseradish peroxidase-conjugated secondary IgG antibody was purchased from Jackson ImmunoResearch Laboratories, PA.

Statistical Analyses

The two-way multivariate analysis of variance (two-way MANOVA) was used to analyze main and interaction effects, whereas the group comparisons were conducted by using multivariate Tukey's test unless stated otherwise (IBM SPSS Statistics, version 26 for Windows, SPSS Chicago, IL). The Spearman's correlation coefficient was used to analyze correlations (SPSS). The VIsualization and Integration of Metabolomics Experiments (VIIME) software [https://viime.org (28)] was used to generate the heat maps and principal components analyses. The results are presented as means ± SE. The level of significance was set at $P < 0.05$.

RESULTS

EL-EPS Yielded Different Metabolic Responses under LG and HG Conditions

We studied the effects of chronic low-frequency EL-EPS and medium glucose content on the metabolism of C2C12 myotubes using untargeted ^{1}H NMR-based metabolomics analysis of the conditioned media and cell extracts. The cell-free media controls were incubated for 24 h with and without EL-EPS. This allowed us to show that EL-EPS does not induce changes in the metabolite profiles in the cell-free media (Supplemental Fig. S2 and Table S1). The principal component analysis (PCA) of the metabolite profiles demonstrated that the four study groups were clearly separated, especially in the media (Fig. 1*A*). Interestingly, in the PCA of the media, the first principal component separates the groups based on glucose levels and the second principal component separates them based on the application of EL-EPS (Fig. 1*A*).

The NMR-based metabolomics analysis resulted in identification of 47 individual metabolites. More specifically, we quantified 39 metabolites from the cells and 37 metabolites from the media and the reporting threshold (i.e., the metabolite was detected in over 50% of cases) was met by 37 and 34 metabolites, respectively (Supplemental Table S2). Among the cells and the media, 24 metabolites were shared (Fig. 1*B*). Overall, the heat map clustering of the metabolites quantified from the cells and media demonstrated that the stimulation-induced differences in the metabolites between LG and HG conditions were greater in the latter, especially in the cells (Fig. 1, *D* and *E*). The hierarchical cluster analysis of heat maps from the cell extracts suggests that the metabolites clustered into three categories including those responsive to EL-EPS and to distinct media glucose contents, whereas in the media more categories were observed (Fig. 1, *D* and *E*).

Similar to a previous study (12), most of the identified metabolites were distributed among four biological groups. These were *1*) metabolism of energy related metabolites (creatine, carbohydrates, and TCA cycle intermediates; 14 metabolites), *2*) short- and branched-chain fatty acids (SCFAs and BCFAs, respectively) and ketone bodies (six metabolites), *3*) amino acids and related metabolites (24 metabolites) as well as *4*) vitamins and others (three metabolites) (Fig. 1*C*, for individual metabolites, see Supplemental Table S2). In the cells, 18 metabolites were altered due to either EL-EPS or medium glucose content (i.e., EPS and HG main effects, respectively), while eight metabolites demonstrated an interaction effect (EPS × HG) (Supplemental Table S3). In the media, EPS had a main effect on 17 and HG

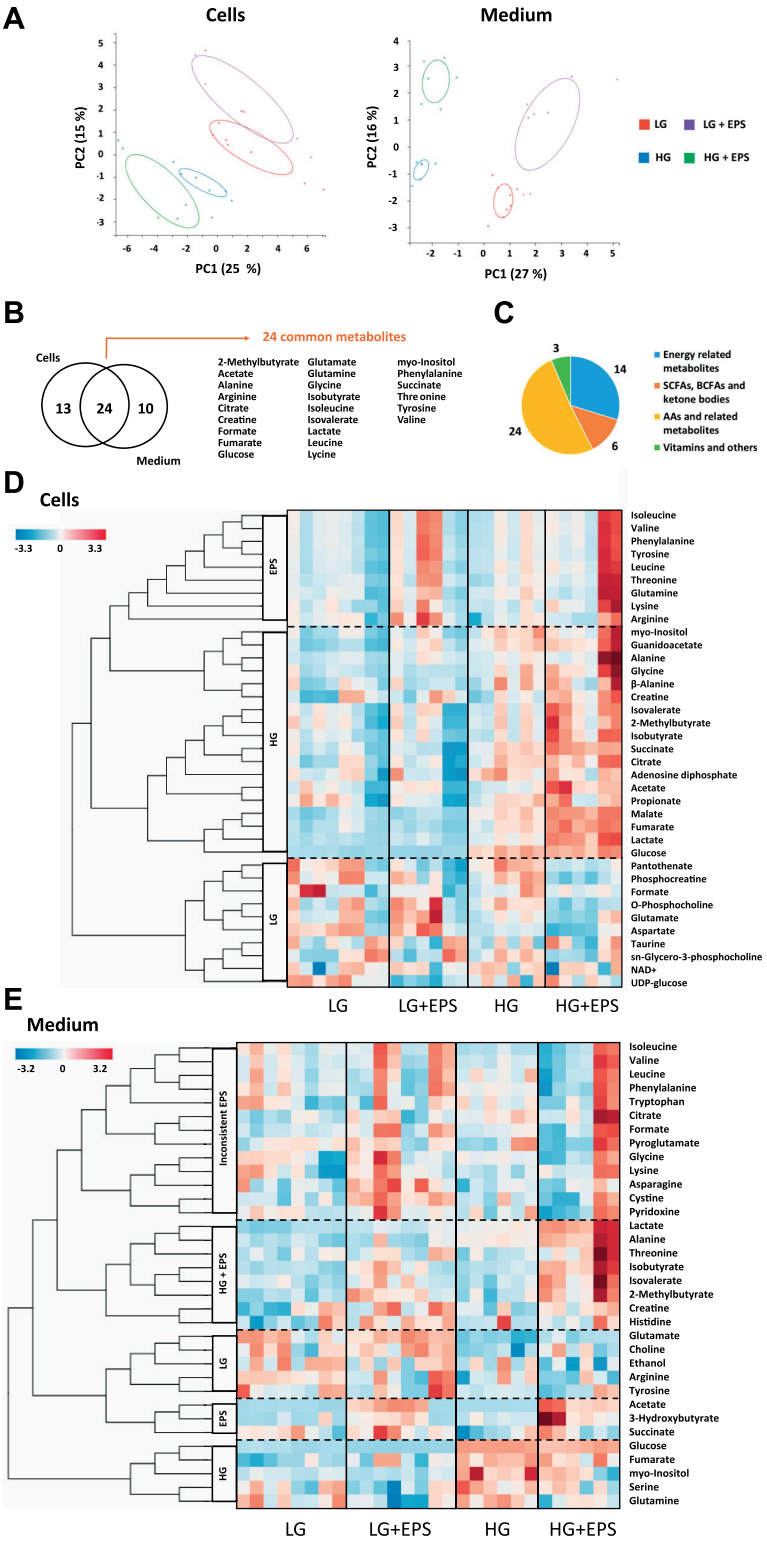

Figure 1. The principal component analysis (PCA), Venn diagram, and heat map visualizations of the identified metabolites with and without exercise-like electrical pulse stimulation (EL-EPS). *A*: the PCA score plots. Fold changes were logarithmically transformed (log_2) and pareto scaling was used to create the plots. *B*: overall, 37 and 34 metabolites were identified from the C2C12 cells and from the media, respectively, and of these 24 metabolites were common among groups. *C*: the identified metabolites were distributed among four biological groups. The heat map categorization (*k*-means clustering) of the analyzed metabolites in the cells (*D*) and in the media (*E*). The dashed lines cluster the metabolites that respond similarly to EL-EPS or to media glucose content. Heat map coloring is based on *z*-scores. $n = 6–8$ samples per group. See MANOVA statistics in Supplemental Table S3 for the significant main and interaction effects of EL-EPS or HG. AAs, amino acids; BCFAs, branched-chain fatty acids; LG/HG, low-/high-glucose condition; LG/HG + EPS, EL-EPS in low-/high-glucose condition; SCFAs, short-chain fatty acids.

on 13 metabolites, while the interaction effect was detected in seven metabolites (Supplemental Table S3).

Glycolytic ATP Production and Acetate Responded Strongly to EL-EPS

During the EL-EPS, the glucose content in the media decreased when compared with cell-free media indicating increased consumption to support the contraction-induced increase in the energy demand in the cells (Fig. 2*A*). Simultaneously, lactate content increased both in the cells and in the media, whereas the level of phosphocreatine decreased and dephosphorylated creatine increased suggesting that both glycolytic and phosphocreatine energy sources were utilized (Fig. 2, *B–D*). In agreement with the increased lactate production and secretion in our experiments, the lactate dehydrogenase (LDH) activity was increased in the cells after EL-EPS, especially in the HG condition (Fig. 2*E*). Finally, we observed an increase in the cell and media content of acetate, a short-chain fatty acid (SCFA) that can act as a potential fuel source during exercise (29). It appears that in the resting C2C12 cells, the net uptake of acetate was enhanced based on substantially lower acetate content in the cell media than in the cell-free media (LG or HG vs. cell-free LG or HG, Student's *t* test, $P < 0.001$, Fig. 2*F*). In contrast, during EL-EPS acetate secretion exceeded its uptake partly due to the increased cellular production, at least in HG condition (HG + EPS vs. cell-free HG + EPS, Student's *t* test, $P < 0.05$, Fig. 2*F*). The effect of the increased glycolysis in response to EL-EPS was accompanied by unaltered content of citrate, the first TCA cycle intermediate, and unaltered citrate synthase (CS) enzyme activity, whereas the levels of the intermediates observed later in the cycle including succinate, fumarate, and malate were increased in the cells in HG condition (Fig. 3, *A–E*).

Increased Intracellular Amino Acid Levels after EL-EPS

Overall, amino acids were more affected by the EL-EPS than by the glucose availability and only minor effects were observed between HG and LG conditions. Figure 4*A* shows a forest plot of the amino acids with the $\log_2$ fold changes of the metabolites in response to EL-EPS shown along the *x*-axis (for individual amino acid box plots, see Supplemental Fig. S3). The plot shows the levels of each of the amino acids under both LG and HG conditions. A set of seven amino acids were increased and eight remained unchanged in response to EL-EPS in the cells, whereas in the media five amino acids increased, two decreased, and ten remained unaltered (Fig. 4*B*). In contrast, a shared increasing HG effect was observed in three amino acids in the cells and media, whereas a decreasing HG effect was observed in one and two amino acids, respectively (Fig. 4*C*). The contents of cysteine (Student's *t*-test, media vs. cell-free media, $P < 0.01$), glycine ($P < 0.001$), histidine ($P < 0.05$), and lysine ($P < 0.001$) were lower in the cell-free than in the cell-containing media suggesting release of these amino acids from the C2C12 cells and for cystine and lysine release appears to be further increased during EL-EPS (Supplemental Fig. S3). In contrast, serine ($P < 0.001$) and glutamine ($P < 0.001$) contents were greater in the cell-free media controls suggesting active uptake of these amino acids by the C2C12 cells and this appears to be further increased during EL-EPS (Supplemental Fig. S3).

Increased Intra- and Extracellular Contents of Branched-Chain Fatty Acids after EL-EPS

A set of branched-chain fatty acids (BCFAs) demonstrated significant increases induced by EL-EPS. The levels of 2-methylbutyrate, isobutyrate, and isovalerate were increased in the media after EL-EPS independent of the glucose availability showing their release/secretion from the cells (BCFAs were not detected from the cell-free media) (Fig. 5, *A–C*). Of these BCFAs, isobutyrate and isovalerate were also increased in the cells after EL-EPS, but this was explained by the increase in HG condition (Fig. 5, *A–C*). Indeed, the responses of BCFAs to EL-EPS were overall greater in HG condition. The observation of the BCFAs was unanticipated and the source of these metabolites was not entirely clear. Based simply upon chemical structure, we suspected that these metabolites could be the result of branched-chain amino acid (BCAA) catabolism. To test this, we evaluated the correlations between the BCFAs and the BCAAs. As shown in Supplemental Table S4, we found no significant correlations in the media, but very strong correlations were found between the BCAA and BCFAs in the cells. Figure 5*D* postulates the pathway through which the BCAAs are transformed.

To unequivocally confirm the identity of the BCFAs, we conducted spike-in ^{1}H NMR experiments, where authentic standards of these compounds were added to the samples to show that the spectral patterns were clearly matching. Finally, we also confirmed by culturing the C2C12 myotubes in BCAA-free media that indeed, BCFAs appear to originate from the BCAA breakdown based on their greater abundance in standard BCAA containing media (pilot results, Supplemental Fig. S3).

Increased Ketone Body Levels in the Media after EL-EPS

The ketone body 3-hydroxybutyrate was identified in the cell-free and the C2C12 media (Fig. 5*E*). It should be noted that the signals for 3-hydroxybutyrate in the cell-free and unstimulated media samples were near the limit of detection and thus the quantitation is only approximate. Application of EL-EPS led to a significant increase in the signals for 3-hydroxybutyrate in the C2C12 media enabling confident identification and quantitation. The increase in 3-hydroxybutyrate content was greater under HG condition demonstrating that ketone body production in these cells was affected by the glucose availability.

Glucose Availability Resulted in Variable Changes in Exercise and Stress Associated Markers

As the glucose content together with the EL-EPS influenced the metabolite levels, we investigated next whether this was also translated to the phosphorylation levels of the mitogen-activated protein kinases (MAPKs) that are common markers of skeletal muscle after energetic stress and exercise (30). We observed that EL-EPS increased the phosphorylation of stress-activated protein kinase/c-Jun N-terminal kinase (SAPK/JNK)$^{Thr183/Tyr185}$ independent of the glucose availability (Fig. 6*A*), whereas the phosphorylation

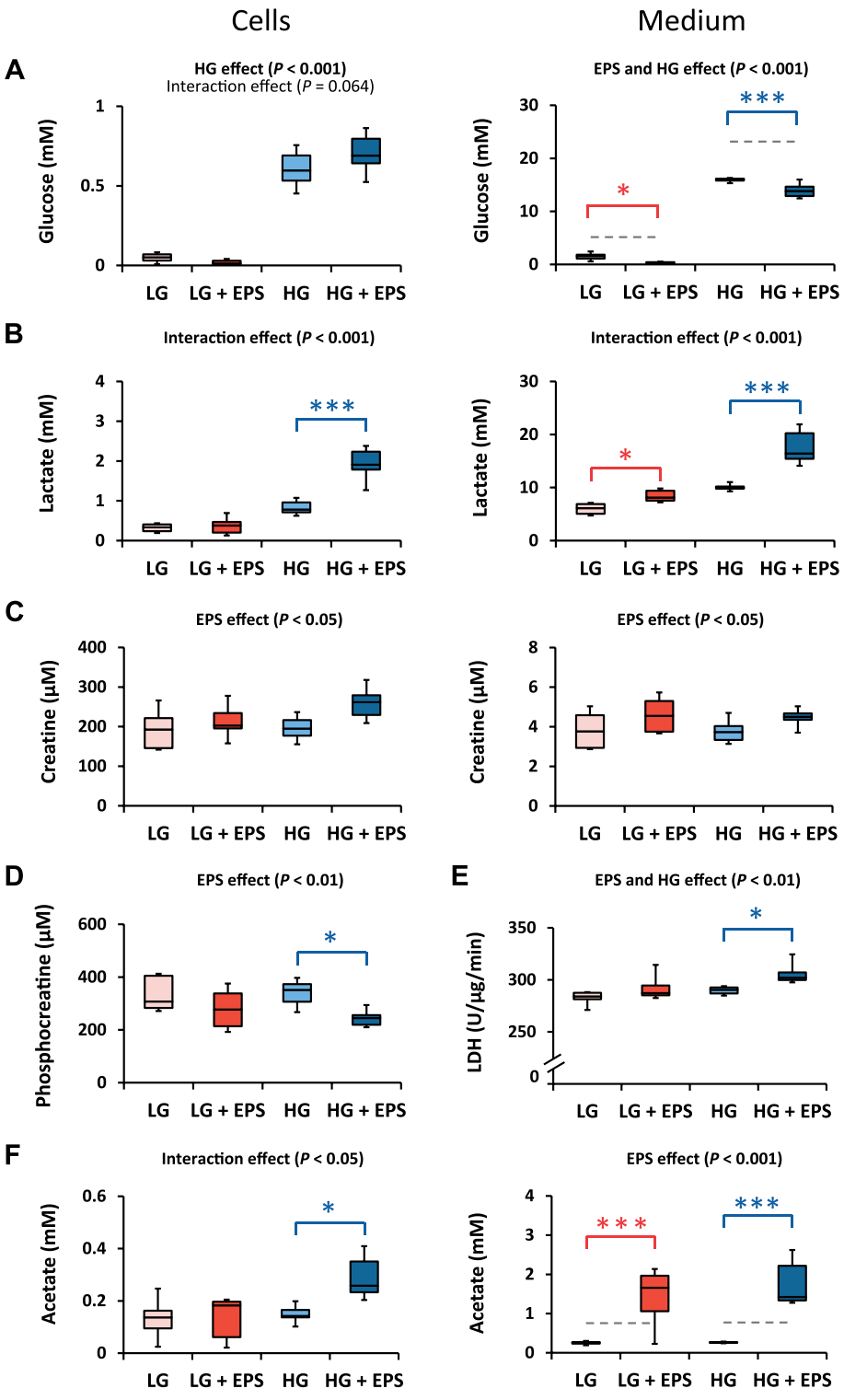

Figure 2. Exercise-like electrical pulse stimulation (EL-EPS) increased energy utilization via glycolytic pathways and readily available energy stores. Glucose (*A*), lactate (*B*), dephosphorylated creatine (*C*), and phosphocreatine contents (*D*) in the C2C12 cells and/or in the media. *E*: lactate dehydrogenase (LDH) enzyme activity in the cells. *F*: acetate content. $*P < 0.05$; $***P < 0.001$, respectively. $n = 6–8$ samples per group. The two-way MANOVA was used to analyze the effects of the applied EL-EPS and media glucose content (EPS and HG effects, respectively) and their interaction effect, whereas group comparisons were analyzed with multivariate Tukey's test. In *A* and *F*, the dashed lines represent the levels of the cell-free low-glucose (LG) and high-glucose (HG) media controls (i.e., mean of the stimulated and nonstimulated media). Lack of the dashed lines refers to the undetected metabolite content from the cell-free media controls. LG/HG + EPS, EL-EPS in low-/high-glucose condition.

of $p38^{Thr180/Tyr182}$ and extracellular regulated kinase $(ERK1/2)^{Thr202/Tyr204}$ remained unaltered (Supplemental Fig. S4). Because SAPK/JNK has been shown to regulate IL-6 signaling in the C2C12 myotubes after EL-EPS (31), we examined the common exercise-responsive cytokines from the media and found that only IL-6 was detectable after EL-EPS. The IL-6 concentration was increased independent of the glucose availability (Fig. 6*B*). Furthermore, Hojman et al. (32) showed

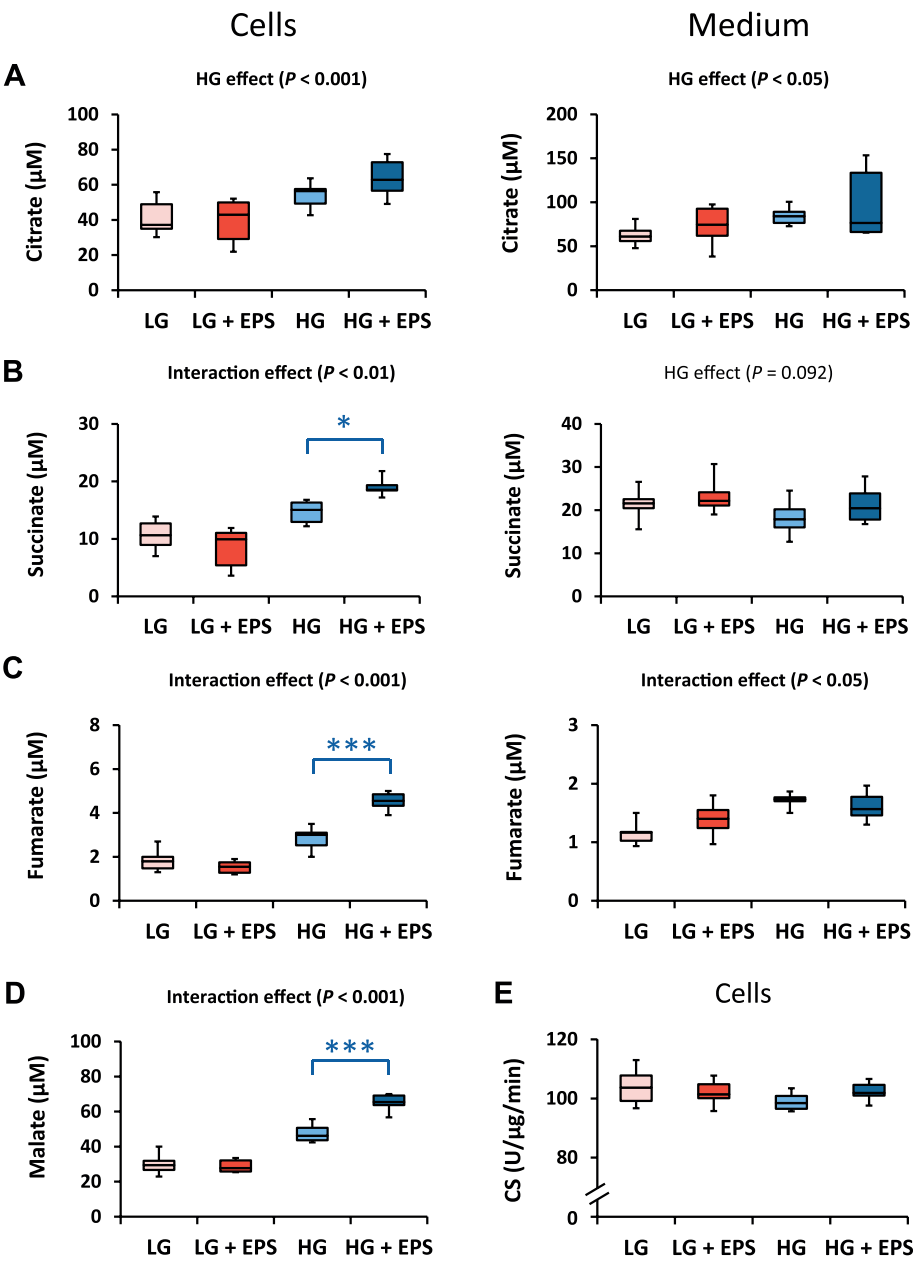

Figure 3. Increase in the content of tricarboxylic acid (TCA) cycle intermediates in the C2C12 cells after exercise-like electrical pulse stimulation (EL-EPS) was dependent on medium-glucose availability. The contents of citrate (*A*), succinate (*B*), fumarate (C), and malate (*D*). *E*: citrate synthase (CS) enzyme activity in the cells. $*P < 0.05$, $***P < 0.001$, respectively. $n = 6–8$ samples per group. The two-way MANOVA was used to analyze the effects of the applied EL-EPS and media glucose content [EPS and high-glucose (HG) effects, respectively] and their interaction effect, whereas group comparisons were analyzed with multivariate Tukey's test. LG, low-glucose condition; LG/HG + EPS, EL-EPS in low-/high-glucose condition.

that IL-6 release from the muscle cells is at least in part dependent on the lactate production, and similarly our correlation analysis demonstrated a positive association between the media IL-6 content and the content of lactate in the cells ($r = 0.551$, $P < 0.01$) and in the media ($r = 0.660$, $P < 0.001$). For the full list of the IL-6 and metabolite correlations, see Supplemental Table S4.

The changes in the metabolites in response to EL-EPS suggest that the C2C12 cell line is very glycolytic in nature even under low-frequency stimulation and therefore in addition to the unaltered activity of the citrate synthase as a TCA cycle marker (Fig. 3*E*), we expected that the fatty acid oxidation might not increase. To test this hypothesis, oleic acid and L-carnitine acclimatized C2C12 myotubes were applied with 24-h EL-EPS during which radiolabeled [9,10-^{3}H(N)] oleic acid was added together with unlabeled oleic acid and L-carnitine in fresh media. The rate of oleate oxidation was analyzed as the amount of ^3H_2O produced and secreted by the myotubes to the culture media. Indeed, the analysis of the metabolic effects of EL-EPS demonstrated that oleate oxidation even decreased in the cells under HG condition (Fig. 6*C*). This occurred without EL-EPS-induced changes in triacylglycerol content, although media glycerol content as a marker of lipolysis was increased in HG condition after EL-EPS (Fig. 6, *D* and *E*).

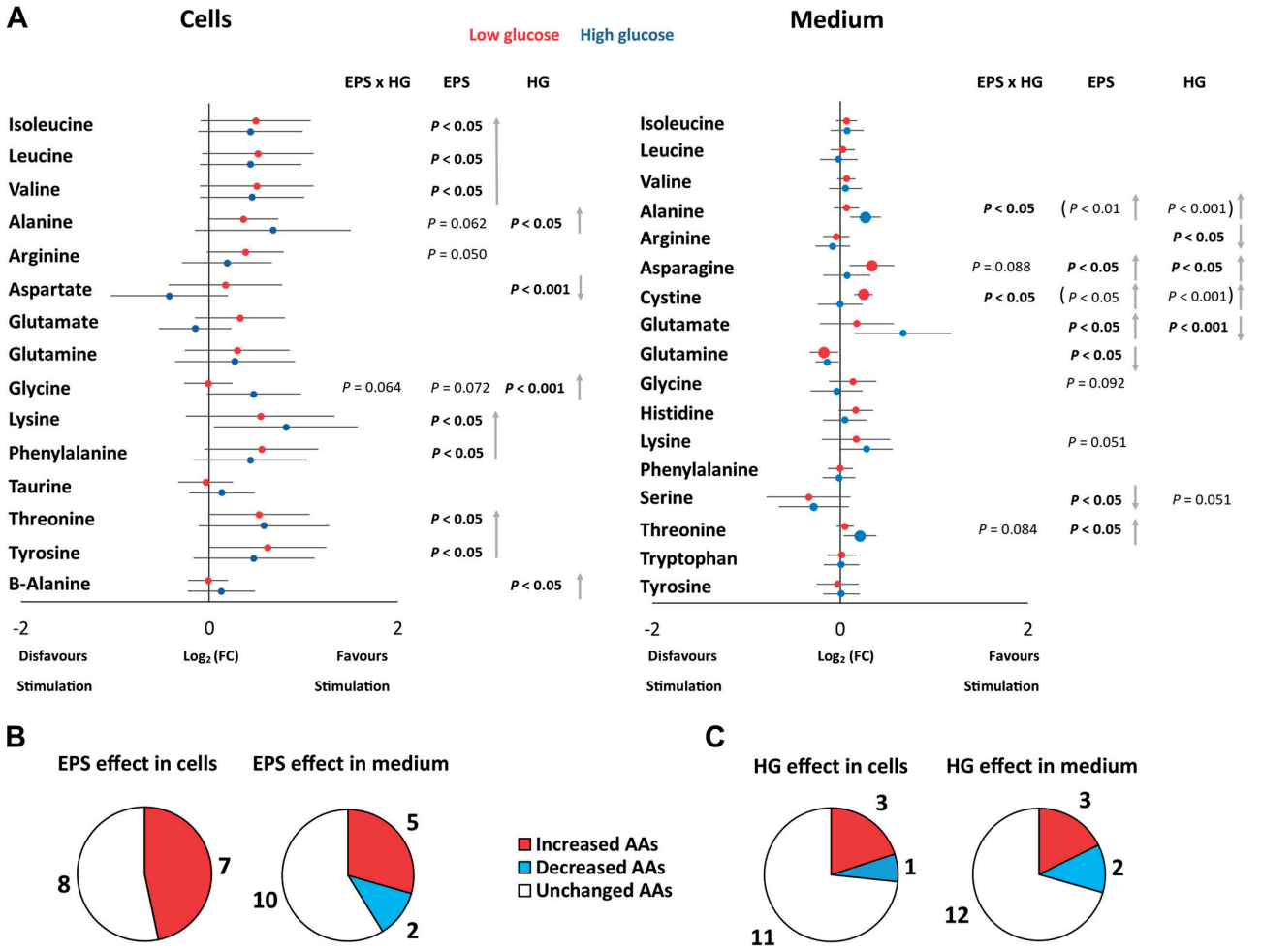

Figure 4. The effects of exercise-like electrical pulse stimulation (EL-EPS) on the analyzed amino acids were greater than the effect of the glucose availability. Forest plots of the amino acids in the C2C12 cells (*A*) and in the medium (*B*) analyzed as logarithmically transformed fold changes [Log_2 (FC)], $n = 6–8$ samples per group. The error bars demonstrate 95% confidence intervals of the analyzed groups [low-glucose (LG) and EL-EPS in low-glucose condition (LG + EPS) or high-glucose (HG) and EL-EPS in high-glucose condition (HG + EPS)]. Next to the plots are shown the interaction effect (EPS × HG) and the main effects of the applied EL-EPS (EPS) and media glucose content (HG) analyzed by the two-way MANOVA. If the interaction effect is significant, the main effects are shown in the brackets. Multivariate Tukey's test was used to analyze the group comparisons and significant results are depicted as larger dots. Red = low glucose samples, blue = high glucose samples. Gray arrows depict the direction (increase or decrease) of the main effect. Pie charts of the amino acids demonstrating EPS (*B*) and HG main effects (*C*) in the cells and in the medium. Of note: the 95% confidence intervals were calculated based on Student's *t* distribution, whereas the group comparisons were conducted using more stringent Tukey's test.

EL-EPS Has No Effect on Cell Viability but Myotubes Grown in HG May Be More Viable

To understand whether the myotubes were more viable and thus perhaps more metabolically active in the HG condition, which could partly explain some of the observed results, LDH enzyme activity was measured from the media as a marker of cell rupture (16) (Supplemental Fig. S5). Overall, the cell viability remained unaffected by the EL-EPS protocol. However, LDH activity tended to be lower in HG condition in NMR experiments thus suggesting possibly better viability than in LG condition (Supplemental Fig. S5).

Potential Myotube-Derived Exerkines Had Little Effect on Normal and Steatotic Hepatocytes

An initial goal of this study was to search for potential, myotube-derived metabolites that could act as exerkines. To test whether myotube-derived exerkines can alter hepatic steatosis, we cultured HepG2 hepatocytes and induced the accumulation of triacylglycerol by supplementation of the media with oleic acid (Supplemental Fig. S1). Steatosis was not accompanied with inflammation because inflammatory markers (IL-4, IL-6, IL-10, and INF-γ) in the media remained below the detection limit (data not shown). As acetate was the metabolite secreted with the largest fold change in response to EL-EPS, we administrated normal and steatotic hepatocytes with 1.5 mM acetate or with EL-EPS CM. The acetate concentration was chosen based on the ^{1}H NMR analysis results. After the 24-h incubation, we observed that neither of the approaches had adverse effects on the triacylglycerol content of the hepatocytes or the glycerol content in the media (Fig. 7, *A*–*D*). That said, the level of glycerol in the media as a marker of lipolysis approached an increasing

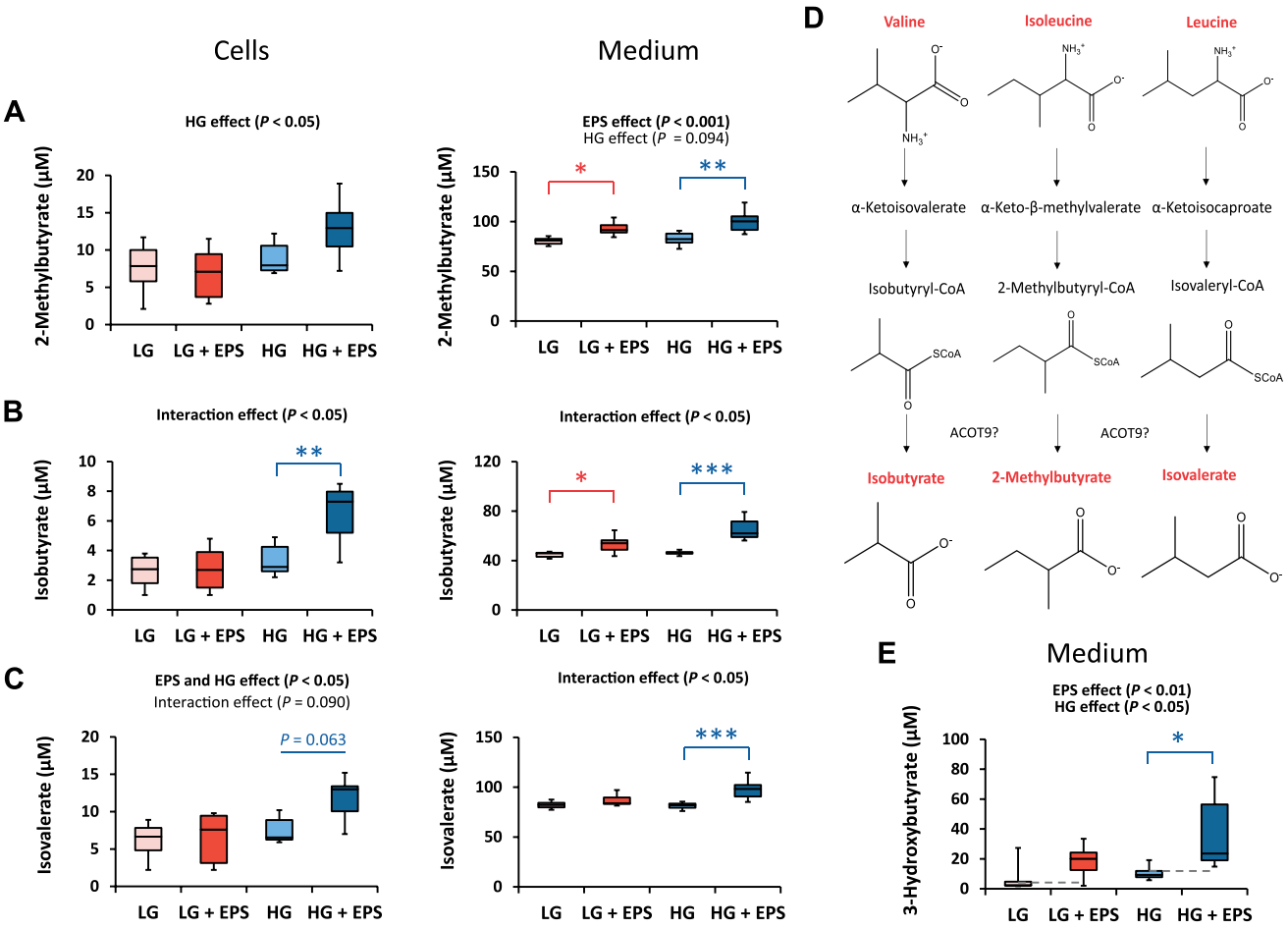

Figure 5. The production and secretion of branched chain fatty acids (BCFAs) and ketone bodies were increased after exercise-like electrical pulse stimulation (EL-EPS) independent of the glucose availability. The contents of 2-methylbutyrate (*A*), isobutyrate (*B*), and isovalerate (*C*). *D*: schematic presentation of the branched-chain amino acids and their breakdown metabolites, BCFAs. *E*: the content of ketone body 3-hydroxybutyrate in the media. $*P < 0.05$, $**P < 0.01$, and $***P < 0.001$. $n = 6–8$ samples per group. The two-way MANOVA was used to analyze the effects of the applied EL-EPS and media glucose content (EPS and high-glucose (HG) effects, respectively) and their interaction effect, whereas group comparisons were analyzed with multivariate Tukey's test *E*: dashed lines represent the level of the cell-free low-glucose (LG) and HG media controls (i.e., mean of the no cells/no power and co cells/power content). Lack of the dashed lines refers to the undetected metabolite content from the cell-free media controls. ACOT9, acyl-CoA thioesterase 9.

trend after EL-EPS CM administration (EPS main effect, $P = 0.098$, Fig. 7*D*).

DISCUSSION

Skeletal muscle metabolism is known to increase dramatically from rest to exercise and the ability of the cells to adapt to increased energy demand is vital (33). In agreement with these known in vivo physiological facts and similar to previous in vivo studies (11, 12, 34), we observed a number of perturbations to energy metabolism that were affected by EL-EPS. Our studies also observed a significant impact of nutrient availability on the EL-EPS-induced metabolic changes. Most, but not all of the EL-EPS responses were of larger magnitude in high-glucose conditions, which may be due to the fact that in low-glucose condition the 24-h EL-EPS almost completely depleted media and cells from glucose. The decreased glucose content in the media after EL-EPS is in line with previous studies demonstrating that EL-EPS promotes glucose uptake into the myotubes (16) and the well-known fact that exercise in vivo increases glucose uptake into the skeletal muscle (35). Similarly, in agreement with in vitro (16) and in vivo (36) findings, we observed an increased production and secretion of lactate and decreased intracellular content of phosphocreatine demonstrating that the applied EL-EPS induced anaerobic and especially glycolytic ATP production and energy demands in the C2C12 myotubes. Indeed, the C2C12 cell line has been considered to be glycolytic in nature (37) and rely on anaerobic glycolysis at rest (38), which may explain the increased lactate production and decreased fat oxidation during the applied low-frequency EL-EPS. As lactate plays an important role in intercellular signaling of nearby and/or distant cells (39), its role as an exerkine has probably been underappreciated and should be further studied.

Our studies revealed alterations in a set of short- and branched-chain fatty acids (S/BCFAs) and ketone bodies

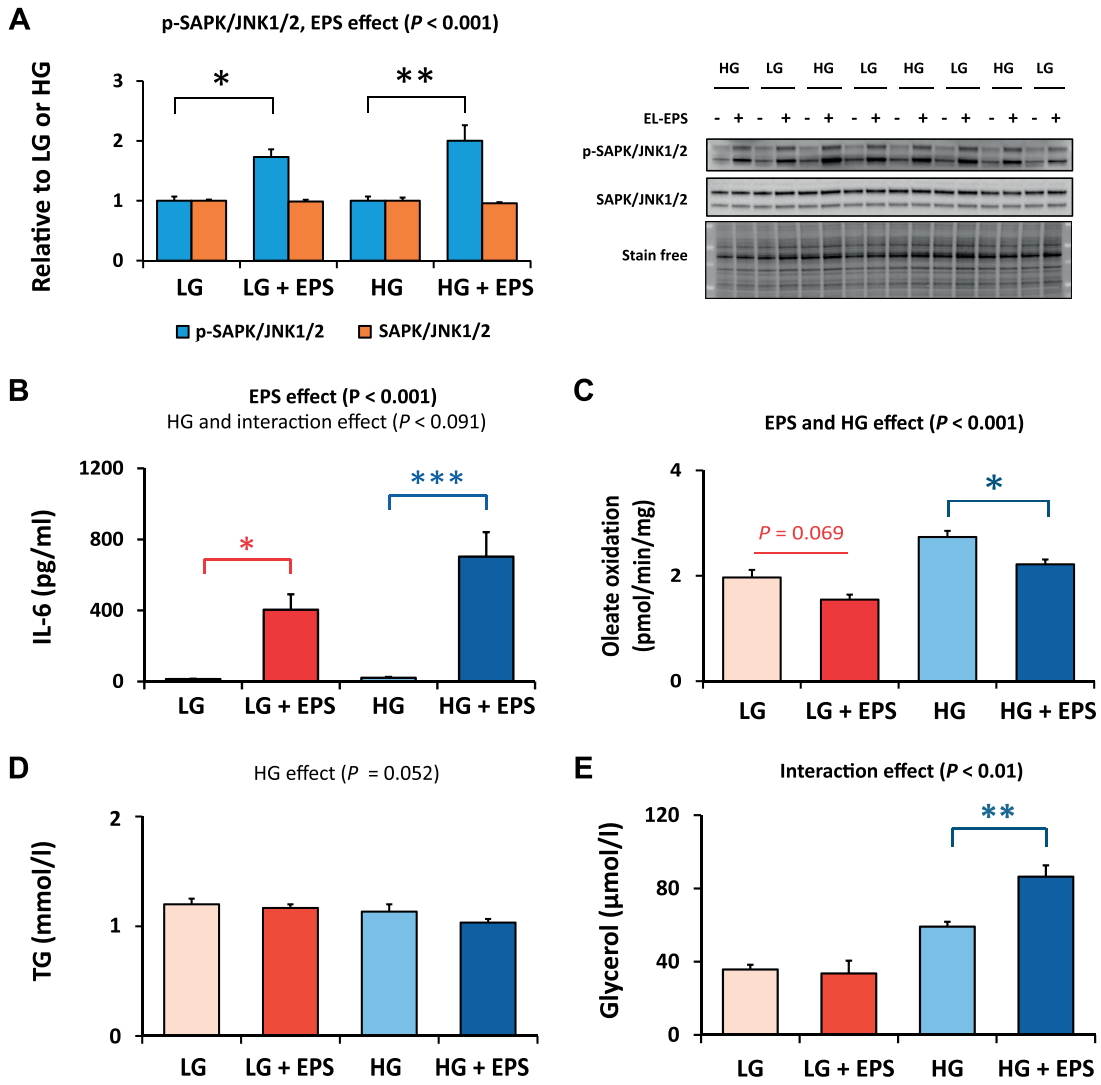

Figure 6. Exercise-like electrical pulse stimulation (EL-EPS) promoted protein phosphorylation and cell metabolism especially under high-glucose (HG) condition. *A*: phosphorylated stress-activated protein kinase/c-Jun N-terminal kinase (SAPK/JNK1/2)$^{Thr183/Tyr185}$, total SAPK/JNK1/2, and representative blots. −, no stimulation; +, stimulation. In the figure, the values are presented as normalized to low-glucose (LG) = 1 or HG = 1. Interleukin-6 (IL-6) concentration in the media (*B*), oleate oxidation rate (*C*), intracellular triacylglycerol (TG) content (*D*), and media glycerol content (*E*). $*P < 0.05$, $**P < 0.01$, and $***P < 0.001$. In *A* and *D–E*, $n = 6$, in *B*, $n = 12$ [pool of the ^{1}H NMR and oleate oxidation (22-h timepoint) experiments] and in *C*, $n = 8–10$ samples per group. The two-way MANOVA was used to analyze the effects of the applied EL-EPS and media glucose content (EPS and HG effects, respectively) and their interaction effect, whereas group comparisons were analyzed with multivariate Tukey's test.

with EL-EPS. SCFAs such as acetate, propionate, and butyrate are commonly observed with in vivo studies and are common products of gut microbial metabolism (40), while also other tissues can produce SCFAs. For example, Van Hall et al. (41) showed that exercise increased leg acetate release by ninefold when compared with rest. In the present study, we showed that intra- and extracellular contents of acetate were increased after EL-EPS, while the former was more pronounced in high-glucose condition. During increased energy demand or restricted TCA cycle function, all of the pyruvate-derived acetyl-CoA might have not successfully entered the TCA cycle and thus the excess can be hydrolyzed to acetate and released into the circulation (42, 43). Acetate can also be produced from pyruvate via enzymatic and nonenzymatic reactions including pyruvate dehydrogenase (PDH) and reactive oxygen species (ROS) (44), respectively, and PDH activity (45) and ROS levels (16) are increased by exercise and/or myotube contractions. In addition, hyperactive glucose metabolism and nutritional excess have been related to incomplete metabolism and excretion of metabolites, which lead to promoted conversion of pyruvate to acetate (44). This might have been the case also in our study since in high-glucose condition, the accumulation of succinate, fumarate, and malate suggests that substrate availability and entry to the TCA cycle might have exceeded the capacity of the oxidative phosphorylation machinery thus resulting in incomplete substrate oxidation. It is possible that the reduced need for full TCA cycle activity is due to enhanced glycolysis,

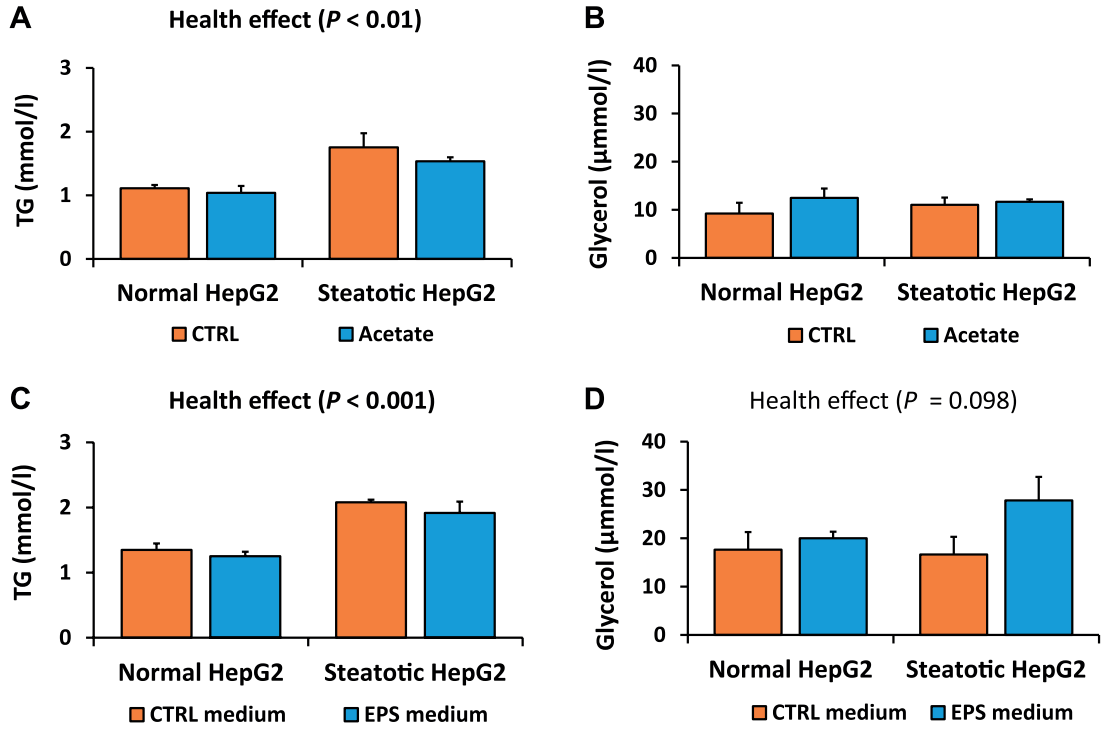

Figure 7. The 24-h administration of acetate and conditioned medium from the stimulated C2C12 cells had only minor effects on normal and steatotic HepG2 hepatocytes. Cell triacylglycerol (*A*) and media glycerol (*B*) contents after administration of 1.5 mM acetate (diluted in PBS) or PBS control. Cell triacylglycerol (*C*) and media glycerol (*D*) contents after administration of the media from the stimulated or unstimulated C2C12 cells grown under high-glucose conditions [electrical pulse stimulation (EPS) and CTRL medium, respectively]. $n = 3$ samples per group. The two-way MANOVA was used to analyze the effects of the applied exercise-like (EL)-EPS and steatosis (EPS and health effects, respectively) and their interaction effect, whereas group comparisons were analyzed with multivariate Tukey's test.

which may provide enough ATP for the working myotubes based on the strongly increased lactate levels.

As acetate has been shown to positively modify liver lipid metabolism (46), the effects of myotube-derived acetate and the whole EPS secretome (EL-EPS CM) on hepatocytes were examined. By applying acetate and EL-EPS CM to normal and steatotic hepatocytes, we found that the intracellular triacylglycerol content in the hepatocytes remained unaltered in the studied conditions. However, the molecules originated from the contracted muscle cells (EL-EPS CM) had a tendency for increased lipolysis in the hepatocytes, inferred from the increased media content of glycerol. In long-term, this could lead to reduced intracellular triacylglycerol content, but further studies are needed. Also more studies investigating dose-response effects of acetate are also warranted. This is because we found high levels of acetate from the cell-free media controls similar to a previous study (47), meaning that hepatocyte culture already had high levels of acetate before further adding it into the media. Future physiology studies should also investigate whether the high levels of acetate use and release from muscle cells have physiological effects in vivo.

Besides acetate, the media content of 3-hydroxybutyrate, a common ketone body, increased after EL-EPS and the response was greater in high-glucose condition. Previously, an increased content of circulating 3-hydroxybutyrate after exercise has been considered to act as a biomarker of metabolic shift from the utilization of carbohydrates toward fats (34) and SCFAs and ketone bodies have been reported to positively modify lipid, carbohydrate, and protein metabolism in the muscle and in other tissues (48). Although 3-hydroxybutyrate has been considered to be produced mainly by the liver, the growing body of evidence demonstrates that during exercise skeletal muscle could secrete certain ketone bodies and thus contribute to the circulating ketone body pool (13). The 3-hydroxybutyrate has been detected in the muscle interstitial fluid after exercise (13), and the enzyme regulating 3-hydroxybutyrate synthesis, HMG-CoA synthase (*HMGCS2*), has been shown to be elevated in skeletal muscle after exercise (49). In addition, 3-hydroxybutyrate dehydrogenase (*BDH1*), which converts acetoacetate into 3-hydroxybutyrate has been shown to be increased in the skeletal muscle by exercise and decreased by inactivity (49) (https://metamex.com). Thus, 3-hydroxybutyrate could be an exerkine, however, further studies are needed to verify its functions on nearby cells and the whole body metabolism and cross talk after exercise.

In addition to the more routinely observed SCFAs, we observed a set of unique changes in several BCFAs including 2-methylbutyrate, isobutyrate, and isovalerate that all increased after EL-EPS. Correlations between BCFAs and BCAAs along with studies using BCAA-depleted media strongly indicate that the BCFAs are indeed derived from BCAA catabolism. Previous in vivo study suggested that

during exercise BCFA precursors derived from the BCAA catabolism were increased in the skeletal muscle (50) and identified from the circulation (51). Concordant with this finding, we demonstrated that BCFAs can be produced and released by muscle cells in response to EL-EPS. Furthermore, we simultaneously observed an increase in the BCAAs in the cells after EL-EPS, identical as reported in glycolytic human type II-muscle fibers after exercise (52). Previous studies have shown that increased levels of circulating BCAAs and decreased BCAA degradation has been associated with poor metabolic health (53). In this study, we reported *1*) unaltered media BCAA content, *2*) increased content of BCAA breakdown products, and *3*) increased intracellular content of many amino acids (including BCAAs) after EL-EPS. Together these results suggest that the EL-EPS perhaps enhanced protein breakdown and amino acid recycling similarly as in vivo exercise (54). In summary, high correlations of the BCAAs and their breakdown products as well as very low levels of BCFAs in the experiment with BCAA-depleted media support the evidence that in the C2C12 cells the origin of BCFAs seems to be BCAA catabolism.

The enzymes needed for the conversion of the acyl-CoA derivatives originated from the BCAA catabolism [2-methylbutyryl-CoA, isobutyryl-CoA, and isovaleryl-CoA (55)] into 2-methylbutyrate, isobutyrate, and isovalerate may include acyl-CoA thioesterases (ACOTs), of which skeletal muscle expresses different isoforms (56) and the C2C12 cell line at least *Acot3* and *Acot9* (57). The ACOT9 isoform has been shown to have a unique substrate specificity with the ability to hydrolyze short-chain acyl-CoA esters, including isobutyryl-CoA and isovaleryl-CoA (56, 58). This further suggests that the mitochondrial link between branched-chain fatty acid and amino acid metabolism could be ACOT9 (58).

The effect of EL-EPS on the amino acids was consistently greater than the high-glucose effect both in the cells and in the media. The in vivo changes in the circulating amino acids have been reported to be controversial and dependent on their specific glucogenic versus ketogenic, nonessential versus essential or other properties (11, 12) as well as exercise intensity (59). To summarize, although our results are mainly in agreement with recent in vivo systematic reviews on exercise metabolomics (11, 12), more research is needed to better understand the stimulation-induced changes in myotube and media metabolites. Indeed, the number of studies analyzing the metabolome after EL-EPS is small (60) and, to best of our knowledge, this study is the first to study metabolites after EL-EPS under distinct nutritional loads.

We observed a decline in oleate oxidation during EL-EPS under high-glucose condition, whereas under low-glucose condition the decrease approached a trend. Decreased oleate oxidation may be related to the aforementioned *1*) incomplete oxidation of the energetic intermediates during hyperactive metabolism and nutrient overloading (44) and *2*) glycolytic nature of the C2C12 cell line (37). Addition of the fresh media containing the radiolabeled and unlabeled oleic acid in right proportion is an essential step for accurate oxidation measurement when using our protocol. Based on our results, the 24-h EL-EPS almost completely depleted the glucose from the media in LG condition. In oleate oxidation experiments, we had to replace the EL-EPS media with the fresh ^{3}H oleic acid-containing media after 22 h of stimulation and thus, we simultaneously provided the cells with fresh glucose for the remaining 2 h of the EL-EPS. This may have temporarily stimulated the cells to rely heavily on glucose, perhaps, at least in LG condition. Furthermore, increased glycolysis causes accumulation of acetyl-CoA that could inhibit β-oxidation via downregulation of β-ketoacyl-CoA thiolase (61). That said, because acetyl-CoA cannot be transported across membrane, the excess might also be transformed to acetate via the action of ACOT enzymes (58) or via nonenzymatic processes (44) and then secreted from the cells to balance the intracellular state of TCA cycle substrates (42) as we observed in the present study. Besides decreased oleate oxidation, we observed no changes in intracellular triacylglycerol content similar to the work by Laurens et al. (62), although our observation of the increased glycerol release may be associated with enhanced lipolysis under high-glucose condition after EL-EPS. In addition, contraction-induced changes in triacylglycerol content may be pretreatment specific because acclimatization of the C2C12 myotubes to fatty acids has been shown to cause intramyocellular triacylglycerol accumulation, which was prevented by short-duration low-frequency EL-EPS (63). Moreover, previous studies have reported controversial results on fatty acid oxidation after EL-EPS and the main factors affecting the rate of β-oxidation seem to be related to the stimulation protocol, duration of the measurement, fatty acid analyzed (e.g., oleate or palmitate), analysis protocol/method, and the cell line used (37, 38, 63–66).

In addition to changes in the metabolome, the applied EL-EPS altered the phosphorylation and secretion of stress-inducible markers, such as MAPKs and cytokines, commonly analyzed after in vivo exercise and in vitro EL-EPS (16). The phosphorylation of SAPK/JNK increased after EL-EPS independent of glucose availability, which is supported by in vivo studies demonstrating that glycolytic exercise increases SAPK/JNK phosphorylation (67, 68). Of the exercise-responsive cytokines, we observed an increase in the secretion of IL-6 after EL-EPS, also independent of glucose availability. Interestingly, muscle IL-6 secretion may occur in part through proteasome-dependent release initiated by lactate production (32). Indeed, the IL-6 in the media correlated positively with the intra- and extracellular lactate content in the present study (Supplemental Table S4). In addition, SAPK/JNK has been shown to regulate IL-6 metabolism (31) and indeed we observed that IL-6 and phosphorylated SAPK/JNK responded similarly to EL-EPS.

Strengths of the Study

To the best of our knowledge, the present study is the first to examine and compare the intra- and extracellular metabolome of myotubes after EL-EPS. Importantly, although we did not use tracers, we included analysis of the cell-free media controls with or without EL-EPS to the present study. This enabled us to roughly estimate whether the metabolites were taken up to the cells or released into the media. Moreover, these cell-free controls also validated the experiments showing that the effects of EL-EPS on media metabolite levels were most probably through myotube contractions and not through unspecific effects of EL-EPS on media. In

addition, the number of studies analyzing the effects of glucose availability on the myotube metabolism after EL-EPS is surprisingly small (21), although the nutritional status is known to regulate many intracellular processes even under nonexercising conditions (69). That said, the limitation of the existing literature is that not all studies have clearly reported the medium glucose content (e.g., only a few of the EL-EPS articles reviewed by Nikolić et al. (16)] although it is highly recommended in other in vitro studies (17, 70). Overall, our study improves understanding of the role of nutrient availability on the metabolic changes induced by EL-EPS.

Limitations of the Study

In the present study, the selected metabolomics platform (^{1}H NMR) provided an introductory insight into the differences in the C2C12 myotube and media metabolites, whereas future studies using mass spectrometry (MS)-based metabolomics would be beneficial for the analysis of lower abundance metabolites. Indeed, combination of the NMR and MS platforms in metabolomics research has been recommended (71). Moreover, studies using dynamic turnover of metabolomics [i.e., fluxomics (72)] are warranted to investigate the flux of the metabolites in vitro and in vivo. We also acknowledge that we detected some minor differences between LG and HG DMEMs in some metabolites in addition to glucose (Supplemental Table S1), but unlike myo-inositol that is derived from glucose, those are likely explained by batch-to-batch differences. Finally, time series data collection after different modes of EL-EPS in upcoming studies would provide a broader understanding of the metabolite characteristics in recovery phase both in the cells and in the media.

Conclusions

By using the C2C12 myotubes, we found that EL-EPS enhanced energy source utilization as well as production and secretion of lactate, acetate, and BCFAs (see summary in Fig. 8). Many of the EL-EPS induced changes in the myotube and/or media metabolites, such as contents of lactate, acetate, BCFAs, and TCA cycle intermediates, were affected by the glucose availability. This is possibly at least in part because low-glucose condition almost fully depleted glycolytic C2C12 cells from glucose in 24 h. Thus, we recommended to consider the effect of nutrition and the choice of media in future EL-EPS studies. Lastly, the novel increase in BCFAs with EL-EPS leads to the enticing notion that these metabolites may act as exerkines warranting more research on their physiological significance and regulation by in vivo exercise.

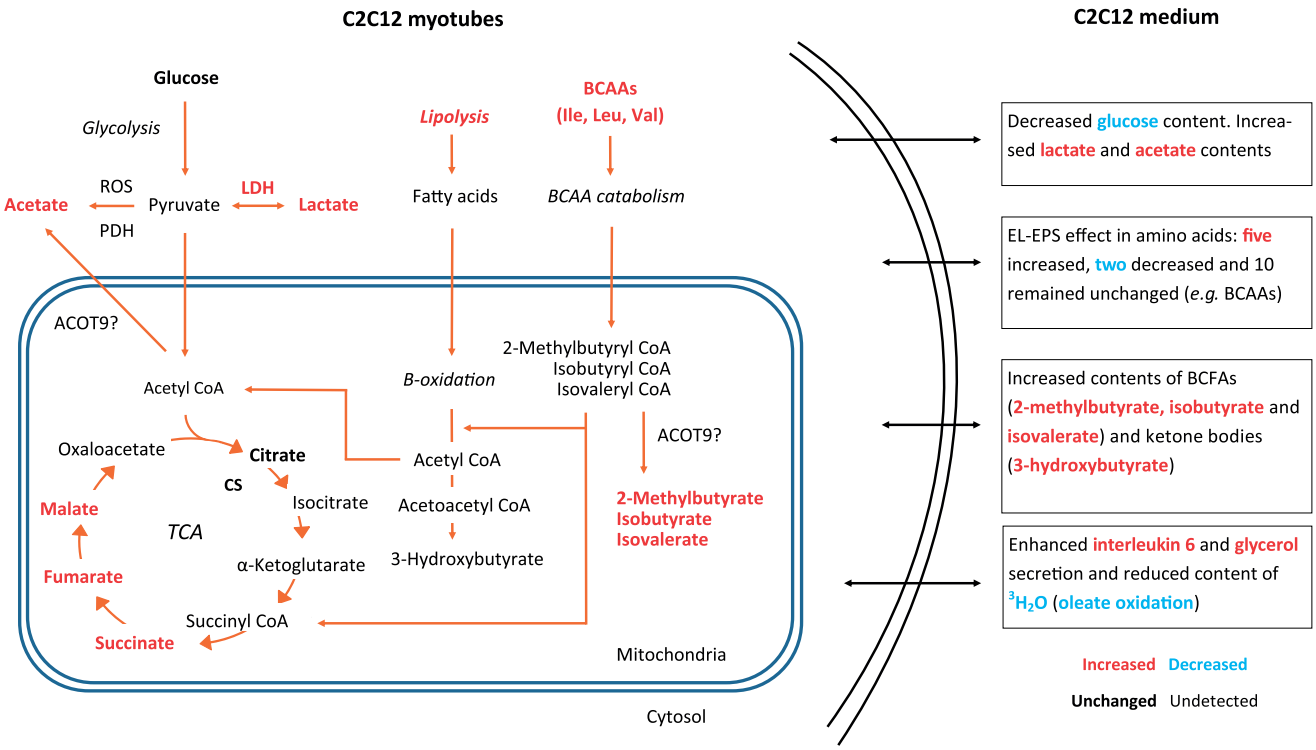

Figure 8. Summary of the effects of exercise-like electrical pulse stimulation (EL-EPS) on C2C12 myotube metabolism. The application of EL-EPS increased ATP production pathways, including glycolysis and lipolysis. The resulting pyruvate and acetyl-CoA were converted to lactate by lactate dehydrogenase (LDH) and to acetate possibly through reactive oxygen species (ROS) and pyruvate dehydrogenase (PDH). A buildup of several TCA intermediates suggests an overall reduction in oxidative metabolism. This is also consistent with the observed reduction in fatty acid oxidation suggested by the reduced oleate metabolism. The intermediates of the branched-chain amino acid (BCAA) catabolism include 2-methylbutyrate, isobutyrate, and isovalerate that are in part produced by the acyl-CoA thioesterases (ACOTs), possibly ACOT9. These BCAA breakdown products belong to the branched-chain fatty acids (BCFAs) and they can be directed to the TCA cycle, production of ketone bodies (e.g., 3-hydroxybutyrate) or as we observed they might also be released out of the cells. Blue = decreased, red = increased, bold black = unchanged, and black = undetected content.

SUPPLEMENTAL DATA

Supplemental Figs. S1–S5 and Supplemental Tables S1–S4: https://doi.org/10.6084/m9.figshare.14376413.v1.

ACKNOWLEDGMENTS

We thank Hannah Crossland, Jouni Tukiainen, and Eija Laakkonen for help with the EL-EPS setup. Mika Silvennoinen, Ulla Sahinaho, and Jari Ylänne are thanked for suggestions and help regarding the oleate oxidation experiments. We appreciate the help received from Maarit Lehti and Emilia Lähteenmäki with methodological issues and Hanne Tähti and Mervi Matero are thanked for help in sample collection. We thank Susanna Luoma, Tanja Toivanen, and Jukka Hintikka for helping with the sample and data analysis.

GRANTS

This work was funded by the Academy of Finland Grant 298875 (to H. Kainulainen), 308042 (to S. Pekkala), 323435 (to P. Permi), and 275922 (to J. J. Hulmi). T. M. O'Connell is supported by grants from National Institutes of Health, National Institute of Arthritis and Musculoskeletal, and Skin Diseases (P01AG039355 and P30AR072581) as well as the Additional Ventures, Single Ventricle Research Fund.

DISCLOSURES

No conflicts of interest, financial or otherwise, are declared by the authors.

AUTHOR CONTRIBUTIONS

J.H.L., S.P., and J.J.H. conceived and designed research; J.H.L., S.M., J.P., and P.P. performed experiments; J.H.L., T.M.O., S.M., and J.P. analyzed data; J.H.L., T.M.O., S.M., H.K., S.P., and J.J.H. interpreted results of experiments; J.H.L. prepared figures; J.H.L. drafted manuscript; T.M.O., S.M., H.K., S.P., P.P., and J.J.H. edited and revised manuscript; J.H.L., T.M.O., S.M., J.P., H.K., S.P., P.P., and J.J.H. approved final version of manuscript.

REFERENCES

1. **Pedersen BK**, **Saltin B.** Exercise as medicine—evidence for prescribing exercise as therapy in 26 different chronic diseases. *Scand J Med Sci Sports* 25: 1–72, 2015. doi:10.1111/sms.12581.
2. **Fiuza-Luces C**, **Garatachea N**, **Berger NA**, **Lucia A.** Exercise is the real polypill. *Physiology (Bethesda)* 28: 330–358, 2013. doi:10.1152/physiol.00019.2013.
3. **Whitham M**, **Parker BL**, **Friedrichsen M**, **Hingst JR**, **Hjorth M**, **Hughes WE**, **Egan CL**, **Cron L**, **Watt KI**, **Kuchel RP**, **Jayasooriah N**, **Estevez E**, **Petzold T**, **Suter CM**, **Gregorevic P**, **Kiens B**, **Richter EA**, **James DE**, **Wojtaszewski JFP**, **Febbraio MA.** Extracellular vesicles provide a means for tissue crosstalk during exercise. *Cell Metab* 27: 237–251.e4, 2018. doi:10.1016/j.cmet.2017.12.001.
4. **Castaño C**, **Mirasierra M**, **Vallejo M**, **Novials A**, **Párrizas M.** Delivery of muscle-derived exosomal miRNAs induced by HIIT improves insulin sensitivity through down-regulation of hepatic FoxO1 in mice. *Proc Natl Acad Sci USA* 117: 30335–30343, 2020. doi:10.1073/pnas.2016112117.
5. **Febbraio MA**, **Pedersen BK.** Contraction-induced myokine production and release: is skeletal muscle an endocrine organ? *Exerc Sport Sci Rev* 33: 114–119, 2005. doi:10.1097/00003677-200507000-00003.
6. **Pedersen BK**, **Febbraio MA.** Muscles, exercise and obesity: skeletal muscle as a secretory organ. *Nat Rev Endocrinol* 8: 457–465, 2012. doi:10.1038/nrendo.2012.49.
7. **Pedersen BK**, **Steensberg A**, **Fischer C**, **Keller C**, **Keller P**, **Plomgaard P**, **Febbraio M**, **Saltin B.** Searching for the exercise factor: is IL-6 a candidate? *J Muscle Res Cell Motil* 24: 113–113, 2003. doi:10.1023/A:1026070911202.
8. **Safdar A**, **Saleem A**, **Tarnopolsky MA.** The potential of endurance exercise-derived exosomes to treat metabolic diseases. *Nat Rev Endocrinol* 12: 504–517, 2016. doi:10.1038/nrendo.2016.76.
9. **Weigert C**, **Lehmann R**, **Hartwig S**, **Lehr S.** The secretome of the working human skeletal muscle—a promising opportunity to combat the metabolic disaster? *Proteomics Clin Appl* 8: 5–18, 2014. doi:10.1002/prca.201300094.
10. **Piccirillo R.** Exercise-induced myokines with therapeutic potential for muscle wasting. *Front Physiol* 10: 287, 2019. doi:10.3389/fphys.2019.00287.
11. **Sakaguchi CA**, **Nieman DC**, **Signini EF**, **Abreu RM**, **Catai AM.** Metabolomics-based studies assessing exercise-induced alterations of the human metabolome: a systematic review. *Metabolites* 9: 164, 2019. doi:10.3390/metabo9080164.
12. **Schranner D**, **Kastenmüller G**, **Schönfelder M**, **Römisch-Margl W**, **Wackerhage H.** Metabolite concentration changes in humans after a bout of exercise: a systematic review of exercise metabolomics studies. *Sports Med Open* 6: 11, 2020. doi:10.1186/s40798-020-0238-4.
13. **Zhang J**, **Bhattacharyya S**, **Hickner RC**, **Light AR**, **Lambert CJ**, **Gale BK**, **Fiehn O**, **Sh A.** Skeletal muscle interstitial fluid metabolomics at rest and associated with an exercise bout: application in rats and humans. *Am J Physiol Endocrinol Metab* 316: E43–E53, 2019. doi:10.1152/ajpendo.00156.2018.
14. **Murphy RM**, **Watt MJ**, **Febbraio MA.** Metabolic communication during exercise. *Nat Metab* 2: 805–812, 2020. doi:10.1038/s42255-020-0258-x.
15. **Carter S**, **Solomon TP.** In vitro experimental models for examining the skeletal muscle cell biology of exercise: the possibilities, challenges and future developments. *Pflugers Arch* 471: 3, 413–429, 2019. doi:10.1007/s00424-018-2210-4.
16. **Nikolić N**, **Görgens SW**, **Thoresen GH**, **Aas V**, **Eckel J**, **Eckardt K.** Electrical pulse stimulation of cultured skeletal muscle cells as a model for in vitro exercise—possibilities and limitations. *Acta Physiol (Oxf)* 220: 310–331, 2017. doi:10.1111/apha.12830.
17. **Lagziel S**, **Gottlieb E**, **Shlomi T.** Mind your media. *Nat Metab* 2: 1369–1364, 2020. doi:10.1038/s42255-020-00299-y.
18. **Daskalaki E**, **Pillon NJ**, **Krook A**, **Wheelock CE**, **Checa A.** The influence of culture media upon observed cell secretome metabolite profiles: the balance between cell viability and data interpretability. *Anal Chim Acta* 1037: 338–350, 2018. doi:10.1016/j.aca.2018.04.034.
19. **Emerging Risk Factors Collaboration**. Diabetes mellitus, fasting blood glucose concentration, and risk of vascular disease: a collaborative meta-analysis of 102 prospective studies. *Lancet* 375: 2215–2222, 2010. doi:10.1016/S0140-6736(10)60484-9.
20. **Lautaoja JH**, **Pekkala S**, **Pasternack A**, **Laitinen M**, **Ritvos O**, **Hulmi JJ.** Differentiation of murine C2C12 myoblasts strongly reduces the effects of myostatin on intracellular signaling. *Biomolecules* 10: 695, 2020. doi:10.3390/biom10050695.
21. **Farmawati A**, **Kitajima Y**, **Nedachi T**, **Sato M**, **Kanzaki M**, **Nagatomi R.** Characterization of contraction-induced IL-6 up-regulation using contractile C2C12 myotubes. *Endocr J* 60: EJ12–E0316, 2012. doi:10.1507/endocrj.ej12-0316.
22. **Evers-van Gogh IJA**, **Alex S**, **Stienstra R**, **Brenkman AB**, **Kersten S**, **Kalkhoven E.** Electric pulse stimulation of myotubes as an in vitro exercise model: cell-mediated and non-cell-mediated effects. *Sci Rep* 5: 10944, 2015. doi:10.1038/srep10944.
23. **Son YH**, **Lee S**, **Lee SH**, **Yoon JH**, **Kang JS**, **Yang YR**, **Kwon K.** Comparative molecular analysis of endurance exercise in vivo with electrically stimulated in vitro myotube contraction. *J Appl Physiol (1985)* 127: 1742–1753, 2019. doi:10.1152/japplphysiol.00091.2019.
24. **Furuichi Y**, **Manabe Y**, **Takagi M**, **Aoki M**, **Fujii NL.** Evidence for acute contraction-induced myokine secretion by C2C12 myotubes. *PLoS One* 13: e0206146, 2018. doi:10.1371/journal.pone.0206146.
25. **Wang H**, **Kuusela S**, **Rinnankoski-Tuikka R**, **Dumont V**, **Bouslama R**, **Ramadan UA**, **Waaler J**, **Linden A-M**, **Chi N-W**, **Krauss S**, **Pirinen E**, **Lehtonen S.** Tankyrase inhibition ameliorates lipid disorder via suppression of PGC-1α PARylation in db/db mice. *Int J Obes (Lond)*. 44: 1691–1702, 2020. doi:10.1038/s41366-020-0573-z.
26. **Kostidis S**, **Addie RD**, **Morreau H**, **Mayboroda OA**, **Giera M.** Quantitative NMR analysis of intra-and extracellular metabolism of

mammalian cells: a tutorial. *Anal Chim Acta* 980: 1–24, 2017. doi:10.1016/j.aca.2017.05.011.
27. **Lautaoja JH**, **Lalowski M**, **Nissinen TA**, **Hentilä J**, **Shi Y**, **Ritvos O**, **Cheng S**, **Hulmi JJ.** Muscle and serum metabolomes are dysregulated in colon-26 tumor-bearing mice despite amelioration of cachexia with activin receptor type 2B ligand blockade. *Am J Physiol Endocrinol Metab* 316: E852–E865, 2019. doi:10.1152/ajpendo.00526.2018.
28. **Choudhury R**, **Beezley J**, **Davis B**, **Tomeck J**, **Gratzl S**, **Golzarri-Arroyo L**, **Wan J**, **Raftery D**, **Baumes J**, **O'Connell TM.** Viime: visualization and integration of metabolomics experiments. *Journal Open Source Softw* 5: 2410–2410, 2020. doi:10.21105/joss.02410.
29. **Hargreaves M**, **Spriet LL.** Skeletal muscle energy metabolism during exercise. *Nat Metab* 2: 817–828, 2020 [Erratum in *Nat Metab* 2: 990, 2020]. doi:10.1038/s42255-020-0251-4.
30. **Kramer HF**, **Goodyear LJ.** Exercise, MAPK, and NF-κB signaling in skeletal muscle. *J Appl Physiol (1985)* 103: 388–395, 2007. doi:10.1152/japplphysiol.00085.2007.
31. **Whitham M**, **Chan MHS**, **Pal M**, **Matthews VB**, **Prelovsek O**, **Lunke S**, **El-Osta A**, **Broenneke H**, **Alber J**, **Brüning JC**, **Wunderlich FT**, **Lancaster GI**, **Febbraio MA.** Contraction-induced interleukin-6 gene transcription in skeletal muscle is regulated by c-Jun terminal kinase/activator protein-1. *J Biol Chem* 287: 10771–10779, 2012. doi:10.1074/jbc.M111.310581.
32. **Hojman P**, **Brolin C**, **Nørgaard-Christensen N**, **Dethlefsen C**, **Lauenborg B**, **Olsen CK**, **Åbom MM**, **Krag T**, **Gehl J**, **Pedersen BK.** IL-6 release from muscles during exercise is stimulated by lactate-dependent protease activity. *Am J Physiol Endocrinol Metab* 316: E940–E947, 2019. doi:10.1152/ajpendo.00414.2018.
33. **Romijn JA**, **Coyle EF**, **Sidossis LS**, **Gastaldelli A**, **Horowitz JF**, **Endert E**, **Wolfe RR.** Regulation of endogenous fat and carbohydrate metabolism in relation to exercise intensity and duration. *Am J Physiol Endocrinol Physiol* 265: E380–E391, 1993. doi:10.1152/ajpendo.1993.265.3.E380.
34. **Morville T**, **Sahl RE**, **Moritz T**, **Helge JW**, **Clemmensen C.** Plasma metabolome profiling of resistance exercise and endurance exercise in humans. *Cell Rep* 33: 108554, 2020. doi:10.1016/j.celrep.2020.108554.
35. **Richter EA**, **Hargreaves M.** Exercise, GLUT4, and skeletal muscle glucose uptake. *Physiol Rev* 93: 993–1017, 2013. doi:10.1152/physrev.00038.2012.
36. **Hirvonen J**, **Nummela A**, **Rusko H**, **Rehunen S**, **Härkönen M.** Fatigue and changes of ATP, creatine phosphate, and lactate during the 400-m sprint. *Can J Sport Sci* 17: 141–144, 1992.
37. **Burch N**, **Arnold A-S**, **Item F**, **Summermatter S**, **Brochmann Santana Santos G**, **Christe M**, **Boutellier U**, **Toigo M**, **Handschin C.** Electric pulse stimulation of cultured murine muscle cells reproduces gene expression changes of trained mouse muscle. *PloS One* 5: e10970, 2010. doi:10.1371/journal.pone.0010970.
38. **Abdelmoez AM**, **Sardón Puig L**, **Smith JA**, **Gabriel BM**, **Savikj M**, **Dollet L**, **Chibalin AV**, **Krook A**, **Zierath JR**, **Pillon NJ.** Comparative profiling of skeletal muscle models reveals heterogeneity of transcriptome and metabolism. *Am J Physiol Cell Physiol* 318: C615–C626, 2020. doi:10.1152/ajpcell.00540.2019.
39. **Brooks GA.** Lactate as a fulcrum of metabolism. *Redox Biol* 35: 101454, 2020. doi:10.1016/j.redox.2020.101454.
40. **Tan J**, **McKenzie C**, **Potamitis M**, **Thorburn AN**, **Mackay CR**, **Macia L.** The role of short-chain fatty acids in health and disease. *Adv Immunol* 121: 91–119, 2014. doi:10.1016/B978-0-12-800100-4.00003-9.
41. **Van Hall G**, **Sacchetti M**, **Rådegran G.** Whole body and leg acetate kinetics at rest, during exercise and recovery in humans. *J Physiol* 542: 263–272, 2002. doi:10.1113/jphysiol.2001.014340.
42. **Kistner S**, **Rist MJ**, **Döring M**, **Dörr C**, **Neumann R**, **Härtel S**, **Bub A.** An NMR-based approach to identify urinary metabolites associated with acute physical exercise and cardiorespiratory fitness in healthy humans—results of the KarMeN study. *Metabolites* 10: 212, 2020. doi:10.3390/metabo10050212.
43. **Knowles SE**, **Jarrett IG**, **Filsell OH**, **Ballard FJ.** Production and utilization of acetate in mammals. *Biochem J* 142: 401–411, 1974. doi:10.1042/bj1420401.
44. **Liu X**, **Cooper DE**, **Cluntun AA**, **Warmoes MO**, **Zhao S**, **Reid MA**, **Liu J**, **Lund PJ**, **Lopes M**, **Garcia BA**, **Wellen KE**, **Kirsch DG**, **Locasale JW.** Acetate production from glucose and coupling to mitochondrial metabolism in mammals. *Cell* 175: 502–513.e13, 2018. doi:10.1016/j.cell.2018.08.040.
45. **Spriet LL**, **Heigenhauser GJ.** Regulation of pyruvate dehydrogenase (PDH) activity in human skeletal muscle during exercise. *Exerc Sport Sci Rev* 30: 91–95, 2002. doi:10.1097/00003677-200204000-00009.
46. **Liu L**, **Fu C**, **Li F.** Acetate affects the process of lipid metabolism in rabbit liver, skeletal muscle and adipose tissue. *Animals* 9: 799, 2019. doi:10.3390/ani9100799.
47. **Kamphorst JJ**, **Chung MK**, **Fan J**, **Rabinowitz JD.** Quantitative analysis of acetyl-CoA production in hypoxic cancer cells reveals substantial contribution from acetate. *Cancer Metab* 2: 23–28, 2014. doi:10.1186/2049-3002-2-23.
48. **Frampton J**, **Murphy KG**, **Frost G**, **Chambers ES.** Short-chain fatty acids as potential regulators of skeletal muscle metabolism and function. *Nat Metab* 2: 840–849, 2020. doi:10.1038/s42255-020-0188-7.
49. **Pillon NJ**, **Gabriel BM**, **Dollet L**, **Smith JA**, **Puig LS**, **Botella J**, **Bishop DJ**, **Krook A**, **Zierath JR.** Transcriptomic profiling of skeletal muscle adaptations to exercise and inactivity. *Nat Commun* 11: 1–15, 2020. doi:10.1038/s41467-019-13869-w.
50. **Klein DJ**, **McKeever KH**, **Mirek ET**, **Anthony TG.** Metabolomic response of equine skeletal muscle to acute fatiguing exercise and training. *Front Physiol* 11: 110, 2020. doi:10.3389/fphys.2020.00110.
51. **Contrepois K**, **Wu S**, **Moneghetti KJ**, **Hornburg D**, **Ahadi S**, **Tsai M-S**, **Metwally AA**, **Wei E**, **Lee-McMullen B**, **Quijada JV**, **Chen S**, **Christle JW**, **Ellenberger M**, **Balliu B**, **Taylor S**, **Durrant MG**, **Knowles DA**, **Choudhry H**, **Ashland M**, **Bahmani A**, **Enslen B**, **Amsallem M**, **Kobayashi Y**, **Avina M**, **Parelman D**, **Schussler-Fiorenza Rose SM**, **Zhou W**, **Ashley EA**, **Montgomery SB**, **Chaib H**, **Haddad F**, **Snyder MP.** Molecular choreography of acute exercise. *Cell* 181: 1112–1130.e16, 2020. doi:10.1016/j.cell.2020.04.043.
52. **Blomstrand E**, **Essén-Gustavsson B.** Changes in amino acid concentration in plasma and type I and type II fibres during resistance exercise and recovery in human subjects. *Amino Acids* 37: 629–636, 2009. doi:10.1007/s00726-008-0182-y.
53. **Kainulainen H**, **Hulmi JJ**, **Kujala UM.** Potential role of branched-chain amino acid catabolism in regulating fat oxidation. *Exerc Sport Sci Rev* 41: 194–200, 2013. doi:10.1097/JES.0b013e3182a4e6b6.
54. **Tipton KD**, **Hamilton DL**, **Gallagher IJ.** Assessing the role of muscle protein breakdown in response to nutrition and exercise in humans. *Sports Med* 48: 53–64, 2018. doi:10.1007/s40279-017-0845-5.
55. **Dhanani ZN**, **Mann G**, **Adegoke OA.** Depletion of branched-chain aminotransferase 2 (BCAT2) enzyme impairs myoblast survival and myotube formation. *Physiol Rep* 7: e14299, 2019. doi:10.14814/phy2.14299.
56. **Bekeova C**, **Anderson-Pullinger L**, **Boye K**, **Boos F**, **Sharpadskaya Y**, **Herrmann JM**, **Seifert EL.** Multiple mitochondrial thioesterases have distinct tissue and substrate specificity and CoA regulation, suggesting unique functional roles. *J Biol Chem* 294: 19034–19047, 2019. doi:10.1074/jbc.RA119.010901.
57. **Zhou L**, **Wang L**, **Lu L**, **Jiang P**, **Sun H**, **Wang H.** Inhibition of miR-29 by TGF-beta-Smad3 signaling through dual mechanisms promotes transdifferentiation of mouse myoblasts into myofibroblasts. *PLoS One* 7: e33766, 2012. doi:10.1371/journal.pone.0033766.
58. **Tillander V**, **Nordström EA**, **Reilly J**, **Strozyk M**, **Van Veldhoven PP**, **Hunt MC**, **Alexson SE.** Acyl-CoA thioesterase 9 (ACOT9) in mouse may provide a novel link between fatty acid and amino acid metabolism in mitochondria. *Cell Mol Life Sci* 71: 933–948, 2014. doi:10.1007/s00018-013-1422-1.
59. **Peake JM**, **Tan SJ**, **Markworth JF**, **Broadbent JA**, **Skinner TL**, **Cameron-Smith D.** Metabolic and hormonal responses to isoenergetic high-intensity interval exercise and continuous moderate-intensity exercise. *Am J Physiol Endocrinol Metab* 307: E539–E552, 2014. doi:10.1152/ajpendo.00276.2014.
60. **Hoshino D**, **Kawata K**, **Kunida K**, **Hatano A**, **Yugi K**, **Wada T**, **Fujii M**, **Sano T**, **Ito Y**, **Furuichi Y**, **Manabe Y**, **Suzuki Y**, **Fujii NL**, **Soga T**, **Kuroda S.** Trans-omic analysis reveals ROS-dependent pentose phosphate pathway activation after high-frequency electrical stimulation in C2C12 myotubes. *Iscience* 23: 101558, 2020. doi:10.1016/j.isci.2020.101558.
61. **Saddik M**, **Gamble J**, **Witters LA**, **Lopaschuk GD.** Acetyl-CoA carboxylase regulation of fatty acid oxidation in the heart. *J Biol Chem* 268: 25836–25845, 1993.

62. **Laurens C**, **Bourlier V**, **Mairal A**, **Louche K**, **Badin P-M**, **Mouisel E**, **Montagner A**, **Marette A**, **Tremblay A**, **Weisnagel JS**, **Guillou H**, **Langin D**, **Joanisse DR**, **Moro C.** Perilipin 5 fine-tunes lipid oxidation to metabolic demand and protects against lipotoxicity in skeletal muscle. *Sci Rep* 6: 38310, 2016. doi:10.1038/srep38310.
63. **Li L**, **Ma J**, **Li S**, **Chen X**, **Zhang J.** Electric pulse stimulation inhibited lipid accumulation on C2C12 myotubes incubated with oleic acid and palmitic acid. *Arch Physiol Biochem* 1–7, 2019. doi:10.1080/13813455.2019.1639763.
64. **Nikolić N**, **Bakke SS**, **Kase ET**, **Rudberg I**, **Halle IF**, **Rustan AC**, **Thoresen GH**, **Aas V.** Electrical pulse stimulation of cultured human skeletal muscle cells as an in vitro model of exercise. *PLoS One* 7: e33203, 2012. doi:10.1371/journal.pone.0033203.
65. **Lambernd S**, **Taube A**, **Schober A**, **Platzbecker B**, **Görgens SW**, **Schlich R**, **Jeruschke K**, **Weiss J**, **Eckardt K**, **Eckel J.** Contractile activity of human skeletal muscle cells prevents insulin resistance by inhibiting pro-inflammatory signalling pathways. *Diabetologia* 55: 1128–1139, 2012. doi:10.1007/s00125-012-2454-z.
66. **Marš T**, **Miš K**, **Meznarič M**, **Prpar Mihevc S**, **Vid J**, **Haugen F**, **Rogelj B**, **Raustan AC**, **Thoresen GH**, **Pirkmajer S**, **Nikolić N.** Innervation and electrical pulse stimulation–in vitro effects on human skeletal muscle cells. *Appl Physiol Nutr Metab* 99: 1–10, 2020. doi:10.1139/apnm-2019-0575.
67. **Lessard SJ**, **MacDonald TL**, **Pathak P**, **Han MS**, **Coffey VG**, **Edge J**, **Rivas DA**, **Hirshman MF**, **Davis RJ**, **Goodyear LJ.** JNK regulates muscle remodeling via myostatin/SMAD inhibition. *Nat Commun* 9: 3030, 2018. doi:10.1038/s41467-018-05439-3.
68. **Hentilä J**, **Ahtiainen JP**, **Paulsen G**, **Raastad T**, **Häkkinen K**, **Mero AA**, **Hulmi JJ.** Autophagy is induced by resistance exercise in young men, but unfolded protein response is induced regardless of age. *Acta Physiol* 224: e13069, 2018. doi:10.1111/apha.13069.
69. **MacDonald TL**, **Pattamaprapanont P**, **Pathak P**, **Fernandez N**, **Freitas EC**, **Hafida S**, **Mitri J**, **Britton SL**, **Koch LG**, **Lessard SJ.** Hyperglycaemia is associated with impaired muscle signalling and aerobic adaptation to exercise. *Nat Metab* 2: 902–917, 2020. doi:10.1038/s42255-020-0240-7.
70. **Théry C**, **Witwer KW**, **Aikawa E**, **Alcaraz MJ**, **Anderson JD**, **Andriantsitohaina R**, et al**.** Minimal information for studies of extracellular vesicles 2018 (MISEV2018): a position statement of the International Society for Extracellular Vesicles and update of the MISEV2014 guidelines. *J Extracell Vesicles* 7: 1535750, 2018. doi:10.1080/20013078.2018.1535750.
71. **Marshall DD**, **Powers R.** Beyond the paradigm: combining mass spectrometry and nuclear magnetic resonance for metabolomics. *Prog Nucl Magn Reson Spectrosc* 100: 1–16, 2017. doi:10.1016/j.pnmrs.2017.01.001.
72. **Hui S**, **Cowan AJ**, **Zeng X**, **Yang L**, **TeSlaa T**, **Li X**, **Bartman C**, **Zhang Z**, **Jang C**, **Wang L**, **Lu W**, **Rojas J**, **Baur J**, **Rabinowitz JD.** Quantitative fluxomics of circulating metabolites. *Cell Metab* 32: 676–688.e4, 2020. doi:10.1016/j.cmet.2020.07.013.

IV

CONTRACTION-INDUCED CHANGES IN THE C2C12 MYOTUBE TRANSCRIPTOME, BUT NOT MYOMIRNA RELEASE, ARE AUGMENTED BY HIGHER GLUCOSE AVAILABILITY

by

Lautaoja, J.H., Karvinen, S., Korhonen, T-M., O´Connell T.M., Tiirola, M., Hulmi, J.J & Pekkala, S.

Manuscript in preparation.

Request a copy from the author.